SHEAR CONTROLLED ORIENTATION EFFECTS WITH INJECTION MOULDINGS PRODUCED BY THE SCORIM PROCESS

A thesis submitted for the degree of Doctor of Philosophy

by

Keith William Rawson

Department of Materials Engineering, Brunel University

May 1997

Brunel University, Department of Materials Engineering, Uxbridge, Middlesex, UB8 3PH, UK
Shear Controlled Orientation Effects With Injection Mouldings Produced by the SCORIM Process
Keith William Rawson; Ph.D. Degree 1997.

Abstract

Injection moulding using the process of Shear Controlled Orientation Injection Moulding (SCORIM) to enhance the aesthetic characteristics of plastics was investigated. Unsightly surface weld lines were successfully removed from highly reflective aluminium flake pigmented plastics by the application of a single macroscopic SCORIM shear when used in series with Bright Surface Moulding (BSM). A gonio spectrophotometer (GSP) was used for the quantitative characterisation of the Al flake pigmented mouldings as a measure of surface reflectivity and preferred angle of reflection. The different directional properties of surface reflectivities to either side of a conventional weld line are unacceptable, but were successfully reoriented approximately uniformly with the use of SCORIM and BSM moulding (i.e. SBM) used in series. SBM therefore provided an acceptable quality of surface finish for mouldings originally containing a weld line, without deterioration of mechanical properties. Indeed, some improvements in mechanical properties were observed.

Translucent two-colour mouldings were used to successfully demonstrate the flow paths taken by sheared material during the application of macroscopic shears. The use of intermittent shearing to encapsulate shear oriented material in the solidifying layers, manifested original and profound aesthetic effects. This resulted from mixing the two colours and was reproducible and widely variable. The morphology of isotactic polypropylene (iPP) processed in this way and examined by light and electron microscopy revealed how only one or two intermittent shears were required to orient a large volume of the moulding in the shear direction. Moreover, U-shaped flow paths demonstrated that the easiest shear route was close to the mouldings edges, an observation supported by x-ray analysis. The addition of Al flake pigment was found to act as a heterogeneous nucleant for β-spherulites. This acted as a suitable marker for the clear identification of the displaced weld interface using polarised light microscopy, of filled and unfilled iPP.

γ-phase was identified with the use of only one or two intermittent shears which reflects an increase in molecular alignment and consequent improved mechanical properties. The intensity of the γ-phase increased with the volume of material sheared. Strong evidence was also obtained of a linear relationship between the logarithm of the time lapse between two intermittent shears and the corresponding values of α-phase index, crystallinity index and percentage crystallinity. The values of each increasing proportionally with the length of time used.

Microhardness characterisation revealed anisotropy within SCORIM samples consistent with preferred orientation and increased modulus in the shear direction. The skin layers were characterised as the softest region through the thickness of SCORIM mouldings.

The results of this work were used to provide the basis of a computer simulation of the SCORIM process under development at the University of Wales Swansea.

Table of Contents

Table of Contents

Acknowledgements

Sincere gratitude goes to Professor Mike Bevis for his arrangement of financial support for this work and his selfless guidance and assistance which enabled this progressive and rewarding programme of research to be completed within the timescale.

My appreciation is also extended to Dr Peter Allan for his technical advice and assistance with the practical work and the various members of technical staff for their individual contributions.

The mathematical modelling group headed by Dr J. F. T. Pittman at University of Wales Swansea, are due special recognition for the collaborative development work undertaken by them.

Special thanks are also due to Dr Malcolm Stock of Silberline Ltd for his technical advice and overall research support.

I would also like to acknowledge the financial and technical support of Silberline Ltd, Leven, Scotland.

Nomenclature

A	α-phase index
B	β-phase index
BSM	Bright Surface Moulding
C	crystallinity index
C-PRES	compression pressure
C-TIME	compression time
DLFM	Double Live Feed Moulding
E	Young's Modulus
GSP	Gonio Spectrophotometer
iPP	isotactic polypropylene
LM	Light Microscopy
M	denotes a piston
N	denotes a piston
O	denotes a piston
P	denotes a piston
PA	polyamide
PC	polycarbonate
PBT	polybutylene terephthalate
PP	polypropylene
PS	polystyrene
Q	flow rate
QLFM	Quadruple Live Feed Moulding
R-PRES	relaxation pressure
R-TIME	relaxation time
SBM	SCORIM and BSM Moulding used in series
SCORIM	Shear Controlled Orientation Injection Moulding
SEM	Scanning Electron Microscopy
SLFM	Single Live Feed Moulding
TEM	Transmission Electron Microscopy
T_g	glass transition temperature
U	Toughness

WAXD	Wide Angle X-ray Diffraction
Y	Vickers hardness indentor diagonal length
Z	Vickers hardness indentor diagonal length
ε_p	peak strain
ε_u	ultimate tensile strain
σ_u	ultimate tensile stress

1. INTRODUCTION AND LITERATURE SURVEY

1.1 Introduction

The main principle of the SCORIM process (Shear Controlled ORientation Injection Moulding)[1, 2] is to apply macroscopic shears to the molten material in a mould during the solidification of the polymer. The objective of the process is to impart favourable physical properties to the moulded artefact as a result of the shearing process, through the control of preferred orientation of matrix resin or resin and fibres in a composite[3, 4]. This enables the removal of internal weld lines through the informed application of these macroscopic shears and with suitable processing conditions, surface weld lines can be eliminated also[5].

SCORIM[2] requires a minimum of two strategically positioned gating points within a mould cavity between which the melt shearing pressure can be applied. The development of SCORIM has matured to a stage where a more detailed, fundamental understanding is desired to assist with optimal design and utilisation of the process in technical injection moulding.

This research is an investigation of the polymer and filler orientation effects that can be produced by applying macroscopic shears in mould during solidification of the resin and following completion of mould filling. This collaborative work links the Wolfson Centre for Materials Processing, Brunel University, with Dr J. Pittman, of the University of Wales Swansea, whose group has an established reputation in mathematical modelling and computer simulation of a wide range of polymer processing operations. That research will analyse and model SCORIM, enabling comparative assessment of the modelling with the results of the dedicated SCORIM moulding trials in order to compare theory with experimental. This collaborative research will thus provide a basis for further modelling to put SCORIM on a predictive basis.

There are high costs associated with injection-mould tool manufacture, with much commercial advantage gained from short lead times in taking a product from concept to production. Hence, accurate predictions of 'in-mould' processing using computational techniques are an essential pre-requisite for

today's designers of injection-mould tools. State of the art modelling techniques currently available to industrial mould designers are limited to the mould filling process and related effects. The need to exploit new technologies whilst designing tooling 'right-first-time' to manufacture quality approved parts with the minimum number of processing steps and low-cost, emphasises the importance of this work.

This literature review covers recent work carried out on weld lines and related topics by various workers.

1.1.1 Aims

The initial aims of this work are detailed below.

1. To undertake dedicated SCORIM moulding trials which accurately measure and record the relevant data, as far as practicable, for subsequent evaluations of computer simulations of the SCORIM process developed at the University of Wales Swansea. The aim of the mathematical model is to provide a predictive basis for the controlled erasure of internal weld lines.
2. To apply macroscopic SCORIM shears to translucent two-colour mouldings, within a simple plaque mould tool, to obtain a visual record in the solidified mouldings of the flow dynamics involved, thereby providing for a better understanding of the way in which shear flow influences the preferred orientation and morphological structure of the mouldings.
3. To relate the morphology of isotactic polypropylene SCORIM mouldings and levels of preferred orientation to the processing conditions applied and some of the resultant mechanical properties, thereby providing insight and better understanding of the factors that determine achievement of optimum mechanical properties combined with minimal cycle time increases.
4. To evaluate the removal of surface weld lines from highly reflective aluminium pigmented polypropylene using SCORIM processing with the assistance of accelerated mould heating, to provide the basis for understanding more fully the influence of process method and conditions

on the desirable and undesirable visual effects of incorporating reflective pigment in compounds.

1.2 Weld Lines

In the context of polymer processing, weld lines occur where two or more molten polymer flow fronts impinge and are essentially complex three-dimensional areas of finite dimensions[6]. They are sometimes referred to as knit lines[7], melds, flow defects, flow aberrations etc. and can be formed in several ways during injection-moulding. Occurrences are due to multiple gate moulds and moulds containing flow interruptions (e.g. inserts, changes in section thickness) illustrated in figures 1.1a and b respectively. An insert divides the flow front and the molten polymer flows around it and then rejoins passed the insert resulting in a weld. Changes in section thickness may result in hesitation effects causing backflow of material during mould fill and a consequent weld.

"Jetting"[6, 8-11] is a further cause of welds (figure 1.2) where the melt "squirts" rather than flows across the mould cavity and is compressed in an "accordion" manner.

1.2.1 Flow Patterns During Mould Filling

Tadmor's[12] explanation of the complex molecular orientation distribution observed in injection mouldings of amorphous polymers is used by many workers[7, 13, 14] concerned with fibre orientation development. This is used as the basis for describing mould filling for fibre reinforced thermoplastics.

Flow advances in the cavity with a parabolic flow front and at some distance behind this a velocity profile exists as depicted in figure 1.3. At the mould wall there is zero shear rate, hence elongational flow predominates inducing molecular orientation and row-nucleated structures[15, 16] in this region. Towards the centre of flow, shear rate passes through a maximum before falling to zero in the centre of the cavity. High shear also induces molecular orientation, whereas the low shear at the centre induces little molecular orientation particularly where low heat transfer rates enable molecular relaxation to occur.

The consequence of this flow velocity profile on the advancing melt front is termed the 'volcano' or 'fountain' effect[6, 12, 17]. As the melt adjacent to the wall is cooled, viscosity increases thus decreasing flow in that region. The core region continues to flow and mould filling is sustained by the volcano-like mechanism where, at the melt front, polymer passes from the centre outwards towards the cavity wall (Figure 1.4). Where two melt fronts impinge to form a weld line, an orientation at 90° to the direction of main flow is found at the interface. In addition, air entrapments at the weld may also cause internal voids or a surface 'V' notch at the weld (Figure 1.5).

1.3 Processing Parameters

Investigations[14, 18, 19] have shown that the parameters used during processing directly influence the morphology of the moulded component, which in turn has a direct consequence on its mechanical properties. The morphology of semi-crystalline polymers is influenced not only by orientation. The degree of crystallisation depends on cooling rate[18] as determined by melt and mould temperature, injection pressure and speed.

1.3.1 Melt Temperature

Increasing melt temperature increases melt flow[20] during mould filling by reducing pseudo-plasticity and the extensional flow component. A reduction in transverse orientation around the gate improves the parabolic nature of the velocity profile which enlarges the highly oriented shear layer. However, Hegler[14] reports this to have an insignificant effect on mechanical properties.

At a weld, a higher melt temperature coupled with sufficient time will enable molecular entanglements to establish across the interface, as is characteristic of the bulk material. This interpenetration is necessary for strength and elongation at break to increase. The melt temperature is therefore a very significant injection moulding process parameter.

1.3.2 Mould Temperature

This influences the rate of solidification of the melt. A higher temperature increases the time available for molecular entanglements to occur across a

weld due to a reduced cooling rate. The morphology of crystalline polymers may also be strongly influenced[21].

1.3.3 Injection Pressure

Workers[22-24] have reported higher pressures improve weld strengths, again due to molecular interpenetrations across the interface. However, its influence relative to that of temperature is questioned without further research[18].

1.3.4 Injection Speed

A higher injection speed reduces the time available for the hot melt to be cooled by the relatively cold mould wall. Shear heat generation is also increased. Therefore the additional heat available in the melt at a weld will improve the 'healing' process of the interface at a molecular level.

1.4 Material Parameters

Material parameters, together with processing and design parameters form a complex function which influence the degree of orientation, symmetry and ratio of thicknesses in the skin/core layer structures. As skin/core layers and the influence of altering processing temperatures during the moulding of filled PP samples are the subject of investigation with this research, a review of related topics is presented here.

1.4.1 Matrix

Bright and Darlington[25] have shown that by simply varying matrix material the ratio of properties in and perpendicular to the mould filling direction can be completely reversed. Glass fibre reinforced PA6 and unfilled PA66[14] have yielded layer structures similar to figure 1.6 where layers 2 and 4 have blurred outlines giving a larger layer 3. Similar results have been noted by Bright *et al*[26] in polypropylene sprues. Alternatively, a glass fibre filled polypropylene matrix gave a pronounced fibre orientation perpendicular to the flow direction with low injection speeds. Here, layers 2 and 4 were exchanged with layer 3.

Bright and Darlington also showed that matrix-specific sensitivity to orientation can result in virtual suppression of the core layer with an increase in injection time. This is true for PA66, whereas conversely, polypropylene shows no fibre pattern change.

Curtis *et al*[27] observed that whilst an unfilled matrix exhibits very ductile mechanical properties the same matrix containing fibres generally fails in a brittle manner. This is partly due to morphological changes induced by the necessity to mould fill matrices at higher temperatures. Thus, this increases the degree of crystallinity and notching effect of fibre ends where stress concentrations exist in the matrix.

1.4.2 Fibres

Fibre concentration, orientation and length distribution as well as the matrix properties influence a mouldings' properties. Using a high volume fraction aligned in the flow direction increases the mechanical properties[27]. Crowson and Folkes[28] noted that a high fibre concentration increased the viscosity at low flow rates due to misaligned fibres colliding. At higher shear rates a blunt velocity profile induced little shearing in the central region. All shearing took place near the wall where fibres were highly aligned in the flow direction. This reduced the incidence of fibres colliding, hence little increase in viscosity with increased fibre content was observed.

This research considers low filler concentrations within a PP matrix. The influence of the application of macroscopic shears upon filler alignment near the cavity walls is investigated.

1.4.3 Orientation Effects of Fibre/Matrix

For all concentrations of fibres, molecular orientation in the matrix is of a magnitude comparable to that observed in unfilled polymers. Folkes and Russell[13] observed that fibres at typical commercial concentrations (20 - 30% by weight) in polypropylene, exhibit little influence on molecular orientation in the matrix. An increase in fibre concentration however, can lead to the molecular orientation in the matrix being dominated by fibre orientation.

For commercial applications the matrix orientation will therefore only be influenced by flow geometry and processing conditions, which is an important consideration for the low filler concentration materials investigated here.

1.4.4 Rheological Behaviour

For fibre filled materials, rheological behaviour is dependent upon fibre orientation and the matrix materials' rheological properties. In addition, the fibre orientation is directly influenced by the rheological behaviour of the melt. Bright *et al*[26] used rheological data to interpret the pattern of fibre orientation in mouldings. However, despite much research on the involved subject of filled polymer melt rheology, a detailed quantitative analysis is still impossible at this time although parts have been analysed theoretically.

1.5 Mould Design

1.5.1 Gate Design

Hegler[14] reviewed the effects of different gate designs on mould filling. Flow conditions during mould filling were ascertained by considering fibres mixed with polymer as independent components or melt particles. Ensuing fibre orientation reflected flow conditions. The relevant observations are reported here.

1.5.1.1 Edge Gated Rectangular Plaque

This design configuration results in a virtually uniaxially expanding flow with a multilayer fibre orientation whose cross-section is symmetrical. Neglecting the edges of the plaque, figure 1.6 shows the fibre orientation. Layer 1 is a low-fibre flow front film, formed close to the wall. Layer 2 has a slight fibre orientation. Layer 3 at the highly viscous 'skin/core interface' undergoes shear flow and can vary in size. Layer 4 is a randomly oriented transitional layer and layer 5 contains fibres predominantly oriented perpendicular to the flow direction. This is explained by expanding flow upon entering the mould

causing transverse orientation and insufficient re-orientation due to a low velocity profile at the centre.

1.5.1.2 Pin-Point Gated Rectangular Plaque

The melt passes through the gate into the cavity with two-dimensional expanding flow. Expansion parallel to the gate axis results in a layer structure similar to that for the edge gate. Flow expansion in the second dimension is radial swell flow, which only exists until the melt reaches the sides of the mould. Thereafter, an approximately single dimensional uniaxially expanding flow similar to the edge gate is observed. Figure 1.7 illustrates the resultant fibre orientation in the core layer 5.

Radial flow near the gate reduces fibre orientation parallel to the gate axis increasing orientation perpendicular to this. The influence of diverging flow is strong enough to alter shear flow conditions and figure 1.8 illustrates the layer structure parallel to the cavity walls which generally results.

1.5.2 Flow Interruptions

Krueger and Tadmor[29] observed advancing melt front profiles during filling of rectangular cavities with inserts. The inserts divided a single melt front into two, creating a long weld downstream of the insert which was the 'meeting line' of the two advancing fronts.

Hegler[14] noted that fibres are oriented transversely in front of obstacles and that at the 'meeting line' no mixing occurs. Instead, a zone with highly longitudinal fibre orientation develops similar to a skin layer at the cavity wall. Mechanical properties perpendicular to the flow direction deteriorate, but may increase in the flow direction. Figure 1.9 illustrates schematically the conditions in the core layer.

1.5.3 Stiffening Ribs

When stiffening ribs are placed perpendicular to the flow direction, disturbances of the fibre pattern before and after the rib are insignificant[14] close to the cavity. However, fibres in the boundary layer of such ribs are perpendicular to the main cavity wall. A greater or lesser degree of inclination

is observed in the layers near the cavity wall when stiffening ribs are either oblique to or along the flow direction. The angle of inclination was a function of the ratio of cavity to rib thicknesses, a thinner rib producing a greater angle.

1.6 Shear Controlled Orientation Injection Moulding

Work carried out by Hengesbach and Schramm[30] and Menges *et al*[31] utilised the moulding machine screw to produce an oscillating packing pressure. This overcame mould filling difficulties such as poor mould packing and dimensional reproducibility. The patented invention of a 'Multiple Live-Feed Moulding' (MLFM) device, figure 1.10, by Allan and Bevis[2] is a more refined method and able to produce 'shear controlled orientation in injection moulding' (SCORIM). The MLFM processing head, positioned between the injection moulder barrel and the mould tool, provides SCORIM by the application of controlled macroscopic shears to the solidifying polymer melt . This shearing acts at the melt/solid interface to orient any alignable fillers, including fibres, platelets and polymer molecules. This control route also provides control over the solidification process and physical properties.

The SCORIM equipment consists of three components, the MLFM processing head, the hydraulic driving package and the microprocessor control and interface package[1, 2]. The MLFM processing head is mounted directly onto the end of the injection screw barrel with its nozzles in contact with the mould.

The functions of the head are to:

i. Split the molten plastic into two or more streams and direct the molten stream into the mould cavity.
ii. Direct the molten plastic through a chamber where independently controlled pressures are applied to each stream.

The chamber pressures are applied by double acting hydraulic cylinders. These pressures provide the force required to move the plastic in the mould.

The hydraulic drive package provides the pressures to move the hydraulic cylinders in the correct sequence on command from the microprocessor control unit. This unit is a multi function controller for:

1. Setting, monitoring and controlling the head heaters and mould cavity pressures.
2. Programming the activation of the hydraulic drive package.
3. Programming the MLFM cycle activation and termination.
4. Programming the mode of operation of the pistons and number of piston cycles per moulding cycle.

1.6.1 Oscillating Hold Pressure Technique

A schematic representation of the device used at Brunel to produce an oscillating hold pressure is illustrated in figure 1.11. An oscillating, rather than static, post-injection pressure is supplied to the solidifying melt by the packing piston. Controlled oscillations cause viscoelastic heating in the sprue(s) and runner(s) maintaining a channel of molten (live) polymer from the barrel to the moulding. Hold pressure continues to pack the solidifying moulding for a longer period compensating for any shrinkage.

1.6.2 Double Live Feed Moulding

This process divides the feed into two, each of which is independently capable of supplying pressure to the mould cavity. The double live feed mould (DLFM) packing device, is positioned between the machine barrel and mould as illustrated in figure 1.10. The hydraulic pistons are microprocessor controlled and can effectively provide SCORIM[1, 3]. A similar double live feed arrangement utilises a twin barrelled injection moulding machine with each barrel fitted with oscillating packing devices, illustrated in figure 1.12.

1.6.2.1 Packing Modes

There are three principle packing modes available with DLFM:

Mode I: pistons M and N are moved back and forth at the same frequency but with a phase difference of 180°.

Mode II: pistons M and N are moved back and forth at the same frequency and in phase.

Mode III: pistons M and N can be held down under a static pressure.

Mode I has the effect of shearing the melt in the cavity by repetitive alternate injection from each packing chamber, figure 1.13a. This provides a route for the elimination of such conventional moulding defects as internal weld lines and knit lines. Short fibre alignment can also be achieved during material freeze off.

Mode II compresses and decompresses the solidifying melt within the mould cavity. Thereby acting as two oscillating packing heads with resultant elimination of shrinkage defects and the attainment of accurate reproducible dimensions, figure 1.13b.

Mode III applies a static packing to the cavity as with conventional moulding, figure 1.13c.

1.6.2.2 Process Control

SCORIM is controlled by an oscillating packing profile consisting of a combination of five parameters. Four of these parameters are required for the microprocessor to instruct the hydraulic pump to complete one cycle:

1. Compression time (C-TIME)
2. Relaxation time (R-TIME)
3. Compression pressure (C-PRESS)
4. Relaxation pressure (R-PRESS)

The remaining parameter, stage duration, controls the number of complete cycles per stage and is therefore a multiple of the cycle time. The number and sequence of stages in the packing profile is determined by the profile sequence.

When using double live feed moulding in mode I the five parameters have the same values for both pistons with a phase separation of 180° specified by the pistons' sequencing. Table 1.1 shows a typical packing profile with compression and relaxation pressures quoted as a percentage of the maximum hydraulic pressure.

The total cycle time for the packing profile is the sum of stage duration's in the profile sequence, i.e. 4.1 seconds.

1.6.3 Quadruple Live-Feed Moulding

This process divides the injection moulder feed into four independent feeds and it is identical in principle to the double live feed system[3]. A single barrelled injection moulding machine may be used requiring a new fixed platen and a more complex live feed assembly than the DLFM packing device.

Figure 1.14 schematically illustrates a four live feed arrangement with a twin barrelled injection moulding machine, utilising two double live feed devices. This offers greater versatility in the design of multiple live-feed systems, including provision for coupling multiple component moulding and multiple live-feed moulding. Quadruple live-feed moulding (QLFM) also imparts considerably more versatility to the SCORIM process than the double live-feed variant.

QLFM process control is the same as with DLFM with the exception that additional piston sequencing is required. Workers[3, 32] have identified four possible piston sequences effectively capable of producing SCORIM with QLFM. In each case the packing pistons operate at the same frequency with a 180° phase separation. Typical conditions are given in Tables 1.2 to 1.5 with the respective flow paths illustrated in figures 1.15 to 1.18. Using examples (i) with (ii) or (iii) with (iv) in series can produce simple laminates, with more complex structures produced using all four examples in series.

1.7 Bright Surface Moulding (BSM)

Wada *et al*[33] of Asahi Chemical Industry Co., Ltd. have patented (UK patent GB 2081171) a novel injection moulding technology termed Bright Surface Moulding (BSM).

Wada *et al.*[33] investigated the influence of increasing the mould surface temperature using BSM technology. With the cavity surfaces at a temperature exceeding that of the glass transition temperatures for the various thermoplastic resins studied, the surface properties of moulded

artefacts were enhanced. Improvements included the absence of weld lines, jetting and silver streak defects with the inclusion of high gloss finishes with HIPS and ABS. Filled resins were noted to contain no filler particles in the skin layers of mouldings.

1.7.1 Equipment To Produce BSM

Bright Surface Moulding can be achieved by the retrospective adaptation of a conventional injection moulding machine with a high frequency induction heating device schematically illustrated in figure 1.19. The high frequency induction heating device consists of a 'stand alone' high frequency oscillator and process controller (1) and an inductance coil (inductor) (2) which is manoeuvred into position by a robot mounted on top of the fixed platen.

During the moulding cycle the inductor, inserted between both cavity surfaces, is energised by high frequency oscillations for a prescribed duration. The cavity surface rapidly rises in temperature before the inductor is retracted from the tool and the moulding cycle continued in a conventional manner. The injected melt material impinges onto tool cavity surfaces at temperatures temporarily exceeding that of its own T_g.

1.7.2 Application of BSM Technology

Wada and Yasuda[34] developed conjugated moulded parts possessing the properties of both thermosetting and thermoplastic resins. Using BSM technology embedded in the mould tool, an uncured solution of diallylphthalate (DAP) was sprayed onto the mould surface before conventionally injecting a thermoplastic resin (e.g. SAN or ABS). The filled mould was then heated to cure the DAP, the mould cooled and the part ejected.

1.8 Computer Simulation of SCORIM

In order to achieve a more fundamental understanding of the SCORIM process a numerical computer simulation is set up by Pittman *et al*[35, 36]. The simulation enables further development and optimisation of SCORIM by

considering the process in a simplified geometry with unfilled resins. No previous work of this type is available.

1.8.1 Mathematical Model Outline

The one-dimensional transient model considers the cooling and solidification of polymer melt contained between infinite plane parallel plates representing the mould walls, figure 1.20. The initial conditions for SCORIM are those present at the end of cavity filling, when a thin skin layer of solidified material is present adjacent to these mould walls. This model neglects the skin layer for simplicity, assuming an initially uniform molten injection temperature. The model thus considers the polymer to lose heat to the two cavity walls, cool and solidify whilst being subjected to reciprocating shear flows. The model solves for the transient temperature and velocity fields, and post-process, the velocity fields to provide further information on material displacement and deformation, which can be related to alignment and weld line erasure. A non-Newtonian, temperature dependent viscosity is used, together with temperature-dependent thermal properties and latent heat of solidification.

1.8.2 Model Simplifications

In addition to the simplifications outlined above, the model:

- assumes the material density to be constant
- assumes the melt to be incompressible
- treats phase change by means of an effective specific heat which represents an approximation to the physics.

These simplifications avoid the development of complicated, difficult theories and of obtaining the relevant data which is outside the remit of this work. This approach represents the most feasible at present[35].

1.8.3 Material Deformation

SCORIM provides for the controlled alignment of the matrix material at the molecular level and also alignable filler particles, described in section 1.4. The model assesses this alignment in terms of the total material deformation, or strain, frozen into the solidifying polymer during shear. This is not

quantitatively related to material alignment at present but is highly indicative. For low filler particle concentrations (e.g. 2% as with this work), particle-particle interactions may be neglected[35] enabling the model to predict particle alignment using either theoretical results from particle mechanics[37, 38] or a continuum approach[39]. Higher filler particle concentrations influence the rheology and they cannot therefore be considered for accurate predictions of orientation by the model without further fundamental work. Therefore all the filler concentrations used for this work were of low concentrations.

1.8.4 Process Operating Modes

The model considers two operating modes for SCORIM, firstly where shear flow is controlled by a constant hydraulic pressure applied to the SCORIM pistons and secondly where the piston displacement velocity is constant, *viz.*:

I. Where the reciprocating flow is driven by a fixed pressure gradient, $\delta p/\delta x$, of constant magnitude and with periodic sign change. In this case the flowrate, Q, eventually falls to zero as cooling and solidification proceed. This relationship is illustrated graphically in figure 1.21.

One limitation of this operating mode is if the limiting pressure gradient of the mathematical model is set too high. In this case the value may not be reached as a result of viscous heating coming into balance with cooling, leading to a dynamic steady state.

II. Where the flow is driven at a set stroke speed by hydraulically actuated pistons. The speed is maintained until the cavity flow resistance becomes too large for the hydraulics to overcome it, whereupon the stroke speed decreases towards zero. This relationship is illustrated graphically in figure 1.22.

This operating mode is approximated by:

a] a constant flow rate period during which the pressure gradient increases towards a limiting value, followed by

b] a second phase of operation at the constant, limiting pressure gradient, with the flow rate falling towards zero.

Neither operating mode is truly representative of the practical process. This is reflected by a balance between the two operating modes, dependent upon processing parameters, materials rheology etc.

This collaborative development of the numerical simulation of the SCORIM process was carried out at the University of Wales Swansea, by Dr J. F. T. Pittman *et al.* Therefore, the results of this simulation are presented as a separate section in an appendix at the end of this thesis.

1.9 Aesthetic Effects

Two industries with a specific interest in aesthetic effects are the automotive and packaging industries. Consequently, new developments related to injection mouldings with coloured surface decoration are often manifested by these industries first. Therefore an overview of existing technologies for the production of such effects is presented in this section.

1.9.1 In-Mould Decoration

The in-mould decoration (IMD) technique[40, 41] uses PC film and was developed for the manufacture of automotive interior trim fascias. It provides design freedom for the surface decoration of injection mouldings permitting great variety of different designs. The technique has also been adopted by the electrical, domestic and communication goods industries enabling technical and economical competitiveness versus alternative processes. Applications include pressure keys where manufacture within one mould can provide for a variety of different articles by simply changing the symbol on the printed film rather than the mould. The technique affords a scratch and abrasion-resistant decoration in conjunction with uniform surface texture. It is also possible to conceal weld lines if the appropriate gating method has been chosen.

1.9.2 Multi-Colour Injection Moulding

The most common method for the surface decoration of injection mouldings is multi-colour moulding[40], especially two-colour moulding. This method is often used with mass-produced parts not transilluminated and without much printed information. The high mould costs are offset by automation. Disadvantages include poor clarity of symbols with line widths less than 0.5mm. Moreover, three or even four colours involve great machine and mould expenditure, diminishing economical feasibility.

1.9.3 Printing

A low cost alternative to multi-colour injection moulding is the decoration of mouldings by screen printing or pad transfer printing. This is the most economical method where a maximum of three colours is required and the articles are not being transilluminated. However, the short life of the applied inks, which are subject to abrasion by frequent use of the article, is a great problem.

1.9.4 Laser Marking

An example of laser marking would be a clear plastic article which is then coated with a black acrylic paint of high covering power. This is subsequently exposed to laser beams which evaporate the black paint and make the white substrate re-appear. Transilluminated articles are thus obtained. However, this method is expensive and the black paint film is susceptible to abrasive wear.

1.9.5 Labels

The use of labels within the packaging industry has become the main way of communicating information to the consumer. With the number of different variants within particular product ranges expanding, the labels graphics are also vital in positioning the product at the correct level in the market and communicating the products qualities. The films used for labels can provide a variety of qualities themselves including high gloss, moisture and stain resistance, a physical protective barrier and top coatings suited to high

quality printing. Further, they are recyclable and may lend themselves to being die cut into sophisticated shapes. This bodes well with the packaging industries constant demand for unusual shaped containers.

1.9.6 Painting of Plastics

Decoratively coated plastic parts are the hallmarks of modern automobile designs and are manufactured predominantly off-line in the plastics processing supply industry. Only a small proportion are supplied as assembled, semi-finished products and painted on-line together with the carbody or in-line as a separate part in the body painting line. New design specifications such as "zero gap", in which components must fit the body with minimal visible join, have focused attention on colour matching between the body and fitting. Here, the preferred choice is on-line painting where primed fittings are painted with the topcoat of the body for an accurate colour match over the entire vehicle. Hence, this technology is experiencing a revival, at least during the planning of future vehicle production[42].

1.9.6.1 Substrate Precleaning and Pretreatment

The choice of substrate for plastic parts on automobiles is determined by technological, design, ecological and economic factors. Economics have greatly increased the market share of polyolefins for large fittings such as bumpers. To overcome the poor adhesion of paint systems to these plastics, various pretreatment technologies are used (e.g. flame and plasma treatment) or are on the brink of market introduction (e.g. flourination). For economic reasons, developments for coating polyolefins without any form of pretreatment are desired. Projects aimed at modifying the substrate polymers as well as developing directly adhering paints are progressing this production route. The main alternatives to polyolefins for large-area body parts are thermoplastics such as PC/PBT and PPE/PA blends. The latter can be coated on-line with original body paints.

The growing need for customisation sometimes with new effects, complements the necessary cost savings provided by pigmented plastics, optionally with additives for optical effects (e.g. metallic finishes) or process

variants (e.g. marble effects), which are only sometimes painted with a gloss clearcoat.

1.9.6.2 Primer

To comply with stringent quality requirements, primer coats are still necessary for the paint structure on plastic substrates. The main reasons for their use are to provide:

- ♣ the greatest colour accuracy in the case of paints with poor hiding power,
- ♣ smooth surfaces, even on problem substrates,
- ♣ optimum substrate/topcoat adhesion,
- ♣ easy repair because surface can be sanded,
- ♣ surface activation of plastics that are difficult to paint, and
- ♣ maximum UV protection for light-sensitive substrates.

New primer technologies are developing as a result of ecological and economical pressures and include,

- ♠ powder-paint primers,
- ♠ Primecoat,
- ♠ in-mould painting (IMP), in-mould coating (IMC), powder mould-coating (PMC) for injection mouldings, and
- ♠ granular injected-paint technology (GIPT).

Zero emissions, which is the ecological ideal, is currently only possible with powder paints. Whilst these provide the necessary storage stability, their large-scale usage is inhibited for plastics by their requirement for high temperature stoving. Conventional ESTA (electrostatic application) of a powder paint directly is not currently possible though developments are underway.

A primer that is also emission-free could theoretically be achieved via granulated injected-paint technology (GIPT). In this process a plastic is used that is formulated in a similar way to a primer, i.e. which contains fillers and even crosslinking agents typical of a primer. This plastic is then moulded by

the two-component ("2K") injection process. Despite the expense of primer coats, they will remain the more economic route for improving surfaces in many cases, especially where relatively inexpensive but problematic substrates are used.

1.9.6.3 Colour Coatings

Metallic paints for plastics are applied as basecoat/clearcoat layers. The solvent-borne basecoats which emit approximately 70 to 85% organic solvents during application and drying, are particularly suitable for developing the special metallic 'flip-flop' effect. However, basic paint technology will in future be characterised by three main developments:

- ♥ reduction of emissions,
- ♥ economy and
- ♥ new colour effects

Emissions will therefore be reduced by developments both in materials and applications technologies with the use of robots and electrostatically assisted applications being prominent. Both development trends are aimed at increasing the applications efficiency.

A new focus of development work is colour adjustment off-line, where colour matching of fittings to the automotive body is crucial. Examples are plastic fenders painted off-line and new effects based on liquid crystal pigments. Certain mother-of-pearl effects require formulations in which the final shade only results from the combination of a coloured substrate and a transparent pearl-effect coat. As a process control, visual inspection will be supplemented with automatic colourimetric measurements as obtained with gonio-spectrophotometry (GSP) characterisation.

1.9.7 Aluminium Pigments

Traditionally defined as lamellar flakes of high purity aluminium, new spheroidal shaped pigments have been developed and coloured flakes are under development. Leafing grades are Al pigments which orient parallel to the plane of the coating and are distributed only at the surface. Their highly reflective finishes are however easily marked. Non-leafing grades are those

which orientate through the depth of the coating and give good optical effects.

Al pigments influence the colour of coatings when viewed at different angles through their orientation. This is known as the 'flip-flop', 'two-tone' or 'travel' effect. When the painted surface coating is viewed face-on, the colour appears bright and when viewed sideways, the colour appears dark. Different effects can be controlled by varying particle size, shape, distribution and degree of surface polish[43]. Al being a soft metal requires care to avoid high levels of shear during formulation of coatings or plastics, in order to avoid deformation of the pigment which leads to a reduced orientation effect, colour and flop.

The desired properties of the Al pigment are related to the end use and include:

- Heat and light reflectivity, as well as corrosion protection from marine, roof and protective coatings.
- Food contact compliance for can coatings.
- Extrudable grades for powder coatings.
- High sparkle, good 'flip-flop' and acid resistance for coil coatings and general industrial coatings.

Features of such pigments include:

- Bright metallic lustre.
- Brightest sparkle.
- Pearlescent effect.
- Glitter effect.

Recent trends in automotive coatings have been towards finishes brighter on the face and darker in the flop tone. This is achieved by changing the pigment shape from a 'cornflake' to lenticular or lens type, in conjunction with closer control of particle size distribution.

1.9.8 Special-Effect Paints in Car Design

Pearlescent paints possess a characteristic 'deep lustre' which is also present in pearls and mother-of-pearl[44]. This is distinct in quality from the

metallic lustre obtained with metallic pigments. The most important group of pearlescent pigments is that of 'layer-substrate pigments' in which finely ground mica platelets are coated with a thin layer of titanium dioxide. These give a silvery white lustrous pigment which in combination with other colourants impart their character.

Colour effects are obtained by controlled variation of the TiO_2 layer which through the interference of light waves on thin layers, all the colours of the rainbow then appear. The interference pigments are distinguished by a brilliant, coloured, slightly iridescent lustre.

1.9.8.1 Pearlescent\Metallic Paints

The many possibilities for developing attractive paints with interference pigments has particularly inspired automobile paint designers recently. Pearlescent and metallic pigments are used alongside each other to develop completely new metallic finishes. Many plastics used for automobile exterior parts are painted the same colour as the car. In addition to protecting the plastic from weathering, this lends a high degree of homogeneity to the appearance of the car-body, particularly in the case of special-effect paints. However, the additional painting operation required considerably adds to the cost of these parts.

1.9.8.2 Pearlescent Masterbatches

Pearlescent masterbatches provide a more efficient method than painting for producing plastic parts with attractive appearance. The advantages of masterbatches are cost savings, the ability to recycle production scrap and the process is practically emission-free. Moreover, minor damage and scratches e.g. to car exterior trim, bumpers, etc. are better concealed by the deeper colouration of masterbatched plastics over the painted alternative.

Coloured effects for car interior trim are also in demand as these can complement traditional finishes e.g. wood grain. Pearlescent pigments can imitate known metallic effects but also provide new design possibilities e.g. marble effects. Pearlescent pigments reproduce the fine crystalline structure of natural marble and make these effects more lively.

1.9.8.3 Pigment Orientation

To ensure that special-effect pigments achieve their full effect in masterbatched plastics, it is important to consider the typical characteristics of these pigment groups. All platelet-type special-effect pigments, i.e. both metallic and pearlescent pigments, require good orientation of the pigment particles in order to optimally reflect the incident light. This orientation is ensured in virtually all plastics processing methods by flow process's of the plastics matrix[44].

However, the flow disturbances encountered with injection moulding lead to undesirable disturbance of pigment orientation and to optical inconsistencies. These always occur for example when the melt stream is divided requiring careful consideration of melt flow during the design of the mould tool to avoid this. With conventional injection moulding with existing mould tools the visual impact of weld lines can be softened by the selection of suitable processing parameters. Lower melt viscosity, lower injection rate and reduced injection pressure contribute to this. For this reason, the plastic should if possible be processed at the maximum temperature specified by the manufacturer and mould cooling should be at the highest, economically acceptable temperature.

The use of SCORIM and BSM to overcome the visual inconsistencies described above are researched, evaluated and the results presented within this thesis. These technologies therefore represent a development of the conventional injection moulding process.

1.10 Morphology of Isotactic Polypropylene

Polypropylene is one of the most important of the hydrocarbon polymers and was the first synthetic stereoregular polymer to achieve commercial and industrial importance. Among the possible stereoregular configurations, the isotactic form was the most important commercially.

Isotactic polypropylene (iPP), has all its pendant CH_3 groups attached on the same 'side' of the chain, i.e. all units have a spatially identical arrangement of atoms. This stereoregularity of polymer molecules is of high

importance for the properties of materials. It determines the possibility for adjacent molecules to fit together and therefore to crystallise. It also controls the strength of forces between molecules, upon which the mechanical properties of the material depend.

There are three different crystalline forms into which iPP can crystallise, namely α (monoclinic), β (hexagonal) and γ (triclinic, orthorhombic), their chain conformations being the threefold (3_1) helix with different packing geometries [45-47]. The α-form is the most common and stable phase with the β-form observed in only small quantities unless the sample is cooled rapidly from the melt,[45, 48, 49] in the presence of shear forces[50] or certain heterogeneous nuclei[51]. The γ-form may be present in low molecular weight PP or samples crystallised under high pressure[45, 52, 53].

1.10.1 Spherulites

Polymeric spherulites consist of numerous crystals radiating from a central nucleus. They form by nucleation at different points within a sample and grow as spherical entities only stopping growth when impingement of adjacent spherulites occurs[16].

Padden and Keith[54] observed five types of iPP spherulites, crystallised from the melt and characterised by their sign and magnitude of birefringence. Three α spherulites were identified dependent upon temperature of crystallisation; below 134°C a positively birefringent, radial (type I) spherulite, above 138°C a negative, radial (type II) spherulite and a mixed type spherulite in the intermediate range. Two β-spherulite types were also identified; below about 128°C a bright negative, radial (type III) spherulite and between 128 - 132°C a negative, ringed (type IV) spherulite. Electron microscopy revealed the epitaxial deposition of branches upon radial lamellae where the angle of branching is 80°40'. With large amounts of these 'cross-hatched' lamellae filling space between the radial lamellae, the structure may take the appearance of an intimately woven array[47].

1.10.2 Injection Moulded iPP Crystal Structures

The crystal structures obtained during injection moulding of crystalline polymeric products are formed as a consequence of the processing operation, and the thermal and mechanical conditions in the mould cavity. The crystallisation is highly influenced by the parameters of the processing technology. Further, thermal and mechanical conditions vary locally according to the geometry of the mould cavity, feed and gating arrangements. In essence, the material undergoing mould filling during injection moulding experiences particularly complicated thermal and orientation conditions.

The processes of deformation and orientation are widely accepted as those described by the Tadmor[12] model. During this process, the surface layers of flowing melt experience tensile stresses and the adjacent inner layers experience shear stresses. This results in an orientation of molecular coils in the flow direction. In the central core region some degree of relaxation may occur after mould filling and prior to crystallisation, depending on the heat transfer conditions. Consequently, conventionally moulded iPP exhibits non-homogenous anisotropic structure with properties varying widely depending upon processing conditions. Kantz *et al*[55] were the first to demonstrate the skin-core structure of injection moulded iPP. This technique and the relations between structure and properties are the subjects of many workers.[7, 51, 56-73] They cover the supermolecular level of the structure of injection moulded iPP as studied by polarised light microscopy (LM), x-ray diffraction and electron microscopy. Extensive reviews of such publications were carried out by Kalay[72] and Gil Medina[73].

It is worthy of note that LM provides useful information about the structure of samples through their thickness, in spite of the relatively low resolution. From microtomed sections of injection moulded iPP cut in the flow direction, the spherulitic structure of the core layer becomes evident. This relates to relaxation of the melt in this region before the start of crystallisation. The size of the spherulites decrease from the centre of the core towards the mould wall which is a reflection of the heat-transfer (cooling) mechanism of the system[73]. Also evident is the skin layer which appears as a

homogenous, often featureless structure at the level of resolution attained with LM. Sandwiched between these two layers is an intermediate layer or shear zone, which consists of a different spherulitic morphology to that of the core. The shear zone spherulites being row nucleated whilst the core spherulites are randomly nucleated[55]. The boundary between the skin and shear zone having a sharp appearance.

Several workers[5, 72-75] have successfully used this LM technique to illustrate the influence that SCORIM technology has upon managerially modifying the crystal structure obtained through the informed application of macroscopic shears. A skin layer is evident as with conventional mouldings, but adjacent to this layer the SCORIM acts to modify the appearance of both the shear and core zones. Microtomed sections cut parallel to flow exhibit shear bands adjacent and parallel to the skin layer, each band corresponding to the oscillatory motion of the hydraulic pistons producing SCORIM. Hence, the shear flow direction which reverses periodically (mode I of operation, described in section 1.6.2.1) during SCORIM is manifested as alternate bands of lower and higher birefringence when viewed under polarised light. In some such mouldings the spherulitic shear and core zones have been virtually replaced by non-spherulitic shear oriented bands. Only spherulitic cores of much reduced volumes remained in such SCORIM mouldings, the extent of spherulitic crystallisation present being dependent upon the character of the SCORIM conditions selected and the geometry of the mould tool. Through the application of intermittent shears alternate non-spherulitic orientation and spherulitic layers can be sequenced through the microstructure.[70, 72, 76] The ability to select these parameters to optimise the desired properties of the end component, is a skill at the disposal of the informed processor.

Table 1.1 Typical SCORIM packing profile for DLFM in mode I

Stage ID	Duration (Sec's)	C-Time (Sec's)	R-Time (Sec's)	C-Pres (%)	R-Pres (%)	Piston	Piston
S00	0.5	0.5	0.5	40	40	M	N
S01	2.4	0.6	0.6	65	30	M	N
S02	0.6	0.3	0.3	50	15	M	N

PROFILE SEQUENCE: S00, S01, S02, S02.

Table 1.2 Example (i), typical conditions using pistons M and P, figure 1.14

Stage ID	Duration (Sec's)	C-Time (Sec's)	R-Time (Sec's)	C-Pres (%)	R-Pres (%)	Piston	Piston
S00	20	2	2	65	30	M	P

Table 1.3 Example (ii), typical conditions using pistons N and O, figure 1.15

Stage ID	Duration (Sec's)	C-Time (Sec's)	R-Time (Sec's)	C-Pres (%)	R-Pres (%)	Piston	Piston
S00	20	2	2	65	30	N	O

Table 1.4 Example (iii), typical conditions using pistons MO and NP, figure 1.16

Stage ID	Duration (Sec's)	C-Time (Sec's)	R-Time (Sec's)	C-Pres (%)	R-Pres (%)	Piston	Piston
S00	20	2	2	65	30	MO	NP

Table 1.5 Example (iv), typical conditions using pistons MN and OP, figure 1.17

Stage ID	Duration (Sec's)	C-Time (Sec's)	R-Time (Sec's)	C-Pres (%)	R-Pres (%)	Piston	Piston
S00	20	2	2	65	30	MN	OP

N.B. (C-TIME) = Compression time; (R-TIME) = Relaxation time;
(C-PRES) = Compression pressure; (R-PRES) Relaxation pressure.

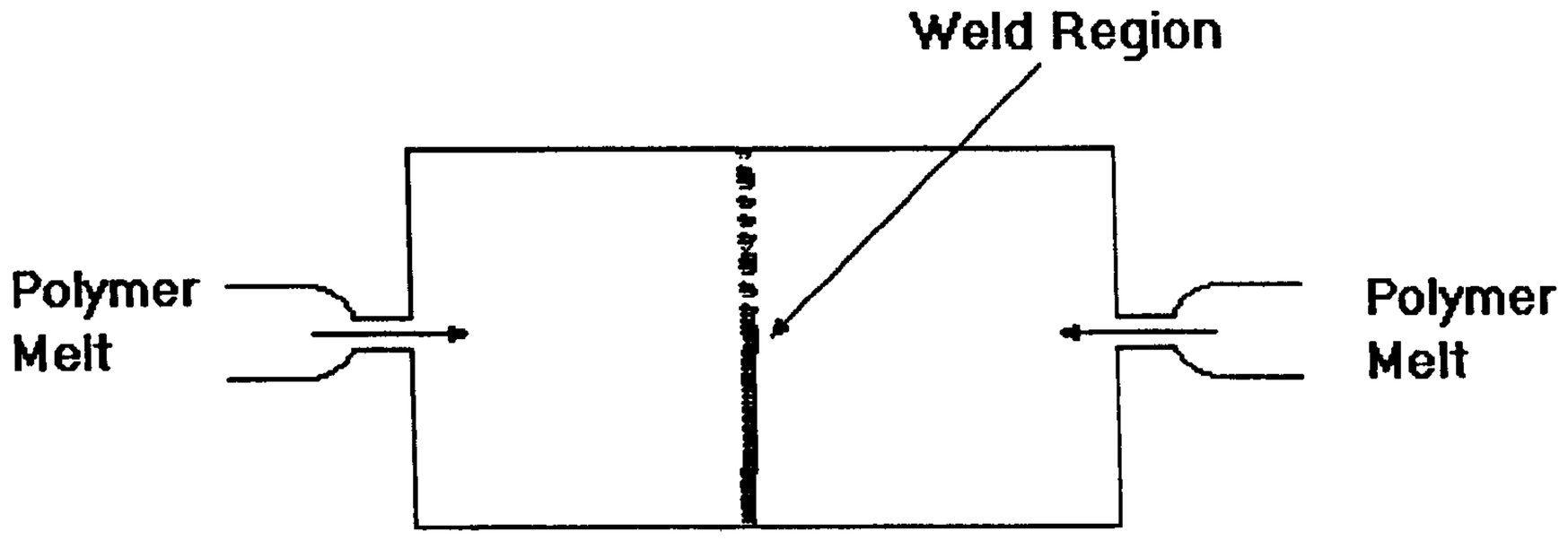

a. Welds Caused by Multiple Gates

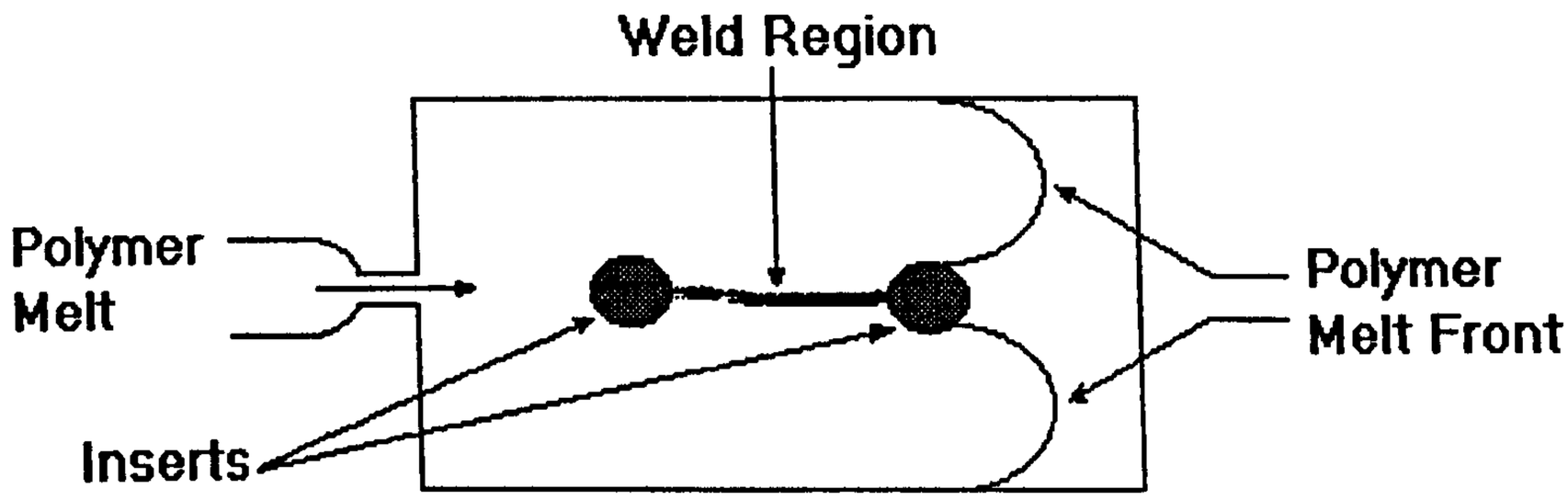

b. Welds Caused by Flow Interuptions

Figure 1.1 Weld lines formed during injection moulding[6]

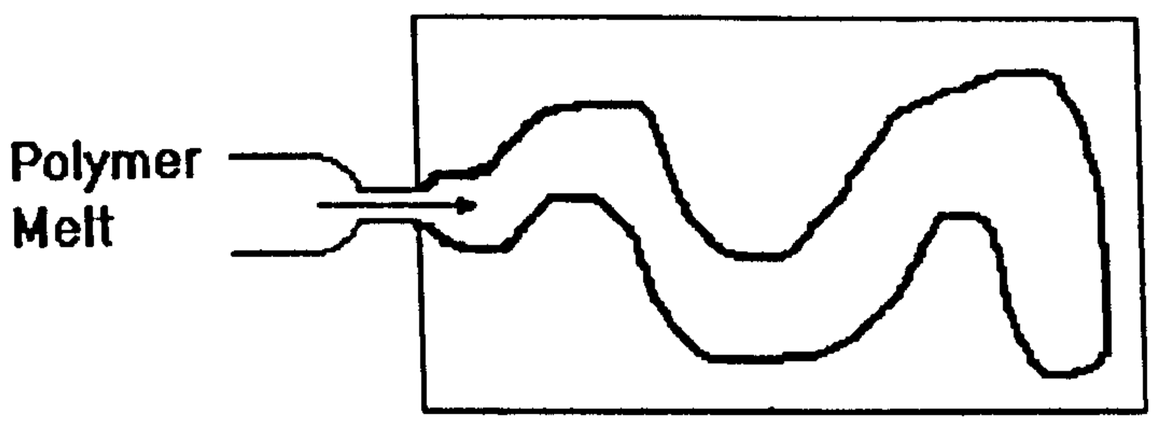

a. Jetting

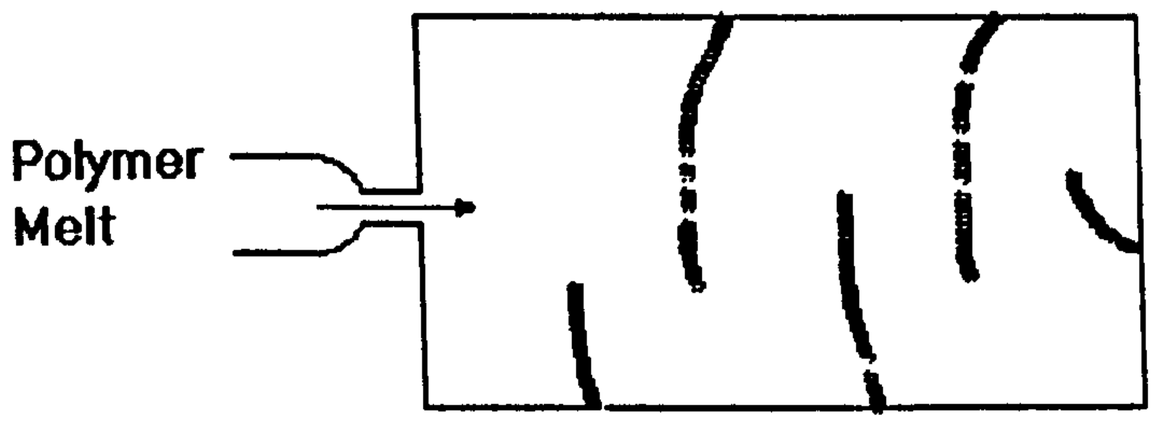

b. Weld Regions

Figure 1.2 Weld line caused by jetting during injection moulding[6]

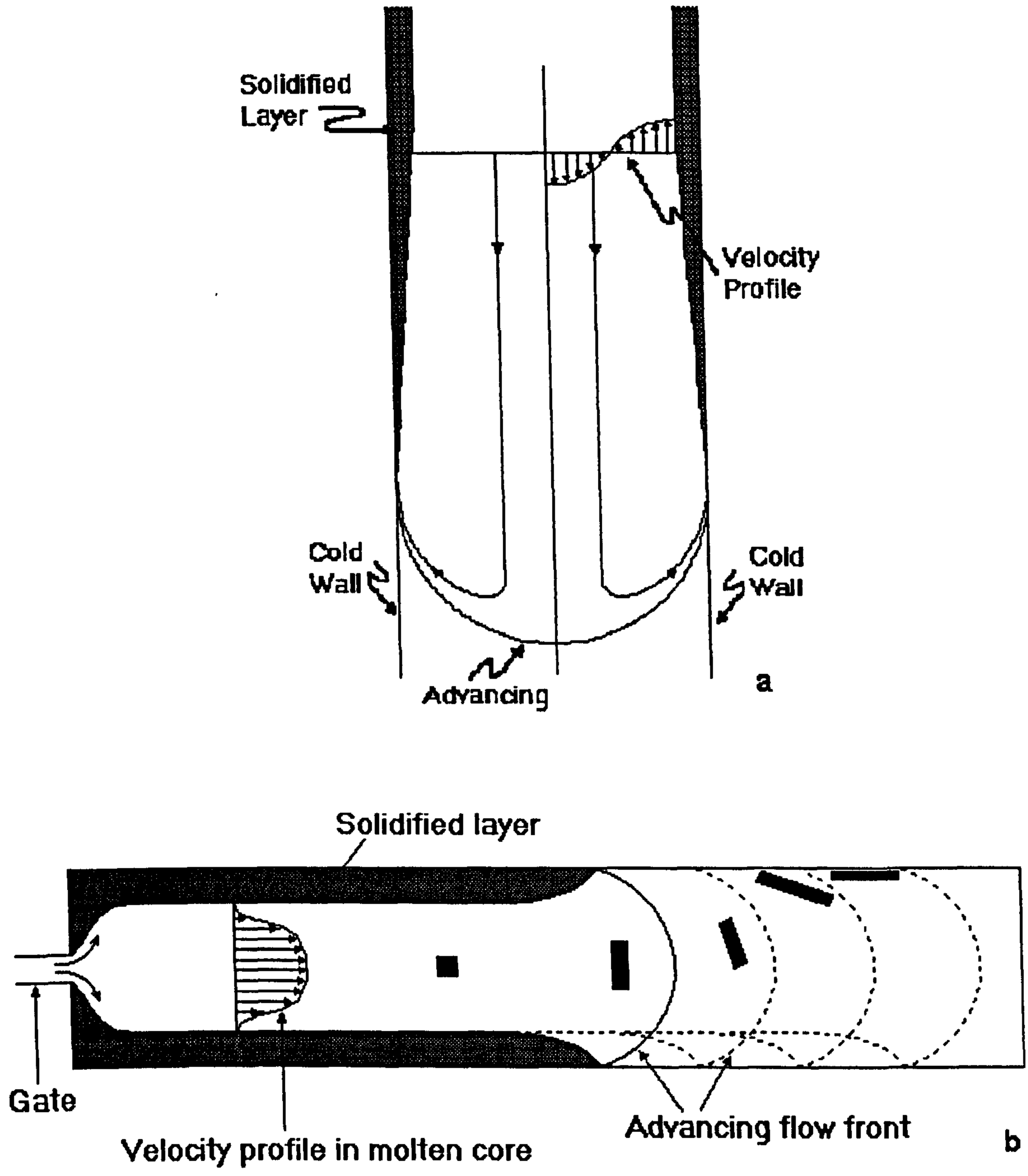

Figure 1.3 Schematic representations of the flow pattern in the advancing front between two parallel plates

a. The shaded areas denote the stretching and orientation of a fluid particle[12].

b. Deformation of an initially square fluid element at successive positions of the advancing flow front[13].

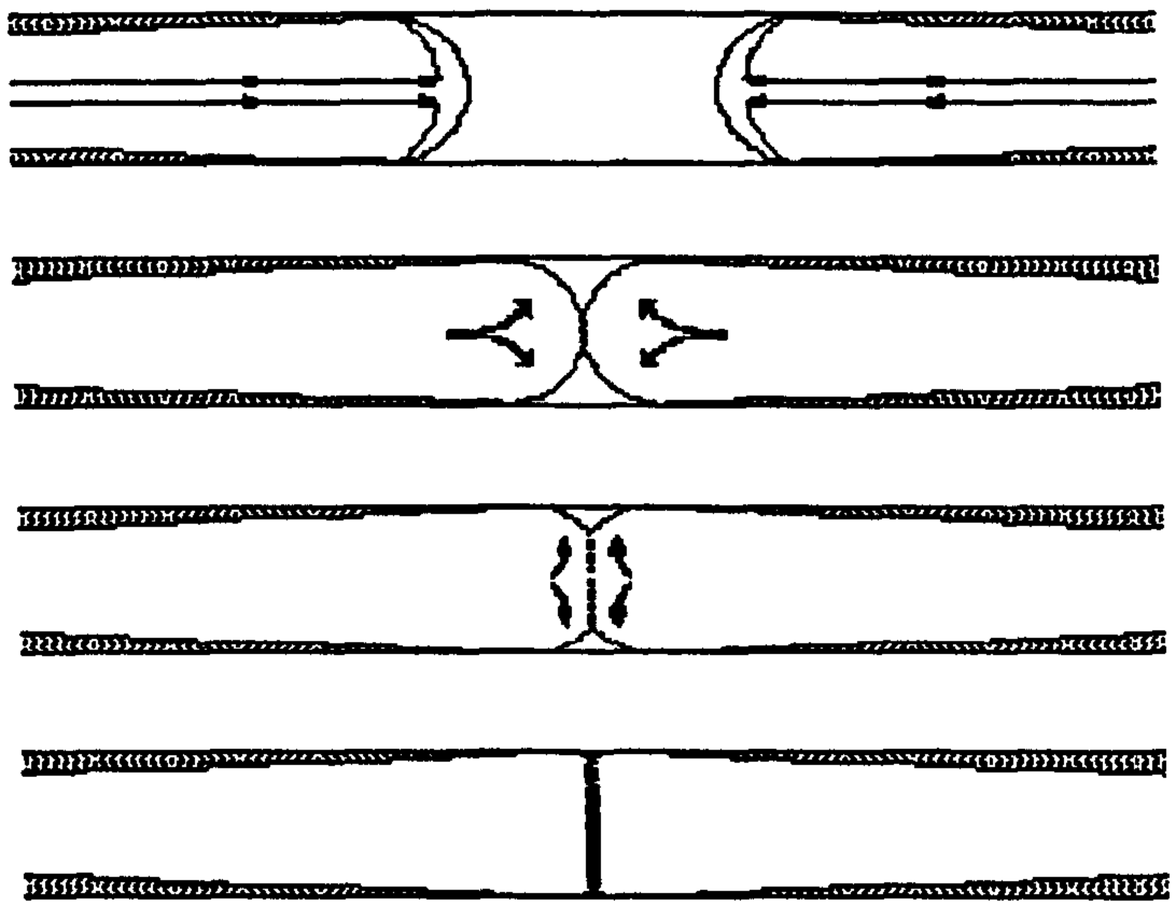

Figure 1.4 Demonstration of volcano-like mechanism which creates orientation at 90° to the main flow direction. Mould walls cool the melt and increase its viscosity at the edges of the channel thus retarding the flow. Flow at the centre of the channel continues at a higher rate, creating melt spill from the centre to the edges of the channel[6].

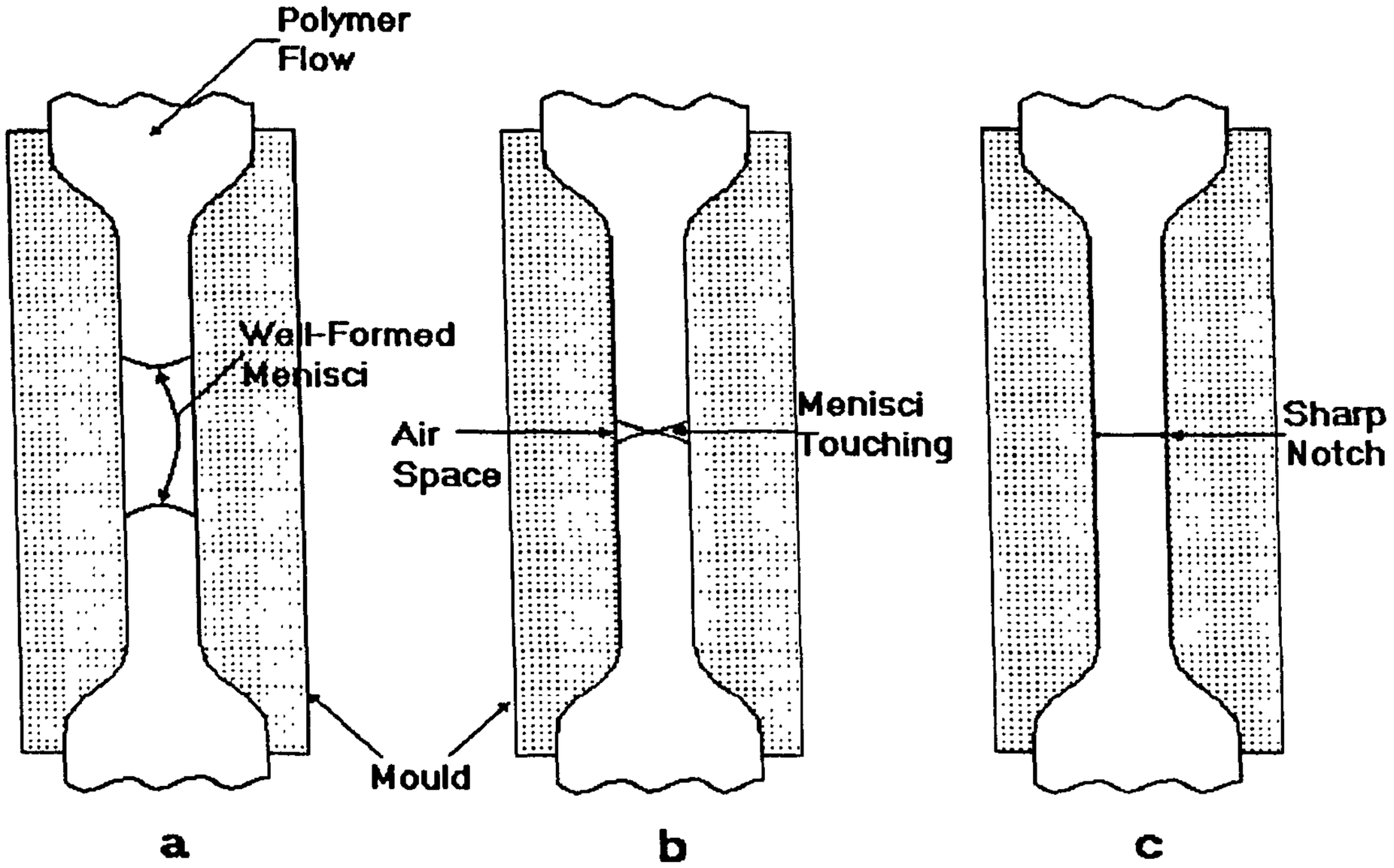

Figure 1.5 Formation of a V-notch. Viscous drag at mould walls (a) forms menisci at front of both polymer melt flows. Menisci meet at centres (b), forcing trapped air towards mould walls. On solidification (c), notch is retained[17].

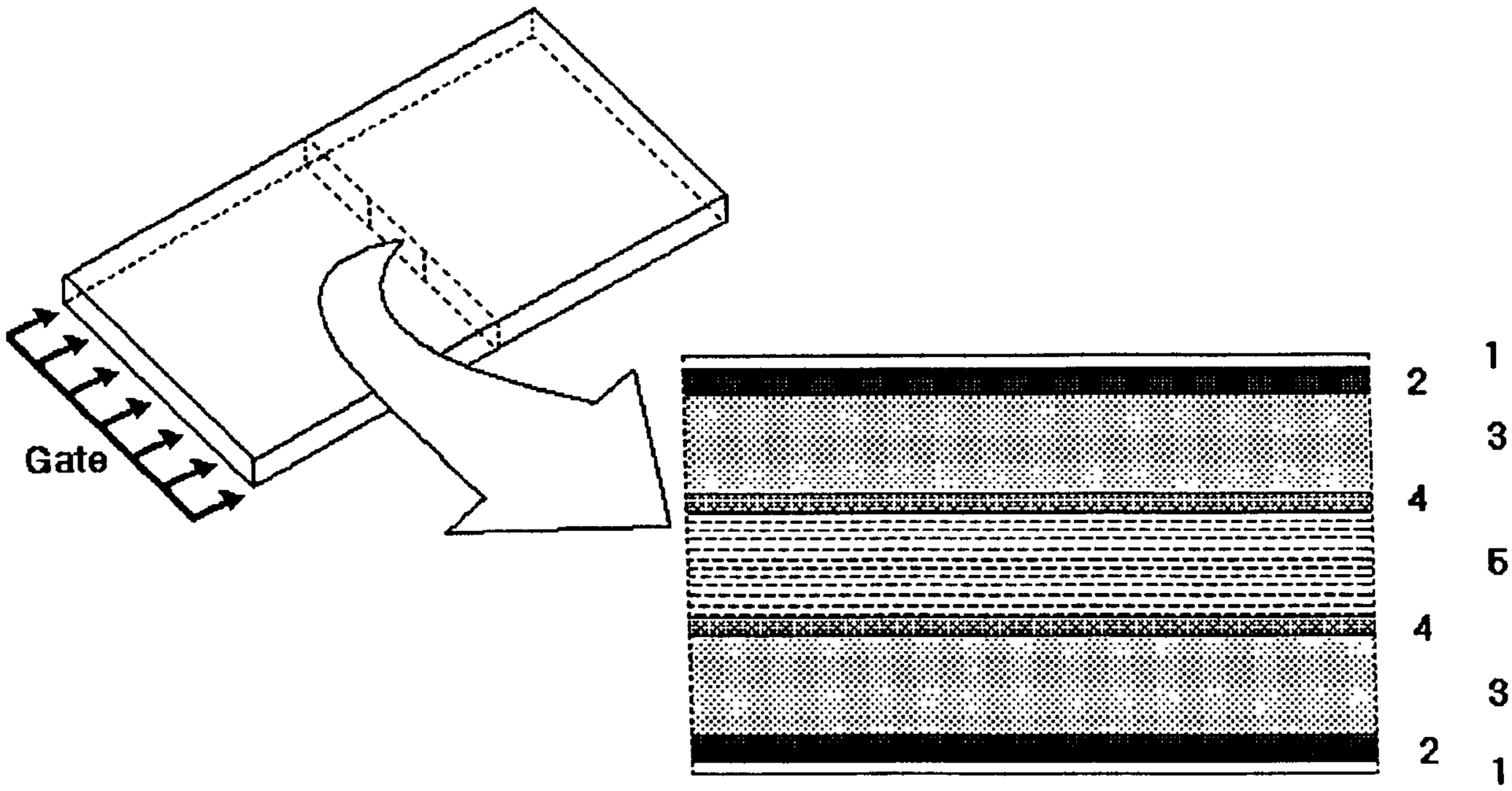

Figure 1.6 Fibre orientation in rectangular plaques with an edge gate[14].

1. low fibre boundary layer,
2. random fibre orientation,
3. fibres predominantly parallel to direction of flow,
4. random fibre orientation,
5. fibres predominantly perpendicular to direction of flow.

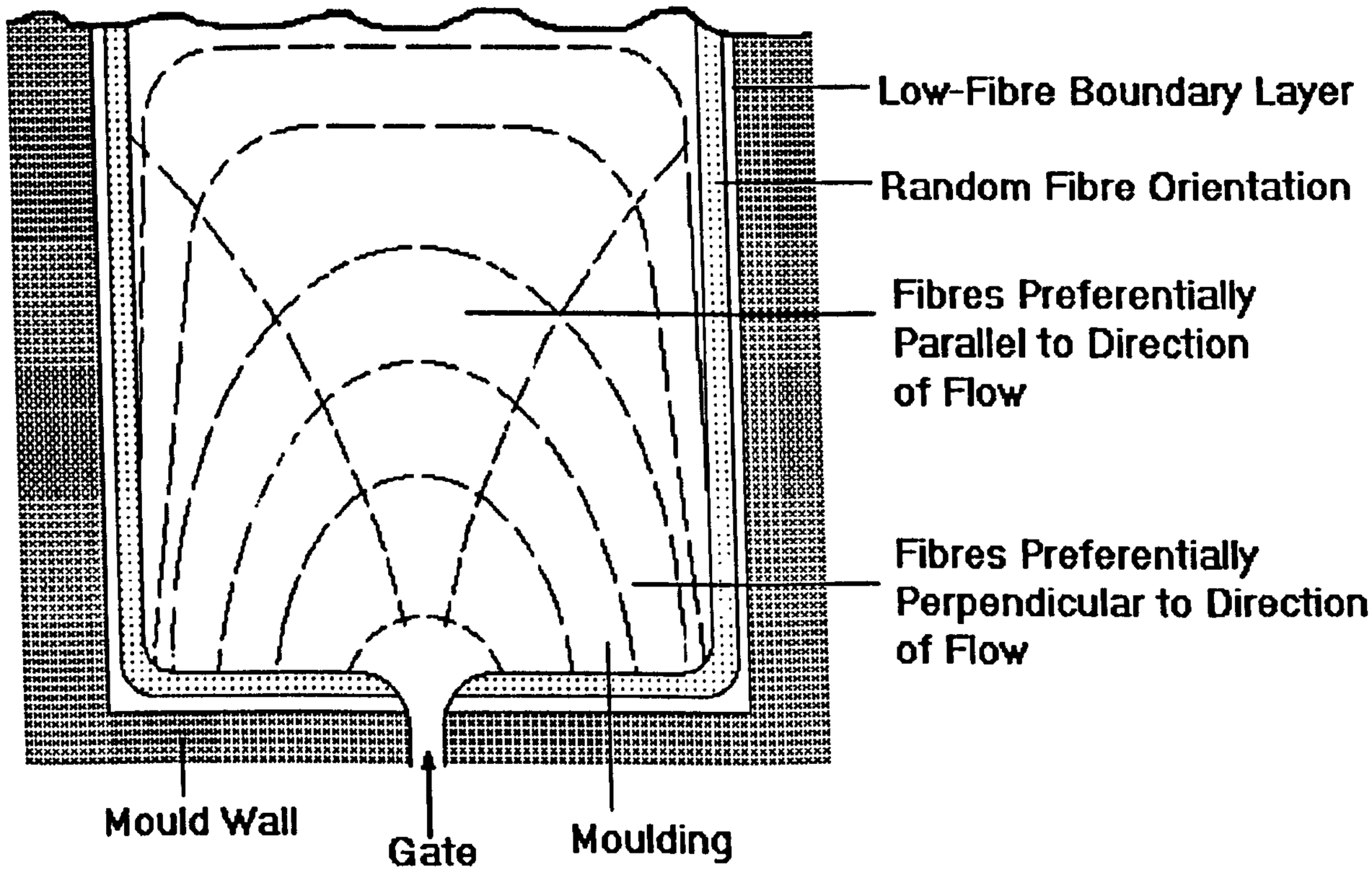

Figure 1.7 Fibre orientation in the core layer of rectangular plaques with pin-point gate[14].

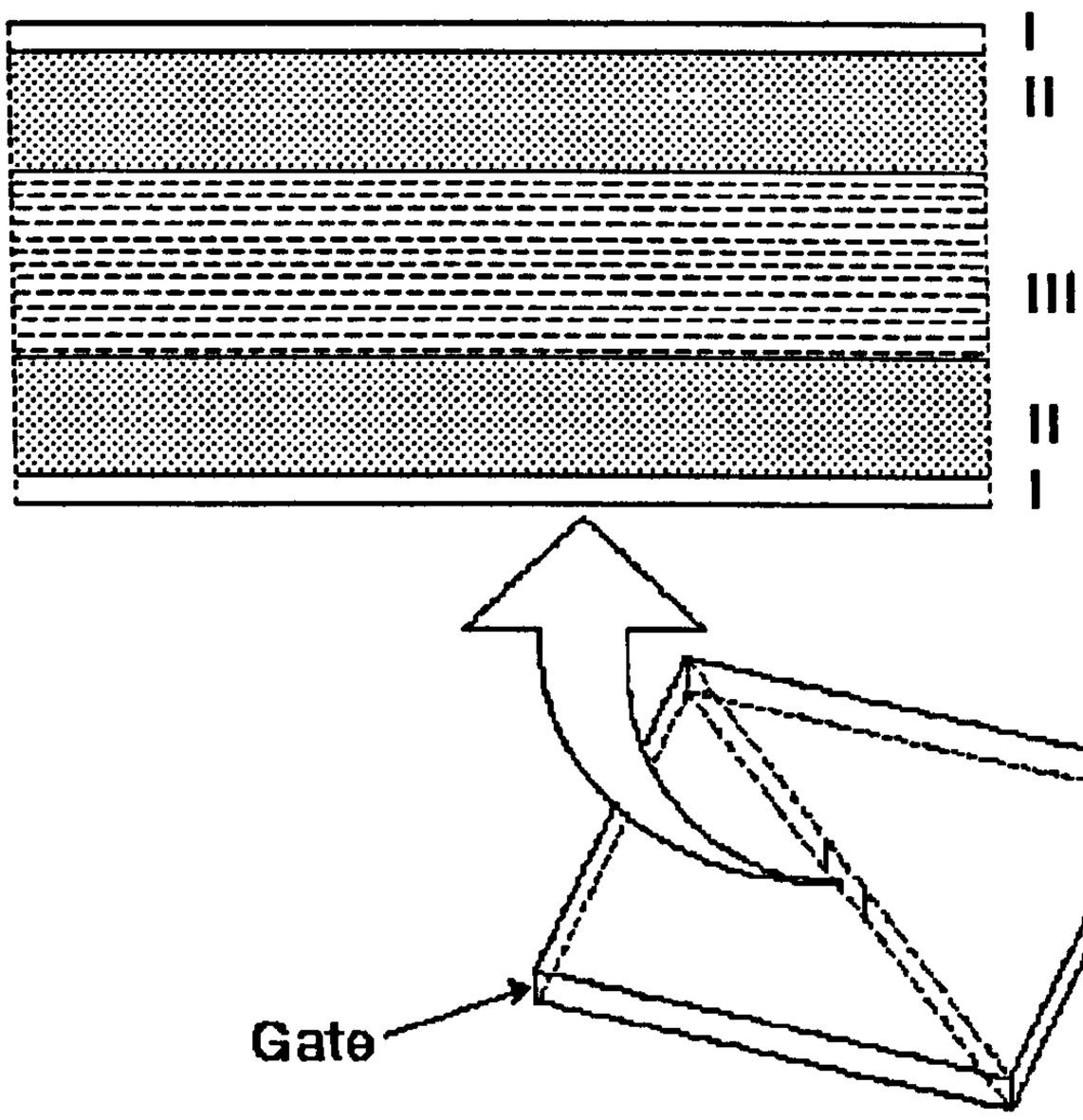

Figure 1.8 Fibre orientation in square plaques with pinpoint gate[14].

I. low fibre boundary layer,

II. random fibre orientation,

III. fibres predominantly perpendicular to direction of flow.

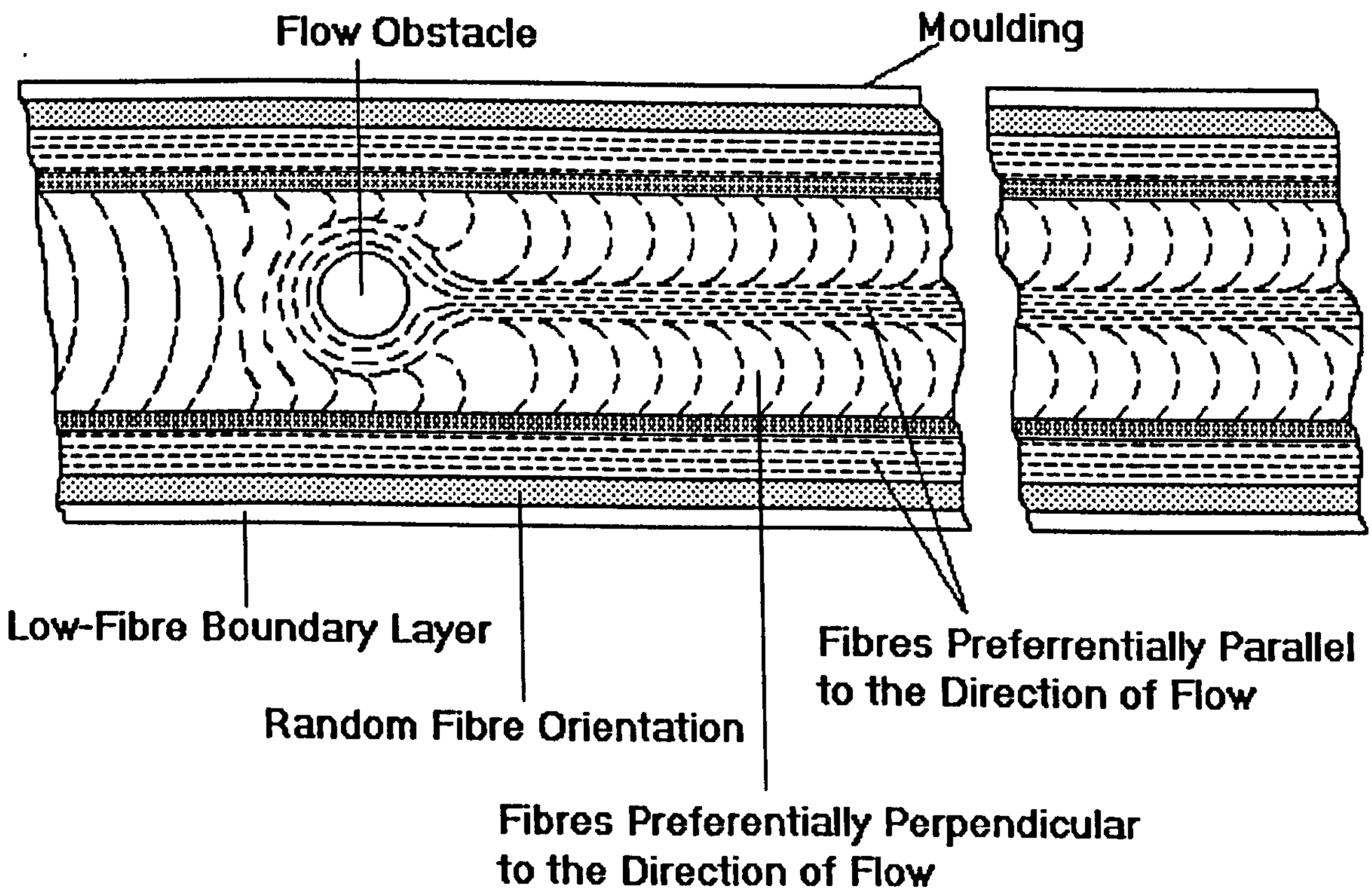

Figure 1.9 Fibre orientation in the core layer of a flat strip with flow obstacle[14].

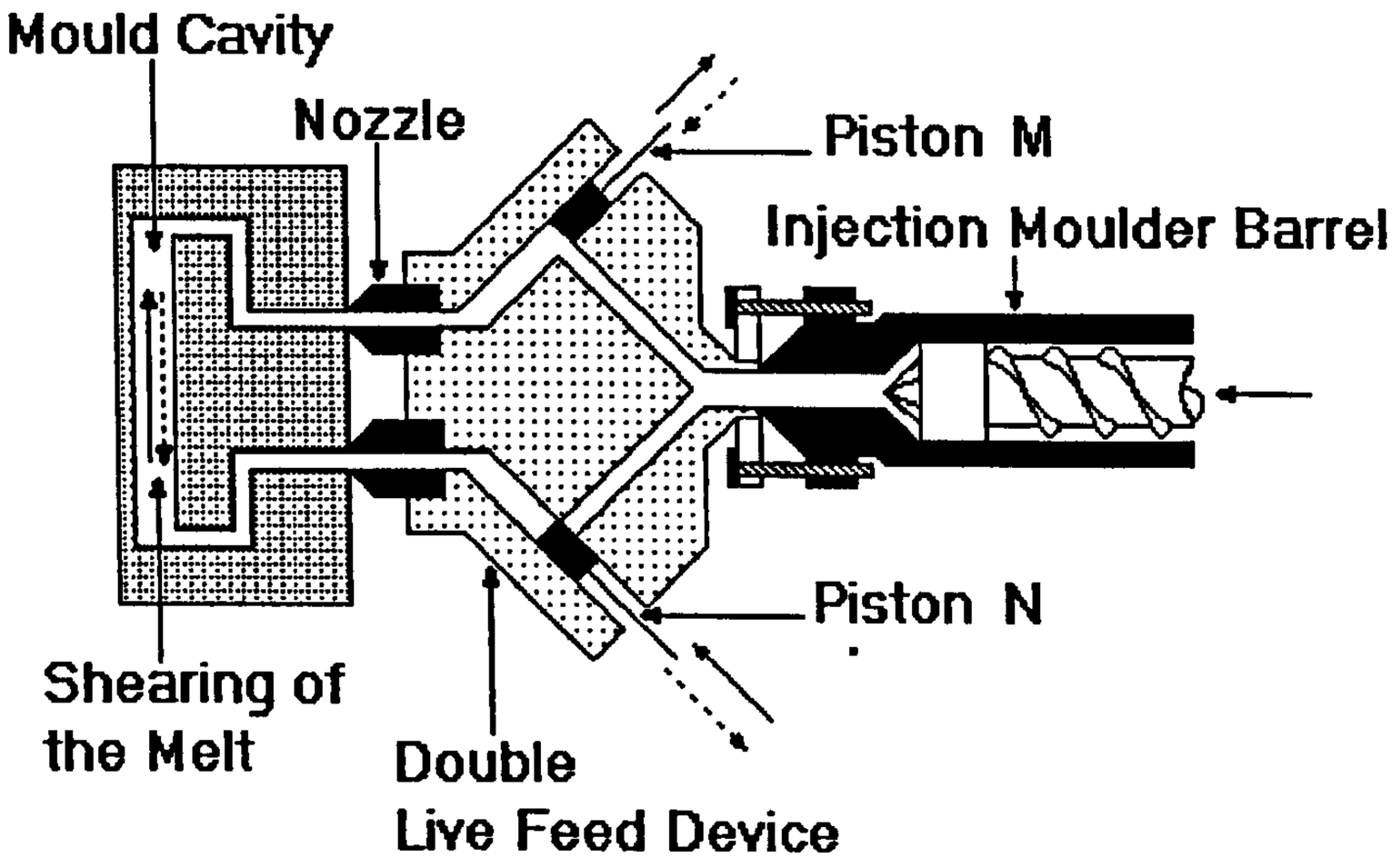

Figure 1.10 Schematic diagram of an arrangement for a double live feed moulding process. The feed for the molten material, the double live feed mould packing device and the mould are the three main constituents of the technique[1].

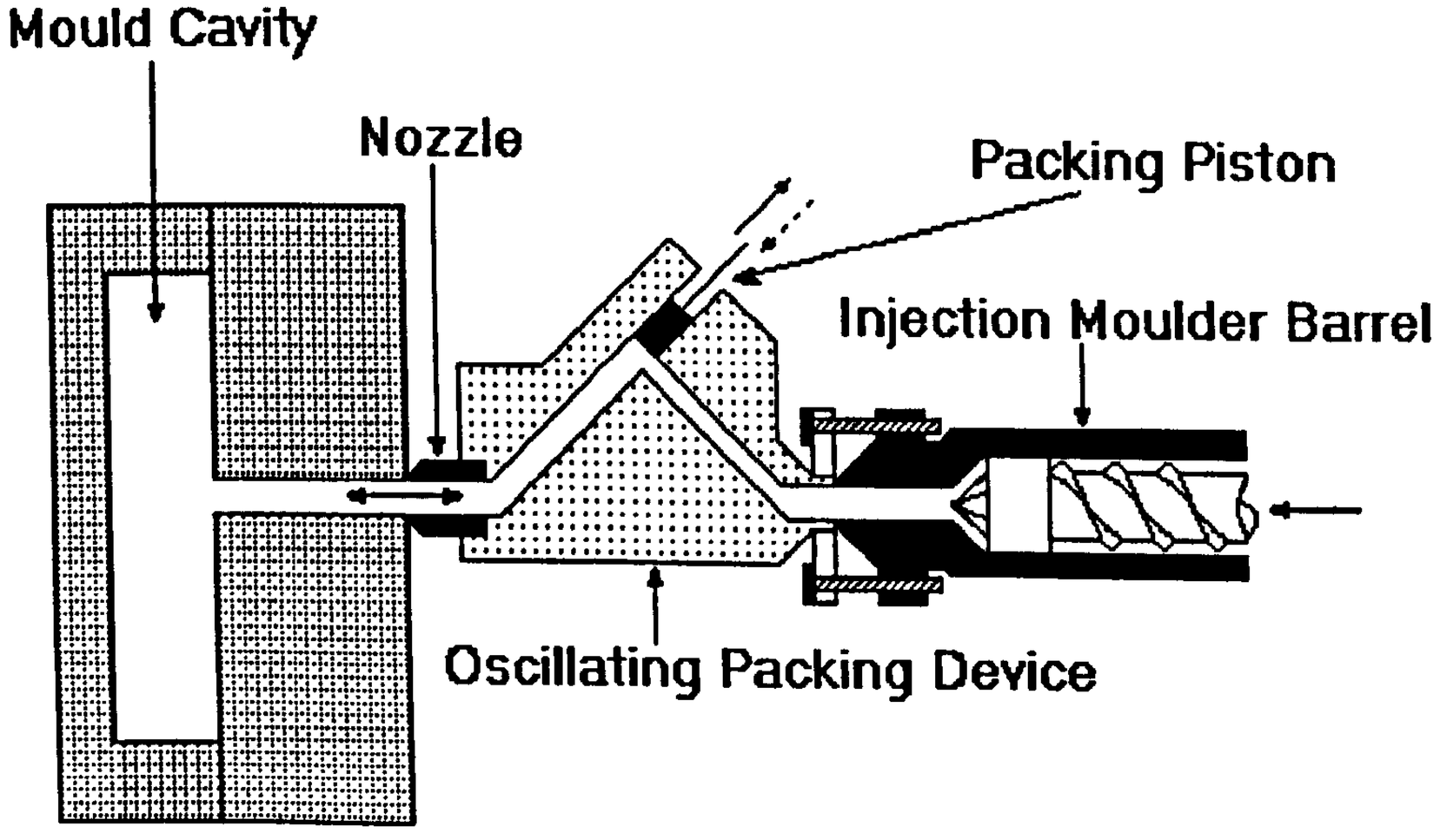

Figure 1.11 Schematic diagram of oscillating packing device in position between die cavity and moulder injection unit[77].

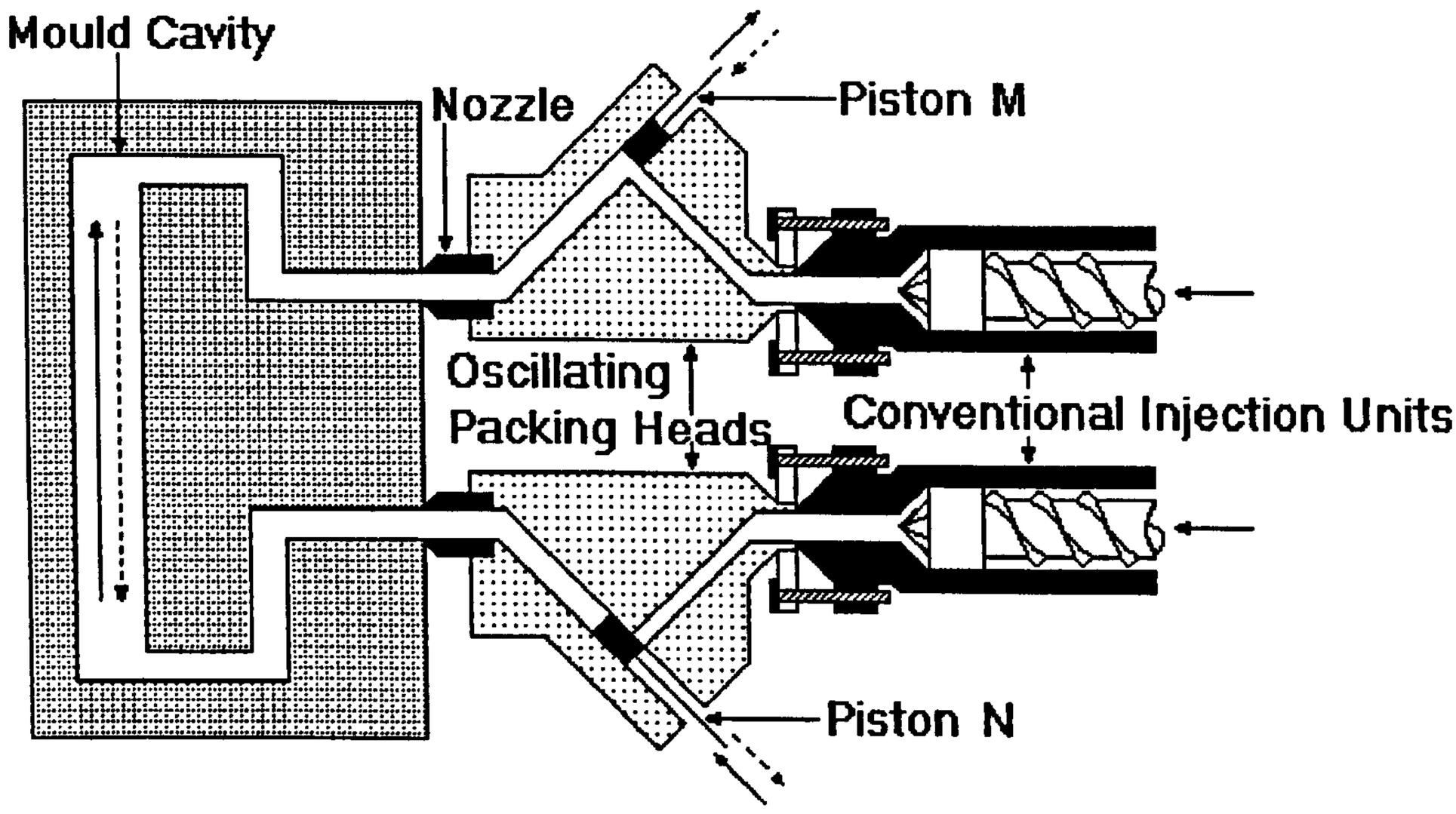

Figure 1.12 Schematic diagram of the two colour double live feed arrangement used. DLFM effectively produced from two SLFM packing devices.

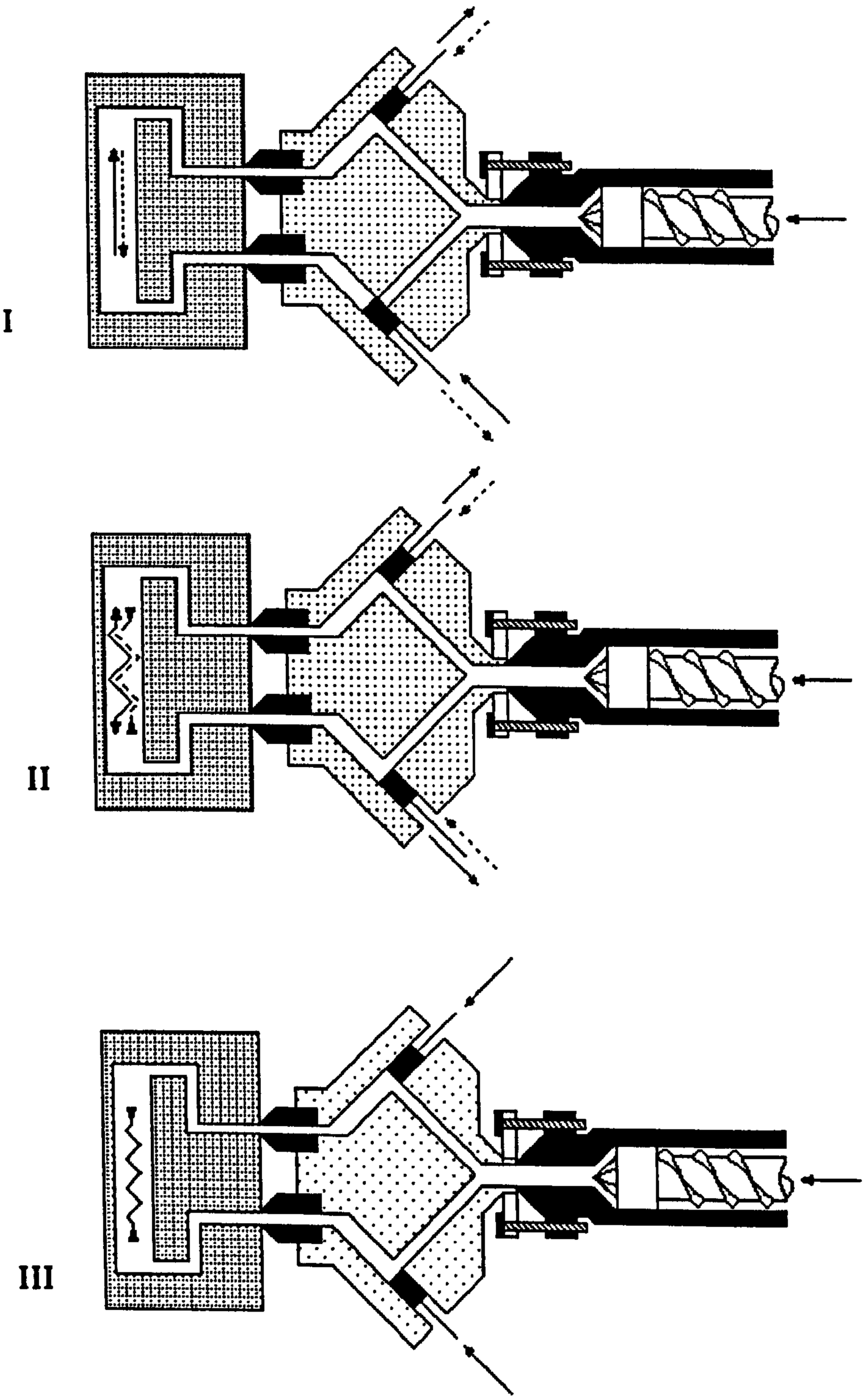

Figure 1.13 Schematic diagrams of the three modes for operation of the two live-feed devices[3].

a) mode I in which the two pistons operate 180° out of phase,

b) mode II in which the two packing pistons operate in phase and

c) mode III in which the two packing pistons compress the melt with an equal pressure.

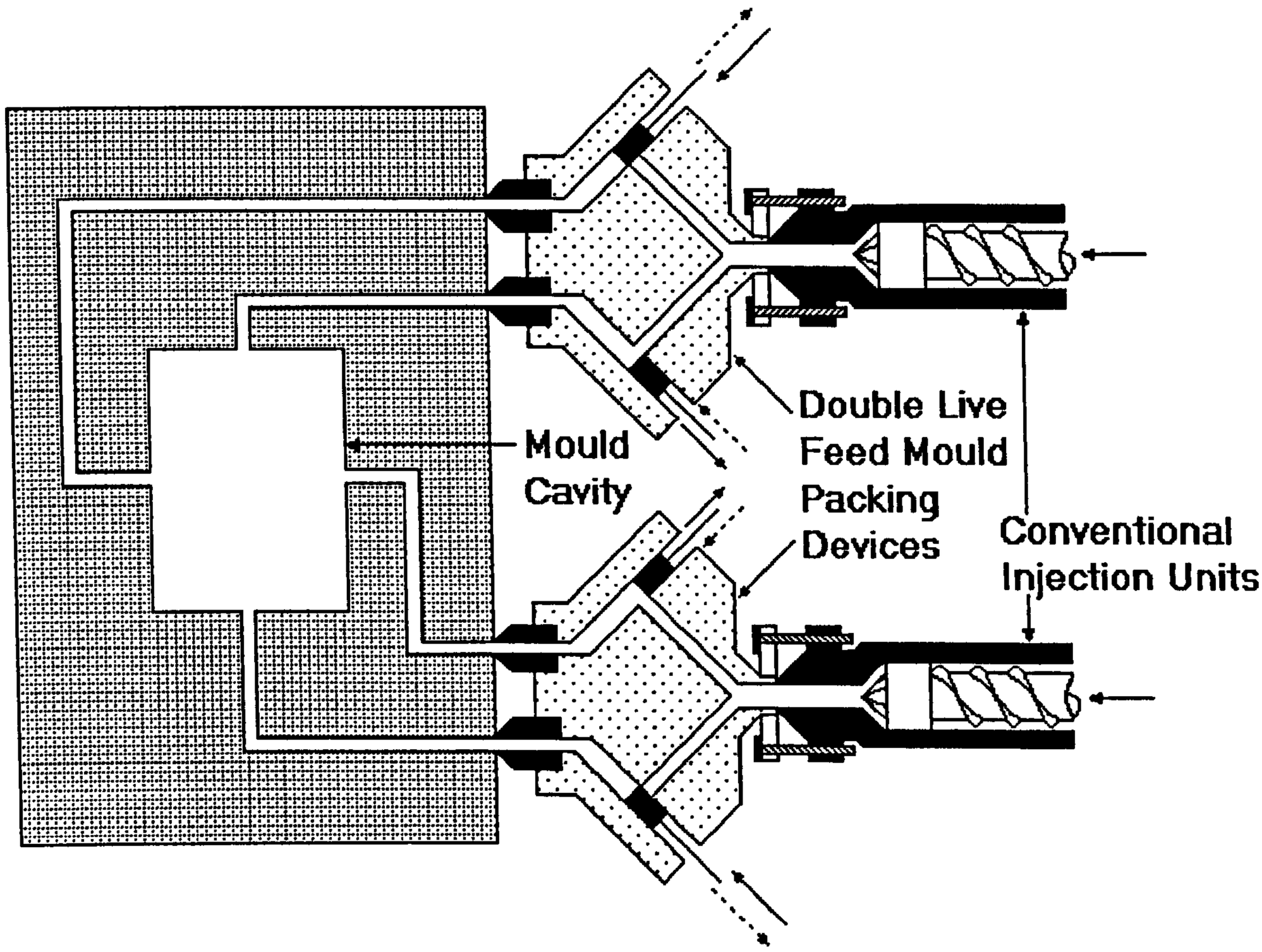

Figure 1.14 Schematic diagram of quadruple live feed arrangement based on a twin injection machine and double live-feed devices[77].

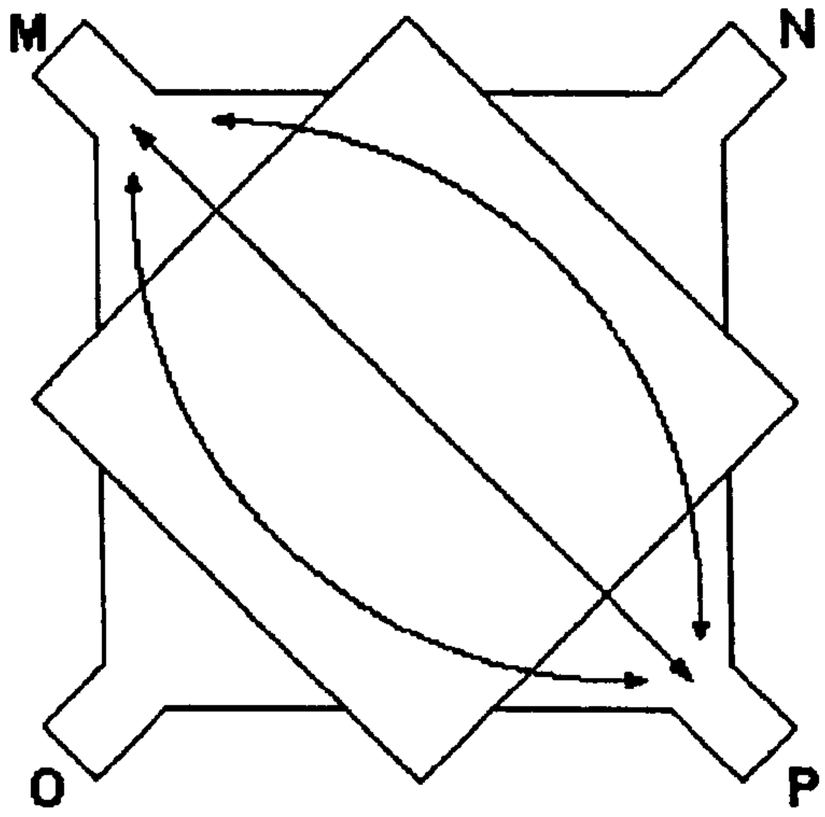

Figure 1.15 Pistons M and P operate using mode I^{32}.

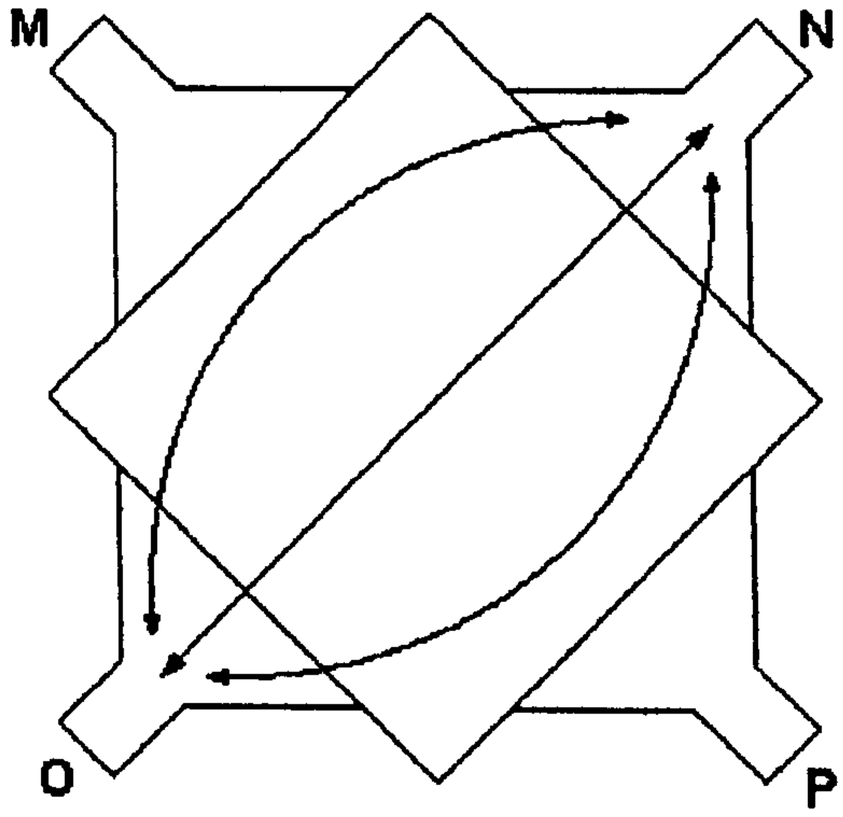

Figure 1.16 Pistons N and O operate using mode I^{32}.

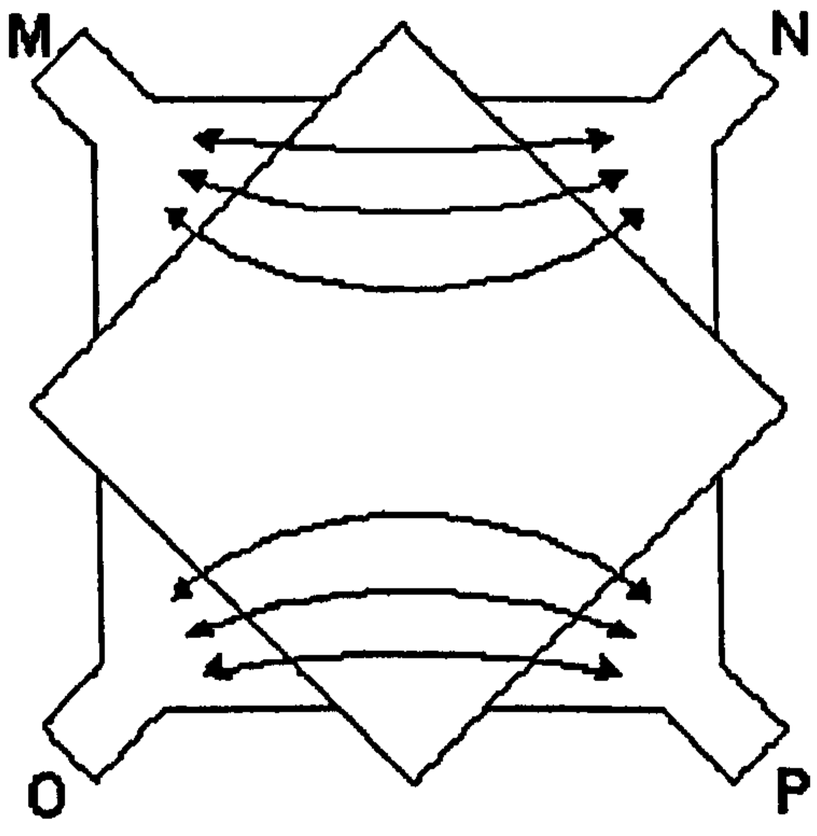

Figure 1.17 Pistons M, O and N, P and operate using mode I^{32}.

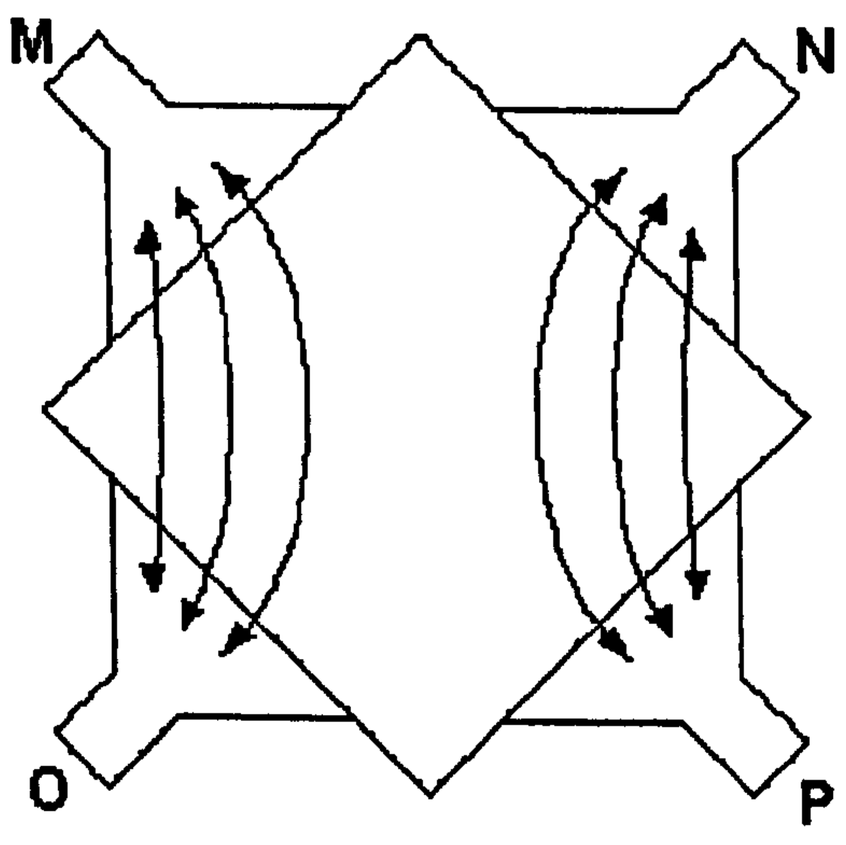

Figure 1.18 Pistons M, N O, P operate using mode I^{32}.

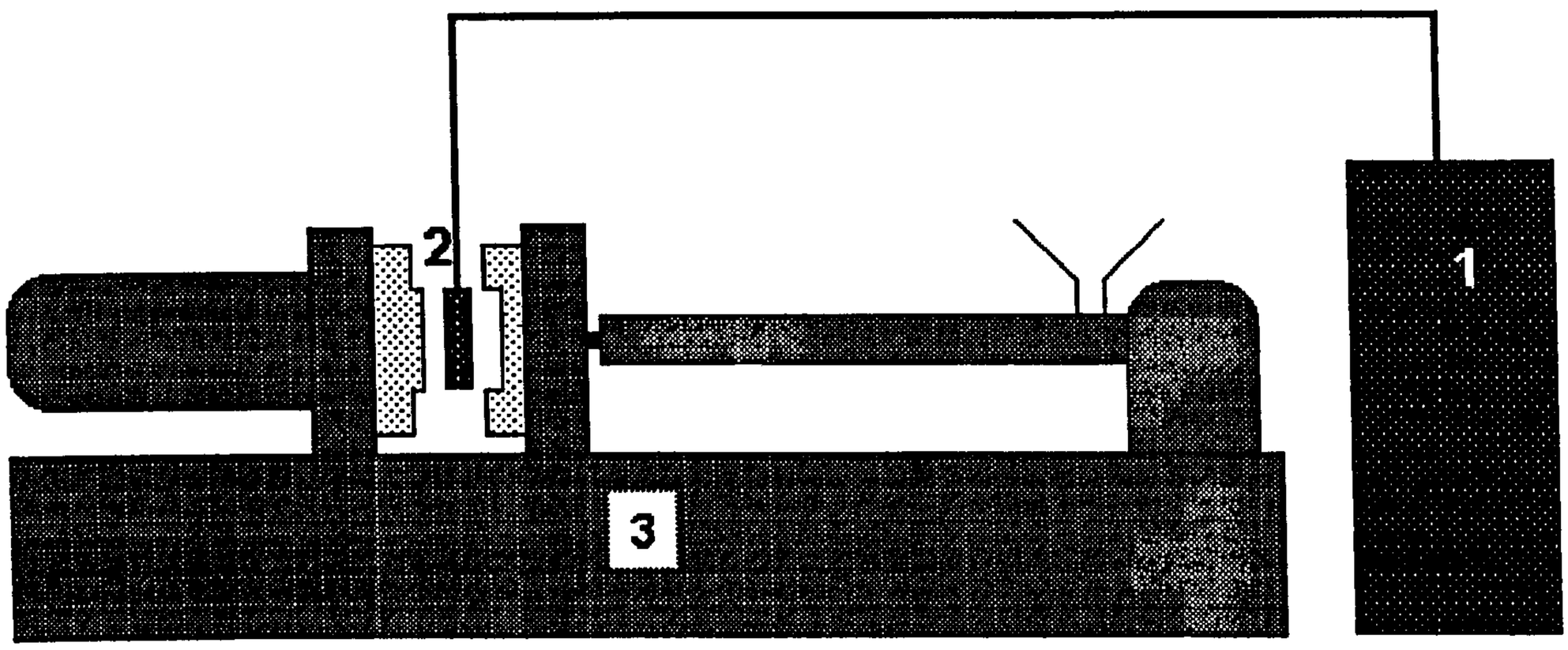

Figure 1.19 Schematic representation of the equipment used for Bright Surface Moulding (BSM)

1. BSM high frequency oscillator and process controller
2. BSM robotically manoeuvred high frequency induction heater coil
3. Conventional injection moulding machine

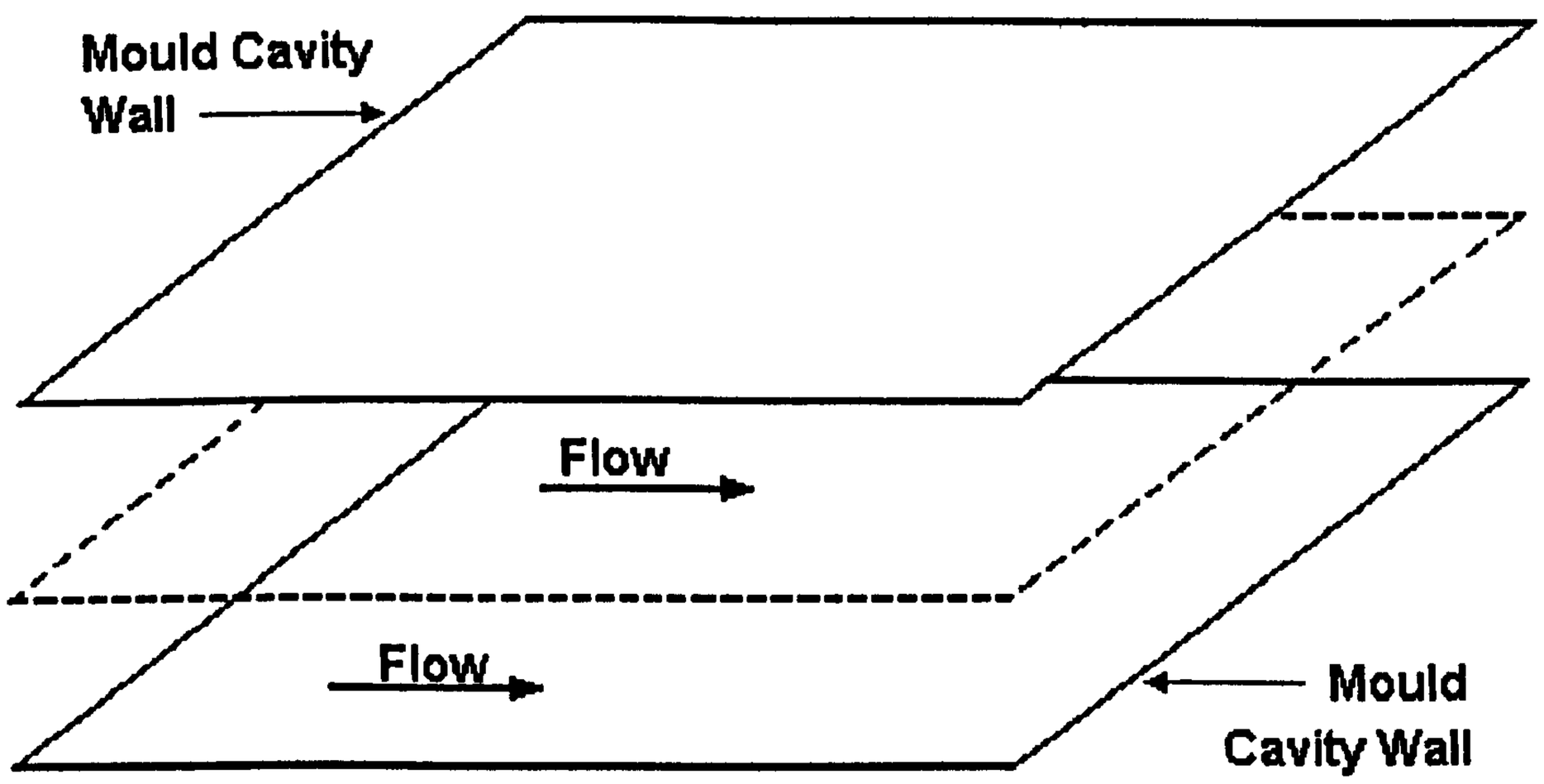

Figure 1.20 2-dimensional transient mathematical model geometry containing only two cavity surfaces for shear flow considerations, i.e. no side walls.

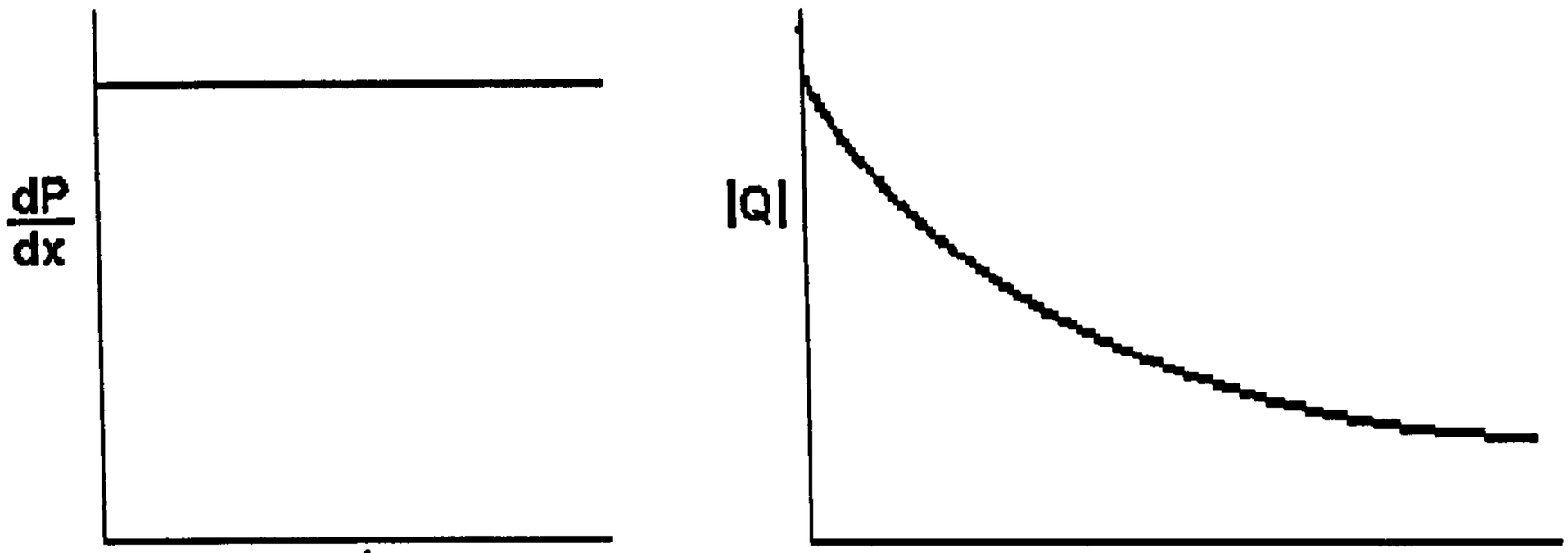

Figure 1.21 Where the reciprocating flow is driven by a fixed pressure gradient, $\delta p/\delta x$, of constant magnitude and with periodic sign change. In this case the flowrate, Q, eventually falls to zero as cooling and solidification proceed.

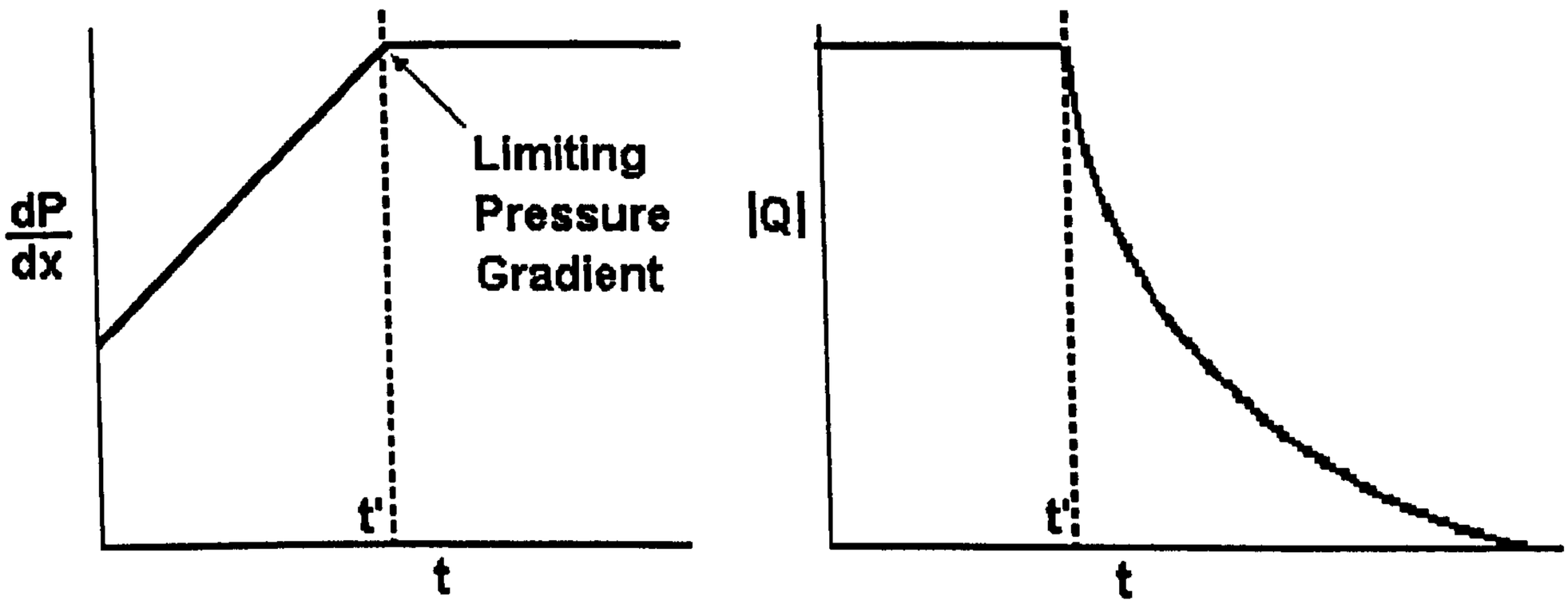

Figure 1.22 Where the flow is driven at a set stroke speed by hydraulically actuated pistons. The speed is maintained until the cavity flow resistance becomes too large for the hydraulics to overcome it, whereupon the stroke speed decreases towards zero.

2. MATERIALS AND CHARACTERISATION TECHNIQUES

2.1 Processing Materials

Polypropylene was selected as a matrix material because PP is of great commercial significance with well documented morphological characteristics which are strongly influenced by the type of processing used. Polystyrene was chosen as it is transparent with suitable rheological properties for the study of flow. Both PP and PS were either moulded in their natural state or after masterbatching or blending with a suitable filler material.

2.1.1 Matrix Materials

A commercial grade of general purpose polypropylene copolymer, BASF Propathene 2300L and transparent polystyrene, BP grade HF888 were used. Property data is given in tables 2.1 and 2.2 respectively.

2.1.2 Filler Materials

Silberline Limited provided their full range of SILVET® and SILVEX® grades of aluminium flake pigments in plasticised paste form for incorporation into the appropriate matrices referred to above. These materials were used as they exacerbate the presence of flow defects such as weld lines virtue of their highly reflective properties. The increasing use of such pigments in commercial applications and the increasing demands for higher quality aesthetics with unpainted injection mouldings, served as a strong impetus for their study. Property data for these pigments is detailed in table 2.3. Carbon black, red and blue dyes were also used as colouring agents with the above matrices.

2.2 Processing Techniques

Filled resins were prepared using a twin screw extruder prior to injection moulding for four main reasons:

I. ease of materials handling

II. a clean injection moulding environment

III. determination of accurate filler concentrations

IV. promotion of good dispersion of the filler material in the resin matrix (especially Al flake).

Injection moulding was then carried out using conventional, SCORIM, Bright Surface Moulding (BSM) and SCORIM & BSM Moulding (SBM) combined.

2.2.1 Materials Compounding

A Betol BTS40 co-rotating twin screw extruder equipped with a single strand die of 3mm diameter was used to compound the virgin resin and filler materials. To ensure homogeneity of the feedstock, the materials were blended together by manual tumbling in a plastic bag, fed at a controlled rate through a feeder into the hopper and processed using the conditions given in table 2.4. On exiting the die the extrudate was immediately quenched in water to minimise any degradation effects and then granulated.

Materials compounding of the virgin resin and filler material was carried out in order to produce a 10% masterbatch when using carbon black. This was further diluted with more resin to produce a 1% carbon black in PP compound before injection moulding. Resins filled with aluminium flake were compounded to the dilutions required for injection moulding to attain uniform dispersion.

Unfilled matrix materials were also extruded with the same processing conditions as the filled materials to attain the same thermal history. This ensured that any difference between the processing characteristics of filled and unfilled materials was a filler related phenomena only.

2.2.2 Injection Moulding

A Negri Bossi 130-90/90 twin barrelled injection moulding machine effectively equipped with two SLFM SCORIM devices and BSM high frequency induction heating device was used in conjunction with various mould tools for sample production. A schematic representation of the equipment used is shown in figure 2.1.

2.2.2.1 Conventional Moulding

A common feature of each of the mould tools used was their double gating arrangement in order to facilitate the formation of a weld line in the centre of moulded articles. Conventional moulding was carried out on either the Negri-Bossi 130 90/90 or Sandretto 6GV-50 moulding machines. Details of the moulding conditions used are given in table 2.5.

2.2.2.2 Bright Surface Moulding (BSM)

The mould tool core and cavity surfaces were heated by a robotically manoeuvred high frequency induction heating coil sequenced by a separate control unit. The unit supplied 15kW of power at 20kHz to the 120mm diameter disc shaped coil for a prescribed duration. The optimum heating rate was attained when the coil was equidistant from the core and cavity surfaces at approximately 8mm, a LED display indicated when this optimisation was achieved.

At the end of the heating cycle the coil was retracted from inside the mould tool, the tool closed and material was injected through the double gating arrangement to produce a centralised weld line as with the conventional moulding cycle. A longer cooling time was then required to remove the additional heat.

2.2.2.3 Shear Controlled Orientation Injection Moulding (SCORIM)

SCORIM processing was applied by hydraulically driven pistons which applied pressure to the solidifying melt cavity of the mould tool. These pistons reciprocated back and forth inside their respective chambers and in order to do this they required two prescribed pressures, one to cause forward piston motion (i.e. compressive pressure) and another to reverse this motion (i.e. relaxation pressure). Timescales were also assigned for the duration of these operations which were termed compression and relaxation times respectively. In this way, the frequency and pitch of the pistons cyclic oscillations were described. The pistons were also sequenced to progress forwards/backwards either simultaneously or alternately. When pistons were motioned forwards simultaneously they both applied a packing pressure to the mould cavity in

unison and this was termed a 'uni-pack'. Conversely, with forward/backward motion of the two pistons occurring alternately the mould cavity experienced shear flow due to their opposite velocities and this was termed a 'bi-pack'. In essence, a uni-pack described whether the pistons moved in modes I or III and a bi-pack described mode II (N.B. modes I, II and III are defined in section 1.6.2.1). The parameters described above constituted one cyclic oscillation for the pistons. However, in some cases there were many repeat cyclic oscillations per moulding cycle so the number of these repeats was defined by the stage duration. Pistons could also be grouped together for sequencing simultaneously, and it was these piston groups which were referenced for processing. This parameter was used to prescribe the order with which each of the pistons used were motioned. Finally, if more than one mode of operation was desired or differing cyclic parameters required within a single moulding cycle, then more than one stage of operation was incorporated. Each stage enabled different SCORIM cycles to be used in succession. Stages were identified with a number (i.e. STAGE ID, e.g. S00, S01, S02, etc.) and then these stages were referred to in the SCORIM sequence. This data was input into the SCORIM microprocessor control unit.

In brief, the salient parameters of the microprocessor control unit of SCORIM are:

- Duration of a given stage i.e. controls the number of piston cycles.
- Compression time (C-TIME), i.e. time the piston(s) forward motion applied a compressive force to the mould cavity.
- Relaxation time (R-TIME), i.e. time the piston(s) return motion applied a decompressive force to the mould cavity.
- Compression pressure (C-PRES), i.e. pressure applied during the pistons forward motion (C-TIME) measured as a percentage of maximum output.
- Relaxation pressure (R-PRES), i.e. pressure applied during the pistons return motion (R-TIME) measured as a percentage of maximum output.
- UNI/BI PACK, i.e. controlled whether the pistons were sequenced simultaneously (UNI) or alternately (BI) i.e. defined the mode of operation.

- Pistons may be grouped together for simultaneous processing by the UNI/BI PACK parameter.

The sequence and frequency of each stage was then described by the profile sequence.

2.2.2.4 SCORIM and BSM Moulding (SBM) In Series

SBM utilised the complementary technologies of SCORIM and BSM in series to good effect. Figure 2.2 schematically represents the main stages in the SBM cycle. These stages are described as follows;

- *High frequency induction heating of the mould tool;* the first stage in the cycle was to rapidly heat the mould tool to elevated temperatures as described in section 1.3.2.2.
- *Injection stage;* upon removal of the heater coil, the mould closed and material was injected into the mould.
- *Stage ID S00;* prior to completion of mould fill, the SCORIM profile sequence was activated in mode I (as described in section 1.6.2.1) for 0.5 seconds. This ensured that upon mould fill and the formation of the centralised weldline, the SCORIM pistons were mid-stroke for the start of the next stage.
- *Stage ID S01;* the melt was sheared by the periodic oscillations of the SCORIM pistons in mode A (as described in section 1.6.2.1).
- *Stage ID S02;* the melt was compressed with a static packing pressure, mode C (as described in section 1.6.2.1) for a suitable period to eliminate sinkage. Material shrinkage occurred during cooling of the mould tool from the elevated temperatures.
- *Ejection stage;* the mould tool opened and the solidified part was ejected.

2.2.3 Temperature Calibration for BSM

Mould temperature was measured by a thermocouple inserted into the centre of the mould cavity insert 3mm beneath its surface. This provided a record of the temperature at this position of the mould tool during processing. To assess the temperatures at other locations of the mould tool, J or K type

thermocouples were placed on the tools moulding surfaces. Readings were taken to calibrate these positions with the inserted thermocouple.

2.2.4 Data Storage and Analysis

Various parameters of the injection moulding process were measured by accurate instrumentation of the process and storage of the acquired data for subsequent analysis. The parameters of interest which were recorded were both the SCORIM pistons' linear displacements and their associated hydraulic pressures, two cavity pressures close to the fan gates and mould tool temperature 3mm beneath the cavity surface.

The transducers and thermocouples used were interfaced with a PC for data acquisition and storage. The raw data thus collected was later manipulated for analysis including comparison with the results of the mathematical model.

2.2.5 Development of Process Control

During the moulding process on the twin barrel Negri-Bossi, an imbalance was noted between the performances of the twin moulder barrels. In order to ensure equal throughput of material from the two barrels, they required constant adjustment of their relative injection speeds to restore balance. As two measurements were acquired for the SCORIM pistons' linear displacements, their associated hydraulic pressures and two cavity pressures, any unexpected differences between these pairs of measurements were readily apparent. In the case of the force transducers measuring cavity pressures, it was necessary to re-calibrate these instruments using an Instron 4206 Universal Testing Instrument in compression mode. This was carried out whilst the transducers were connected to the data acquisition system to ensure the process of acquiring the data was calibrated as a whole. Different correction factors were established ensuring accurate measurements were subsequently made.

Other deleterious effects associated with the process of collecting large amounts of data with development equipment required resolving before commencement of meaningful results could be achieved. A significant

emphasis was placed on the development of the process in order to ensure the accuracy of the data acquired was suited to that needed for the computer modelling of the SCORIM process.

2.2.6 Piston Restrictors

These controlled the length of stroke of the pistons in order to reduce the volume of material displaced. Without these, material was sent into the opposing gate and runner system whence it came, as the piston stroke was too long. Another purpose of these stops was to allow the pistons to 'bottom out' on them and remain in this position for a time prescribed in the SCORIM packing sequence. This allowed the freezing skin layer to thicken, incorporating the shear influenced material, before beginning the reverse piston stroke; i.e. a delay time between oscillations was incorporated.

2.3 Injection Mould Tools

Differently dimensioned mould tools or inserts were used to study the effects of these dimensional changes. Their descriptions and reasons for use are described, *viz.*

2.3.1 Double-Gated Rectangular Plaque

A simple plaque mould was used of dimensions 140 x 50 x 4mm. The plaque was fed by two 2mm thick, 50mm wide fan gates, one at each end of the plaque. This enabled weld lines to be produced at the centre of the plaque as illustrated in figure 2.3.

2.3.2 Square Plaques

Two square plaques were used for moulding, one with rounded corners of dimensions 84 x 84 x 1.5mm illustrated schematically in figure 2.4, and a second with squared corners of dimensions 108 x 108 x 4mm, figure 2.5. Both tools had interchangeable gates to enable between 1 and 4 fan gates along the edges of the squares. The gating configuration ensured good control over weld line placement and subsequent SCORIM processing.

2.3.3 Dumb-Bell Shaped Cavities

Two mould tools were used to produce these mouldings. Schematically illustrated in figure 2.6 one two impression tool used on a single barrelled injection moulding machine produced 190mm long samples. One impression moulded the part through a single gate (a), the other impression moulded through two gates (b) to produce a centralised weld line. The other single impression tool used on a twin barrelled injection moulding machine, moulded 167mm long samples (c) through two gates producing a centralised weld line.

2.3.4 Ring Mould

A ring mould was used for two-colour moulding. The ring had inside and outside diameters of 139 and 159mm respectively, of square cross-section 15mm thick. The two circular gates 6mm in diameter were fed directly onto the outside edges of the ring at opposite locations via cold runners.

2.4 Mechanical Testing

2.4.1 Tensile Testing

This was carried out using an Instron 4206 Universal Testing Instrument interfaced with a PC for data acquisition, storage and analysis. Test samples were injection moulded dumb-bell specimens 167 and 190mm long with gauge length, width and thickness of 115, 10 and 4mm respectively. The test method was in accordance with BS 2782: Part 3: Method 322: 1994 ISO with 5kN load cell.

2.4.2 Tensile Modulus Measurements

A strain gauge extensometer was attached to the specimens under test for greater accuracy, and the tests were carried out with a cross-head speed of 1mm/min. Six specimens of each type were tested and the results derived as the Young's modulus, E.

2.4.3 Ultimate Tensile Properties

Tests were carried out using a cross-head speed of 50mm/min on six specimens of each type. The parameters determined were the ultimate tensile stress σ_u, peak strain ε_p, ultimate tensile strain ε_u and the toughness *U* (i.e. energy absorption during the deformation process) in N/mm.

2.4.4 Vickers Microhardness Testing

Bowman and Bevis[65] reported microhardness testing as a way of characterising polymers, determining microstructural variations and anisotropy through the thickness of injection mouldings. Lopez[78] reported that correlation between microscopic (microhardness) and macroscopic (modulus, yield stress) mechanical properties have been established for a wide range of thermoplastics including polypropylene.

Samples examined were sectioned both parallel and perpendicular to the flow direction as illustrated in figure 2.7. Samples were cut and polished to a 1μm finish with care taken to ensure the base and polished surface were parallel.

A Leitz Miniload 2 Vickers Hardness Tester was used with a 15g load. The Vickers microhardness value, HV, was determined by the formula:

$$HV = \frac{1854.4\,P}{d^2}$$

where P is the load in grams and d is the average of the indentor diagonal lengths in μm. Upon application of the load and completion of the indentation the load was retained in position for one minute before removal and measurement. Time dependent recovery of the indent was not accounted for as most of the recovery occurred at the apex of the indentation and not in the length of the diagonals[79]. Measurements were taken every 0.1mm across the thickness of the samples.

2.5 Morphological Characterisation

This section describes the studies carried out to determine the morphologies of the PP composites using light microscopy (LM), scanning electron microscopy (SEM) and transmission electron microscopy (TEM).

2.5.1 Sample Preparation

Injection moulded samples were sectioned to reveal regions of interest for microscopic examination and to provide a flattened cut surface suitable for etching. After etching a replica was taken of the surface for study with the TEM. The specimen was then gold coated for examination with the SEM.

2.5.2 Microtomy

A Leitz microtome was used to cut thin sections from specimens of SCORIM mouldings. The blade was set at an angle of approximately 45° to the direction of motion, to aid the cutting of sections (≈120mm^2 surface area). The microtome was used to prepare specimens for LM, SEM and TEM.

2.5.3 Specimen Preparation

Injection-moulded rectangular plaques were cut up to obtain specimens which revealed the skin-core morphology. The selected faces were cut either parallel or perpendicular to the direction of flow. Specimens were marked with a sharp blade to aid identification after etching. Microtomed sections about 5μm thick were obtained for examination under the optical microscope.

2.5.4 Etching

Prior to etching specimens were washed in distilled water and acetone which had been filter-cleaned using a sinter funnel. The specimens were then dried, weighed and placed in ground glass stoppered test tubes.

The following reagents were then prepared for use in the etching process:

a) 25cm^3 concentrated (98%) H_2SO_4 + 25cm^3 concentrated (88%) H_3PO_4. The phosphoric acid was slowly added in aliquots of about 2cm^3, and the mixture was cooled in ice.

b) The etchant was made by slowly adding 1% w/w Analar grade $KMnO_4$ to reagent a). Agitation was applied continuously using a glass covered magnetic stirrer. After all the $KMnO_4$ was added, the solution was a deep "sage" green, with undissolved potassium permanganate crystals visible. The flask was sealed and given occasional shaking. Approximately 30 minutes were required for dissolution of all the $KMnO_4$.

c) $12cm^3$ concentrated H_2SO_4 + $42cm^3$ distilled water. This was cooled in dry ice.

d) $25cm^3$ H_2O_2 (100 volumes) + $25cm^3$ distilled water.

2.5.5 Etching Procedure

(i) About $5cm^3$ of the etchant, reagent b), was poured onto each specimen in a test tube. The tube was then sealed, and manually agitated for about one minute before being placed in an ultrasonic bath for one hour.

(ii) The etchant was decanted into excess distilled water and then 2-3 cm^3 of reagent c) was poured onto the specimen. The test tube was returned to the ultrasonic bath and given about 5 minutes agitation.

(iii) Hydrogen peroxide, d), was used to neutralise reagent c) and placed in the ultrasonic bath for 1 minute.

(iv) The contents of the test tube were decanted into excess water. The specimens were removed and given several washes in water and acetone before drying.

2.5.6 Replication

Replicas were made by a two stage process. Firstly, a 20μm thick film of cellulose acetate was softened by immersion in acetone for about two seconds. It was then laid upon the etched surface whereupon it adhered to the contours of the morphological structures. It was then allowed to dry and harden for 30 minutes before being removed.

Once removed, the cellulose acetate film was attached to a glass microscope slide using double-sided sticky-tape, with care taken not to damage the replicated area and with the replicated detail uppermost. This was then placed in the Edward's Coating System E306 before evacuating the

air and depositing a thin layer of carbon on the surface of the film from a carbon arc. A thin shadowing layer was then applied at 45° to the replica surface by evaporation of gold/palladium wire.

The coated replicas were cut up into squares about 2 x 2mm, and placed in acetone for half an hour to dissolve away the cellulose acetate layer. The carbon replicas were then scooped out of the acetone on copper TEM grids (3.05mm diameter, 100 square mesh). The replica was placed on the dull side of the TEM grid for better adhesion. If a fold or roll appeared in the replica, the surface tension of the distilled water was used to try to flatten it out. Once a satisfactory replica was gathered it was dried by dabbing it with filter paper and warming slightly to remove excess water. This prevented damage by water being drawn through the carbon film by capillary forces when the TEM grid was placed down.

2.6 Microscopy Techniques

Three microscopy techniques were employed to study the morphological characteristics of the composites, namely LM, SEM, TEM.

2.6.1 Optical Microscopy

A Reichert microscope fitted with crossed polars was used to take photomicrographs. Microtomed sections (≈5μm thick) of the moulded sections were mounted between slide and cover slip with microscope slide oil. Micrographs were taken to measure the sizes of skin, shear and core zones. A graticule was photographed at each magnification and used to provide a calibration.

2.6.2 Scanning Electron Microscopy

The specimens examined using the SEM were the same ones as used for the replication described in section 2.5.6. They had therefore been etched to reveal their morphology, and were mounted on 0.5" aluminium pin stubs for morphological analysis in the SEM.

The specimens were coated with a thin layer of gold using an Edward's S150B sputter coater to produce a clear topographic image in the

SEM. A beam of 10kV electrons was found to give a clear image with minimal electron beam damage to the specimen surface. At higher magnifications (>$3x10^3$) it was found necessary to lower the beam voltage to 9kV. Micrographs were taken on 35mm black and white film.

2.6.3 Transmission Electron Microscopy

The replicas described in section 2.5.6 were examined in the TEM. They were viewed in the bright field mode with accelerating voltage of 100kV at different magnifications. Micrographs were recorded on 6x9" film plates.

2.7 Wide Angle X-Ray Diffraction

2.7.1 X-Ray Diffraction Profiles and Debye Patterns

Cu K_α radiation was used for sample characterisation with x-ray diffractometry and Debye pattern techniques. The same samples were used for each technique by preparing samples ≈1mm thick from the areas represented in figure 2.8 cut parallel to the flow direction. These parallel, polished surfaces were considered symmetrical about their centreline and therefore the Debye pattern analysis was carried out over half their width at positions 0.25, 0.5, 0.75, 1.0, 1.25, 1.5, 1.75 and 2mm (i.e. centreline) at a distance ≈8mm from the original weld line. The incident x-ray beam was positioned onto the samples through an aperture of 100μm diameter.

Diffraction profiles were initially recorded with an incident x-ray beam scanning at a rate of 0.02° 2θ/sec over an angular range 7°<2θ<60°. Later profiles were recorded over the narrower angular range of 8°<2θ<32° for clarity.

2.7.2 Methods of Calculation for α-, β- and γ-Phases, Percentage Crystallinity and Crystallinity Index

Trotignon *et al*[80] suggest a routine approach to calculating the crystallinity index, β-phase index and α-phase orientation index in injection moulded iPP. This is done from the x-ray diffraction profile of a sample where the crystalline orientation parallel to the flow direction is represented by α_1, α_2, α_3, α_4 and β

peaks which are the $(110)_\alpha$, $(040)_\alpha$, $(130)_\alpha$, $(111)_\alpha$+$(131)_\alpha$+$(041)_\alpha$ and $(300)_\beta$ reflections respectively. Their corresponding crystalline peak heights, $h\alpha_1$, $h\alpha_2$, $h\alpha_3$ and $h\beta$, are subtracted from the amorphous background in accordance with Turner-Jones *et al*[45]. The maximum height of the amorphous background is denoted by *h*a. Therefore,

a crystallinity index

$$C = \frac{h\alpha_1 + h\alpha_2 + h\alpha_3 + h\alpha_4 + h\beta}{5ha}$$

a β-phase index

$$B = \frac{h\beta}{h\alpha_1 + h\alpha_2 + h\alpha_3 + h\beta}$$

an α-phase orientation index

$$A = \frac{h\alpha_1}{h\alpha_1 + h\alpha_4}$$

Further, the percentage crystallinity was determined from the x-ray diffractometer profiles using the following equation,

$$\text{Percentage Crystallinity} = \frac{\text{Area of Crystalline Fraction}}{\text{Area of Crystalline Fraction + Area of Amorphous Fraction}} \times 100$$

2.8 Gonio-Spectrophotometer Tests

Gonio-spectrophotometers (GSP) have been in existence for over 50 years but recent advances in instrument design and paint coatings technology coupled with the growth of special-effect pigments have brought this characterisation equipment into mainstream use. They have been used recently with coatings and cosmetics, but only to a limited extent with conventional coloured plastics[81, 82]. These tests were carried out utilising such characterisation equipment which was installed at Silberline Ltd. The main use of the techniques is on painted samples in order to compare different formulations. It relies on the samples allowing no light transmission during testing as this would give unrepresentative results. The GSP was capable of quantitatively characterising:

1. ***hue*** colour, red, blue, green etc. The perception of colour which discriminates different colours as a result of their wavelengths.
2. ***value***, the lightness or darkness of colour, i.e. brightness.
3. ***chroma***, strength or saturation of a colour. A term to indicate the degree of saturation; low values represent neutral grey, and, depending on the hue, higher values represent complete saturation.

The GSP equipment, an Optronic Multiflash unit interfaced with a PC comprised colour control software for data acquisition and manipulation. It was used for quantitative measurement of light reflectivity from aluminium flake within opaque PP mouldings. Only the second parameter, ***value***, was used for subsequent analysis as this was the measure of reflectivity. The unit was initially calibrated with firstly no sample in place (i.e. dark calibration) and secondly a titanium dioxide sample (i.e. white calibration) as TiO_2 has no directional properties. The unit flashed a white light through a square window of dimensions 22 x 28mm onto the surface of the specimen which was placed over the window and held firmly in position. Measurements were taken over a range of angles, 20, 25, 35, 45, 55, 65, 75 and 115° with an observation angle of 45° as illustrated in figure 2.9. These angles were fixed by design. The amount of light reflected from the moulded samples back onto the photosensitive cell was then recorded as a percentage relative to both calibrations. The equipment was tested initially by repeating the same test on the same sample six times to determine the reproducibility of the tests.

A nomenclature was developed to describe the location of the area of the sample tested. The two injection gates of each moulding were labelled as either the left or right hand to ensure accurate comparison between samples, as illustrated in figure 2.10. To aid discussion, the angle subtended by the Al flakes adjacent to the moulding surface was referred to as the α angle and is illustrated in figure 2.11.

Six samples were tested for each measurement to obtain a mean and standard deviation. All measurements were taken from the surface moulded in contact with the fixed half of the tool. For clarity, only the light reflected at

three of the angles is quoted, namely 25, 45 and 75° or face, gloss and flop angles respectively.

Table 2.1 Properties of the polypropylene matrix.

PROPERTY	TEST METHOD	UNIT	
Melt Flow Index (MFI)	230°C/2.16kg	g/10 mins (dg/min)	0.8 (108)
Specific Gravity		kg/m^3	905
Tensile Yield Stress	ISO 527 ASTM D 638M (50mm/min)	MPa kg/cm^3	27.0 275
Flexural Modulus	ISO 178 (2mm/min) ASTM D 790M	GPa kg/cm^3	1.15 11700
Izod Impact Strength	ISO 180 (0.25mm notch radius)	kJ/m^2 23°C 0°C 20°C	9.5 5.5 3.5
Specific Volume at 23°C Specific Volume at 175°C		m^3/kg m^3/kg	1.09×10^{-3} 1.29×10^{-3}
Bulk Density of Granules		kg/m^3	500
Melting Range		°C	165-175
Specific Heat at 20°C		cal/g°C	0.46
Coefficient of Thermal Expansion at 20°C		K^{-1}	1.1×10^{-4}
Burning Rate ASTM D635 (3mm thickness)		cm/min	2.3
UL 94 Flammability Rating			UL94HB
Mould Shrinkage at 20°C		%	1-2
Typical Applications	Car and domestic appliance components Chair shells Housewares Battery cases Domesticware Car interior trim		

Table 2.2 Properties of the polystyrene matrix.

PROPERTIES	TEST METHOD[1]	UNITS	
Melt Flow Index	R1133	G/10min	7
Vicat Softening Point	306	°C	90
Distortion Temperature Under Load	R75	°C	81
Charpy unnotched	R179	kJ/m^2	13
Strength at Break	R527	MPa	44
Elongation at Break	R527	%	1.8
Tensile Modulus	R527	GPa	3.1
Flexural Strength	178	MPa	80
Flexural Modulus	178	GPa	3.1
Specific Gravity	R1183	g/cm^3	1.05
Recommended Melt Temperature	-	°C	<280

[1] Injection moulded specimens prepared to ISO 294.

Table 2.3 Properties of aluminium flake pigments.

GRADE	SILVET™ 210-30-E1	SILVET™ ET2018	SILVET™ 880-30-E1	SILVET™ ET2025	SILVET™ 790-30-E1	SILVET™ 460-30-E1	SILVET™ 764-30-E1	SILVET™ 440-30-E1	SILVET™ 430-30-E1	SILVET™ 730-30-E1	SILVET™ 420-20-E1	SILVET™ 410-20-E1
Description	Fine, Smooth	Fine, Smooth	Medium Coarse	Medium Coarse	Coarse	Coarse, Thick	Very Coarse	Coarse, Thick	Coarse, Thick	Ultra Coarse	Extremely Coarse	Extremely Coarse
Al Flake Content	≥69%	≥39%	≥69%	≥69%	≥69%	≥68%	≥69%	≥68%	≥68%	≥69%	≥78%	≥78%
Carrier Resin Contents	≥29%	≥59%	≥29%	≥29%	≥29%	≥28%	≥29%	≥28%	≥28%	≥29%	≥18%	≥18%
Volatile Content	≤09%	≤2.0%	≤0.9%	≤0.9%	≤0.9%	≤0.9%	≤0.9%	≤0.9%	≤0.9%	≤0.9%	≤0.9%	≤0.9%
Median Flake Diameter	≈9μm	≈11μm	≈30μm	≈33μm	≈36μm	≈70μm	≈75μm	≈95μm	≈165μm	≈225μm	≈330μm	≈650μm
Metal Purity	≥99.7%	≥99.7%	≥9.7%	≥99.7%	≥99.7%	-	≥99.7%	-	-	≥99.7%	-	-
Loadings (w/w)	0.5-1.5%	0.01-0.1%	1-2.5%	1-2.5%	1.5-3%	1-2%	1-2%	0.5-1.5%	0.5-1.5%	1-2%	0.5-1.5%	0.5-1.5%
Compatible thermo-plastics	PE, PP, PS, ABS, SAN, PA, Polyester, PU, Acetal Polymers, EVA, PC, PVC	PE, PP, PS, ABS, SAN, PA, Polyester, PU, Acetal Polymers, EVA, PC, PVC	PE, PP, PS, ABS, SAN, PA, Polyester, PU, Acetal Polymers, EVA, PC, PVC	PE, PP, PS, ABS, SAN, PA, Polyester, PU, Acetal Polymers, EVA, PC, PVC	PE, PP, PS, ABS, SAN, PA, Polyester, PU, Acetal Polymers, EVA, PC, PVC	Styrene's, Polyolefins, PA, PU, Polyesters, Polyacetol, PVC, PC	PE, PP, PS, ABS, SAN, PA, Polyester, PU, Acetal Polymers, EVA, PC, PVC	Styrene's, Polyolefins, PA, PU, Polyesters, Polyacetol, PVC, PC	Styrene's, Polyolefins, PA, PU, Polyesters, Polyacetol, PVC, PC	PE, PP, PS, ABS, SAN, PA, Polyester, PU, Acetal Polymers, EVA, PC, PVC	Styrene's, Polyolefins, PA, PU, Polyesters, Polyacetol, PVC, PC	Styrene's, Polyolefins, PA, PU, Polyesters, Polyacetol, PVC, PC
Applications	Packaging, agricultural film and sheets	Indirect food contact applications	Toys, cosmetic containers, domestic appliances, jewellery, stationery products	Toys, cosmetic containers, domestic appliances, jewellery, stationery products	Toys, cosmetic containers, domestic appliances, jewellery, stationery products, sports goods	Indirect food contact applications	Toys, cosmetic containers, domestic appliances, jewellery, stationery products, sports goods	Indirect food contact applications	Indirect food contact applications	Toys, cosmetic containers, domestic appliances, jewellery, stationery products	Indirect food contact applications	Indirect food contact applications

Table 2.4 Compounding conditions used for resin preparation prior to injection moulding.

	Temperature (°C) Barrel Zones						Screw Parameters	
Resin	1	2	3	4	5	Die	Speed (rpm)	Melt Pressure (PSI)
Polypropylene	180	200	210	220	230	230	135	210
Polystyrene	180	200	210	220	230	230	135	210

Table 2.5 Optimum moulding conditions for conventional mouldings.

Matrix	Polypropylene	Polystyrene
SCORIM head	220°C	200°C
Nozzle thermocouple	220°C	200°C
Barrel zone 1	210°C	190°C
Barrel zone 2	200°C	180°C
Barrel zone 3	190°C	180°C
Mould temperature	40°C	40°C
Injection speed	35%	35%
Hold pressure	0 bar 40 sec's	0 bar 40 sec's
Shot size	32.0mm	32.0mm
Max. inj. pressure	100 bar	100 bar
Screw trip position	12.0mm	12.0mm
1st screw speed	40%	40%
2nd screw speed	40% 26mm	40% 26mm
1st back pressure	2 bar	2 bar
2nd back pressure	12 bar 5mm	12 bar 5mm
Cooling time	1.0 sec	1.0 sec

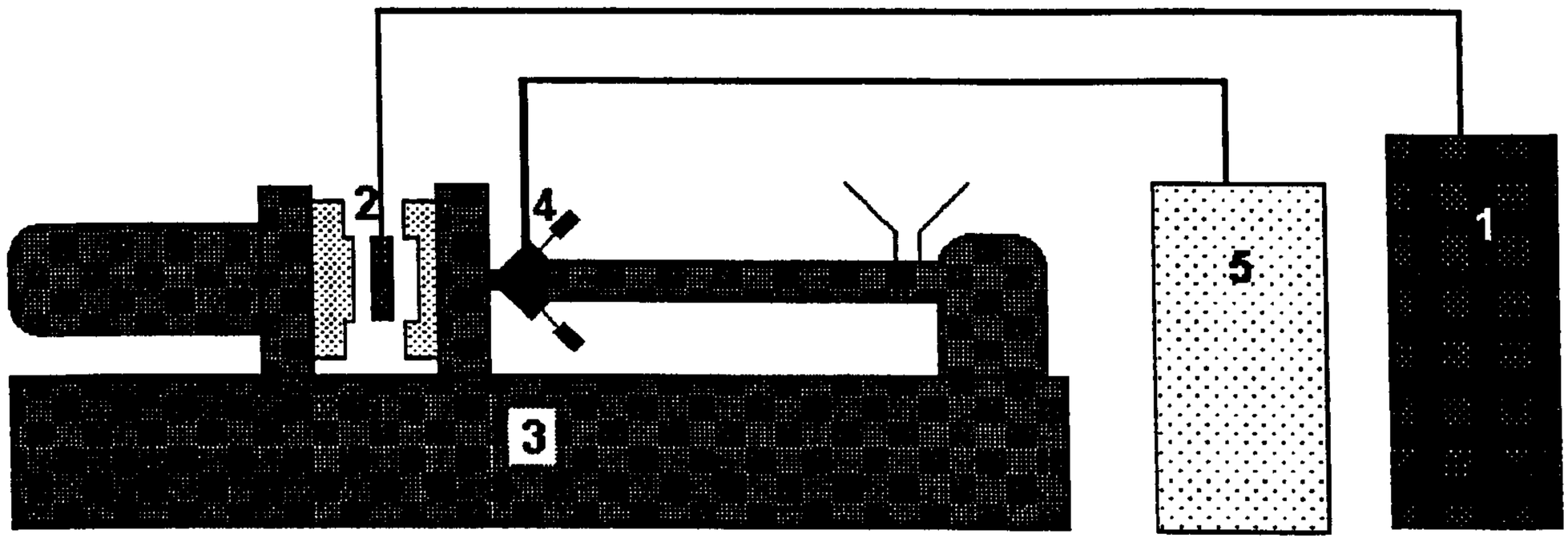

Figure 2.1 Schematic representation of the injection moulding, SCORIM and BSM equipment.

1. BSM process controller
2. BSM robotically manoeuvred high frequency induction heater coil
3. Twin barrelled injection moulding machine
4. SCORIM live feed moulding devices
5. SCORIM microprocessor controller

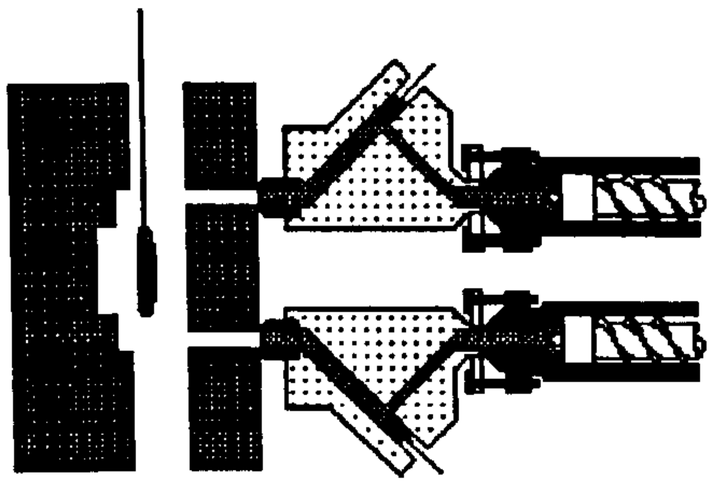

High Frequency Induction Heating of Mould

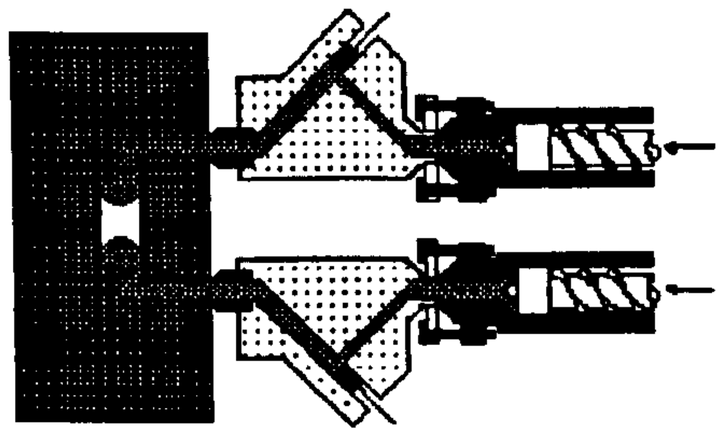

Injection Stage

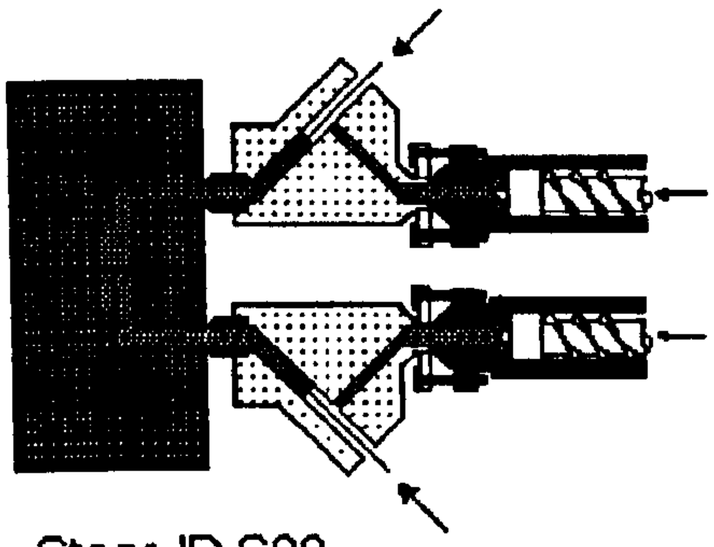

Stage ID S00

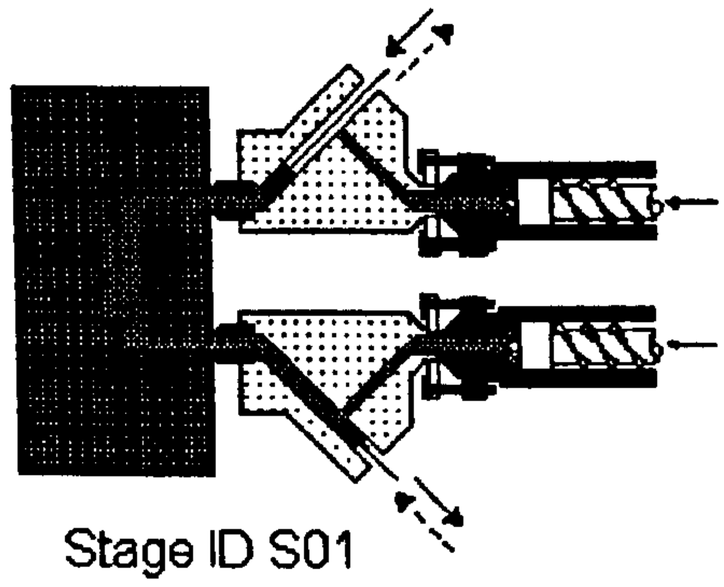

Stage ID S01

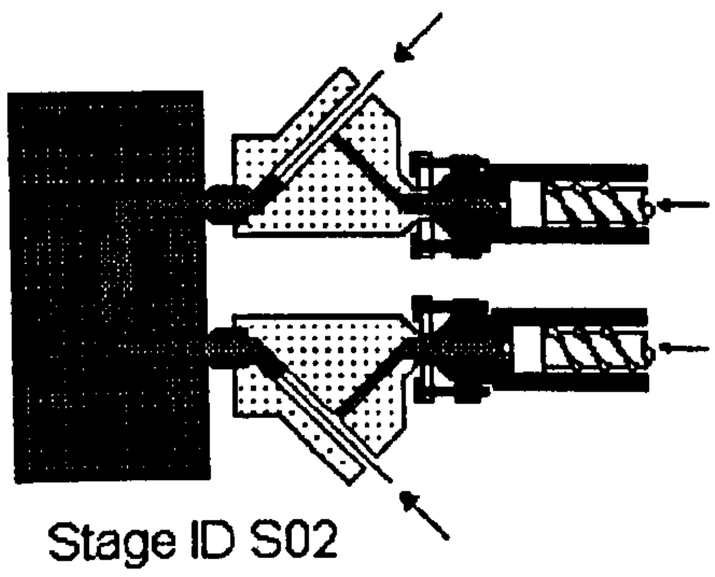

Stage ID S02

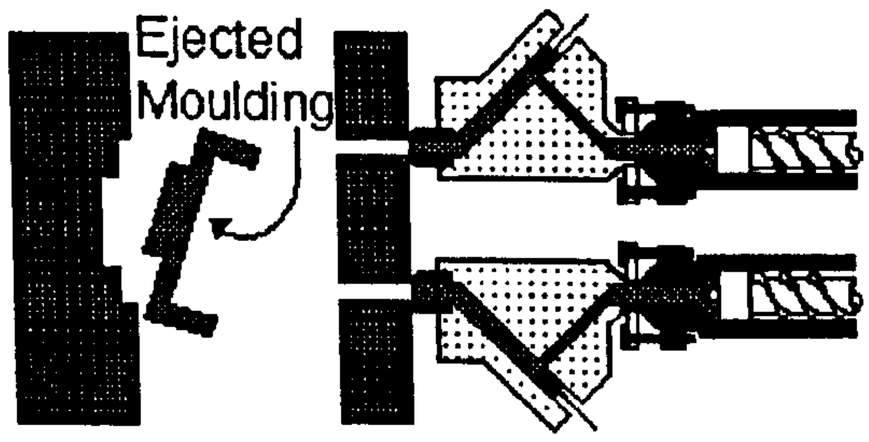

Ejection Stage

Figure 2.2 Schematic representation of the significant stages of the SBM process

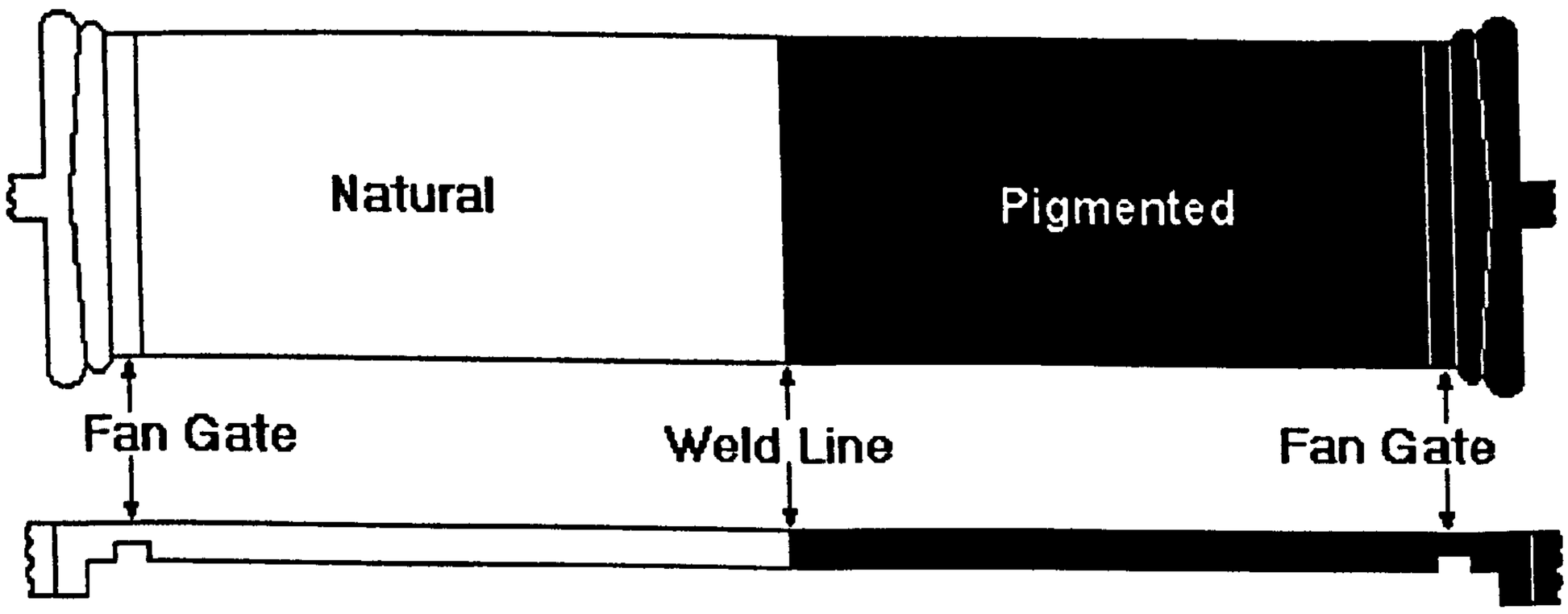

Figure 2.3 Diagram of a 140 x 50 x 4mm moulded plaque showing the two fan gates

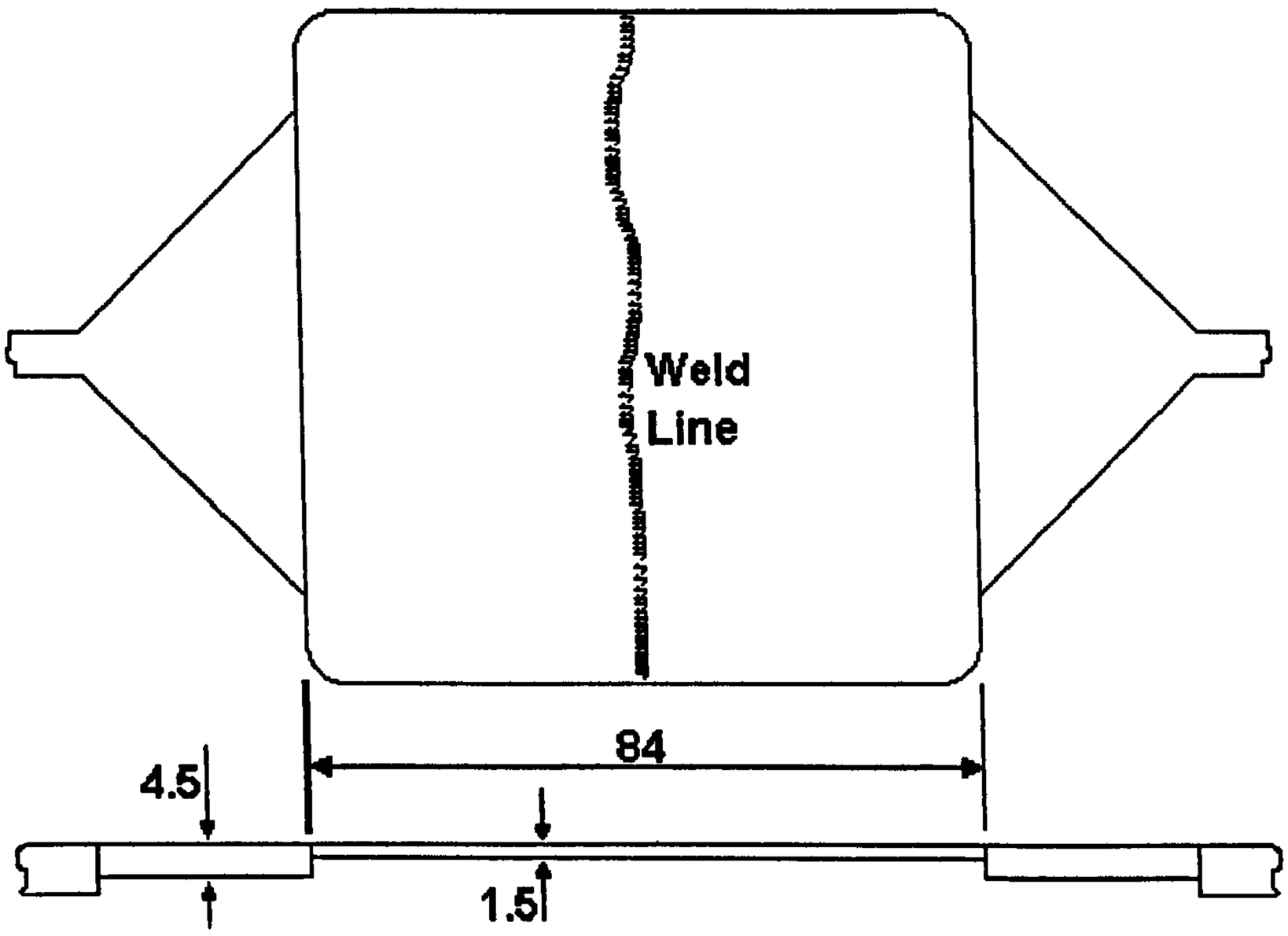

Figure 2.4 Diagram of 84 x 84 x 1.5mm plaque configured with two opposing fan gates.

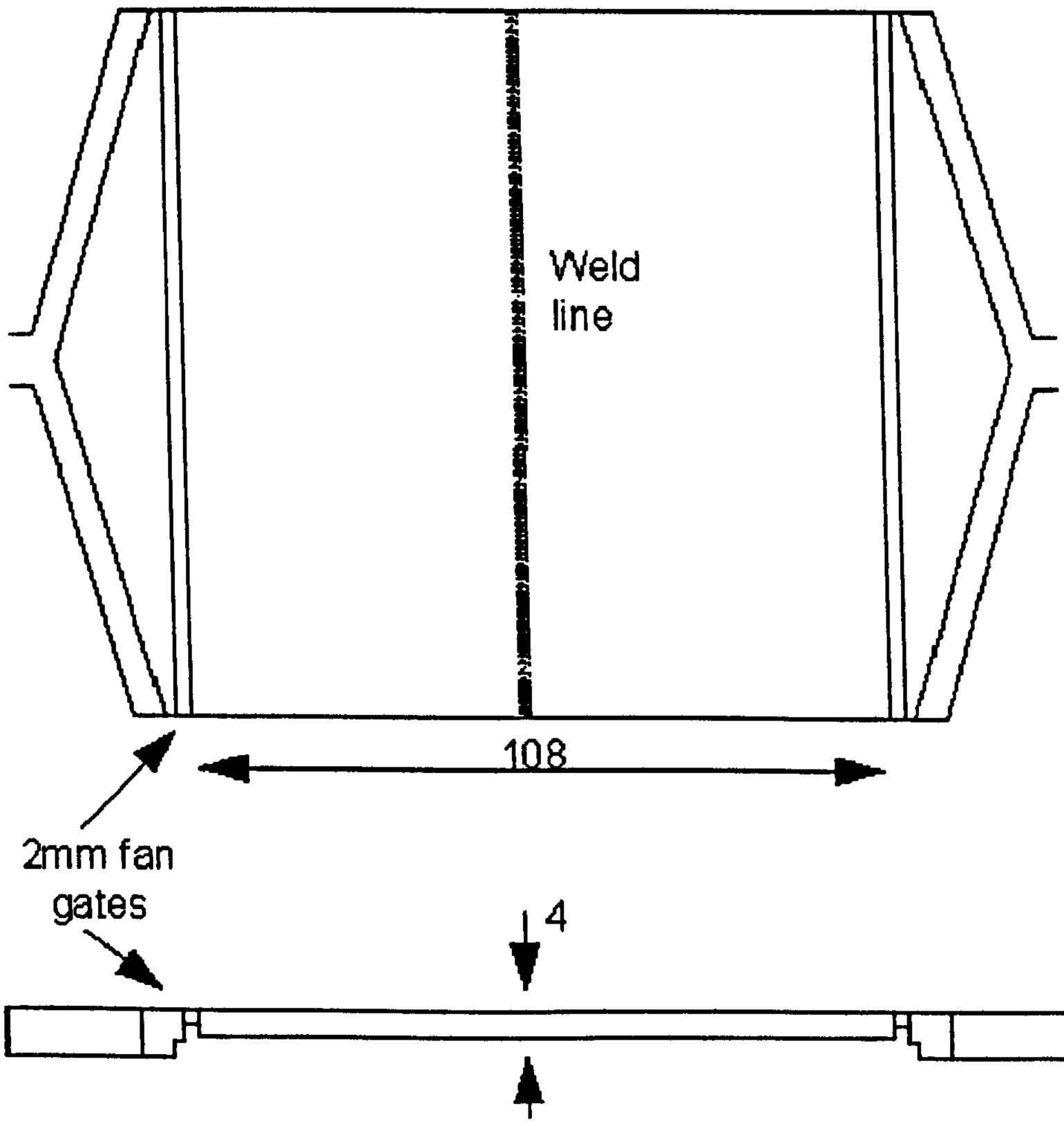

Figure 2.5 Diagram of 108 x 108 x 3mm plaque configured with two opposing fan gates.

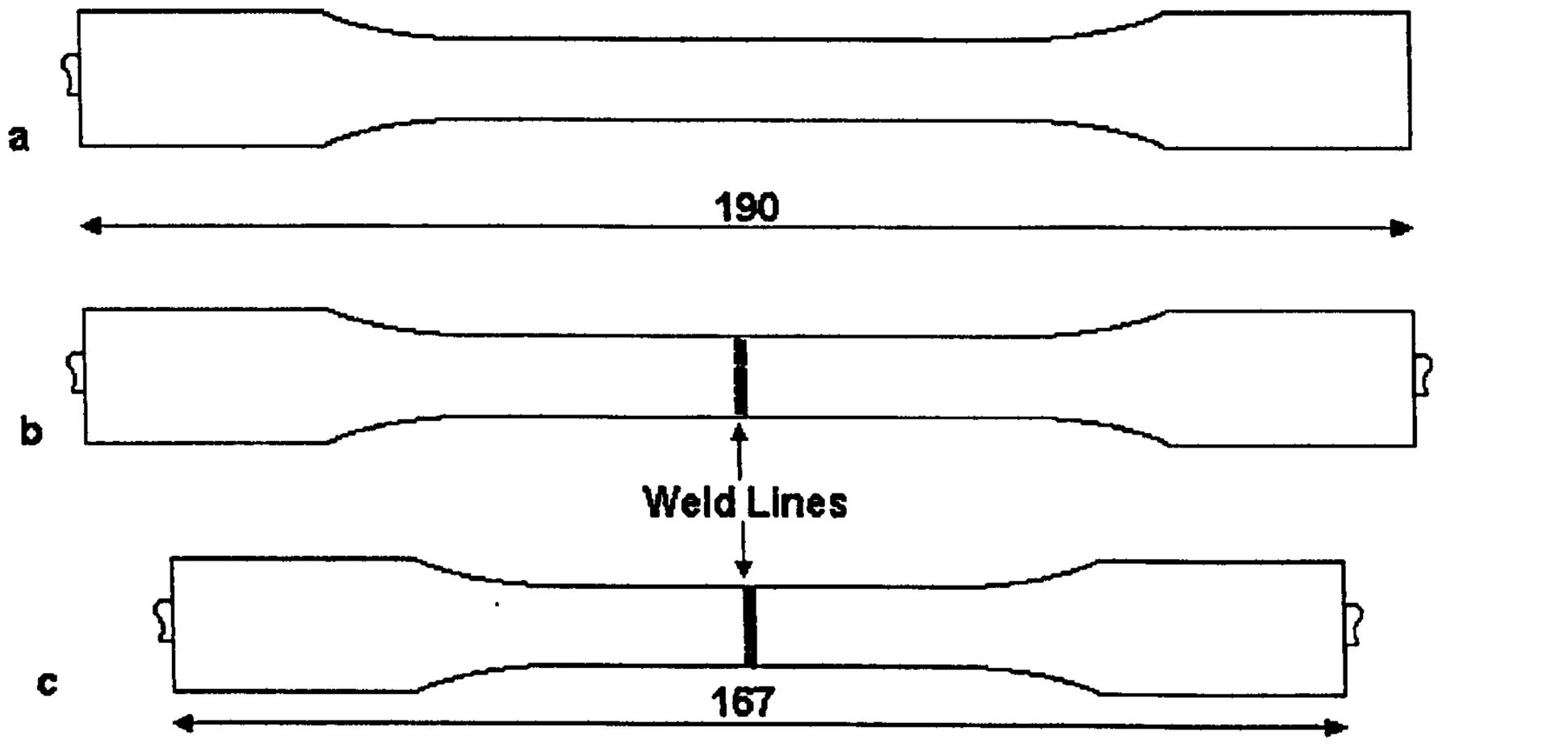

Figure 2.6 Schematic representation of the three types of dumbbell specimens produced

a) Single gated moulding produced by single barrelled injection moulding machine
b) Double gated moulding produced by single barrelled injection moulding machine
c) Double gated moulding produced by twin barrelled injection moulding machine

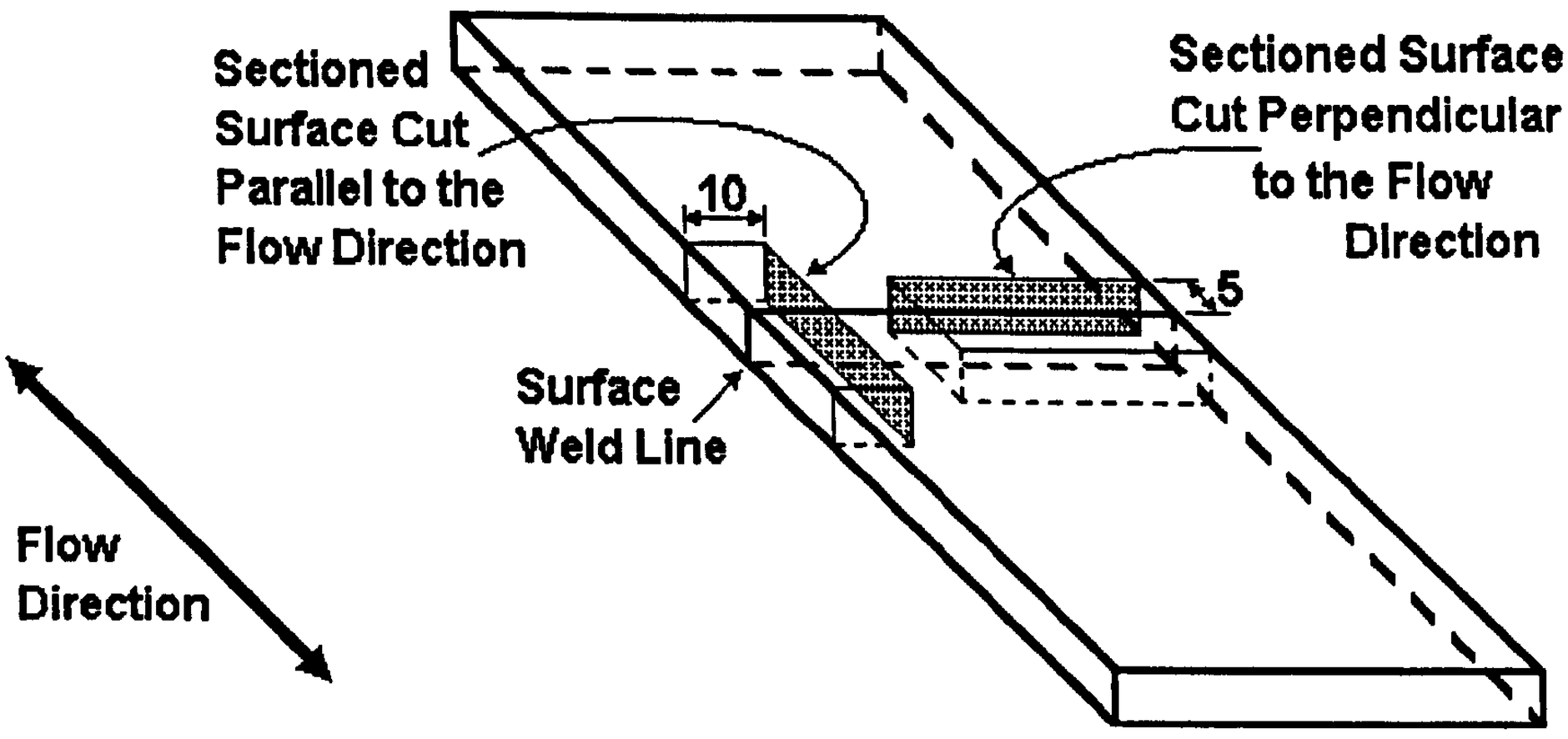

Figure 2.7 Sectioned surfaces of rectangular plaques

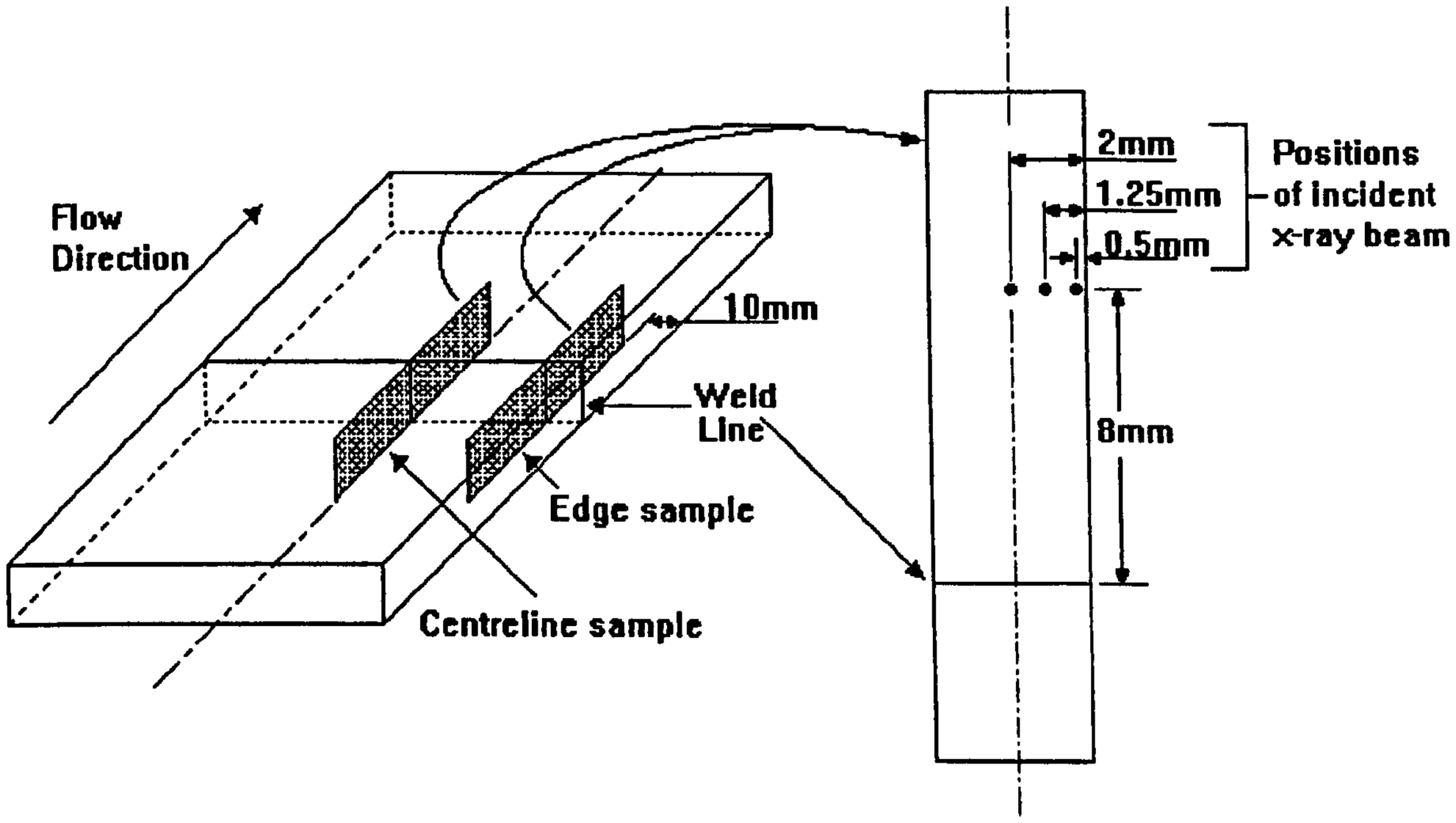

Figure 2.8 Schematic representation of sections taken from moulded samples for use with WAXD and positions of incident x-ray beams for Debye patterns. The same sections were used for both techniques.

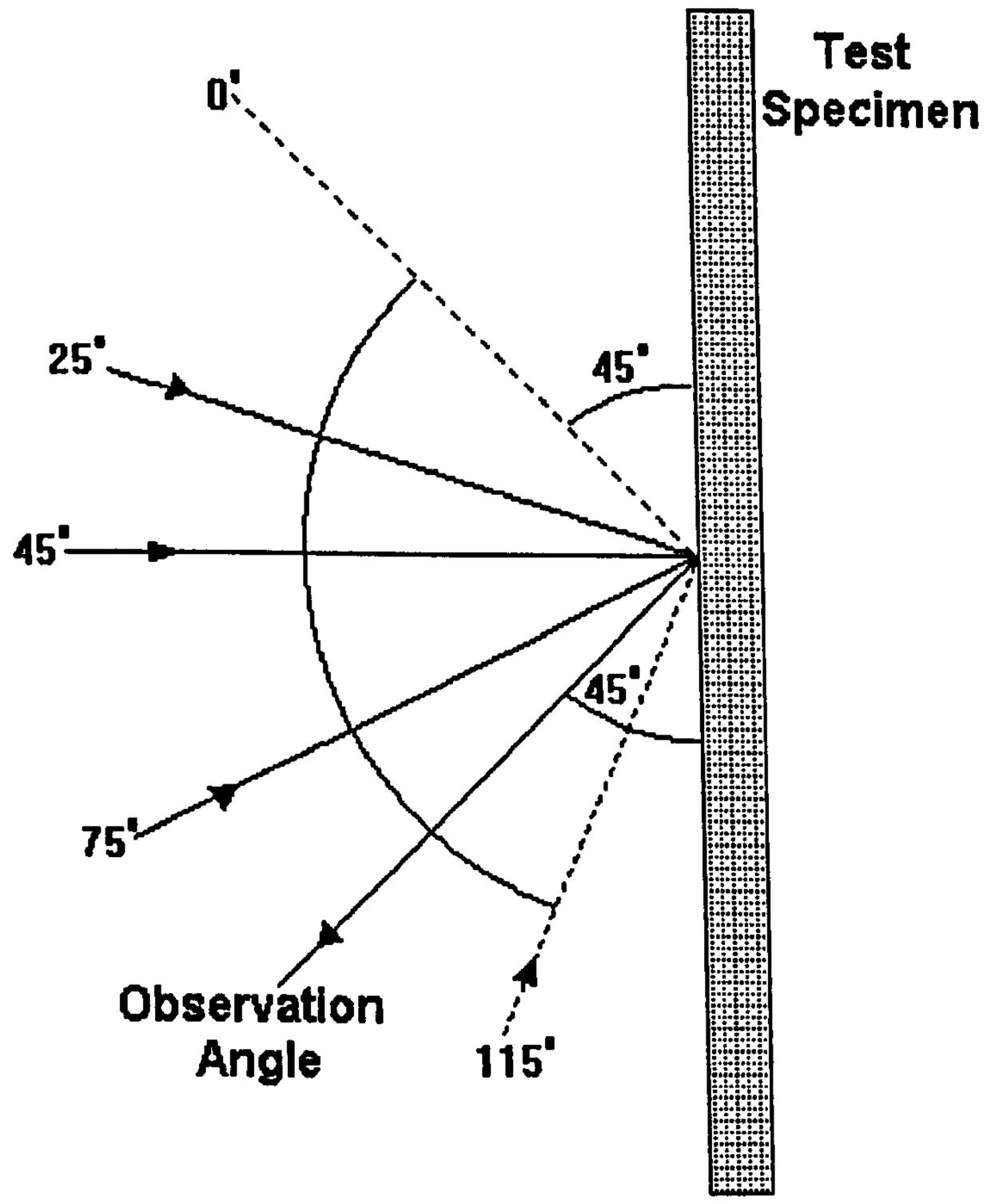

Figure 2.9 Schematic representation of the angles referenced by the GSP and their positions relative to the sample.

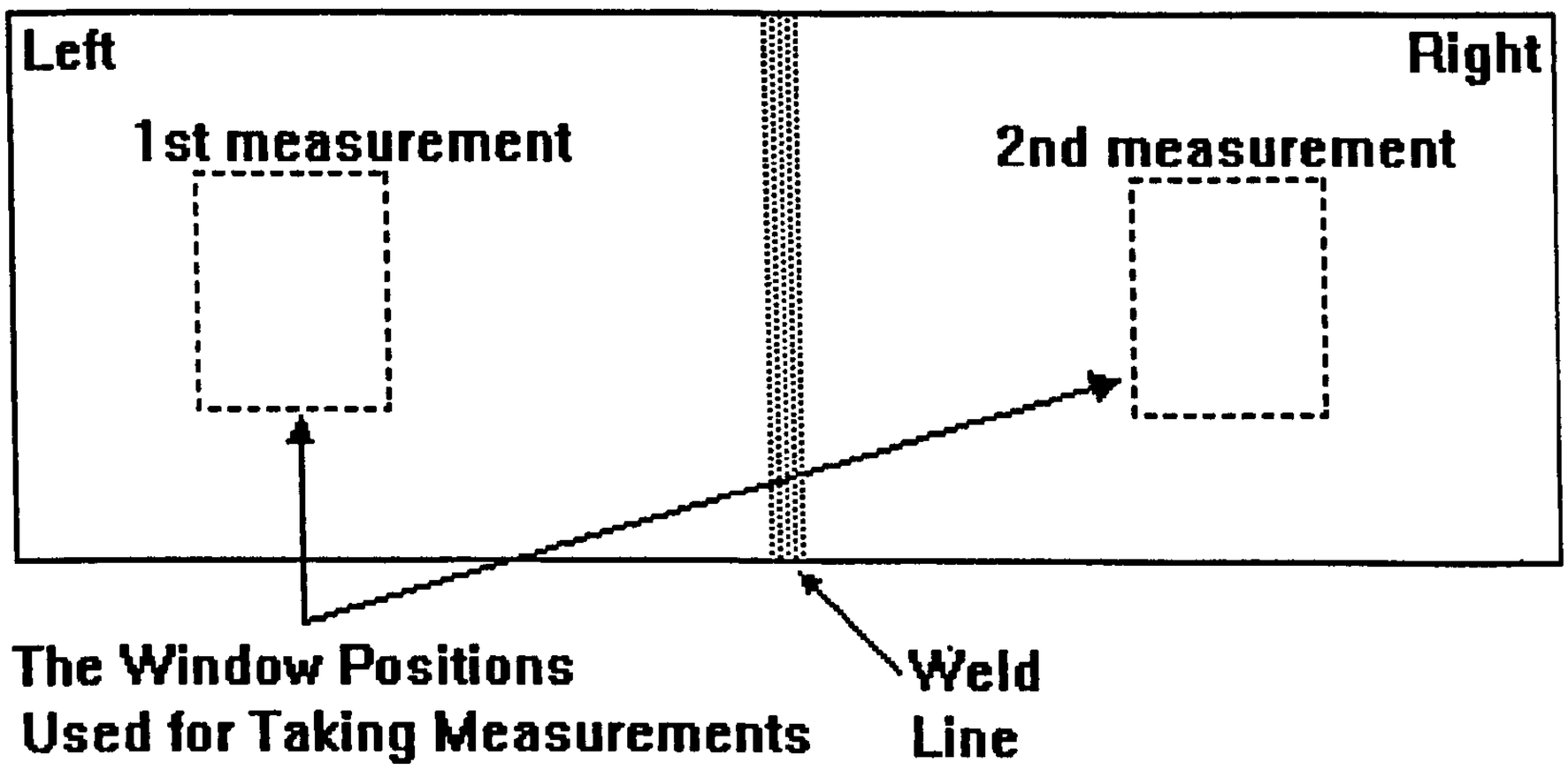

a) With this orientation, the two measurements obtained highlight the directional orientations induced during cavity filling. Consequently, the two values are not directly comparable.

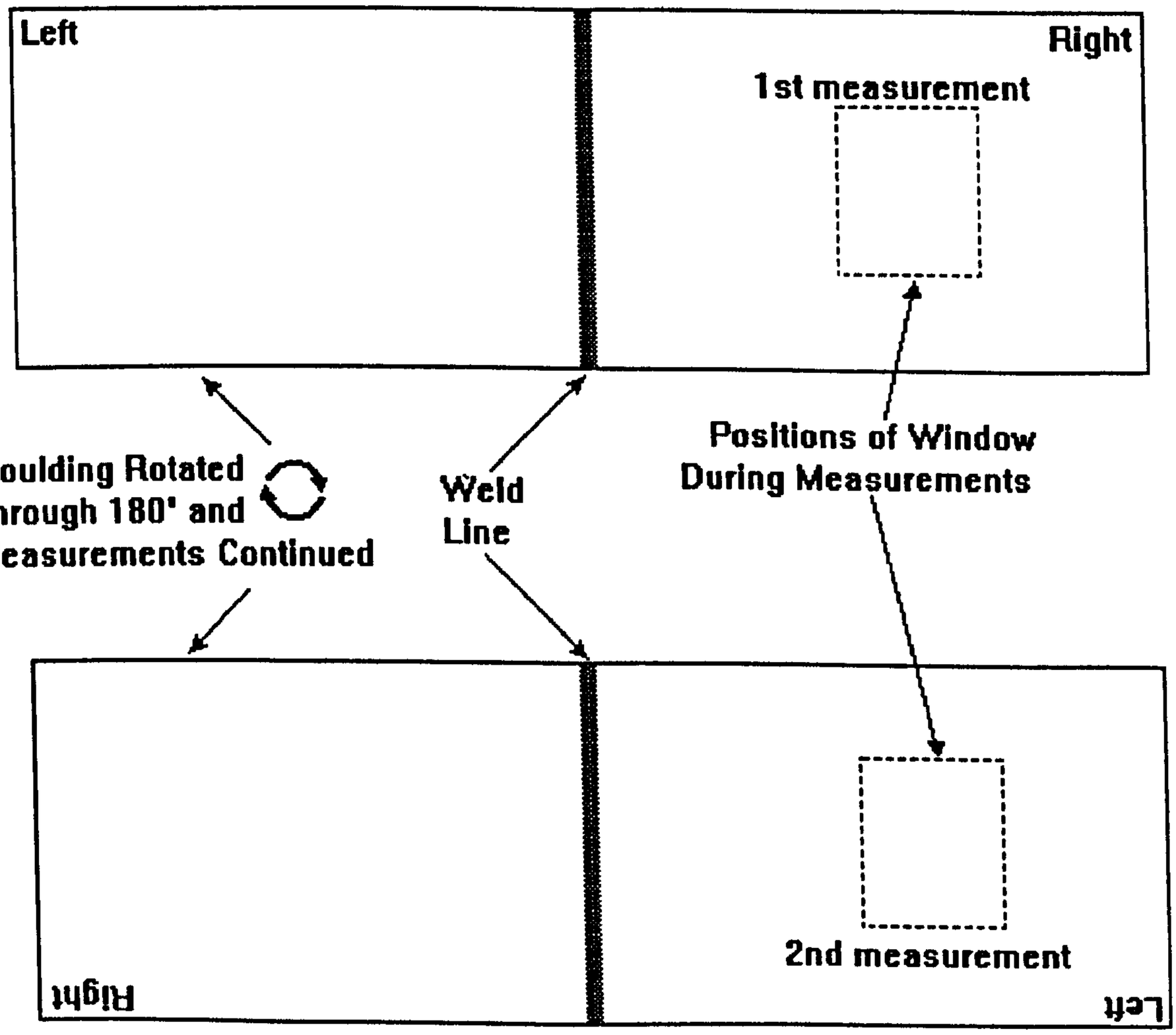

b) With these orientations, the two measurements obtained overcame the directional orientations induced during cavity filling. Therefore the two values are directly comparable.

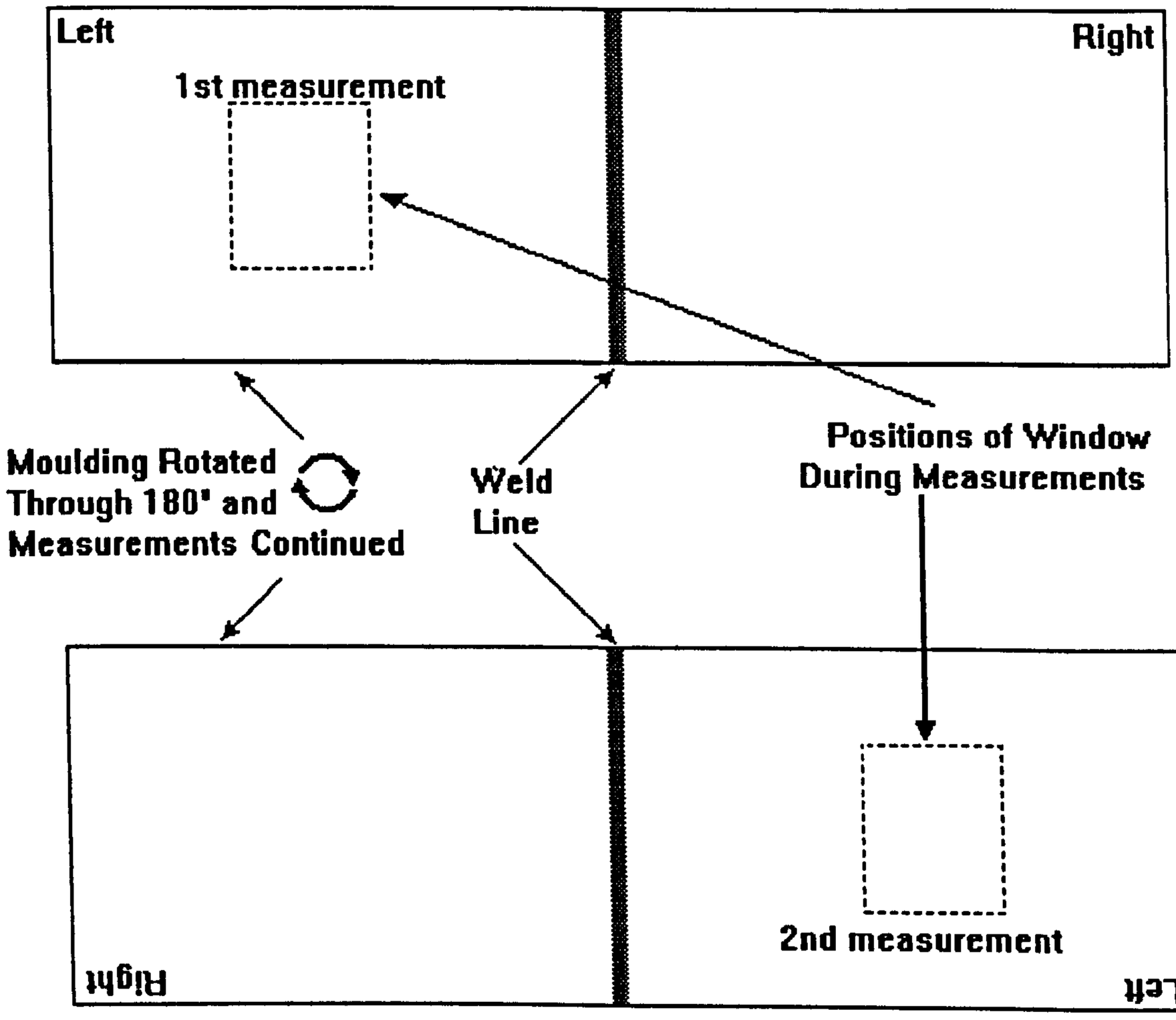

c) With these orientations, the two measurements obtained from the same position enabled evaluation of directional orientations induced during processing.

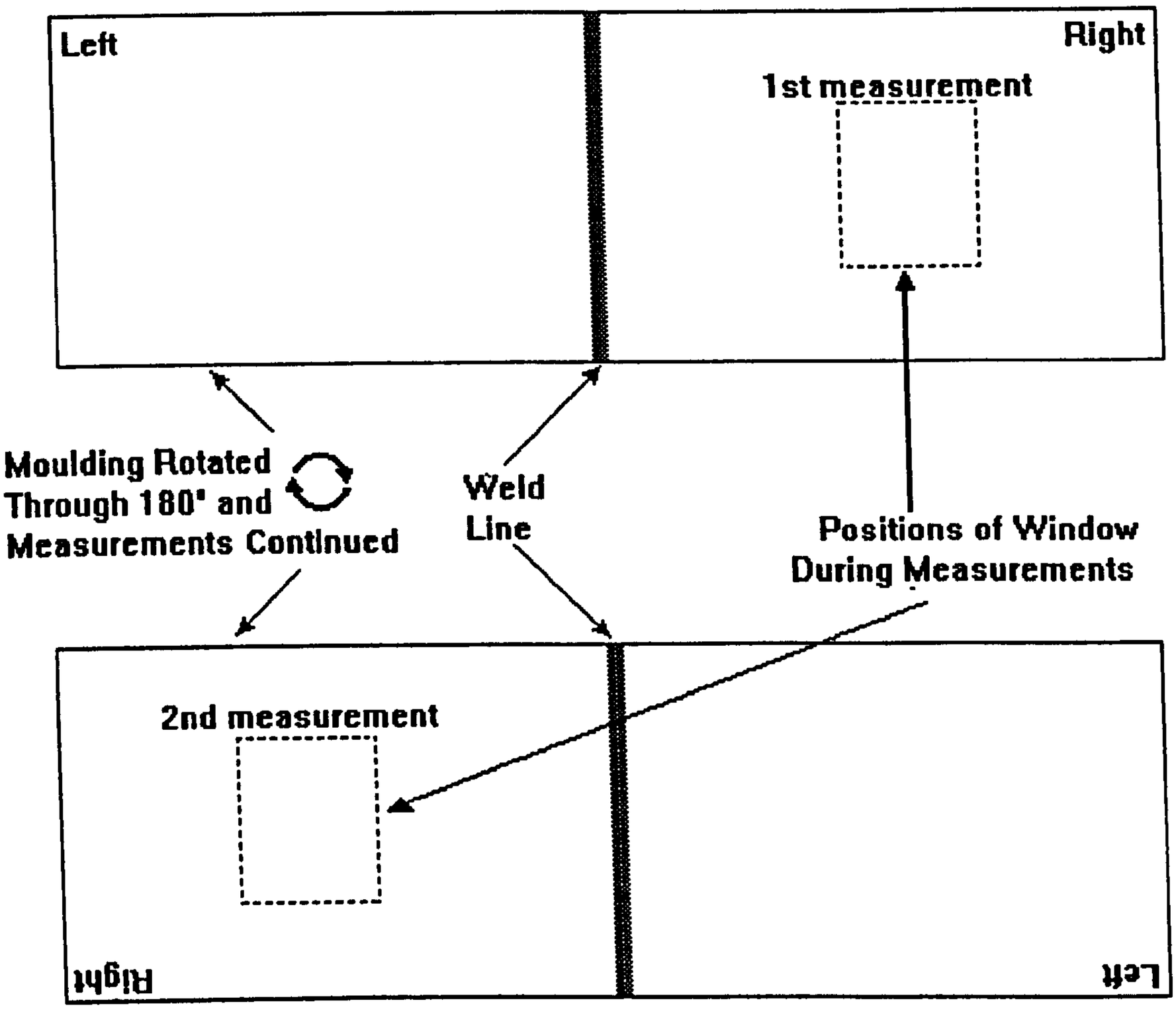

d) With these orientations, the two measurements obtained from the same position enabled evaluation of directional orientations induced during processing, and comparison with **c)**.

Figure 2.10 Schematic representations of the samples and the positions at which measurements were taken using the GSP.

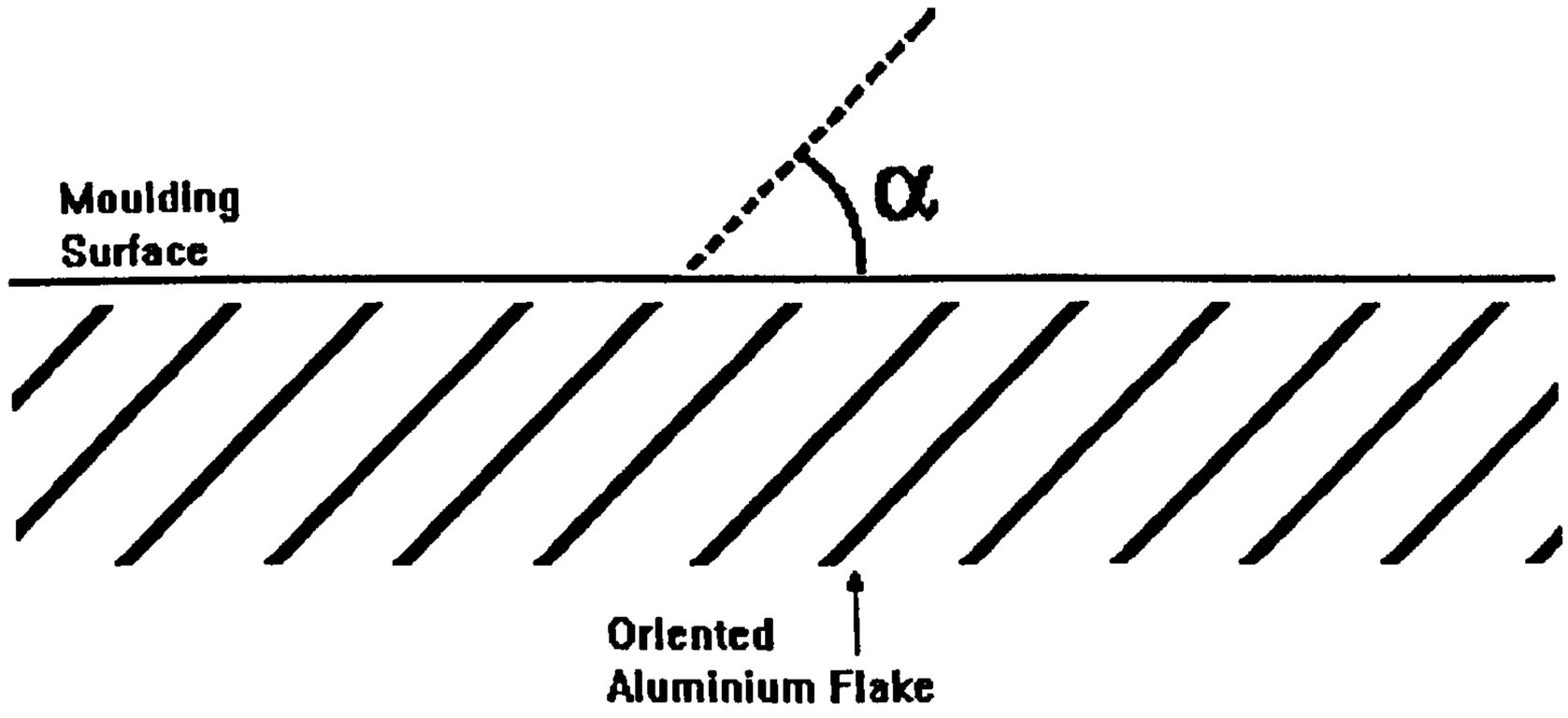

Figure 2.11 Schematic representation of the angle α subtended by the Al flake adjacent to the moulding surface.

3. AESTHETIC EFFECTS OBTAINED WITH THE USE OF SCORIM

3.1 One-Colour Injection Mouldings

Mouldings were produced using polypropylene loaded with 2% ET2025 aluminium flake. The two edge gates resulted in the formation of a single centralised weld interface which formed the basis of these investigations. Mouldings were produced using different cavity geometries and injection moulding techniques, namely conventional, BSM, SCORIM and SBM.

3.1.1 Weld Line Removal

Conventional mouldings resulted in the formation of clearly defined weld lines whose presence was exacerbated by the highly reflective properties of the Al flake as photographed in figure 3.1a. Flow perturbations during mould filling were found to manifest themselves as irregularities in the optical reflectivities of the finished moulding. The smaller sized Al flake particles illustrated this most clearly, hence ET2025 was selected for study as this was relatively small with a median flake diameter of ≈33μm.

Weld line removal for this material was investigated using BSM and then using SCORIM as photographed in figures 3.1b & c. Neither technique proved completely successful when used on its own which is consistent with Yasuda[5]. However, when SBM was used weld line removal was successful in producing mouldings with an acceptably high quality of surface finish in the 'as-moulded' part, figure 3.1d. The discontinuous Al flake orientations exhibited at the weld interface by other processing routes were eliminated in these SBM mouldings. The high temperature of the mould cavity surface induced by BSM, was able to prevent any solidification of a skin layer for sufficient time to enable SCORIM to realign the Al flake and polymer molecules at the moulding surface in the direction of flow. This eliminated or 'washed out' the weld line.

The most successful weld line removal with the SBM process was achieved where the heater coil was large enough to heat the whole of the moulding's surface area. Hence, the dumb-bell mouldings yielded the most

successful results. Figure 3.2 shows mouldings made conventionally, with BSM, SCORIM and SBM. The only wholly successful process for eliminating the weld line was the SBM, showing only a minute witness of any previous weld interface, discernible only upon close inspection. The larger square mouldings in figure 3.3 demonstrate the partial removal of the weld line with SBM where the mould gates were opposite one another. Figure 3.4 shows the same mould cavity with gates feeding onto adjacent sides of the square. The weld line position was therefore across corners in this example, requiring a larger heater coil for heating with BSM, so the SBM process was not as successful at weld line removal in this case as with the previous example. Further, shear flow probably did not influence the corners containing the weld line as this was likely to be a shear flow 'dead spot'. This fact adds emphasis to the importance of applying shears to a mould cavity in an informed and controlled manner. The larger plaques moulded had larger surface areas than the heater coils' area which resulted in variations in gloss level visible in these mouldings, figures 3.1, 3.3 and 3.4. The heater coil used for this work also produced localised 'hot-spots' over portions of the area it was heating, also visible in the larger plaques as gloss variation. Figure 3.5 shows the results of moulding a smaller sized square cavity with surface area similar to that of the heater coil. This cavity was also thinner at 1.5mm than the previous examples, with a consequent smaller cross-sectional area, providing greater resistance to flow during the application of shear forces. Weld line removal was successful with SBM without variation in gloss levels, although flow perturbations are evident around the gate region.

During the high frequency induction heating of the mould tool a temperature gradient was introduced between the high temperature of the cavity surface and the relatively low temperature of the mould tool cooling channels. The distance between the cavity surface and these channels therefore influenced the temperature profile between them and the rate of heat extraction by the tool. As this distance was shorter in the fixed half than in the moving half of the tool a difference in the quality of the mouldings' two surfaces was seen.

The gloss variations and the differences between the mouldings two surfaces are due to the nature of development where prototype equipment is being used; i.e. the heater coil and the fact that the tool used was not initially intended for such work. Knowledge gained during the course of this work could now be used to design out most of these problems. An additional improvement could be made by disabling cooling of the tool during heating and enabling it again only when required. This would conserve energy and reduce cycle times providing the temperature dynamics are kept within control which would require evaluation.

3.1.2 Gonio-Spectrophotometer Results

The gonio-spectrophotometer (GSP) was found to provide highly reproducible results as tabulated 3.1. The coefficient of variation ranged from 0 to 0.14, indicative of a highly reproducible measuring technique. A typical example of the results obtained from the range of angles measured with all the samples is shown in figure 3.6. The results show a decreasing mean and standard deviation as the angle of incident light increased. The values followed a clearly defined curve in each case so only three values were used for discussion, namely 25, 45 and 75°. As a control, unpigmented PP samples moulded using conventional and SBM techniques were tested for levels of reflectivity in the absence of Al flake. These results are presented in figure 3.7 and show that the mean values of the intensities of reflection vary by less than 8%, i.e. between 71 and 79%, over the range of 25 to 75°. This is indicative of a sample that was demonstrating little or no optical directional properties. The decrease in intensity of reflection with increased angle of incident light is consistent with the change in angular relationship between the incident light and observation angle, and not necessarily a materials property, c.f. figure 2.9. The SBM plaques demonstrate a consistently higher reflectivity than the conventional plaques for each angle of incident light, indicative of a brighter surface finish of the polymer. This finding is significant as it shows the contribution from the induction heating device produced a brighter surface finish to the matrix. This is an important aesthetic quality for

the development of injection mouldings with bright metallic finishes comparable to those of similar painted components, and for other colour effect mouldings.

The slight differences between reflectivities at the left and right gate locations is probably due to the orientation of the samples when offered to the GSP for measurement, with a possible contribution from a difference in the mould tool cooling rates at each gate location. This cooling discrepancy, if indeed it was present, would have manifested itself most clearly in the BSM and SBM mouldings where heating cycles were featured. Further, the GSP depends on the full reflectivity of the test piece. The Al flake pigmented samples achieved this but the unfilled control samples did transmit some light during test. Therefore, some light would have been reflected by the backing disc supporting the test piece as well as by the control sample. However, the control results are still informative. A remedy for such light transmission may be to place a matt black material between the sample under test and the support disk in order to absorb transmitted light rays, thus preventing their reflection and influence upon the results.

Figures 3.8 and 3.9 are the results of characterisation using the method depicted in figure 2.10b which ensured the figures are directly comparable. They show the variations in the relative intensities of reflections from rectangular plaque conventional mouldings, SBM, SCORIM and BSM, and how these change with angle of incident light. At 25° the conventional and SCORIM mouldings show similar high values of reflectivity comparable to those of a good sprayed metallic paint e.g. values of 100 plus, whereas the SBM and BSM mouldings show lower but similar values. The intensities of reflection seen here are predominantly due to the sparkle effect of the Al flake with a smaller contribution from the matrix. At 45° all the values are similar to one another. At 75° the conventional and SCORIM mouldings exhibit lower values of intensity than the SBM and BSM mouldings.

One reason for the change in relative intensities between moulding techniques over this angular range may be the orientation induced into the Al flake by the 'fountain flow' effect during mould fill. When moulding

conventionally and with SCORIM, this orientation was frozen into the skin upon impingement of the molten polymer with the cold mould wall. The application of SCORIM appears to alter the intensity of reflectivity slightly over that of a conventional moulding. For discussion, the angle subtended by the Al flake adjacent to the moulding surface is referred to as the α-angle and is illustrated schematically in figure 2.11. Figure 3.10 schematically illustrates how the 'frozen in' Al flake orientation (α-angle) induced by 'fountain flow' is visible to the eye as distinctly bright and dull halves of the same moulding i.e. the 'flip-flop' effect present with two distinctly different orientations. Where SBM was used, this α-angle was purposefully changed to impart uniform Al flake orientation over the surface of the moulding thereby removing the weld line and inducing a uniform direction for the 'flip-flop' effect. With BSM, the weld line was not removed because there was no flow occurring there, but the influence of fountain flow during cavity fill was present at the locations characterised here and therefore the α-angle was affected. Thus, SBM and BSM mouldings exhibit similar properties when characterised in this way. Notably however, the disparity between the two BSM reflectivities is smaller than those for SBM. In essence, the two sets of values shown in figures 3.8 and 3.9 are the same and therefore this discussion will mainly concentrate on the characterisation of one half of the mouldings only.

Figure 3.11 schematically illustrates the importance of the α-angle during GSP characterisation. For example, with the incident light at 25°, it is evident from figure 3.11a that the positive α-angle of the Al flakes will direct more light towards the observation angle than the arrangement in figure 3.11b where the α-angle is 0°. Alternatively, with incident light from 75°, neither positive α-angle nor one of $\alpha = 0°$ is ideally preferenced to direct more light towards the observation angle. Therefore these values are more likely to be a measure of the base polymers' brightness. In this way, the salient interpretation of figures 3.8 and 3.9 is of conventional and SCORIM mouldings with relatively obtuse α-angles and SBM and BSM mouldings with relatively acute α-angles approaching 0° at the locations characterised.

Figure 3.12 represents the left hand gate location measured as shown in figure 2.10a, for the conventional, SBM, SCORIM and BSM mouldings. For conventional and SCORIM mouldings, with the sample presented to the GSP in this orientation, the relationship between the Al flake and the GSP is that illustrated in figure 3.11c. Here, a negative α-angle reflects much of the incident light away from the observation angle at all the incident light angles. For the SBM and BSM mouldings, their acutely negative and positive α-angles were actually approaching 0°. Therefore their relationship with the GSP is again similar to the arrangement in figure 3.11b. Hence, figure 3.12 shows with this orientation conventional and SCORIM mouldings exhibit lower levels of reflectivity than SBM and BSM.

By comparing figures 3.8 with 3.12 it is clear the relative intensities of reflection for the mouldings is directly dependent upon sample orientation during characterisation. At 75° the relative intensities of the four sets of mouldings are the same in both figures. This leads to the interpretation that these reflections may be due more to polymer surface reflectivity than the presence of Al flake. This is commensurate with the knowledge gained from figure 3.7 with unfilled PP, that the use of cyclic heating, as with SBM and BSM, results in higher surface reflectivity of the base polymer. For conventional and SCORIM mouldings the presentation of the moulding to the GSP with positive or negative α-angle resulted in differences between mean intensities of reflection at 25° of 19 and 34% respectively. The SCORIM process re-orienting the Al flake to a more obtuse angle than conventional moulding. The removal of the weld line with SBM would ideally have re-oriented the Al flake to an α-angle of 0°. In this case the differences between mean intensities of reflection at 25° should be 0%. However, in practice with SBM and BSM the actual differences were 11 and 0.5% respectively. This would imply that the use of BSM alone does orient the Al flake virtually parallel to the mould cavity, but when used in conjunction with SCORIM for SBM, the additional shearing applied to remove the weld line re-orients the Al flake to a more obtuse α-angle. It should be noted however that the removal of the weld line was not perfect in these samples due to the nature of the

development equipment used, and therefore the values obtained are only indicative of what could be achieved with an ideal arrangement.

Figure 3.13 shows the reflectivities obtained from conventional and SBM mouldings. These were characterised at the left gate only in two configurations illustrated in figure 2.10c, to demonstrate the relative α-angle acuteness with each process. These mouldings were square plaques of dimensions 108 x 108 x 3mm. The conventional mouldings demonstrate a 37% difference in reflection at 25° between positive and negative α-angles whereas SBM only demonstrates 16%. This quantitative evaluation is commensurate with the qualitative visual assessment that the SBM processing re-orients the Al flake adjacent to the mould surface to an α-angle closer to 0°. Moreover, SBM was able to partially remove the weld line as illustrated in figure 3.3. This re-orientation was unable to produce a 0% difference between positive and negative α-angles at the left gate due to the large surface area of the moulding relative to the heater coil. The relative magnitudes of the four measurements presented for each angle shown remains constant. At 75° the intensities of the reflections are all similar suggesting again that the Al flake is not contributing too much to this value but rather the surface reflectivity of the base polymer.

The differences between positive and negative α-angles for the rectangular and square plaques is related to their respective flow path geometry's and their different surface areas for heating. With conventional moulding, this is probably a measure of the angle of orientation induced by fountain flow during mould filling. As the thinner square plaque has a greater difference between positive and negative α measurements, 37%, than the rectangular plaque, 19%, this may suggest a larger α-angle was induced by a thinner wall section. The SBM mouldings have closer values of reflectivity between positive and negative α with the rectangular plaque, 11%, than the square plaque, 16%. This may be related to the cross-sectional area through which sheared material flows. The rectangular plaques are smaller in cross-section thus increasing the level of shearing and inducing more preferred

orientation in the Al flake adjacent to the surface. The use of SBM therefore appears to have reduced the size of the α-angle.

Figure 3.14 illustrates the influence of increasing the heating time from 11 to 15 seconds during BSM. These heating times were selected as 15 seconds was optimum, therefore 11 and 13s were suitable for comparison without overheating the tool. This figure shows an excellent comparison between positive and negative α-angle for the optimised 15s heating time, with the lesser heating times showing consistently greater differences. For example with incident light from 25° the differences between the mean values for 11, 13 and 15s heating time are 2.9, 2 and 0.5% respectively. This may indicate the influence mould heating has on the orienting of flake by the 'fountain flow' effect. If there is a delayed 'freeze off' of the skin layer during mould filling due to the elevated mould temperature, then the flow shearing past the material in contact with the mould is likely to induce a degree of preferred orientation in this area, and thus align the Al flake approximately parallel to flow. Clearly an optimum level of heating is required in order to achieve this and 15s was found to be suitable with this arrangement. It should be noted that this influence would only occur in regions away from the weld line and that the weld line retained an appearance very similar to that of a conventional moulding. Another contribution to the changes in intensity of reflection may be the influence that BSM has on the reflectivity of the base polymer. The use of BSM increases the surface brightness of the base polymer and this may be detected by the GSP as an increase in reflectivity with little directional property. Again with incident light from 75° this notion appears to be borne out.

Figure 3.15 compares the reflectivities of SCORIM rectangular plaque mouldings which have undergone either one or two shears. Measurements were taken from the left gate as shown in figure 2.10c again to compare positive and negative α-angles. Both sets of data appear to be the same within experimental error. The difference between mean positive and negative α-angles with 25° incident light was 34.7% for both one and two shear mouldings. The equivalent measurement for a conventional moulding

(c.f. figures 3.8 and 3.12) was 19.4%. This therefore implies that applying SCORIM did re-orient the Al flake with the first shear but that the second shear was unable to impart any further influence on the surface reflectivity. The difference between conventional and SCORIM mouldings seen here is probably due to the SCORIM shear re-orienting the Al flake just beneath the surface skin of the moulding before a thicker skin layer solidified. This new orientation was then quickly frozen into the moulding surface before the second shear was applied.

Figure 3.16 illustrates the effect of increasing the heating time from 11 to 15s during SBM. The general trend within experimental error is that the size of the disparity between positive and negative α-angles is reduced with increasing heating time. With incident light from 75° there is no discernible difference between these mouldings. The interpretation here is that a longer heating time enables SCORIM to re-orient the Al flake to a smaller α-angle. The ideal processing conditions with this arrangement were not reached as both positive and negative α-angles were not equal. An ideal arrangement would require a larger heater coil which was of the size of the mouldings' surface being characterised.

Figure 3.17 illustrates the effect of applying one or two SCORIM shears during SBM moulding. Measurements are taken at the left hand gate as shown in figure 2.10c. These two types of moulding appear to exhibit reverse orientations to one another. The two shear moulding exhibits α-angle orientations akin to a conventional moulding at this position, whilst the one shear moulding is the reverse of these. This leads to the interpretation that the orientation induced during the fountain flow of mould fill was re-oriented by the first shear. The second shear then re-oriented the Al flake back to almost its original orientation at this left hand gate position. For clarity, figure 3.18 illustrates the effect upon the right hand gate position in the same way for comparison. Measurements were taken as shown in figure 2.10d. The relative heights of the reflections in these two figures are essentially the same, leading to a clear understanding of what is taking place during the application of shears with SBM. Figure 3.19 schematically illustrates the

interpretation of the latter two figures. Upon the formation of a conventional weld line an orientation would exist whereby the Al flake is oriented dependent upon the direction of fountain flow during cavity fill. The Al flake would attain an α-angle, either positive or negative, dependent upon this, figure 3.19a. With SBM the application of a single shear is able to orient the Al flake in the direction of shear, figure 3.19b. Then, the application of a second shear in the opposite direction reversed the orientation previously induced, figure 3.19c. This process should be repeatable only until such a time as the surface polymer cools to a temperature below its glass transition temperature. Figures 3.17 and 3.18 also show that the disparities between positive and negative α-angles are reduced by the second shear, indicating that the α-angle is approaching 0°.

3.1.3 Light Microscopy Characterisation

Light microscopy (LM) was employed to provide supportive evidence of the angles of the Al flakes at the mouldings surface. Photomicrographs were taken of conventional and SBM rectangular plaque mouldings sectioned and microtomed parallel to flow. Polarised LM was also used as this provided informative skin/core morphological characterisation.

Figure 3.20 contains two photomicrographs of microtomed sections viewed by polarised LM. These show the changing morphologies through the 4mm thickness of rectangular plaques moulded using conventional and SBM techniques. The bright entities present are β-phase spherulites and the darker regions α-phase. The conventional sample appears to have a much thinner bright β-phase band at the surface which encroaches less distance into the core than the SBM sample. This is due to the additional shearing experienced by the SBM sample during the application of SCORIM as well as the higher mould temperature imparted by BSM. Therefore SBM moulding is demonstrated to have a significant influence on the proportions of α- and β-phase present.

As the reflectivity of the samples is a function of the Al flake pigment at the surface of the mouldings, figure 3.21 shows higher magnification

photomicrographs of these regions for the same conventional and SBM rectangular plaque mouldings. In these LM images the Al flake appear dark within the grey PP matrix. Preferred orientation in the flow direction is present within both these samples. The presence of an Al flake α-angle ≠ 0° in the conventionally moulded sample is difficult to discern. However, if this angle is only very small as would be reasonable to expect, this would prove difficult to characterise using this approach. Close scrutiny of the two photomicrographs does show the SBM moulding contains a higher degree of preferred orientation of the flake, where they appear to be oriented parallel to the mouldings surface through a greater thickness of the sample than with the conventional sample. This is a result of the shear induced orientation provided by the macroscopic SCORIM shears.

In figure 3.22 are photomicrographs of the same sections as figure 3.21 but viewed between crossed polars to reveal the crystalline morphology of these two regions. The conventional moulding exhibits bright β-phase in the skin layer which usually contains no visible crystalline structure[63]. The presence of β-phase is probably synonymous with the presence of the Al flake acting as a heterogeneous nucleant for β-phase crystallisation in this region. Adjacent to this large defined β-spherulites are present in the shear zone which then peter out in the α-phase core region.

By comparison the crystalline morphology of the SBM moulding in figure 3.22b demonstrates less β-phase in the region adjacent to the moulding surface. Wright *et al*[67] noted skin thickness decreased with increasing mould temperature. With the very high mould temperatures developed with SBM, it is probable that no skin of any discernible thickness was able to form, before the application of SCORIM shears induced preferred orientation through a greater thickness of the moulding. The polymer and Al flake orientation thus induced was then encapsulated by the advancing solid/melt interface. At a distance of 0.5mm from the moulding surface, polymer relaxation enabled the growth of spherulites which were subsequently frozen into the microstructure. In essence, the elevated mould temperature induced during SBM appears to have prevented the formation of

the skin layer by maintaining the plastic above its T_g for long enough to enable SCORIM shears to re-orient polymer molecules and Al flake in the flow direction (i.e. parallel to the mould surface). One effect of moulding with elevated mould temperature may be the formation of a relatively brittle/hard surface layer due to the increased time for crystallisation to occur, in contrast to the usual tough/soft surface skin found in low temperature mouldings, as characterised by Murphy *et al*[59]. This could have important implications with respect to recent requirements for improved scratch resistance[83] by enabling the production of harder surfaced mouldings. However no surface hardness characterisation was carried out with this work.

These aesthetic effects were dependent upon the successful and informed application of macroscopic shears by the SCORIM process. In order to develop a greater understanding of the shearing mechanisms involved during SCORIM a novel approach was adopted. This involved the simultaneous processing of two translucent materials with different colouration, to obtain a visual record in the finished article of the shearing process, with respect to how a given volume of sheared material was displaced through the mould cavity. The success of this original approach is discussed in the following section.

3.2 Two-Colour Injection Mouldings

This work utilised the two-colour Negri-Bossi 130-90-90 moulding machine effectively equipped with two SLFM as described in section 1.6.2. In order to visualise and record the position of the weld interface at the end of any moulding cycle the same type of polymer was processed through both barrels, each pigmented a different colour, and injection moulded simultaneously into the same mould cavity. This work has focused on accurately measuring the parameters of the SCORIM process of interest for its precise mathematical modelling. The successful co-development of the computer model at Swansea University was wholly dependent upon the authenticity of this real-time *in-situ* evaluation. The ability of the mathematical model output to reflect the experimental results could only be as accurate as

the raw data input into it. Therefore this involved the implementation and calibration of a data acquisition system capable of collecting data on piston displacements, hydraulic pressures, cavity pressures and tool temperatures. The thorough assessment of the system during its preparation was paramount to the successful outcome of this work.

The resultant moulding morphologies subsequently studied can thus be accurately and confidently related to the processing conditions measured. This information will then be used for comparison with the mathematical model and any model modifications which may be required.

3.2.1 Mould Filling

The rectangular cavity used to study the SCORIM process was required to form a flat weld line at the meeting of the two flow fronts from the two gates. Fan gates were chosen to minimise any flow perturbations from the gates during cavity fill and promote flat flow fronts of the advancing melts in the cavity. Figure 3.23 shows clearly how the melt emerging from the fan gate developed into a flat flow front as it advanced through the cavity. This therefore enabled flat weld lines to be produced in the centre of the plaque prior to the application of SCORIM.

3.2.2 Weld Line Displacement

Upon the formation of a flat weld line, SCORIM was applied displacing material across the weld. Initial wisdom suggested a flat flow front would develop similar to that developed during cavity filling, with edge effects. However, in practice mouldings developed U-shaped flow fronts with displaced material showing a clear preference for advancement away from the central region of the plaque. The photograph of figure 3.24 shows this effect for a family of SCORIM mouldings. Much consideration was given to the influence of deleterious effects associated with the differences in the processing parameters. Hold pressures were removed, screw back delayed until after gate freeze off and SCORIM pistons held in their final sequenced positions until gate freeze off. The elimination of these influences ensured the patterns obtained were real phenomena associated with the SCORIM

processing system. The comparable behaviours of different materials ensured the phenomena were not the sole property of one material, but a complex relationship between material rheology, flow path geometry and the processing system.

3.2.3 Gate Geometry Effects

To investigate the influence of the gate design on the formation of the U-shaped flow front, the fan gates were modified so as to be flat, figure 3.25a. These new gates illustrated that the U-shape was not developed due to any subtle changes in fan gate design, but only mildly influenced the flow profile indicating it may be reduced or eliminated by the use of pin gates.

Mouldings then produced using pin gates exhibited different flow fronts depending on the material processed. PP exhibited a parabolic flow front across the weld, figure 3.25b, whereas PS still produced a U-shape, albeit modified by the pin gate design. These results provide further evidence that the phenomenon is due to a complex flow situation dependent upon the processing technologies involved, flow path geometry and the materials rheological properties.

3.2.4 Shear Heating

Melt flowing in a cavity will always take the path offering the least resistance to flow. Therefore, the presence of the U-shaped flow fronts is thought to be a direct consequence of uneven melt shearing of the displaced weld line in the regions close to the cavity's edge walls. In these regions, there is not only melt shearing adjacent to the tool cavity's two large surfaces, but also from the side walls of the tool cavity. This additional melt shearing generates more shear heat in this localised area. Thus, a combination of the low thermal conductivity of the polymer and the additional thermal insulation provided by the frozen skin layer at the cavity edge, act to retain the heat generated. The localised regions close to the cavity edge are therefore temporarily at a higher temperature than the areas of the moulding only influenced by two cavity surfaces.

This temperature profile along the weld interface has a profound influence on the rheological behaviour of the displaced material. As the melt temperature is inversely proportional to the viscosity, the lower viscosity in the regions close to the cavity edges ensures a preferential melt flow path exists there. Displaced material flows most easily through these low viscosity melt regions and consequently generates more shear heating, exacerbating further the temperature variations across the weld interface. Therefore the more time which elapses between the start of material solidification and progressive SCORIM shears the sharper the U-shape becomes. This is a reflection of the varied extent of solidification and cooling across the weld interface. Hence, once a temperature profile exists across an interface, the formation of a U-shaped flow front is self propagating, the exact shape of the profile being dependent upon materials properties and the processing system.

3.2.5 SCORIM Management

During conventional moulding the flat weld lines resulted in no mixing of the two polymers and mechanically weak interfacial bonds due to the limited area of contact between the two materials and the limited molecular entanglements across the interfaces. This is illustrated in figure 3.26. Upon the utilisation of SCORIM technology the weld interface displacement which ensued was visually recorded at the end of the moulding cycle and produced some profound aesthetic effects. Figures 3.27 to 3.32 show examples of some of the patterns produced by informed application of macroscopic shears to the solidifying polymer melt. By the considered management of the

- relative injection speeds of the two materials into the tool cavity,
- timed initiation of injection of the two materials into the tool cavity,
- number of shear oscillations,
- the speed of each oscillation,
- volume of material displaced with each shear,
- incorporation of delays between shears,

- geometry of the material's flow path, especially the gate region and
- careful selection of materials for suitable rheological properties,

a range of patterns were controllably and reproducibly created within the same mould geometry.

The patterns recorded provided clear visual information with which to easily select and manage the

* position of the initial weld line.
* flow paths taken by the polymer melt during SCORIM.
* mixing of materials within the cavity but outside the runners where desired.
* extent to which mixing of the two materials occurred.
* rate and extent of 'freeze off' of material in the cavity.
* most suitable materials by their rheology.

The initial weld line was positioned by controlling the speed of injection into the mould cavity from each of the two moulding machine barrels as each was independently controlled. It would also be possible to achieve the same result by sequencing the start of injection so that one barrel began injection before the other, i.e. timed injection. Upon formation of the conventional weld line the application of SCORIM would produce displacement of material across the weld interface. The process was developed to manage the volume of material displaced by controlling the distance the live feed head pistons were able to reciprocate in their chambers. This development of the control of SCORIM ensured accurate management of the patterns produced, enabling the patterns to be restricted to within the tool cavity and outside of the gates and runners as desired.

The volume displaced was therefore easily altered to produce subtly different patterns. This, coupled with other moulding parameters such as melt temperature, mould temperature, materials rheology, flow path geometry and the SCORIM profile could all be manipulated to provide for new and varied patterns.

The sheared material exhibited a U-shaped flow front with each material processed. The edges of the mouldings therefore seemed to act as the easiest flow path to the polymer melt offering the least resistance to movement. This may be due to the edges of the cavity providing an additional surface upon which shear heat was generated. The additional heat in this region was insulated into the moulding by the solid polymer in contact with the cavity surfaces. This heat then presumably locally lowered the melt viscosity ensuring this route to be the easiest flow path. The flow in this locality would then have exacerbated the temperature profile by creating additional shear heating. Once this temperature profile existed through the tool cavity all subsequent shears would perpetuate the situation. If shear oscillations were repeated without delay sufficient shear heating was generated to maintain a stream of molten polymer through the cavity indefinitely i.e. live feed moulding.

The symmetry which exists in the flow patterns produced is quite different from the pseudo-parabola proposed for mould filling through a cavity of air. Here, fountain flow exhibits a velocity profile discussed by Tadmor[12] and illustrated in figure 1.3a, which is considered to be the mechanism of flow. Clearly, when the medium through which flow takes place changed from air to polymer melt, a different type of melt flow than that of fountain flow developed. The two flow fronts which emerged developed into sharp points reminiscent of carving knives in appearance within the PS. This would therefore require a different type of velocity profile to describe the flow mechanism responsible here.

The mouldings produced were a complimentary source of information for understanding the influence which SCORIM exerted on the microstructure of semi-crystalline polymers such as PP, which was also studied during this work and reported on in the following two chapters.

3.2.6 Pin Gates

The mould cavity was modified to accommodate two opposing pin gates each 1 x 1mm in cross section feeding into a 150 x 110 x 3mm cavity. Figure 3.31

is a photograph showing the successful result of the mould filling and immediate application of one SCORIM shear. The small cross sectioned gates froze off very quickly without the continuous flow of molten polymer through mould fill and SCORIM shear to keep the gates 'live'. However, it was only possible to apply a single shear and with no delays before the gates froze. The pattern produced within this mould arrangement shows how the material made some progress along the edges of the moulding, as seen in the other plaque mouldings, but as the pin gates were positioned centrally along the edges of the plaque flow was forced to occur predominantly along the centrelines of these mouldings, unlike the fan gated plaques. In essence, these mouldings demonstrate that cavity fill and a single SCORIM shear can be successfully applied within this moulding arrangement. In order to facilitate multiple SCORIM shears within this gating geometry a hot runner and sprue tip would be required in order to delay freeze off and enable intermittent shearing.

3.2.7 Recyclate Core and Virgin Skin

Figure 3.32 shows two photographs of PS SCORIM mouldings where the mould cavity was filled from one gate with red plastic, before the SCORIM piston forced the blue plastic into the cavity from the opposite gate to the exclusion of the still molten red core material. This technique of displacing molten core material only and retaining a desired thickness of frozen skin material enables the possible utilisation of SCORIM for the controlled insertion of recyclate into a cavity of virgin plastic. The extent of solidification of plastic in contact with the tool cavity can be controlled by the timing of the recyclate piston's movement. This enables the control of an adequate thickness of virgin skin material to freeze off first, although this thickness may not be uniform over the length of the moulding.

In principle, this technique may also facilitate the production of mouldings consisting of a sandwich of several layers through their thickness. These composite structures would have a number of layers controllably determined by the SCORIM profile. A moulding machine developed to have

more than two processing barrels would offer composite sandwiches containing several materials which may offer improved mechanical properties, e.g. impact performance. Moreover, the materials processed can be aligned by SCORIM in a direction independent of the mould fill direction. This would be achieved by filling the mould cavity in the most appropriate way, and then applying SCORIM with pistons strategically positioned within the mould cavity, and possibly independent of the runner systems. This level of flexibility and control is not offered by other '2K' processing routes.

This combination of a two-colour machine and SCORIM has the flexibility of enabling two materials with quite different rheological characteristics to be processed into the same cavity within the same moulding cycle. These two materials could be any capable of sustaining flow through an injection moulding machine. The managerial control of the moulding cycle capable with SCORIM would also ensure excellent reproducibility from shot to shot, which is a pre-requisite for quality.

3.3 Relationship Between Processing Conditions and Aesthetic Effects

In order to facilitate the continued and growing understanding of the SCORIM process as a technology for imparting excellent managerial control over the preferred orientation and optimised properties of injection mouldings, an original approach was required for visualising the macroscopic shearing encountered during processing. This technical challenge bore the conception of processing a polymer pigmented differently in each moulder barrel of the two-component injection moulding machine fitted with two SLFM devices. The translucent PS used for its visual clarity not only proved an enlightening method of determining an accurate record of shear flow during SCORIM processing, but immediately realised a potential for the enhancement of visual aesthetic effects within a two-colour moulding process.

These two considerations for continuing this two-colour SCORIM investigation bode well together as complementary sources of inspiration. Progressive attempts to produce ever refined visual aesthetic qualities required further development of the management of the SCORIM process.

Moreover, the incorporation of delay times for this end, in order to encapsulate sheared material through solidification, demonstrated for the first time that shear flow occurs along the edges of fan gated mouldings with a U-shaped flow front which cannot be assigned to fountain flow. Without the ability to visualise the shear rheology in the post moulded components this profound and fundamental knowledge would not have been gained. The incorporation of delay times was then selected for study with the PP matrix as without such delays shear heating and cooling equilibrate resulting in a dynamic steady state and stationary shear interface. This, coupled with chain relaxation and re-entanglement of the melt during cooling uninterrupted by shear, reduced the volume of material which bore witness to SCORIM after solidification. Further, the visual aesthetic qualities of the two-colour mouldings are as original and exciting as they are informative.

I) With the use of the SCORIM and BSM technologies (SBM) in series with an adapted conventional moulding machine, and with the informed application of shear to the mould cavity melt, it was possible to reproducibly remove surface weld lines to an acceptably high quality of surface finish. Critically, the application of this technique was successful with the highly visible surface characteristics of an aluminium flake of median diameter $\approx 33\mu m$.

II) The reflective surface properties of the aluminium flake filled mouldings have been successfully quantitatively characterised to complement the qualitative visual assessments made. This characterisation yielded highly informative data on the excellent control over the directional orientation of the flake and the reproducibility of the whole moulding process. Pertinent SBM processing conditions such as mould heating times and controlled melt shearing were found to be salient parameters.

III) The use of SCORIM with two colours of polymer, simultaneously moulded within the same cavity has been successfully evaluated. Unique and distinguished aesthetic effects have been discovered for the first time from the controlled shearing of these materials within the mould cavity. A wide variety of patterns have been achieved controllably and reproducibly within

the same mould geometry. Further, a more informed understanding of the influence of shearing and its preferred flow paths through the filled cavity has been attained with both fan and pin gates.

IV) The potential use of the SCORIM process for the controlled insertion of a recyclate core material within a virgin skin layer has been identified. This technique would allow a substantial quantity of recycled material to be processed with each shot without influencing the surface characteristics of the virgin outer skin.

Table 3.1 Typical values of intensities of reflection obtained from the Al flakes in PP plaques measured with the GSP.

Angle of Measurement	Mean (%)	Standard Deviation	Coefficient of Variation
20°	86.78	0.075	0.09
25°	76.50	0.063	0.08
35°	60.45	0.055	0.09
45°	50.23	0.052	0.10
55°	44.10	0	0
65°	40.60	0	0
75°	39.15	0.055	0.14
115°	37.78	0.041	0.11

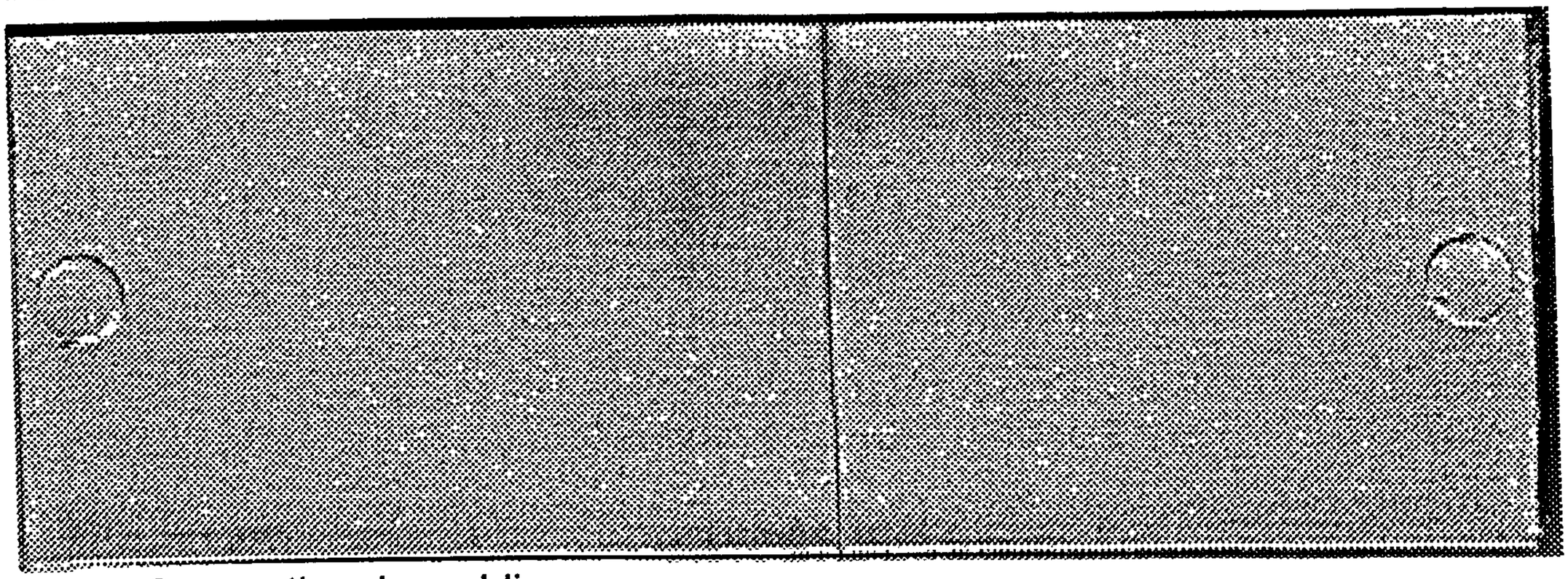

a) Conventional moulding

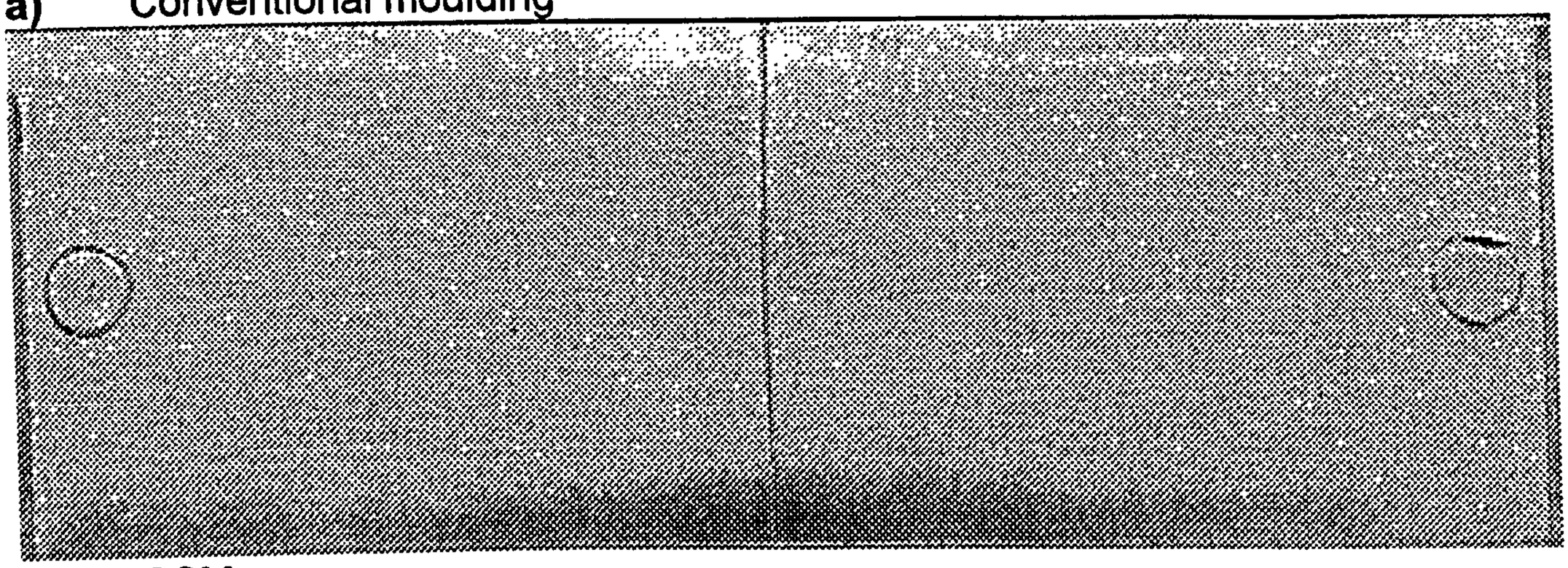

b) BSM

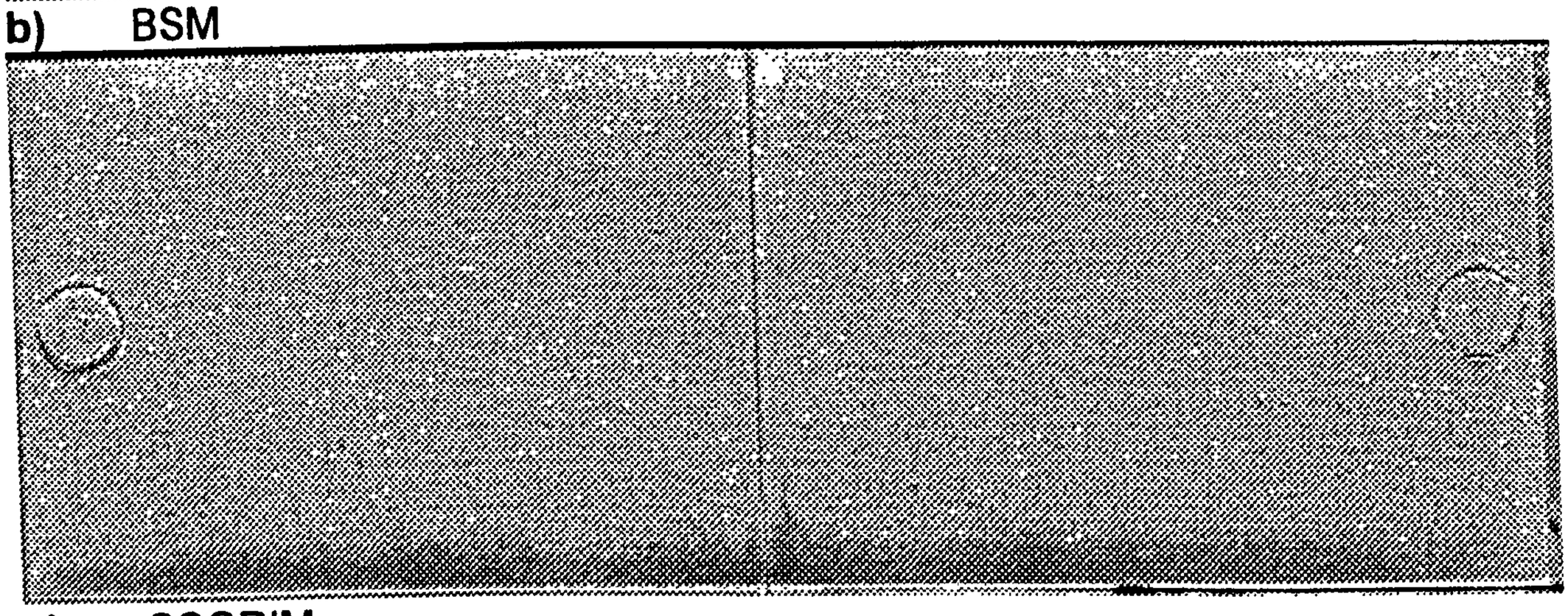

c) SCORIM

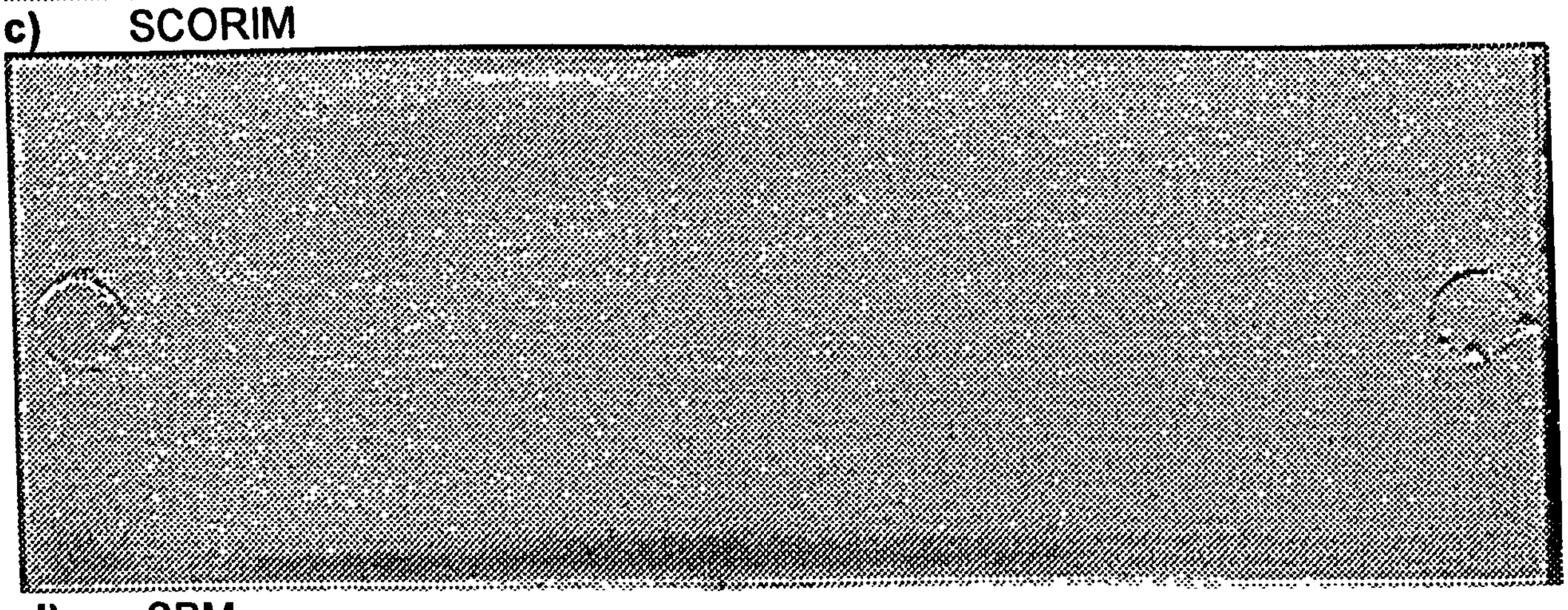

d) SBM

Figure 3.1 Images of the surface appearances of the weld line with 2% ET2025 Al flake in PP after processing with the four techniques

a) Conventional

b) BSM

c) SCORIM

d) SBM

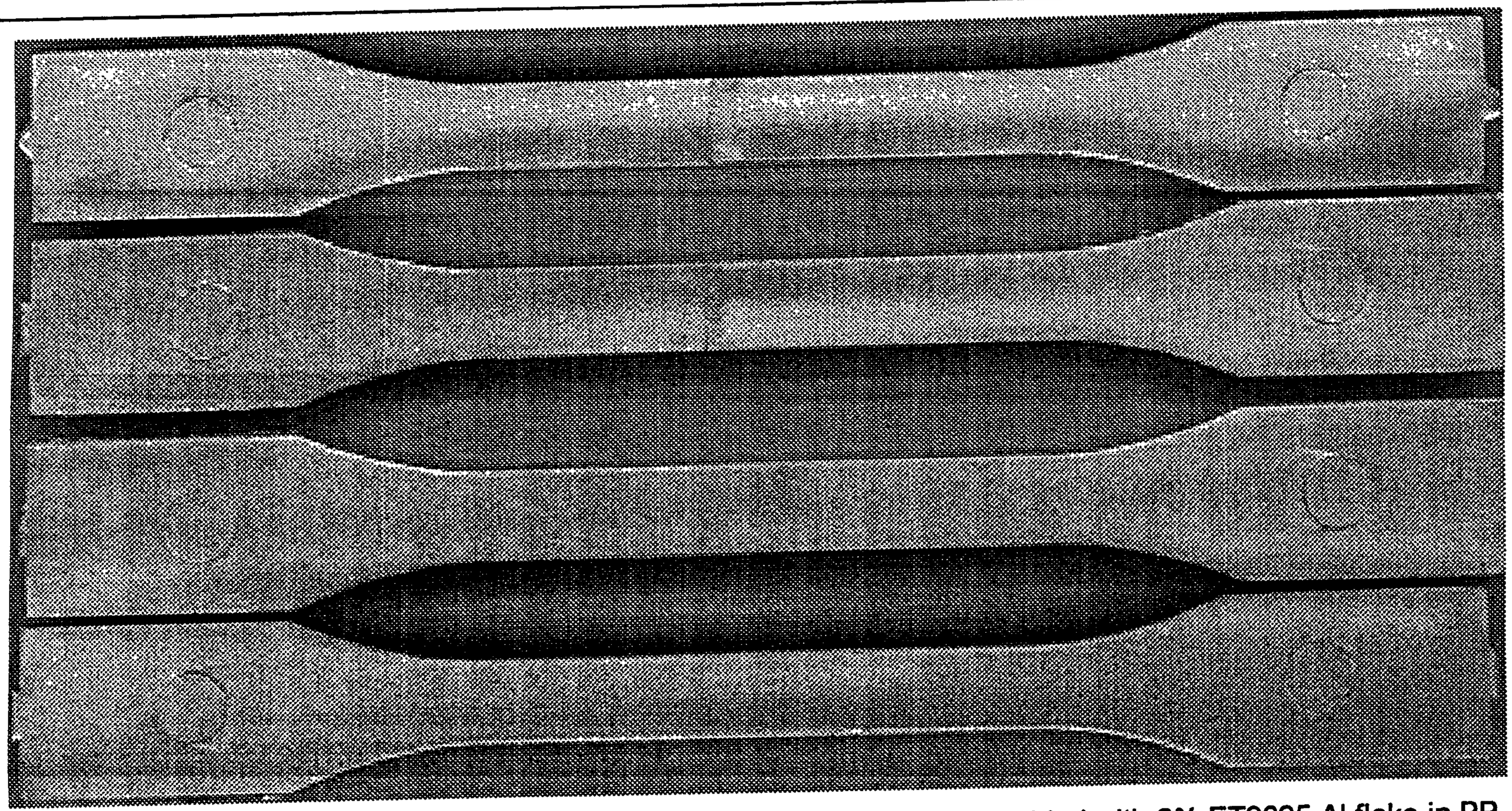

Figure 3.2 Images of the surface appearances of the weld line with dumbbell mouldings moulded with 2% ET2025 Al flake in PP after processing with the four techniques.

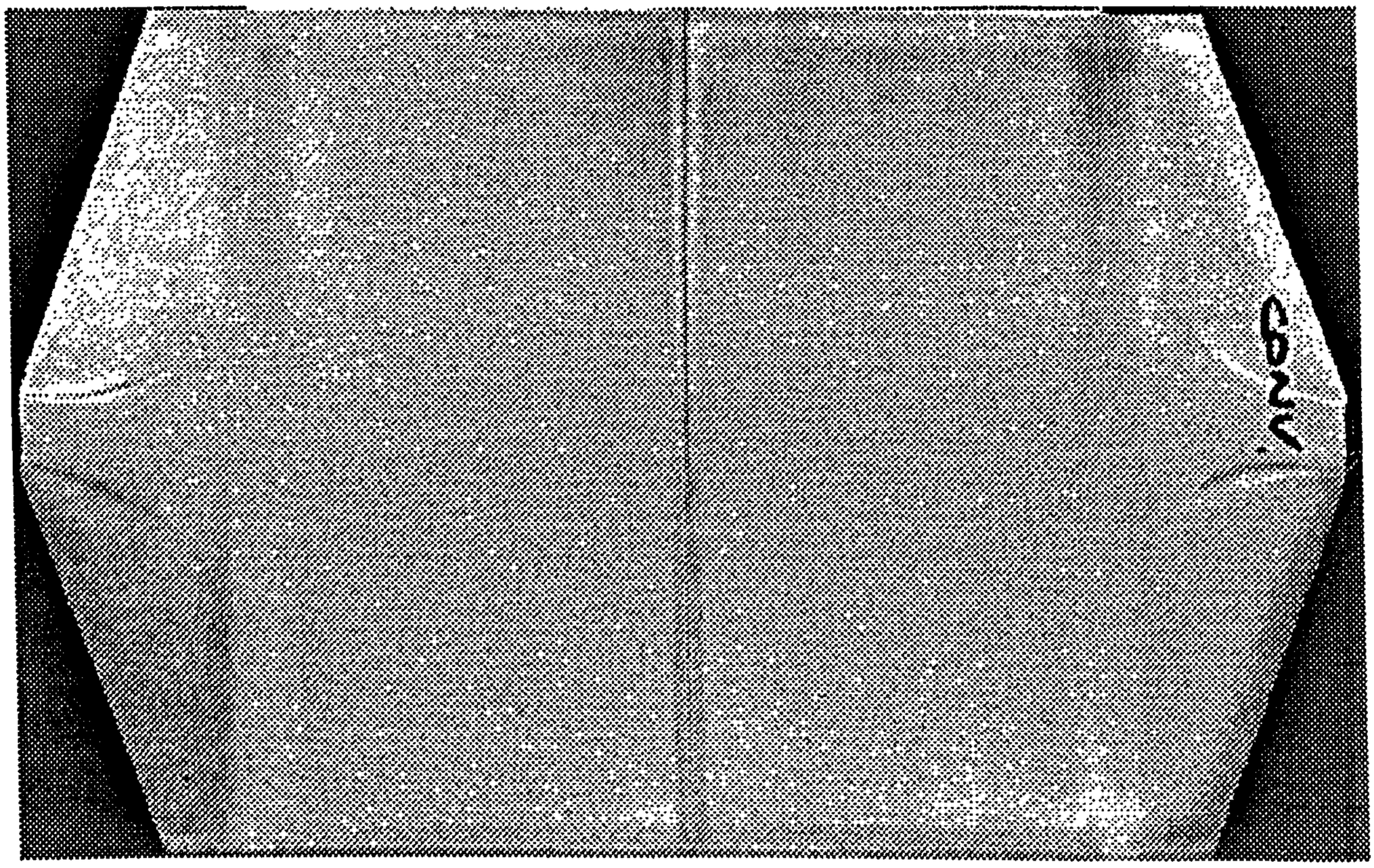

a) Conventional moulding

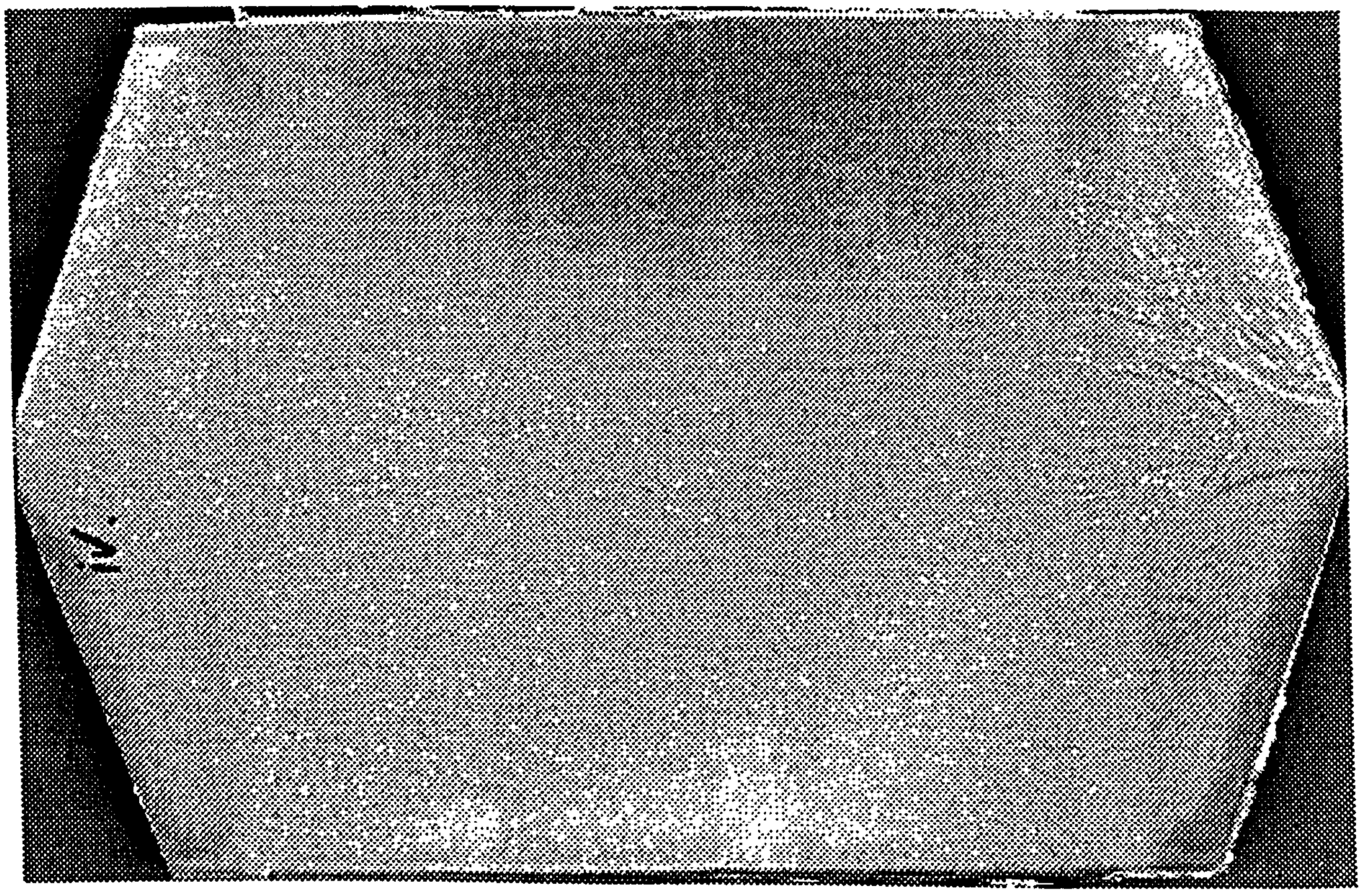

b) SBM

Figure 3.3 Images of the surface appearances of the weld line with 2% ET2025 Al flake in PP after processing conventionally and with SBM. The moulding dimensions are 108 x 108 x 3mm and was fed by two opposite fan gates.

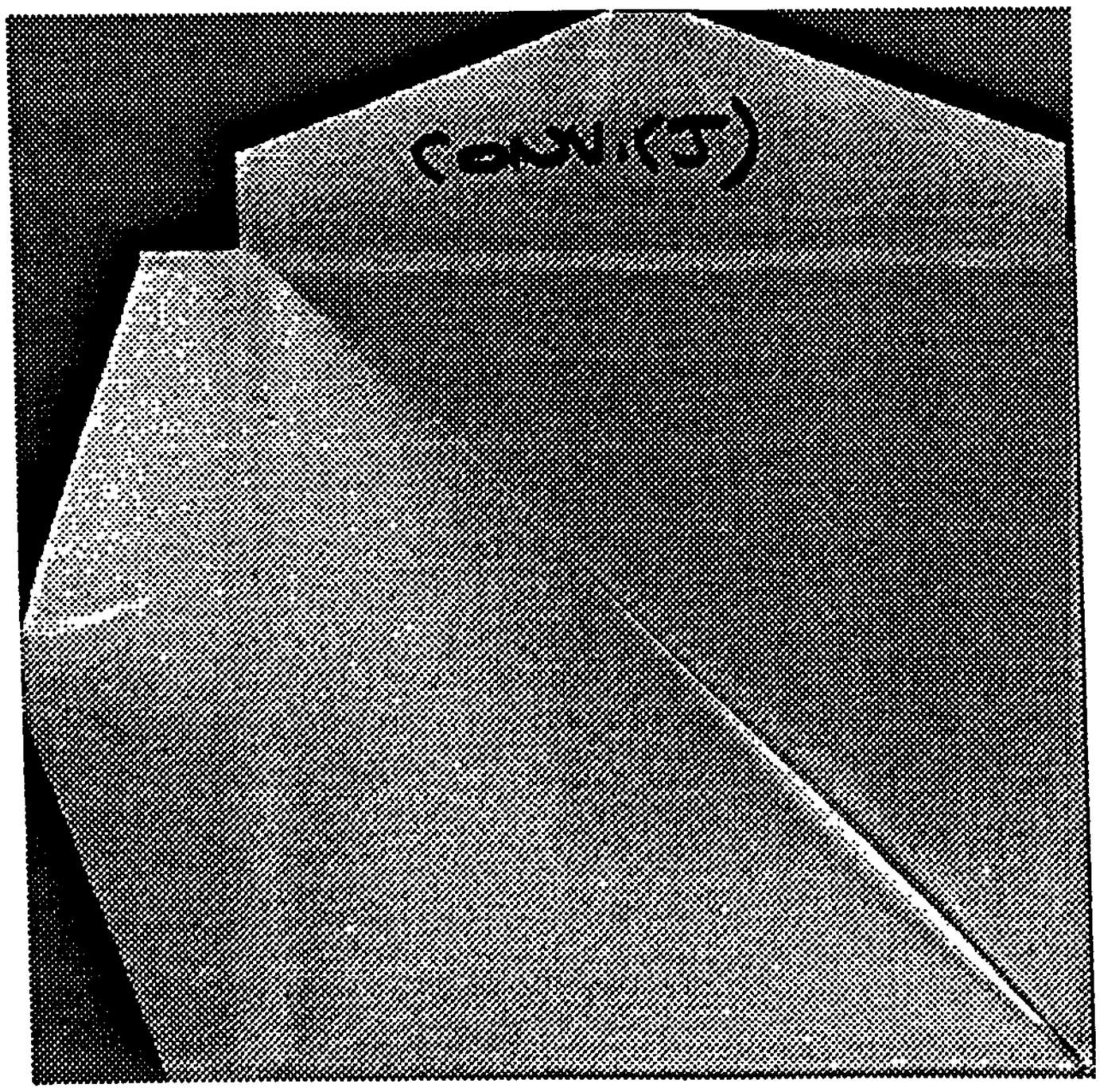

a) Conventional moulding

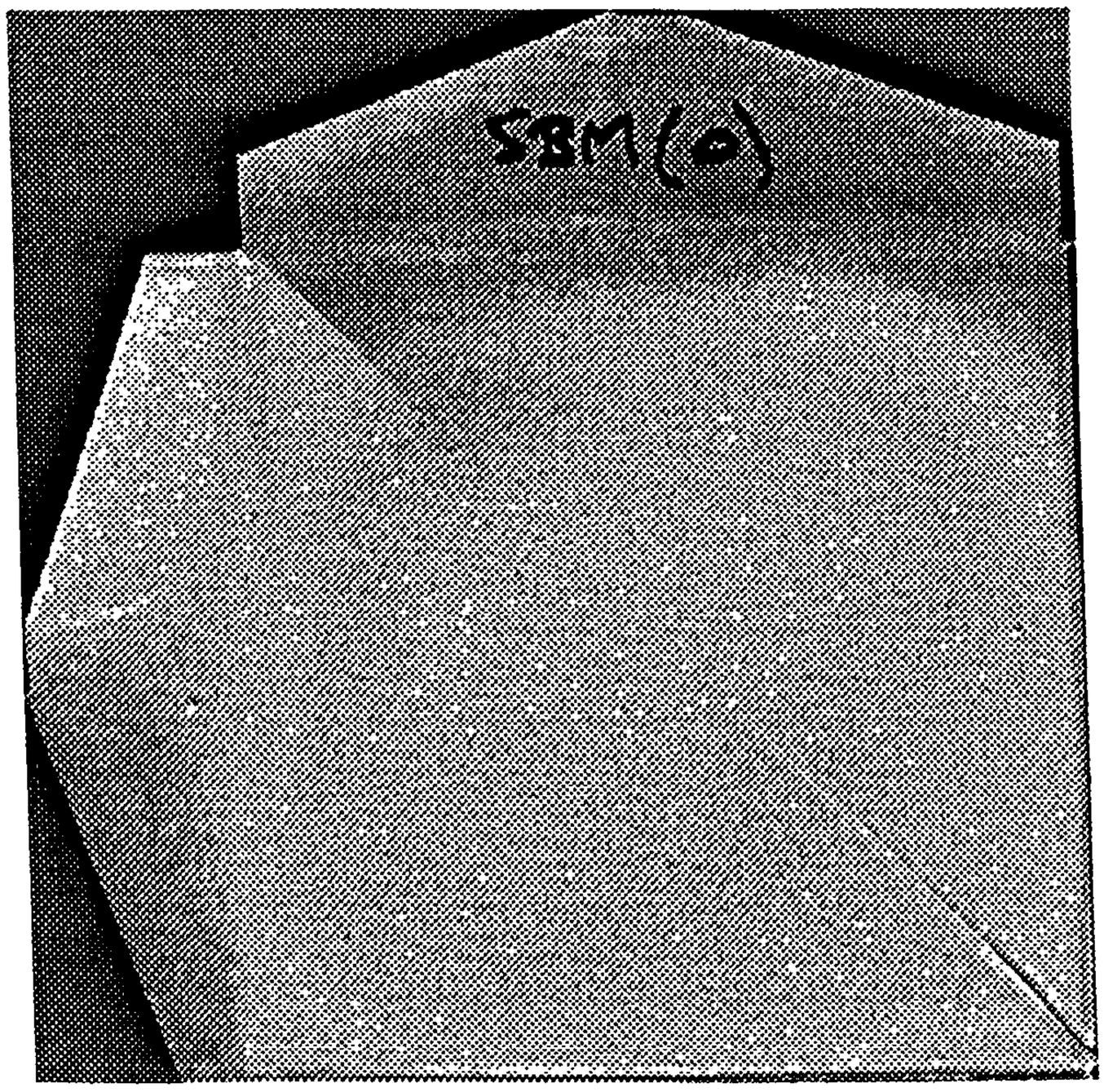

b) SBM

Figure 3.4 Images of the surface appearances of the weld line with 2% ET2025 Al flake in PP after processing conventionally and with SBM. The moulding dimensions are 108 x 108 x 3mm and were fed by two adjacent fan gates.

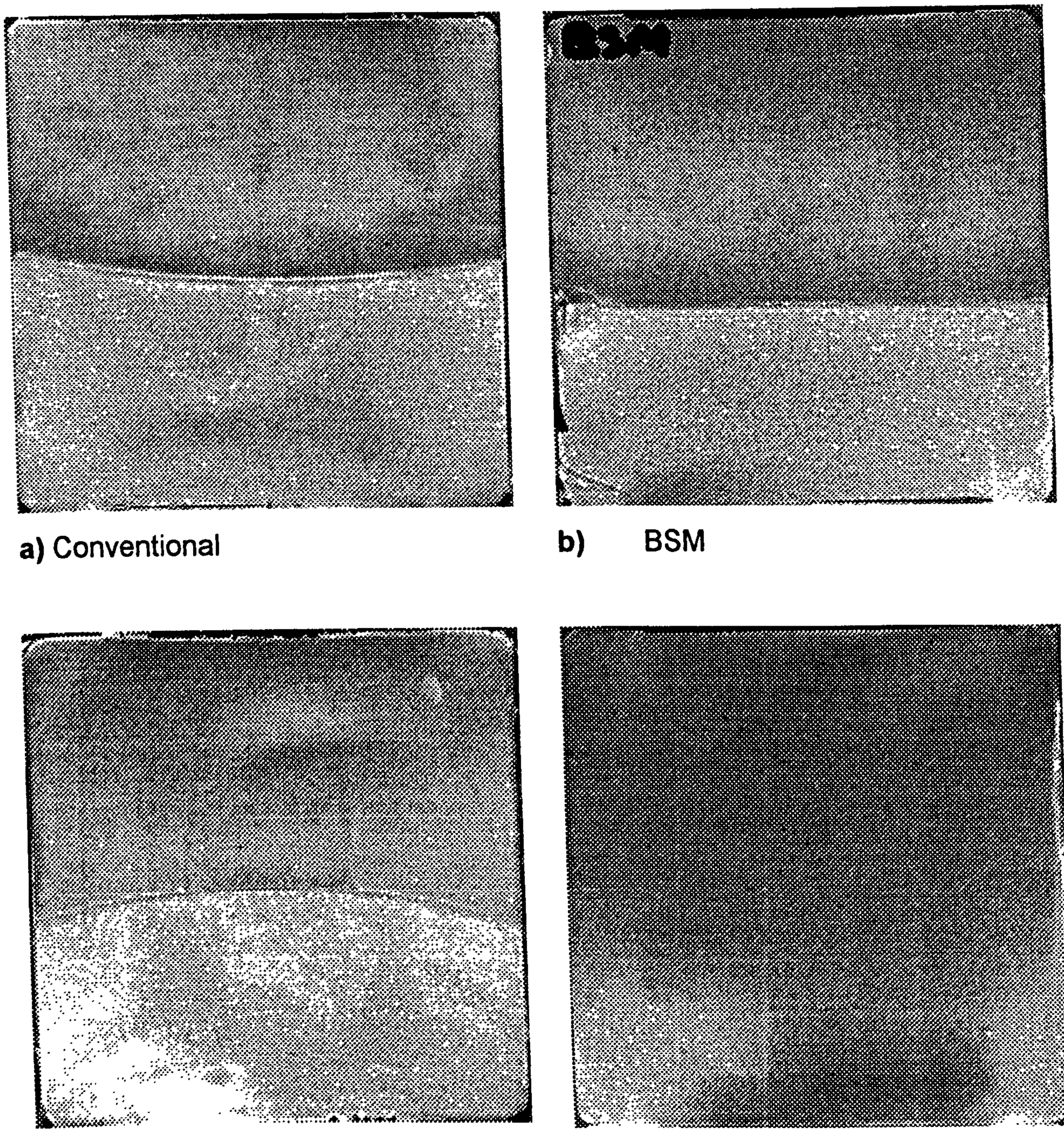

a) Conventional

b) BSM

c) SCORIM

d) SBM

Figure 3.5 Images of the surface appearances of the weld line with 2% ET2025 Al flake in PP after processing using the four techniques. The moulding dimensions are 84 x 84 x 1.5mm and were fed by two opposite fan gates.

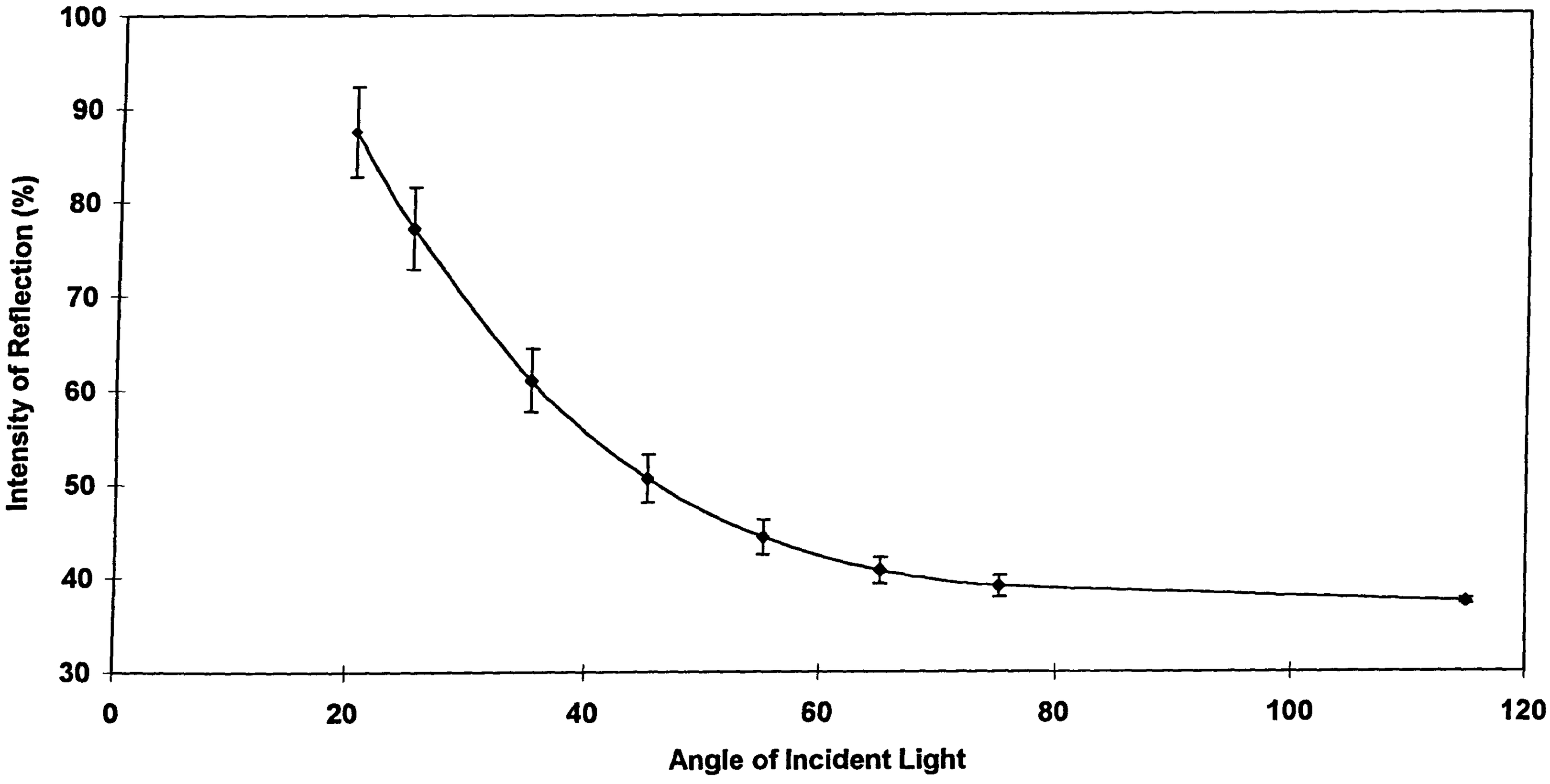

Figure 3.6 Typical results from the range of angles measured of 2% Al flake in PP moulded rectangular plaques. The samples here were moulded conventionally.

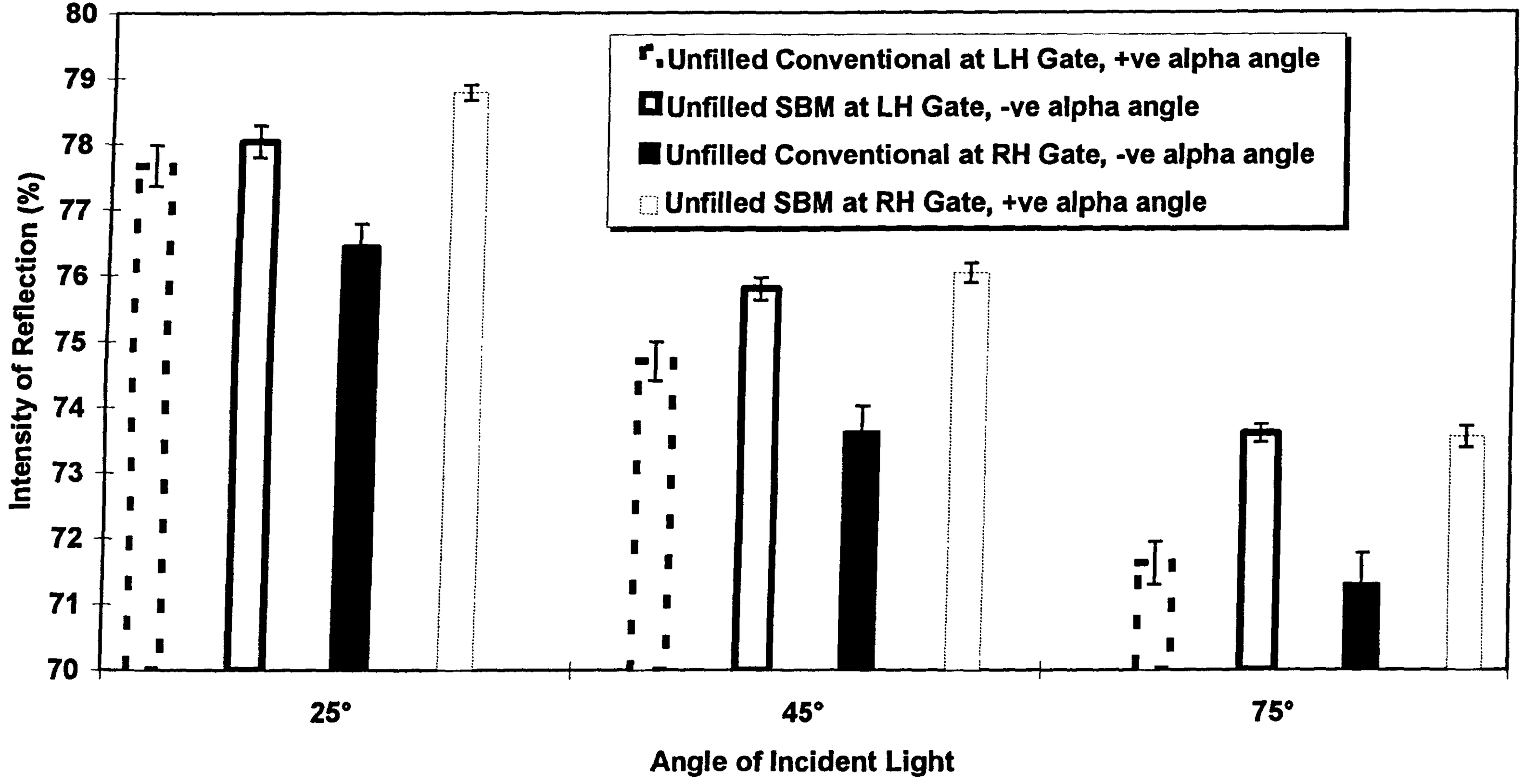

Figure 3.7 Light reflectivity measurements taken from natural PP rectangular plaques moulded conventionally and with SBM. Measurements were taken at both gates as depicted in figure 2.10a.

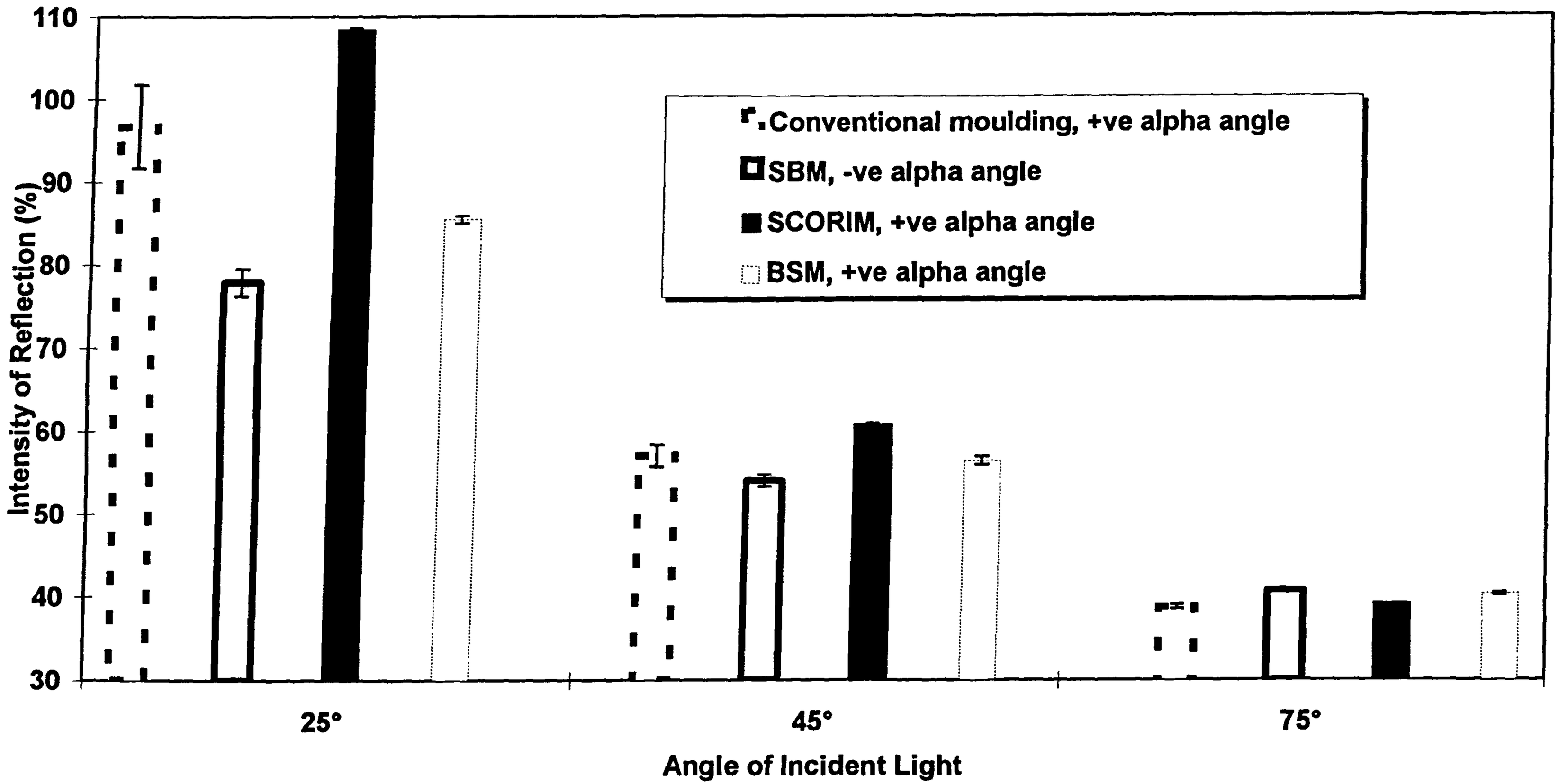

Figure 3.8 Comparisons of reflections from 2% Al flake in PP rectangular plaques moulded conventionally, with SBM, SCORIM and SBM. All measurements taken at the left gate as depicted in figure 2.10b.

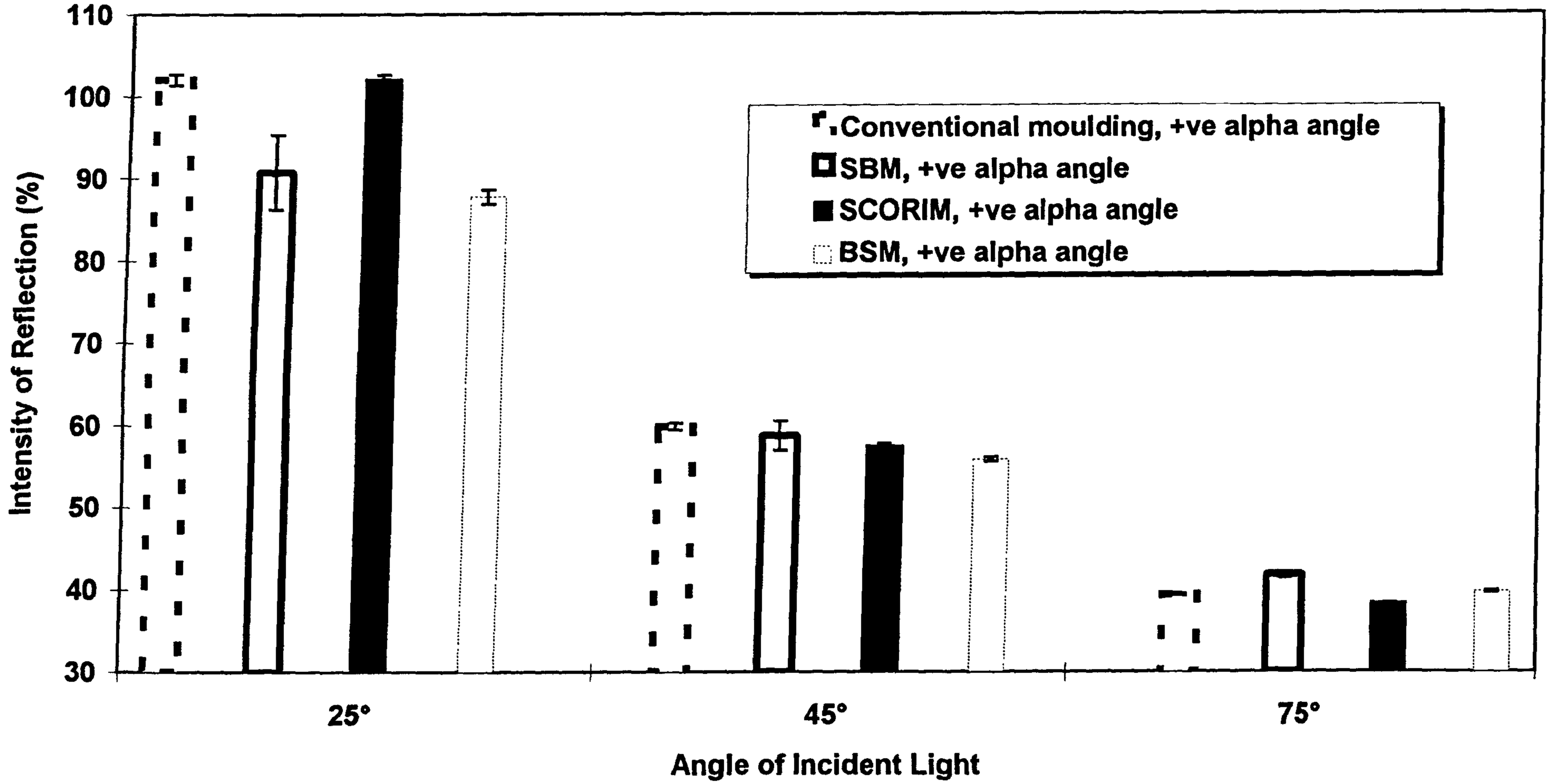

Figure 3.9 Comparisons of reflections from 2% Al flake in PP rectangular plaques moulded conventionally, with SBM, SCORIM and BSM. All measurements taken at the right gate as depicted in figure 2.10b.

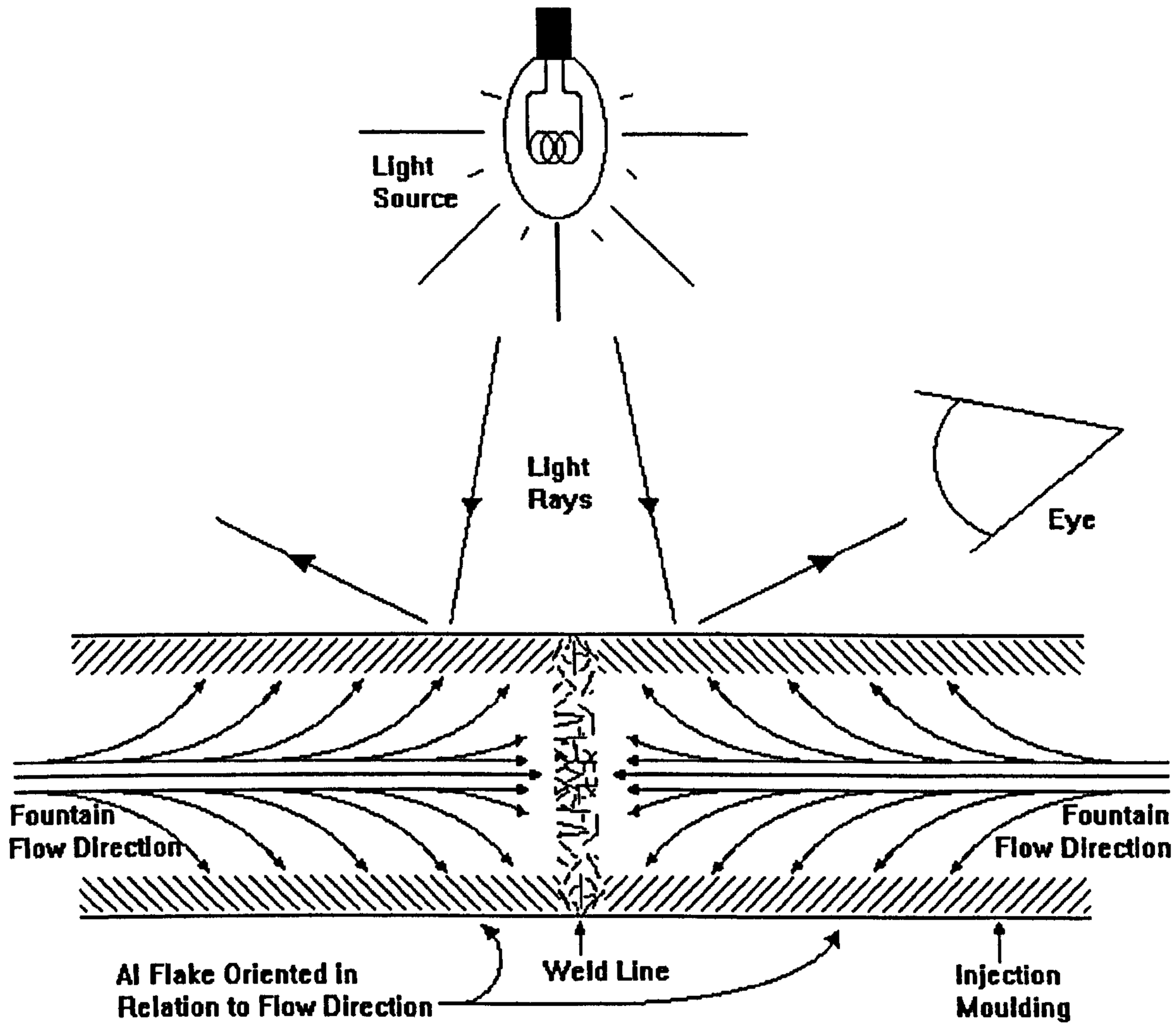

Figure 3.10 Schematic representation of the orientation induced into the Al flake during mould filling by the 'fountain flow' effect. The orientation is visible to the eye as a bright region where the Al flakes reflect light towards the eye and a dull region where light is reflected away., i.e. the 'flip-flop' effect.

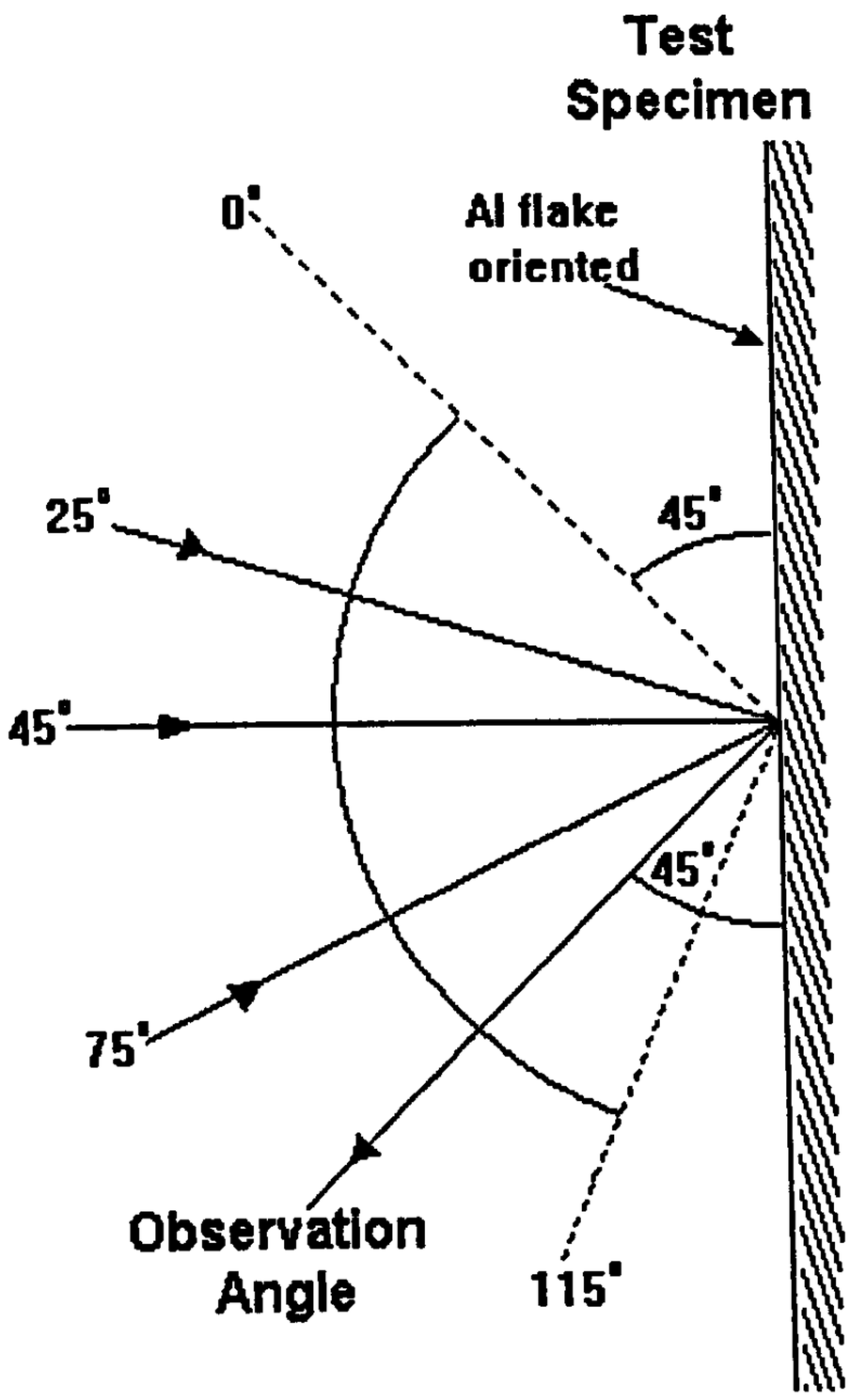

a) Al flake oriented with a positive α-angle

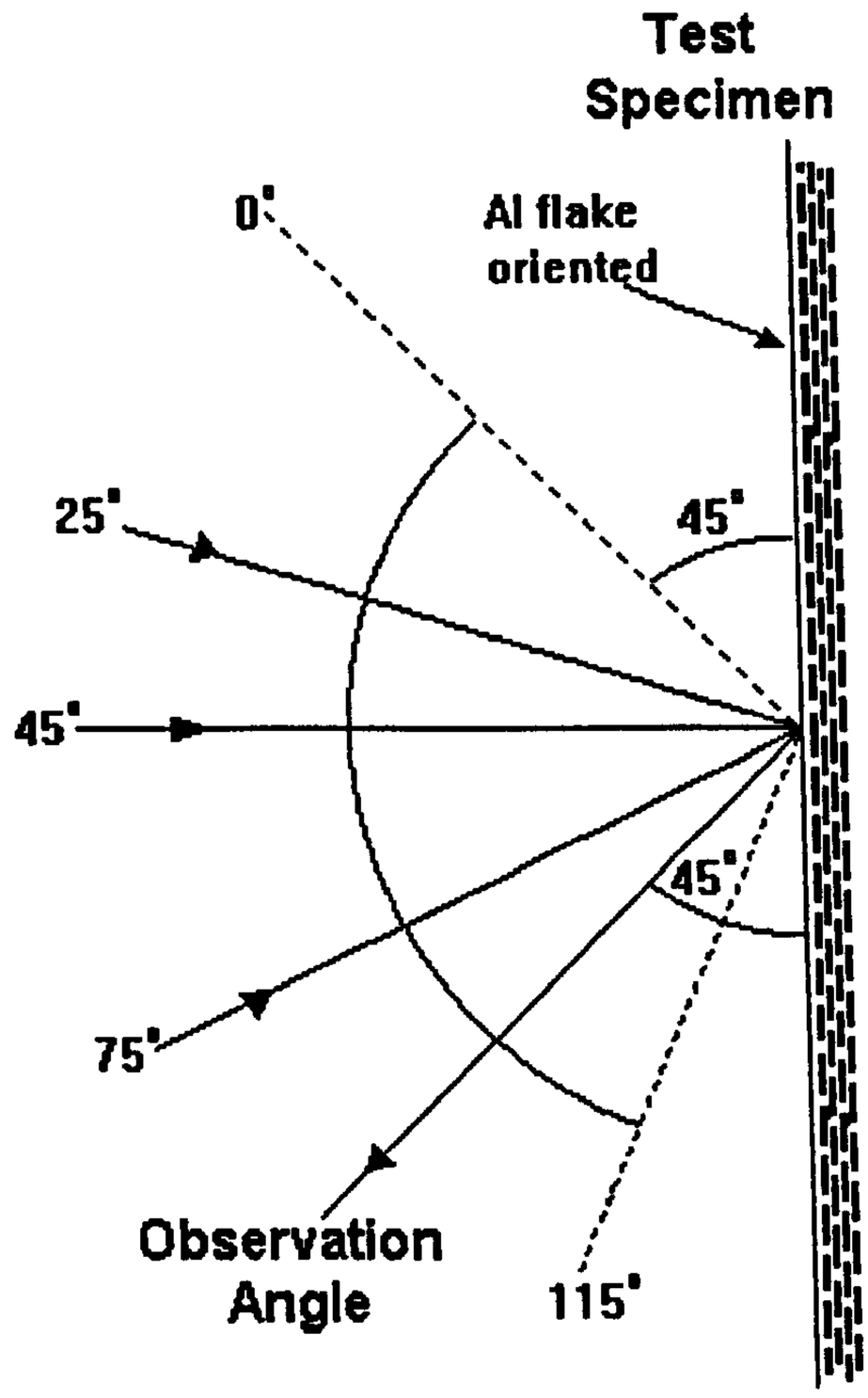

b) Al flake oriented parallel to the moulding surface, i.e. $\alpha = 0°$.

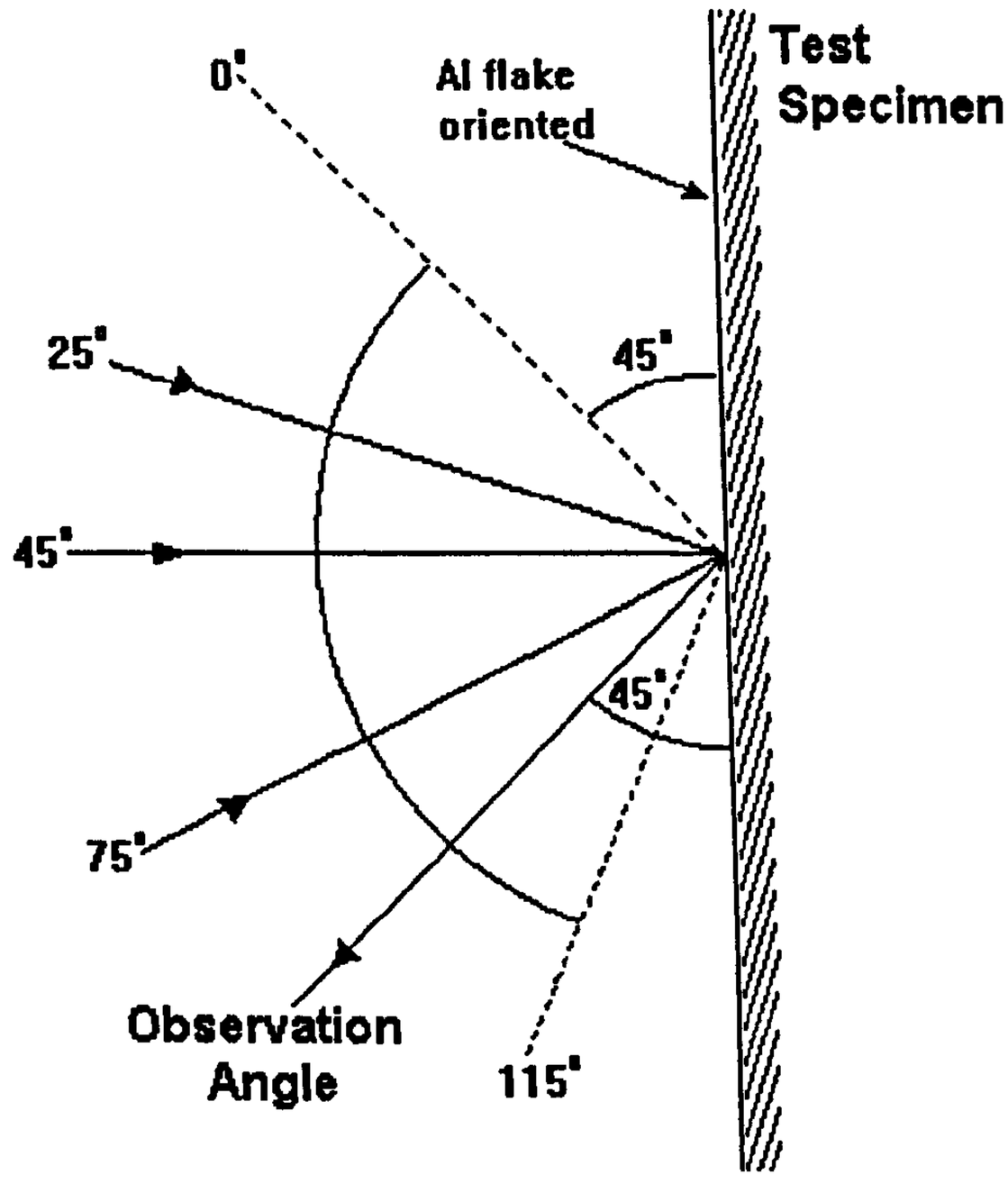

c) Al flake oriented with a negative α-angle.

Figure 3.11 Schematic illustration of the three principle Al flake orientations present in the moulded samples and identified by the GSP.

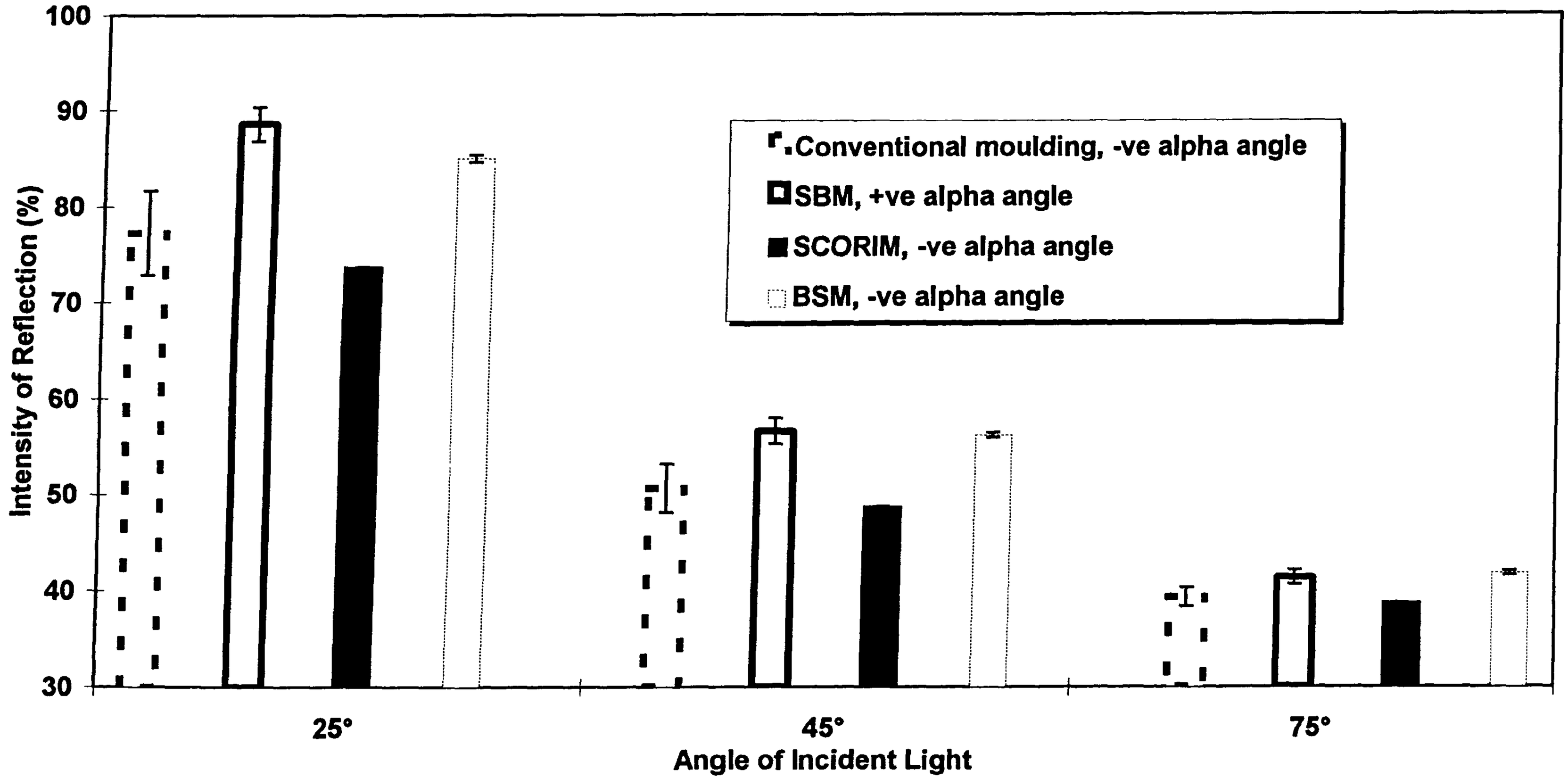

Figure 3.12 Comparisons of reflections from 2% Al flake in PP rectangular plaques moulded conventionally, with SBM, SCORIM and BSM. All measurements taken at the left hand gate as depicted in figure 2.10a.

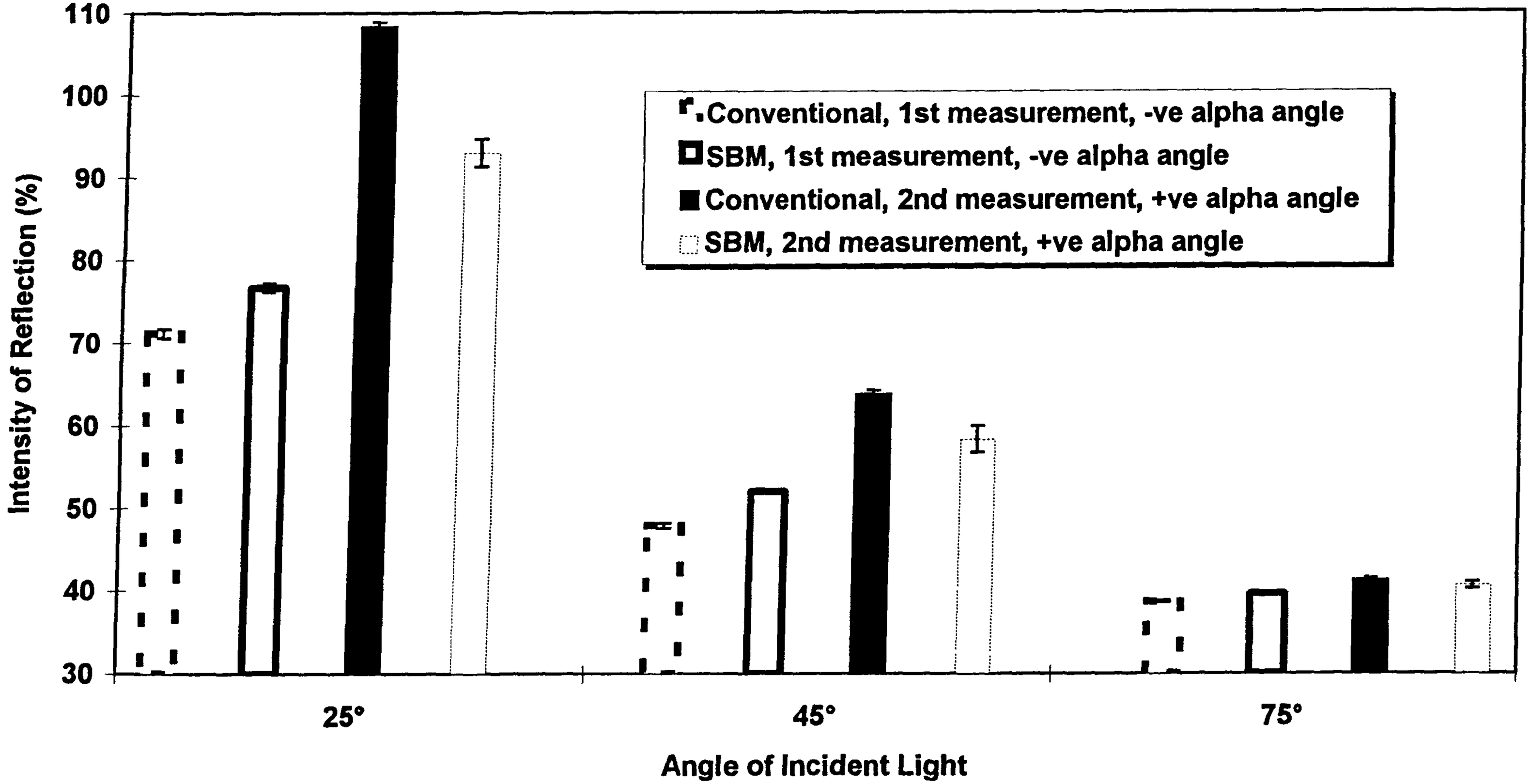

Figure 3.13 Reflectivity's from 2% Al in PP conventional and SBM square plaque mouldings of dimensions 108x 108x 3mm. Measurements taken from the left gate, as shown in figure 2.10c, for comparison of positive and negative α-angles of the Al flake.

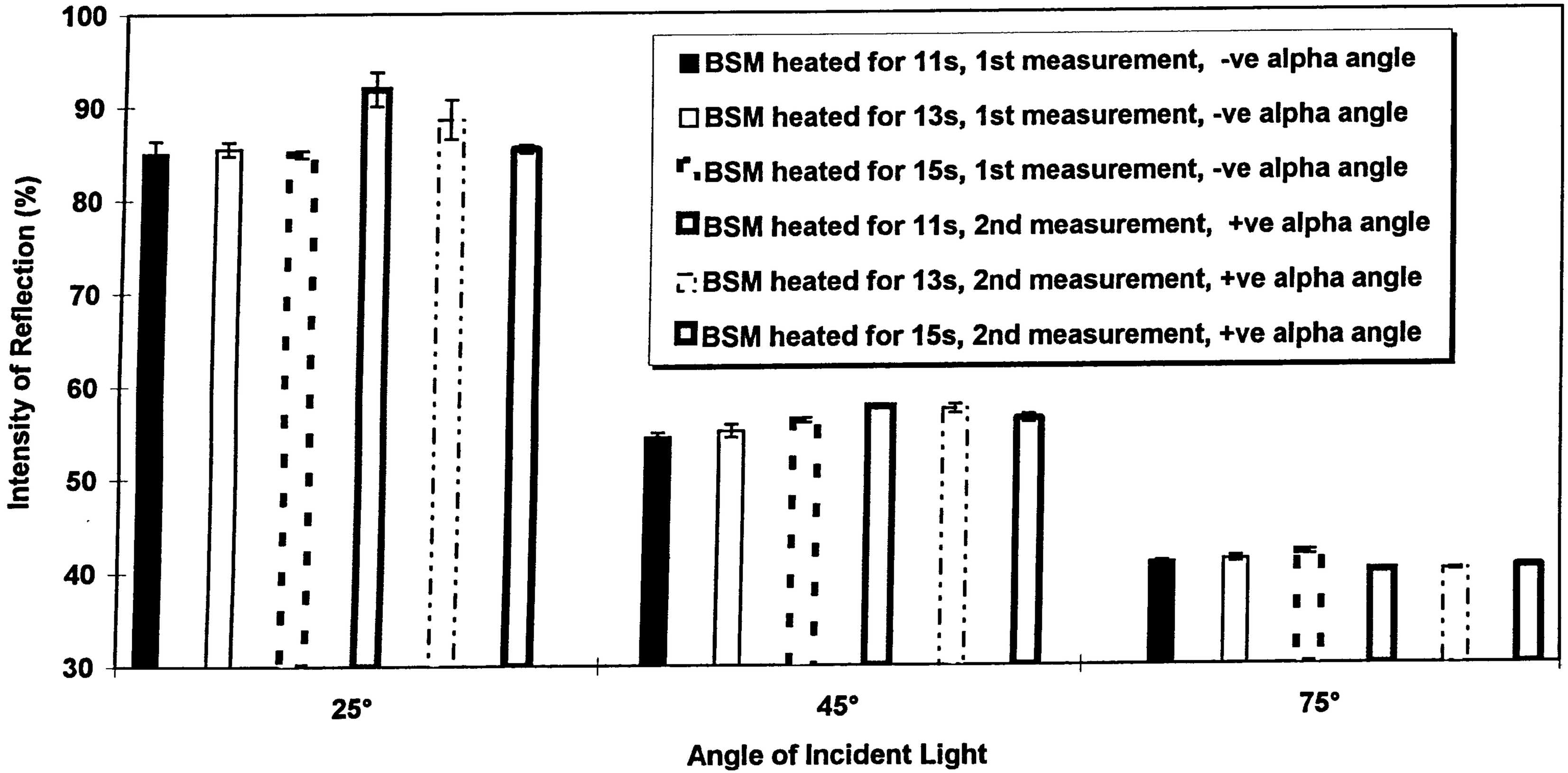

Figure 3.14 Comparisons of 2% Al in PP BSM rectangular plaque mouldings produced with different heating times. Measurements taken from the left gate, as shown in figure 2.10c, for comparison of positive and negative α-angles of the Al flake.

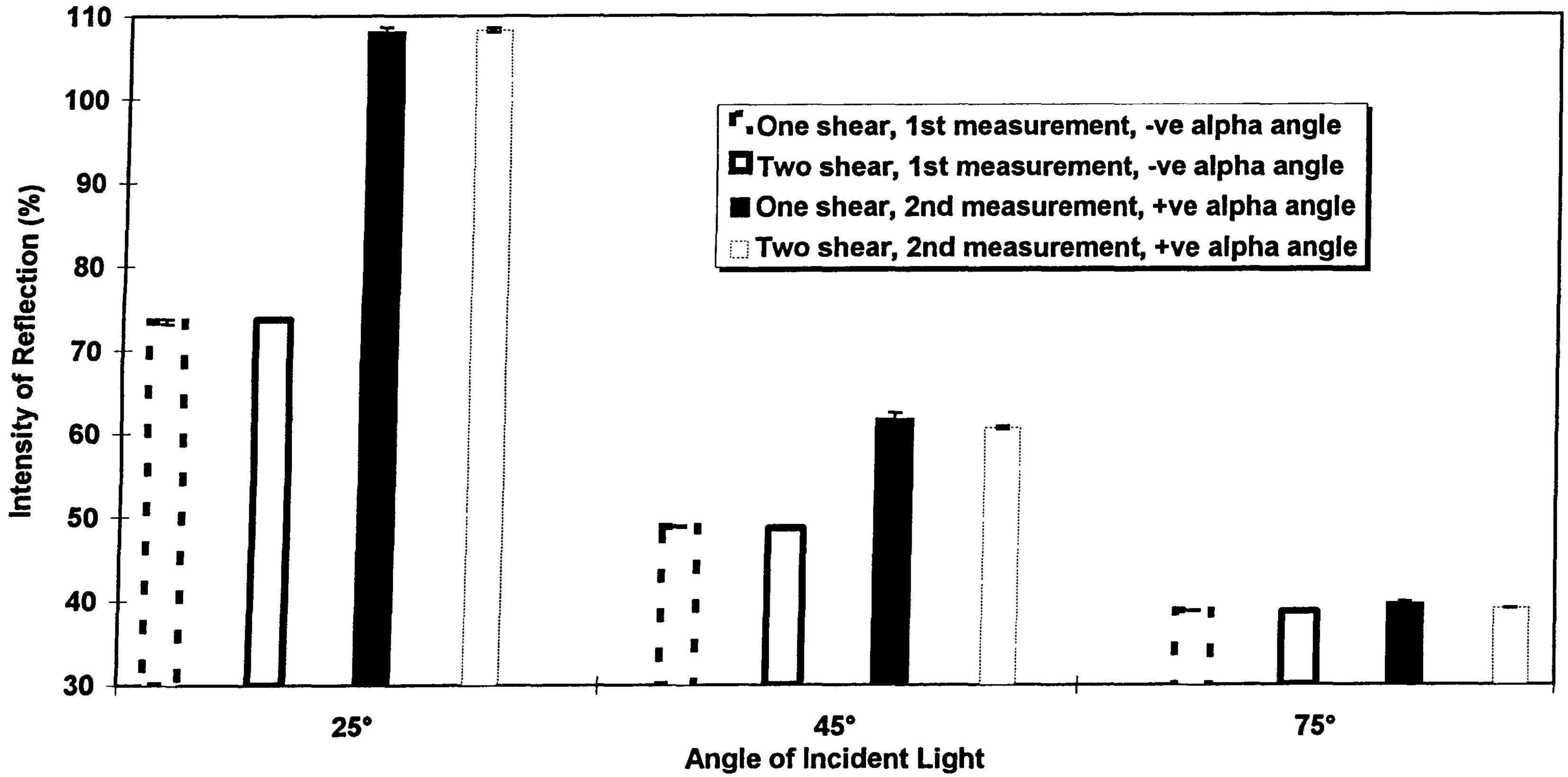

Figure 3.15 Comparisons of reflections from 2% Al in PP SCORIM rectangular plaque mouldings produced using one and two shears. All measurements taken from the left gate as shown in figure 2.10c to compare positive and negative α-angles.

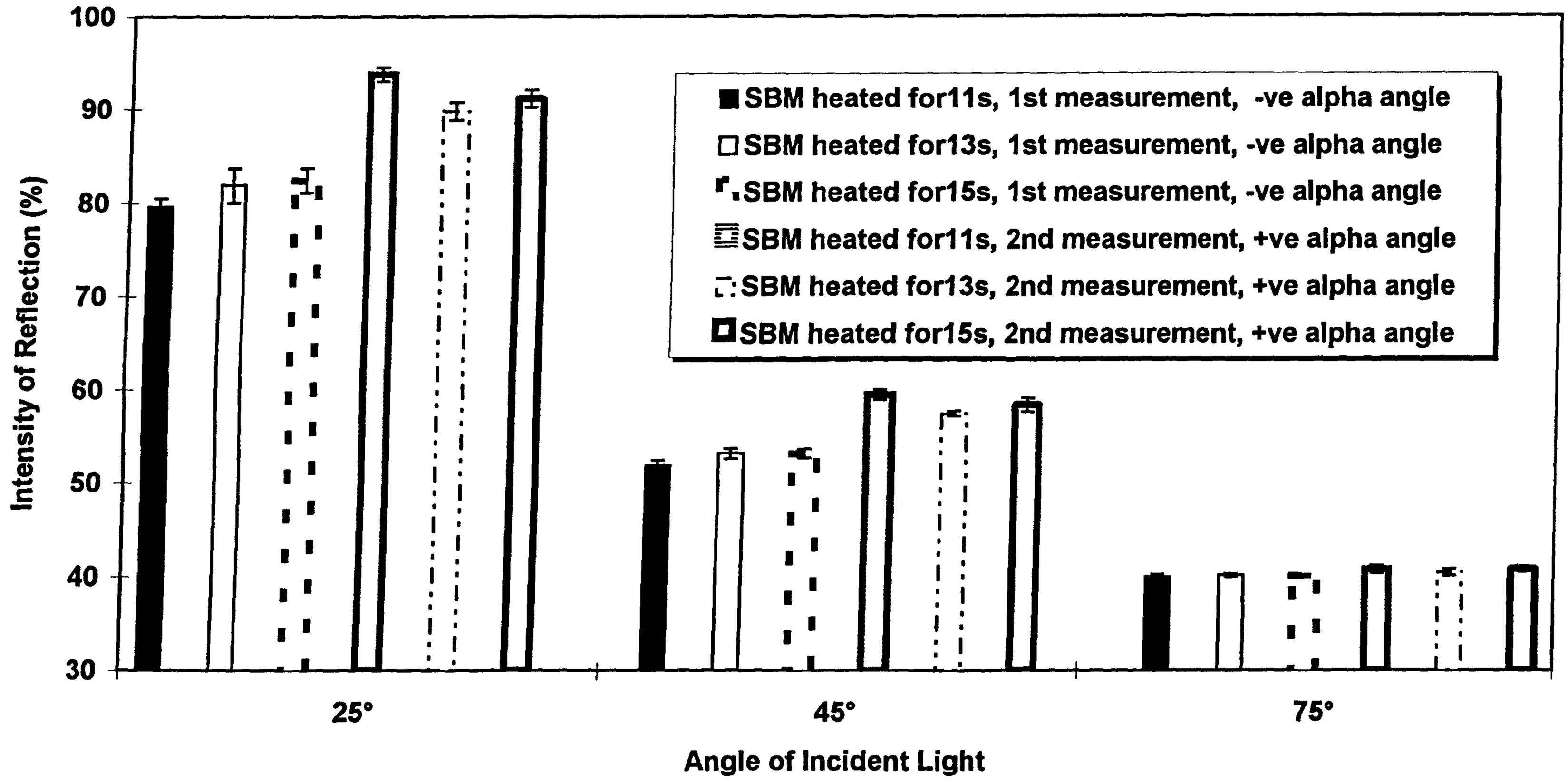

Figure 3.16 Comparisons of 2% Al in PP SBM rectangular plaque mouldings produced with different heating times. All measurements taken at the left gate, as depicted in figure 2.10c, for comparison of positive and negative α-angles of the Al flake.

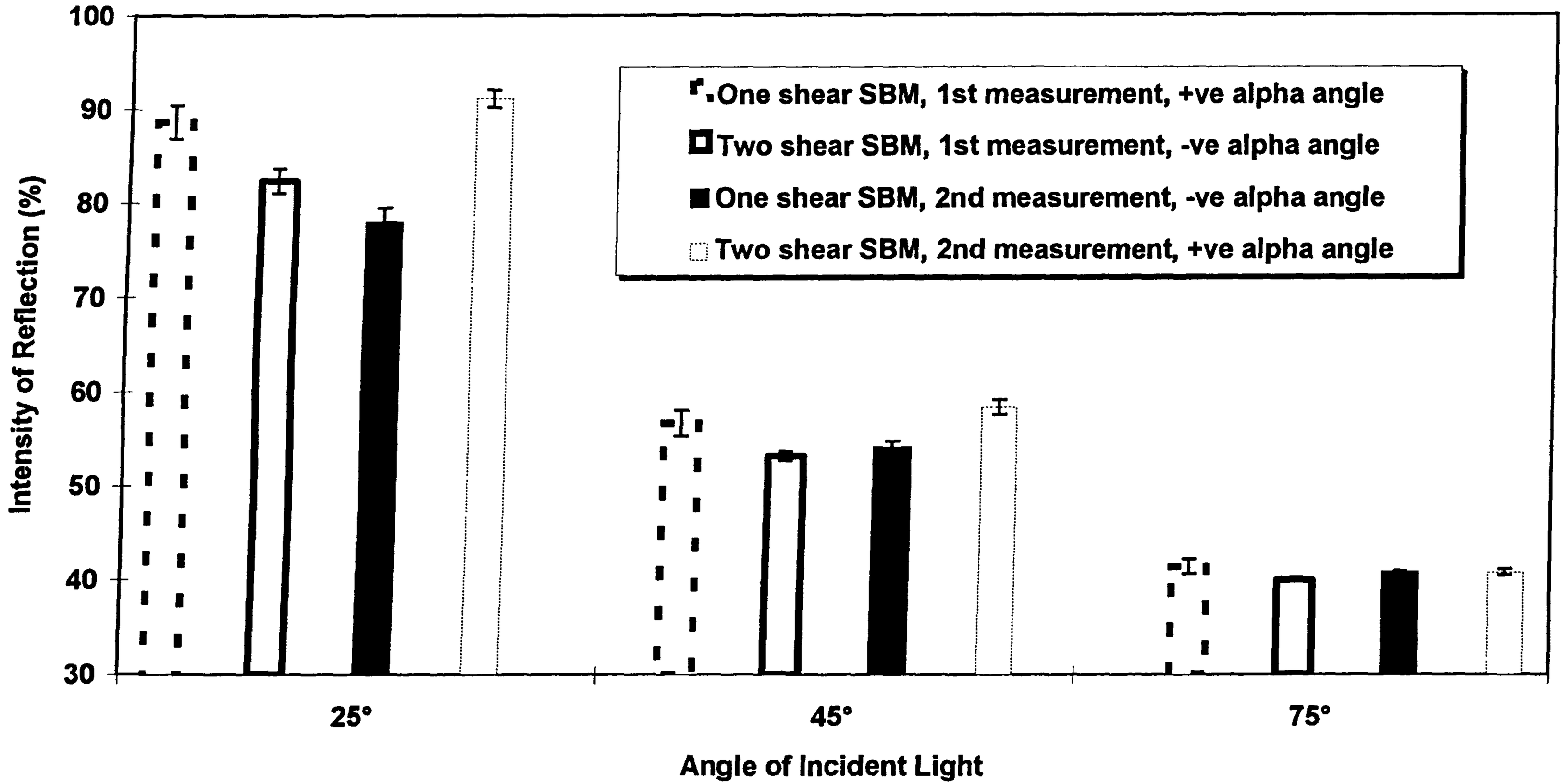

Figure 3.17 Comparisons of reflections from 2% Al in PP SBM rectangular plaque mouldings produced using one and two shears respectively. All measurements taken from the left gate as shown in figure 2.10c to compare positive and negative α-angles.

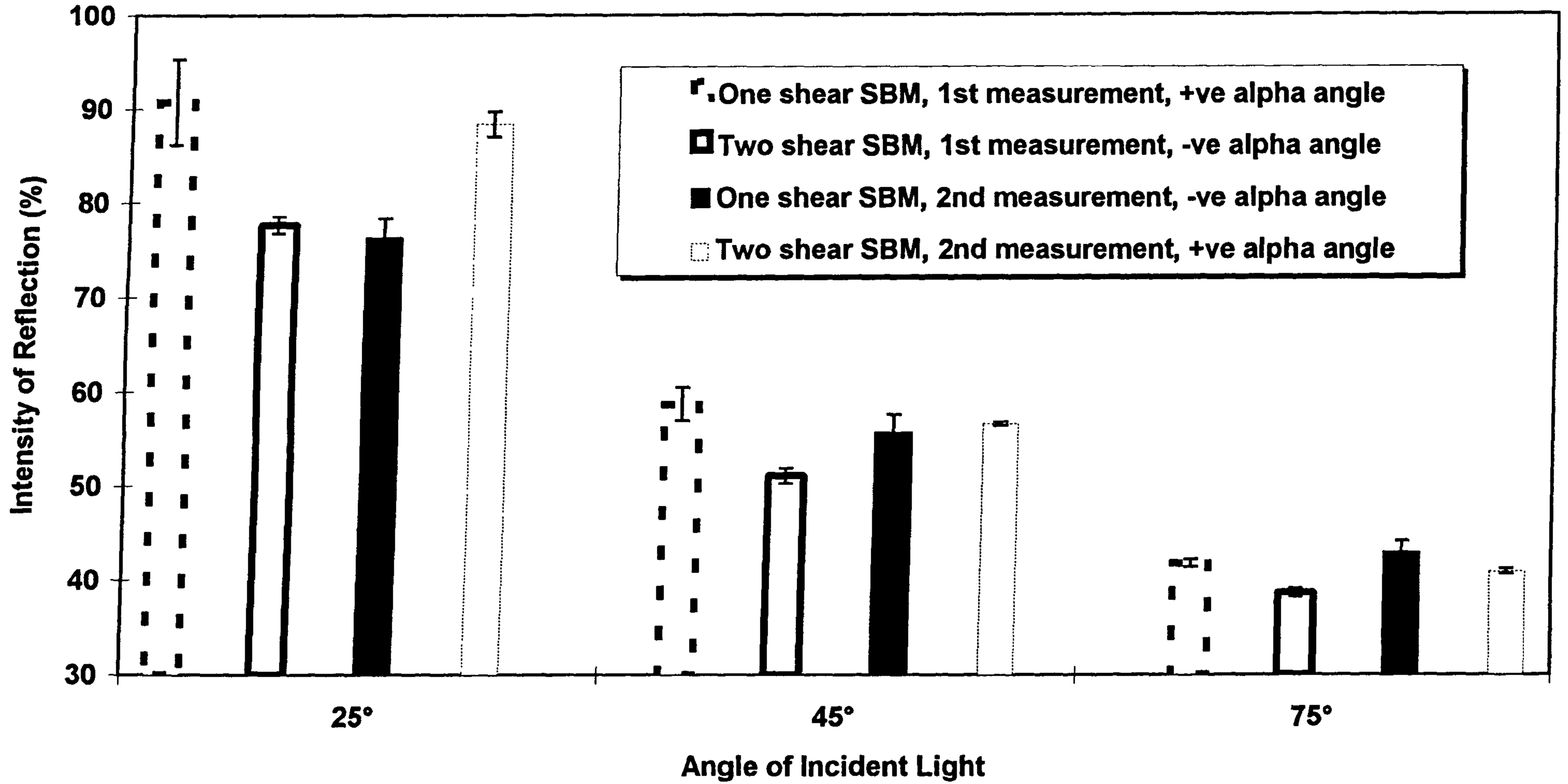

Figure 3.18 Comparisons of reflections from 2% Al in PP SBM rectangular plaque mouldings produced using one and two shears respectively. All measurements taken from the right gate as shown in figure 2.10d to compare positive and negative α-angles.

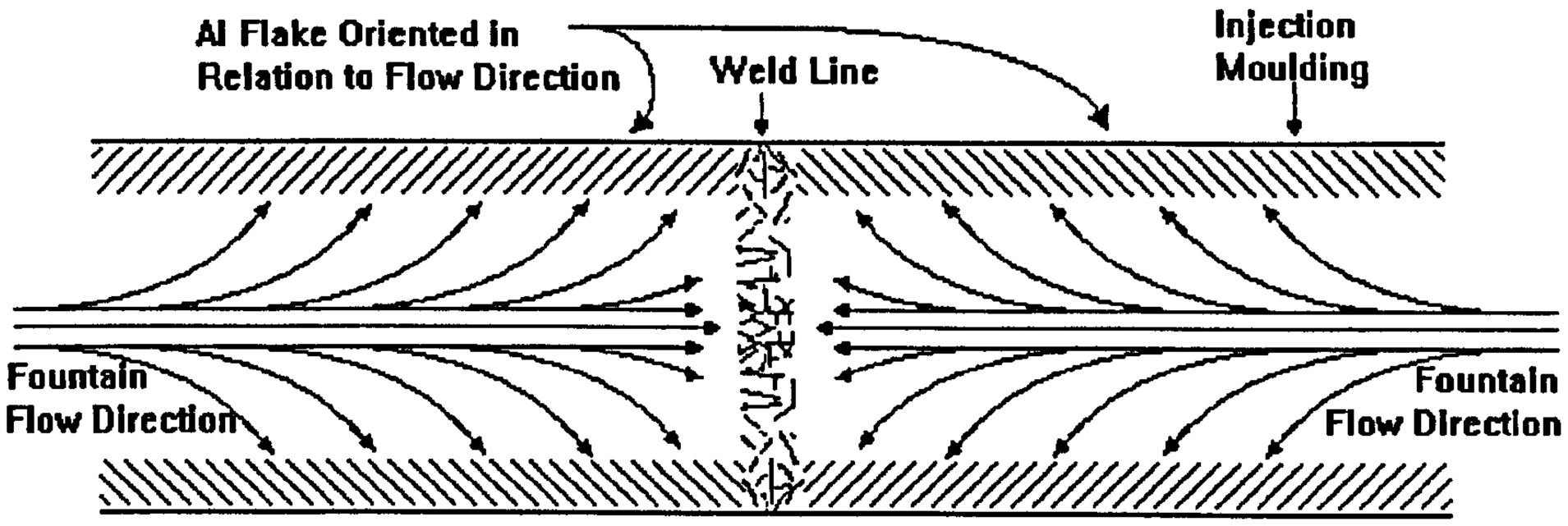

a) Conventional moulding exhibiting both positive and negative α-angles, i.e. the 'flip-flop' effect present with two orientations.

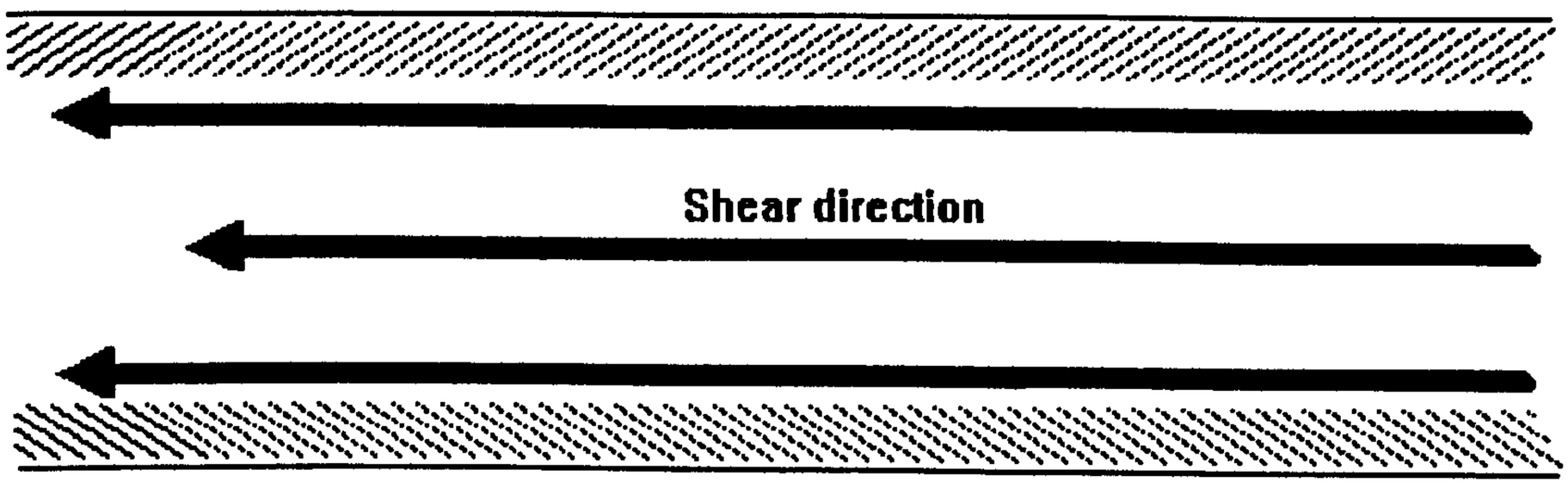

b) SBM moulding with one shear orients all the Al flake in the shear direction eliminating the weld line and unifying the 'flip-flop' effect direction.

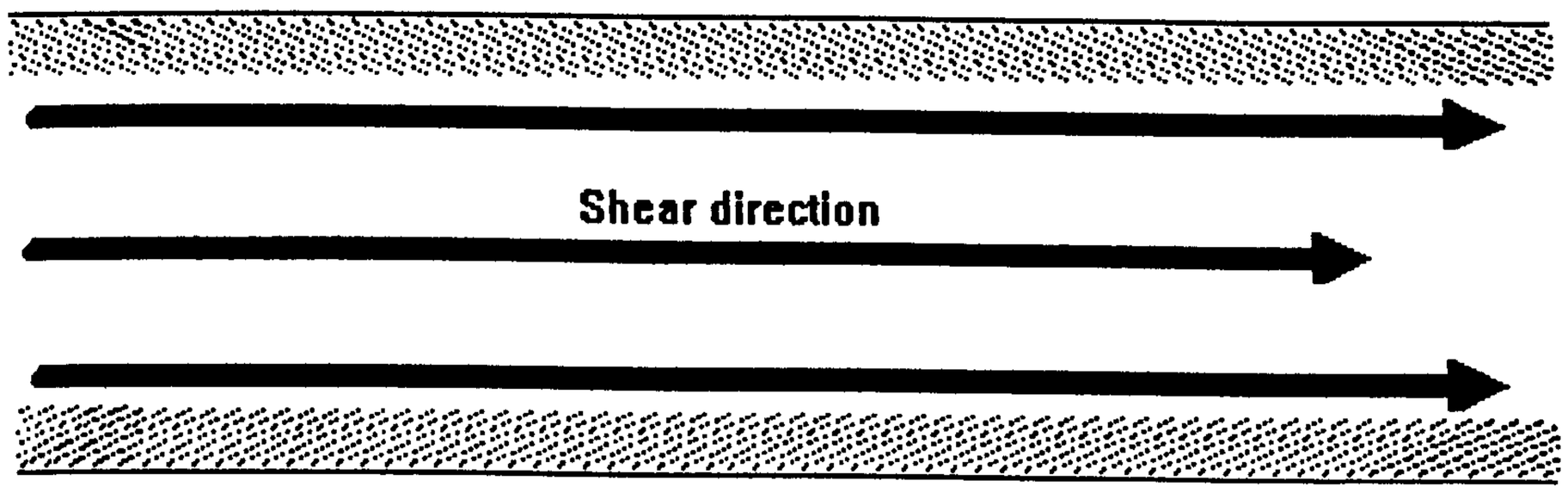

c) SBM moulding with two shears reverses the Al flake orientation induced by the first shear, although the flake orientation with the second shear is more acute to the moulding surface, i.e. $\alpha \rightarrow 0°$.

Figure 3.19 Schematic illustration of the Al flake orientation during conventional moulding and the subsequent orientations induced by the SBM process resulting in weld line removal.

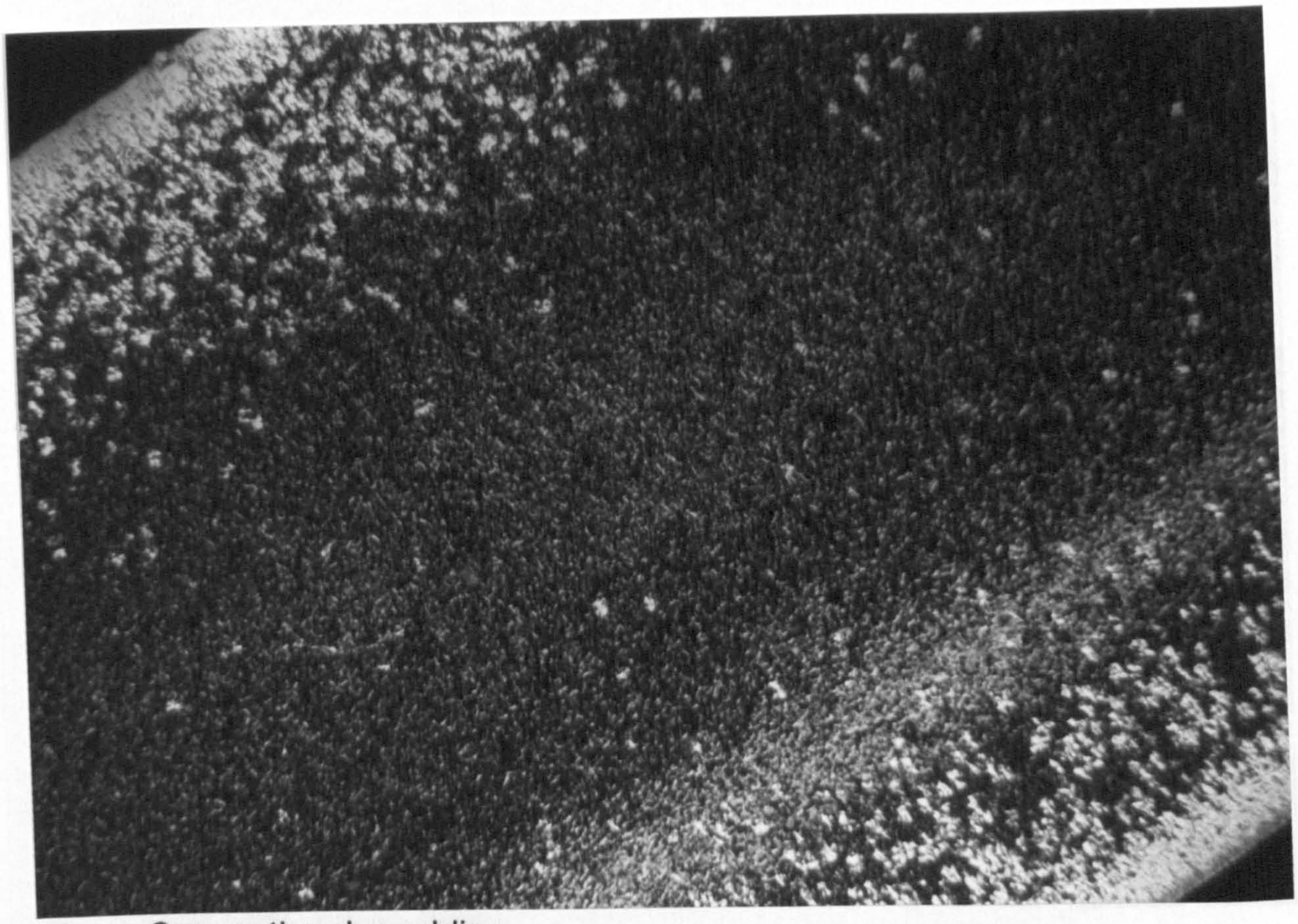

a) Conventional moulding

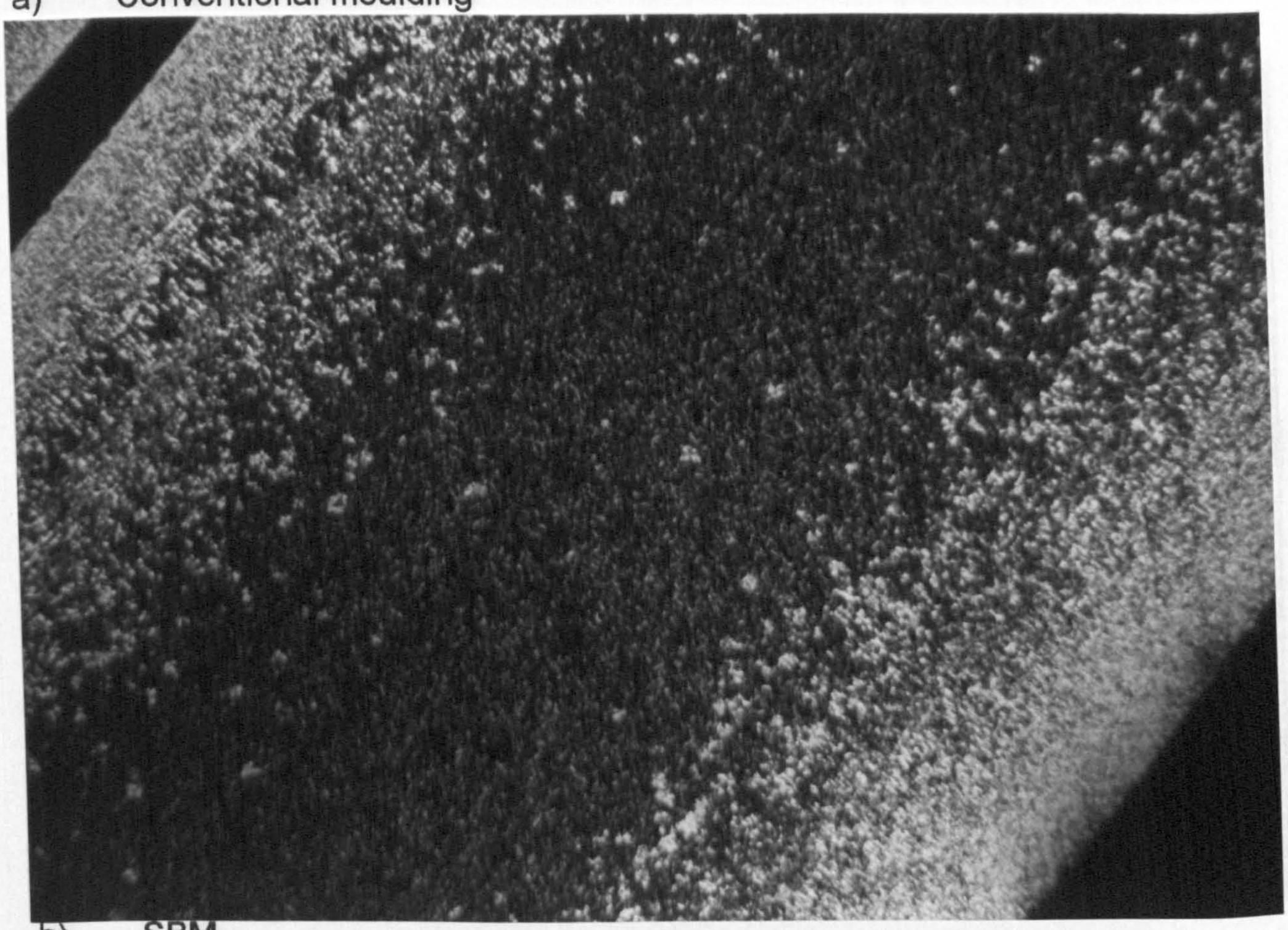

b) SBM

Figure 3.20 Microtomed sections of 4mm thick, 2% ET2025 Al pigmented iPP rectangular plaque mouldings, sectioned parallel to flow and viewed using polarised LM.

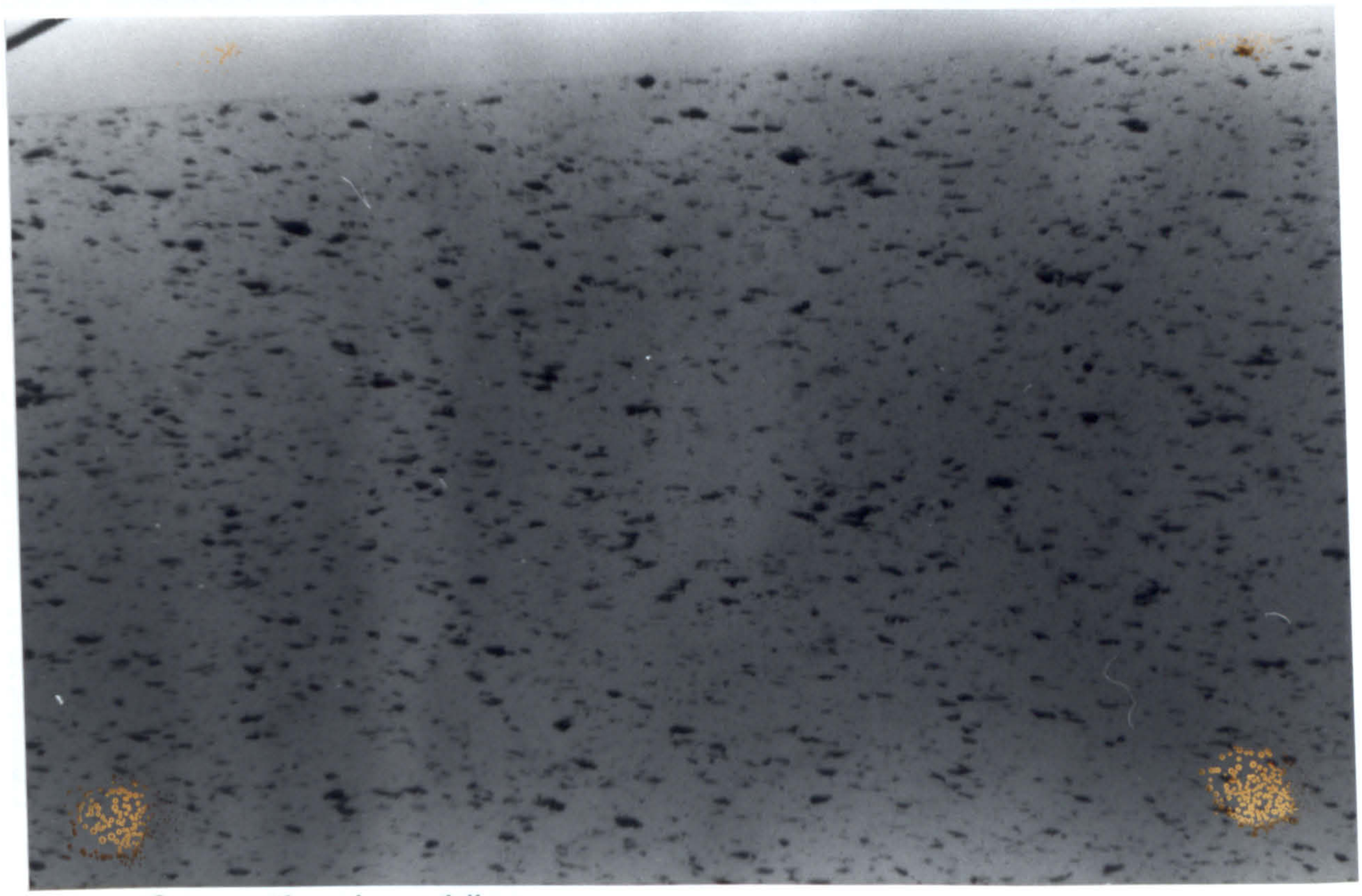

a) Conventional moulding

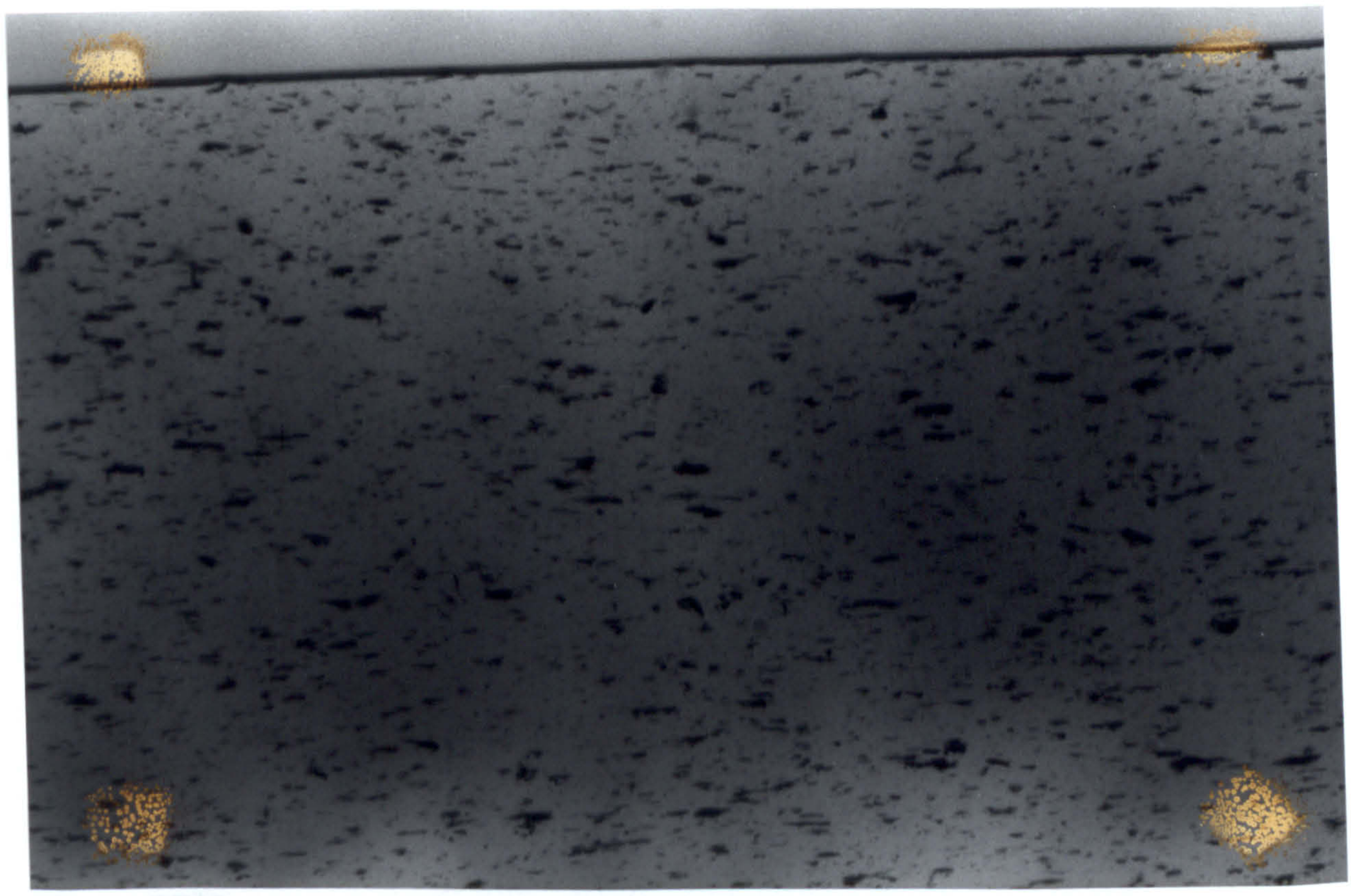

b) SBM

Figure 3.21 Microtomed sections of 2% ET2025 Al pigmented iPP rectangular plaque mouldings, sectioned parallel to flow and viewed using polarised LM (magnification x90).

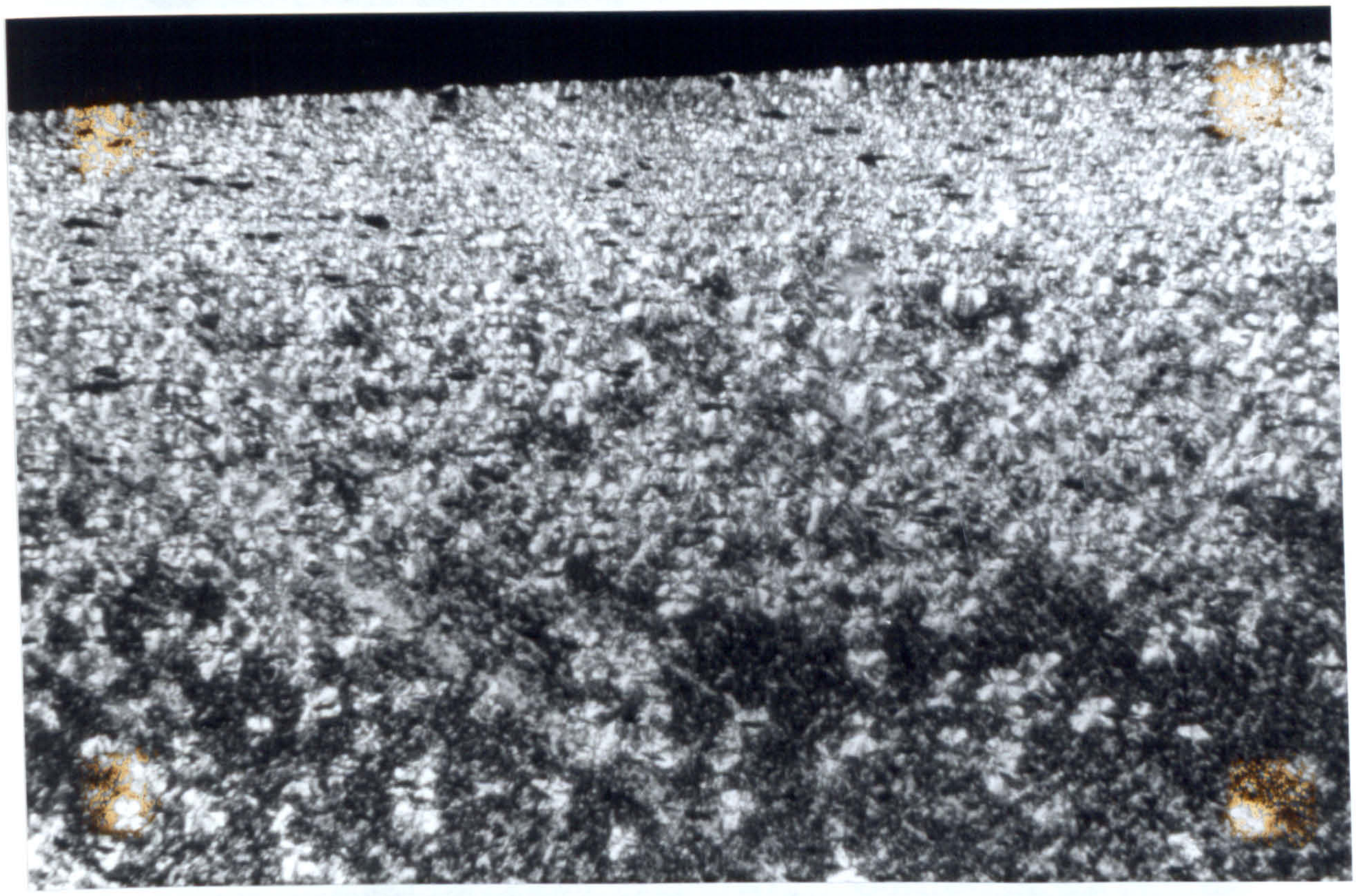

a) Conventional moulding

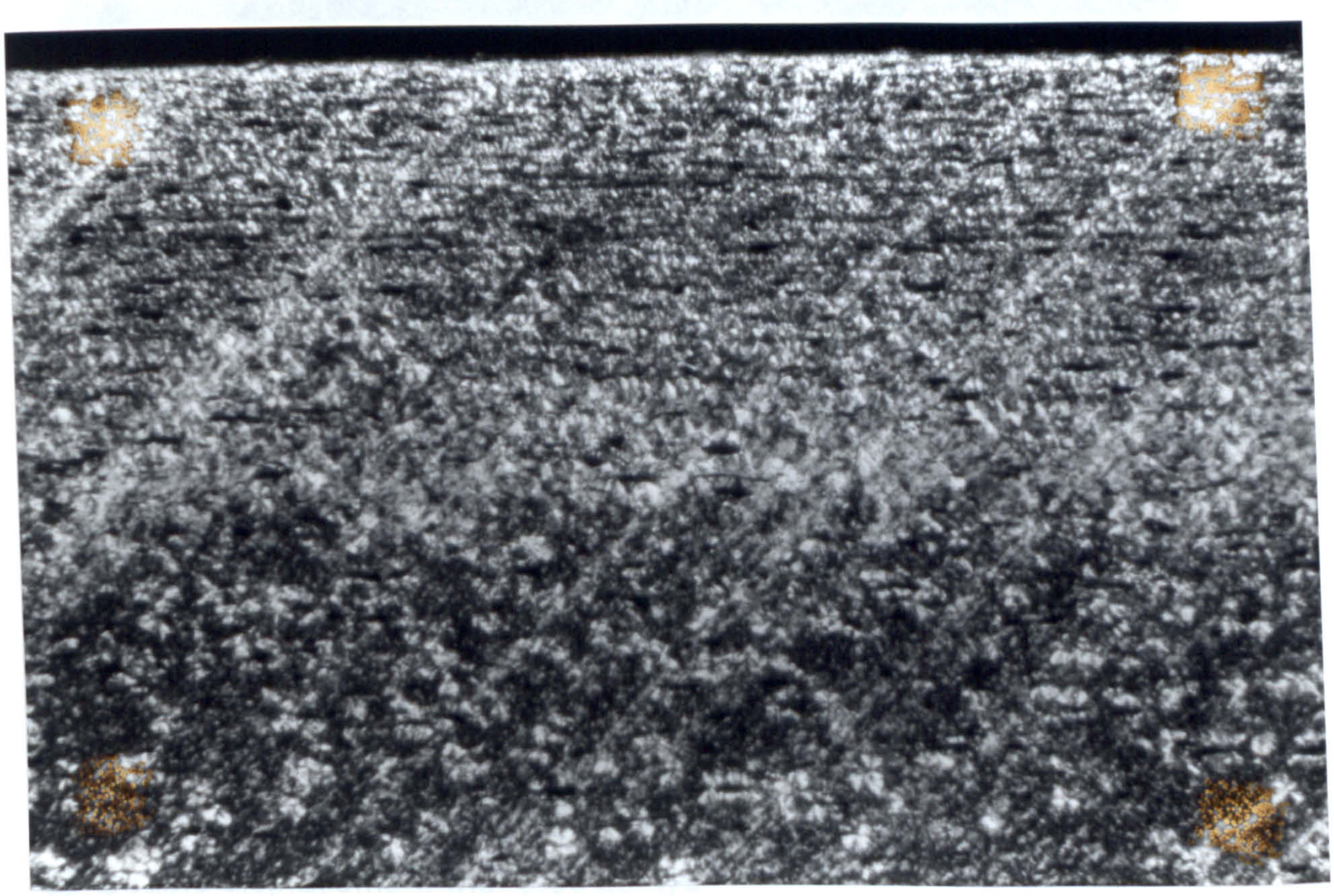

b) SBM

Figure 3.22 Microtomed sections of 2% ET2025 Al pigmented iPP rectangular plaque mouldings, sectioned parallel to flow and viewed using polarised LM (magnification x90) i.e. as figure 3.21.

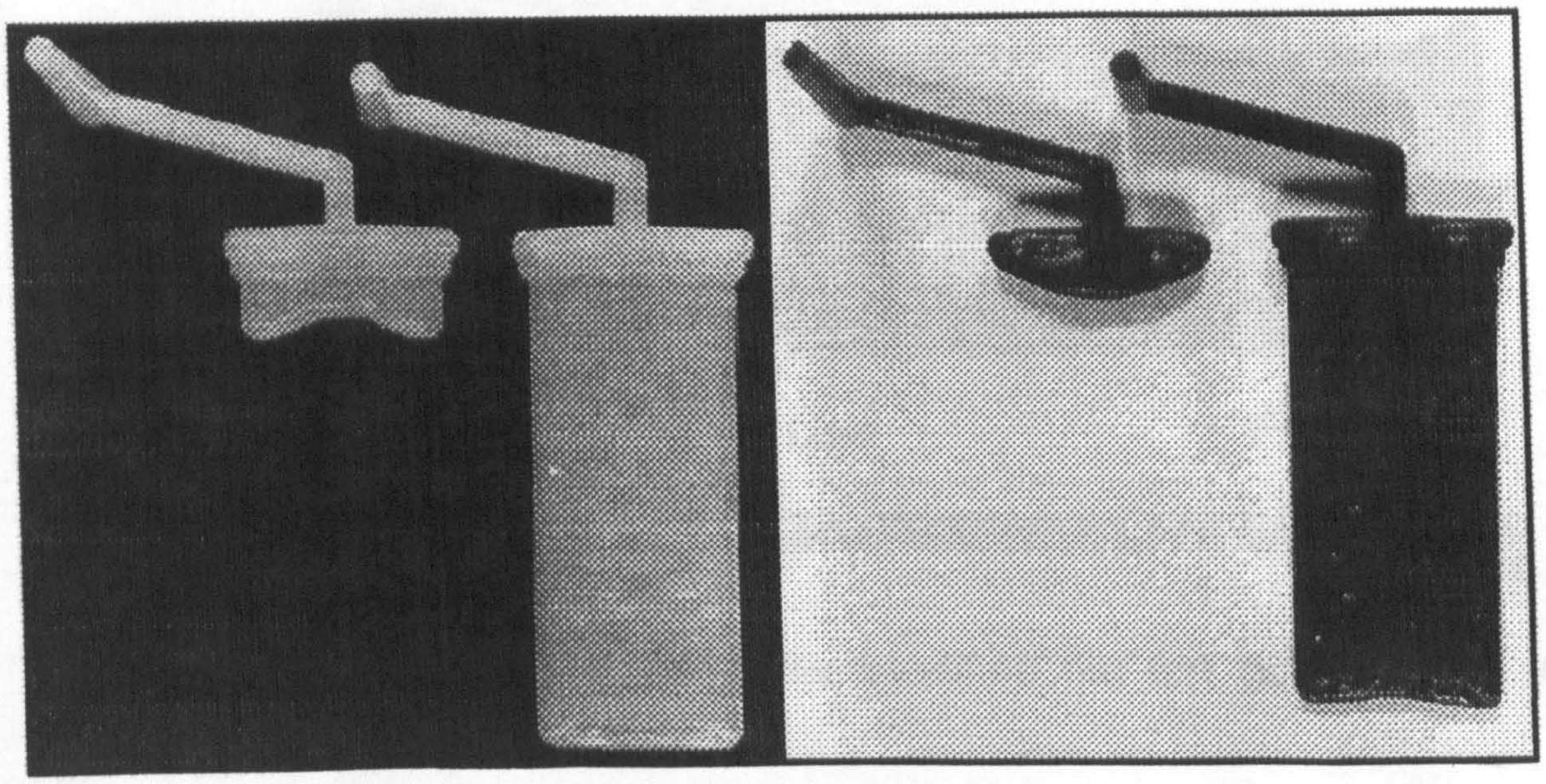

Figure 3.23 Development of a flat flow front during cavity filling

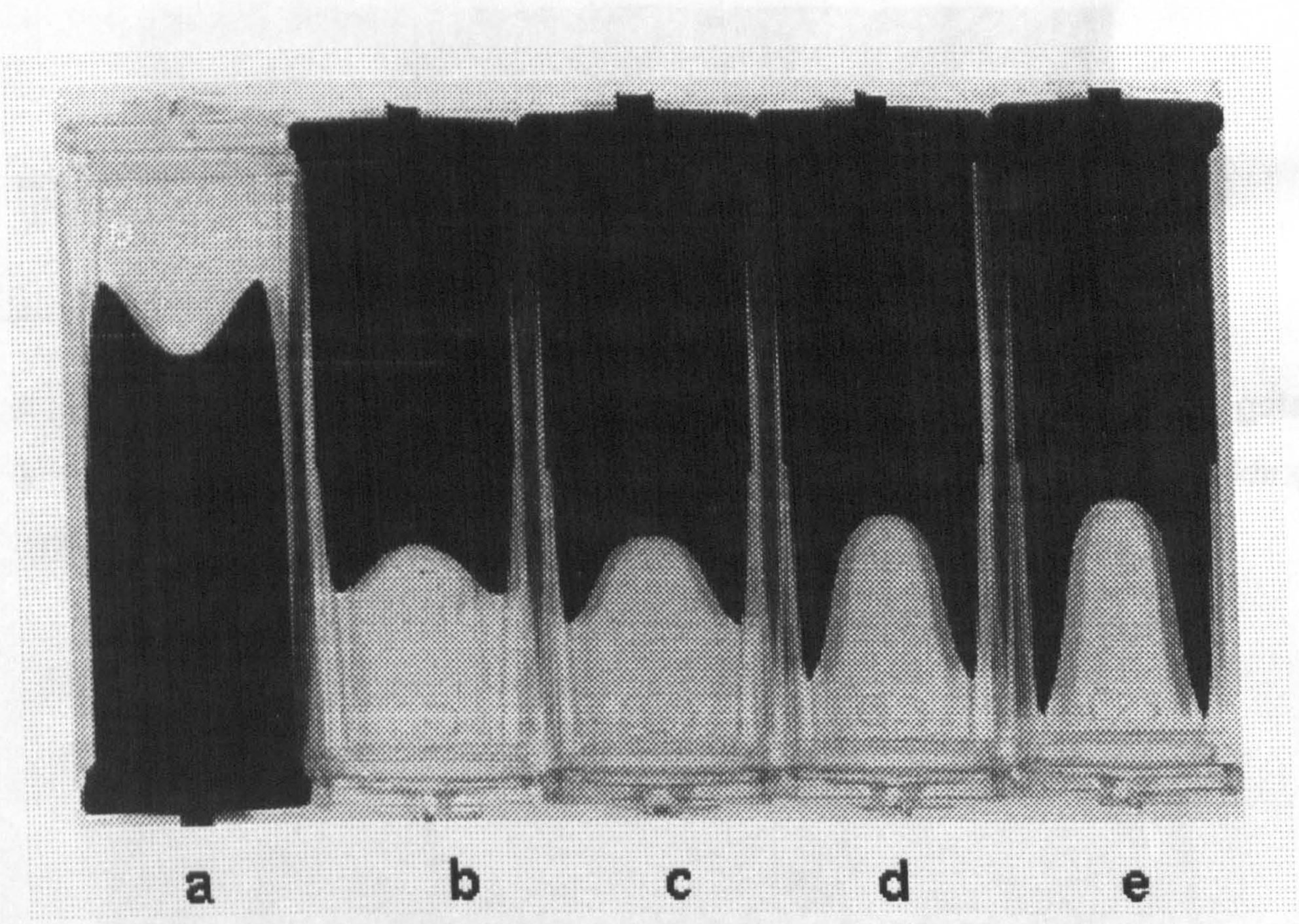

Figure 3.24 The U-shaped flow front in a family of SCORIM mouldings of natural and pigmented PS.

a) Single displacement with 0.5s delay
b) Double displacement with 0.5s delays
c) Double displacement, with 1.0s delays
d) Double displacement, with 1.5s delays
e) Double displacement, with 2.0s delays.

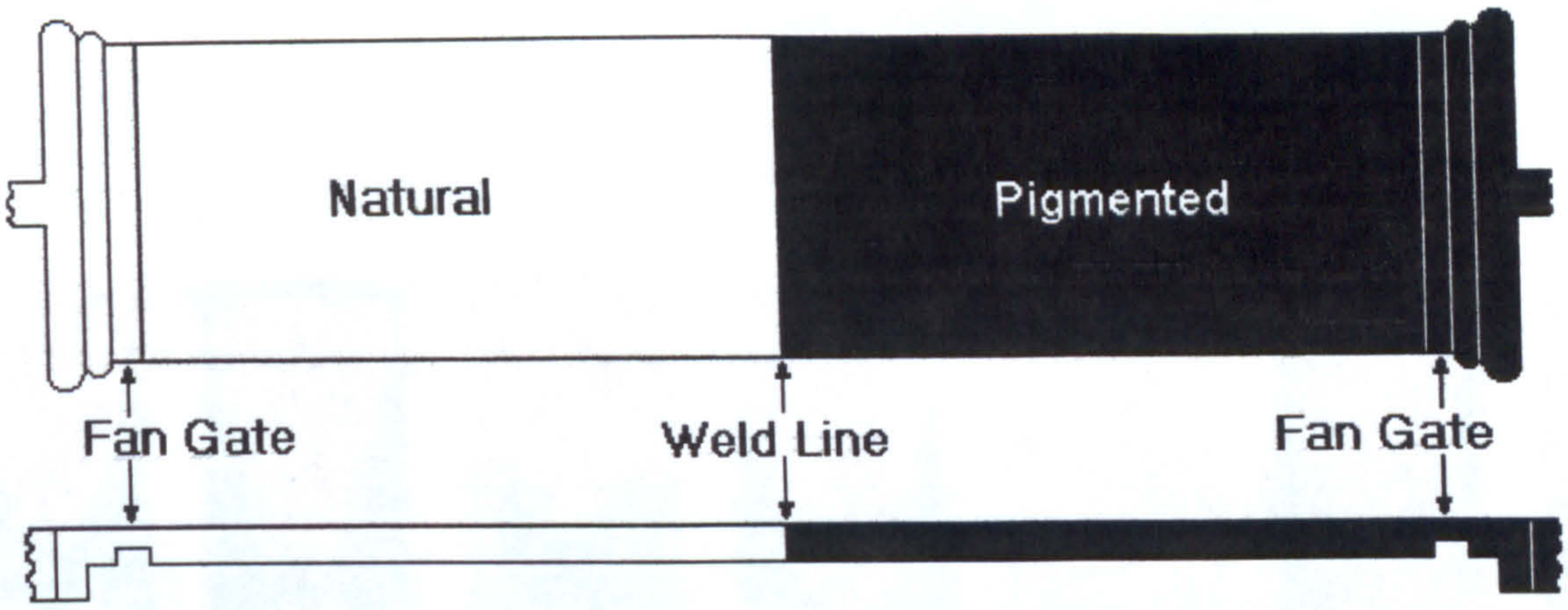

Figure 3.25a Schematic diagram of the modified flat fan gate design. (c.f. figure 2.3).

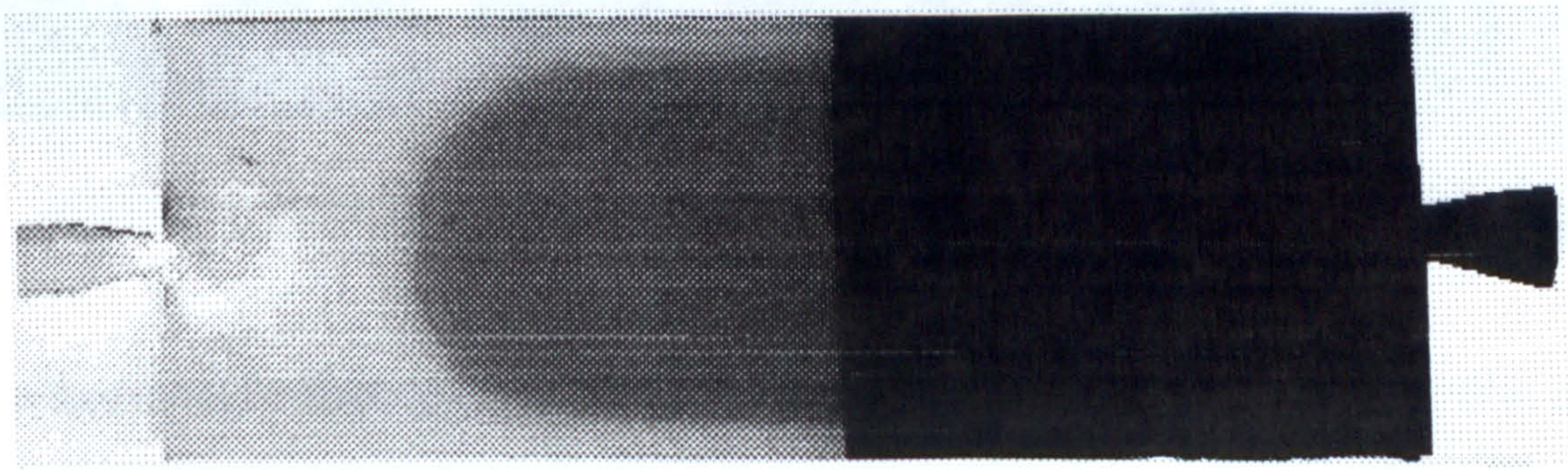

Figure 3.25b Photograph of the parabolic flow front obtained with a pin gate and PP. The material was a carbon black and natural 2-colour PP moulding produced with 2 SCORIM shears.

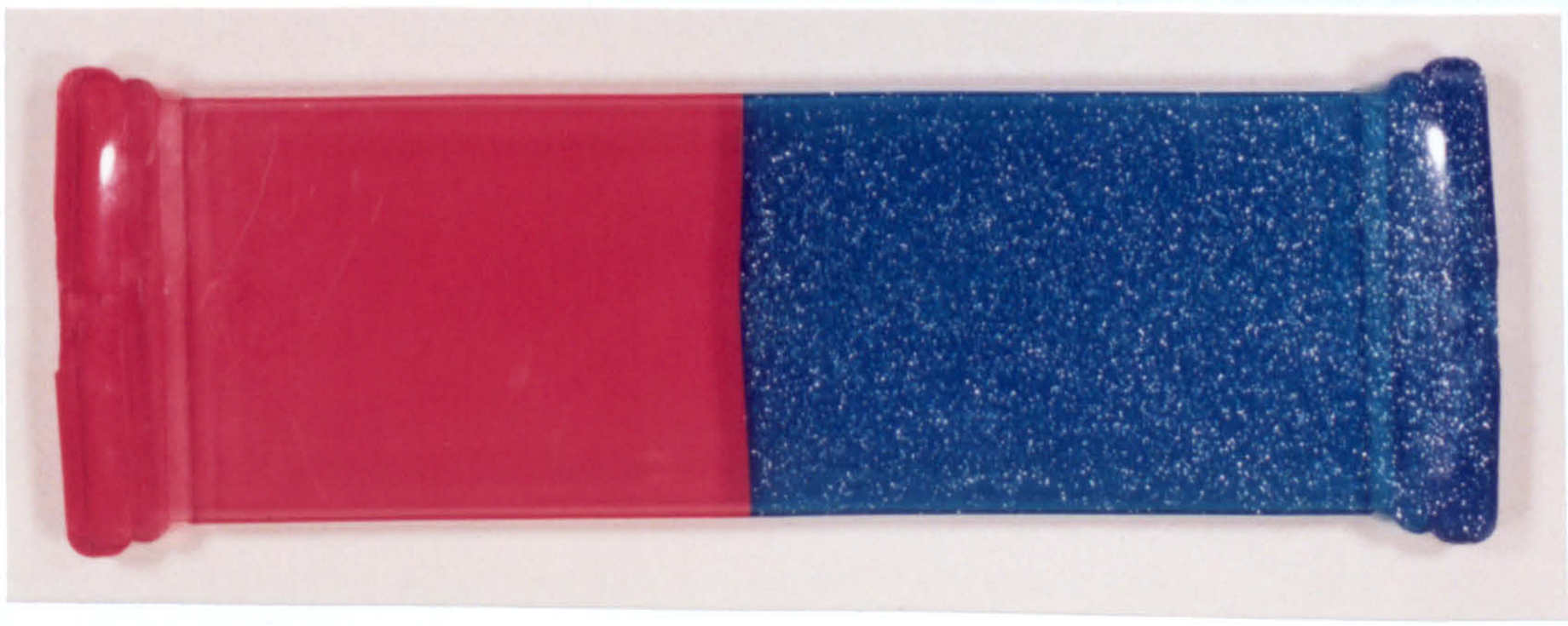

Figure 3.26 A conventional weld line produced with a two-colour moulding showing the flat interface with minimal surface area for adhesive contact and molecular entanglements to occur.

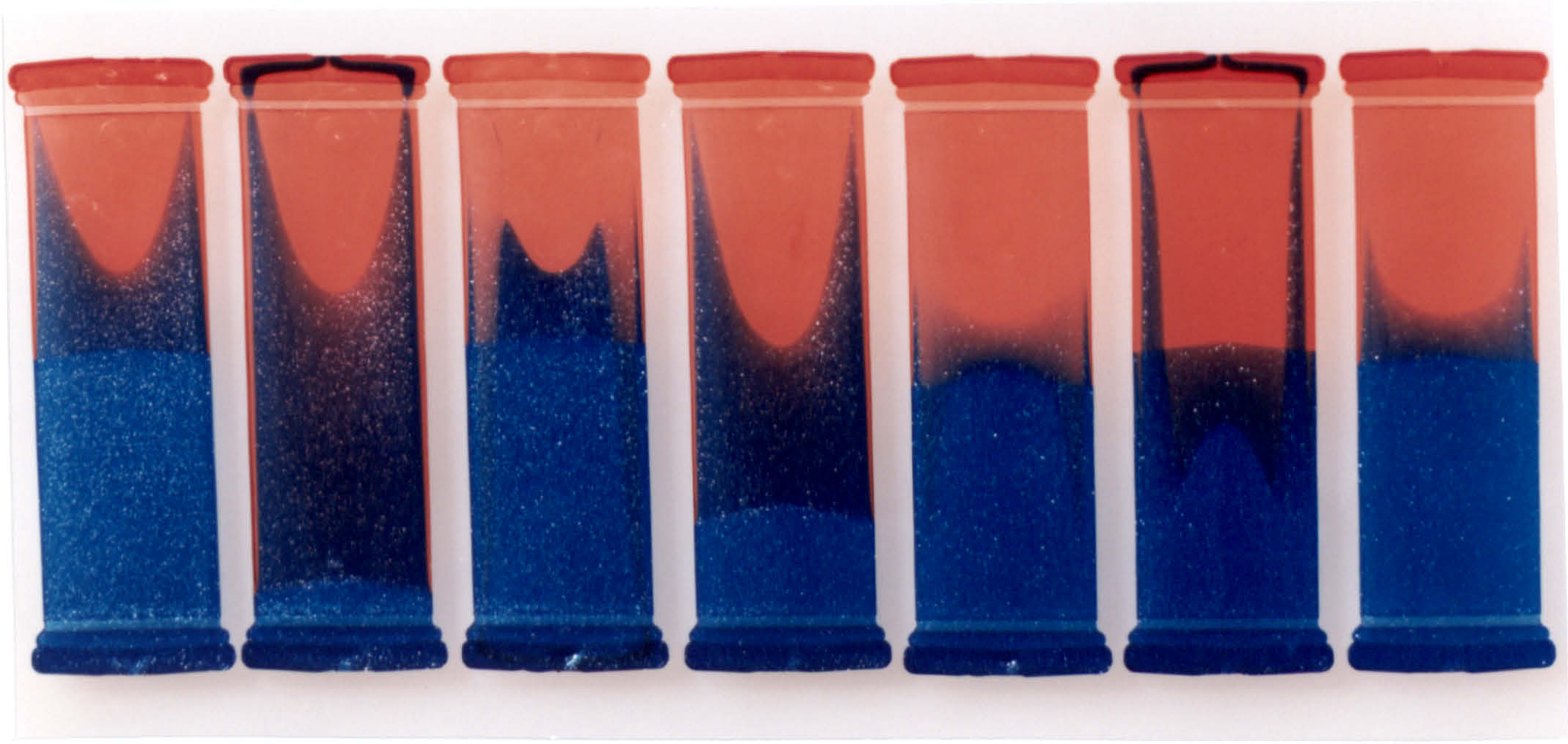

Figure 3.27 Examples of the two-colour patterns produced within the same mould geometry by the informed application of intermittent SCORIM shears.

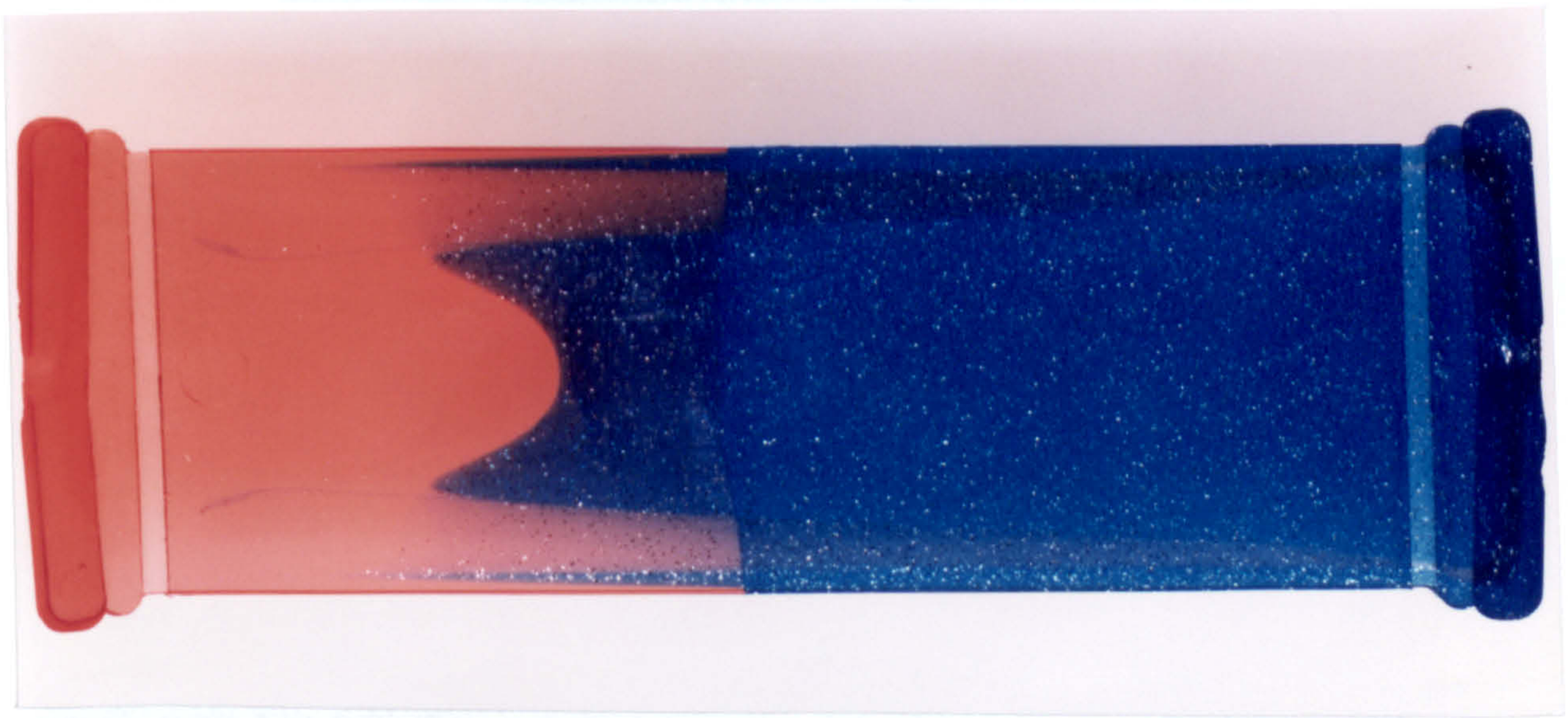

Figure 3.28 An enlarged view of one of the two-colour mouldings produced by the application of two intermittent shears.

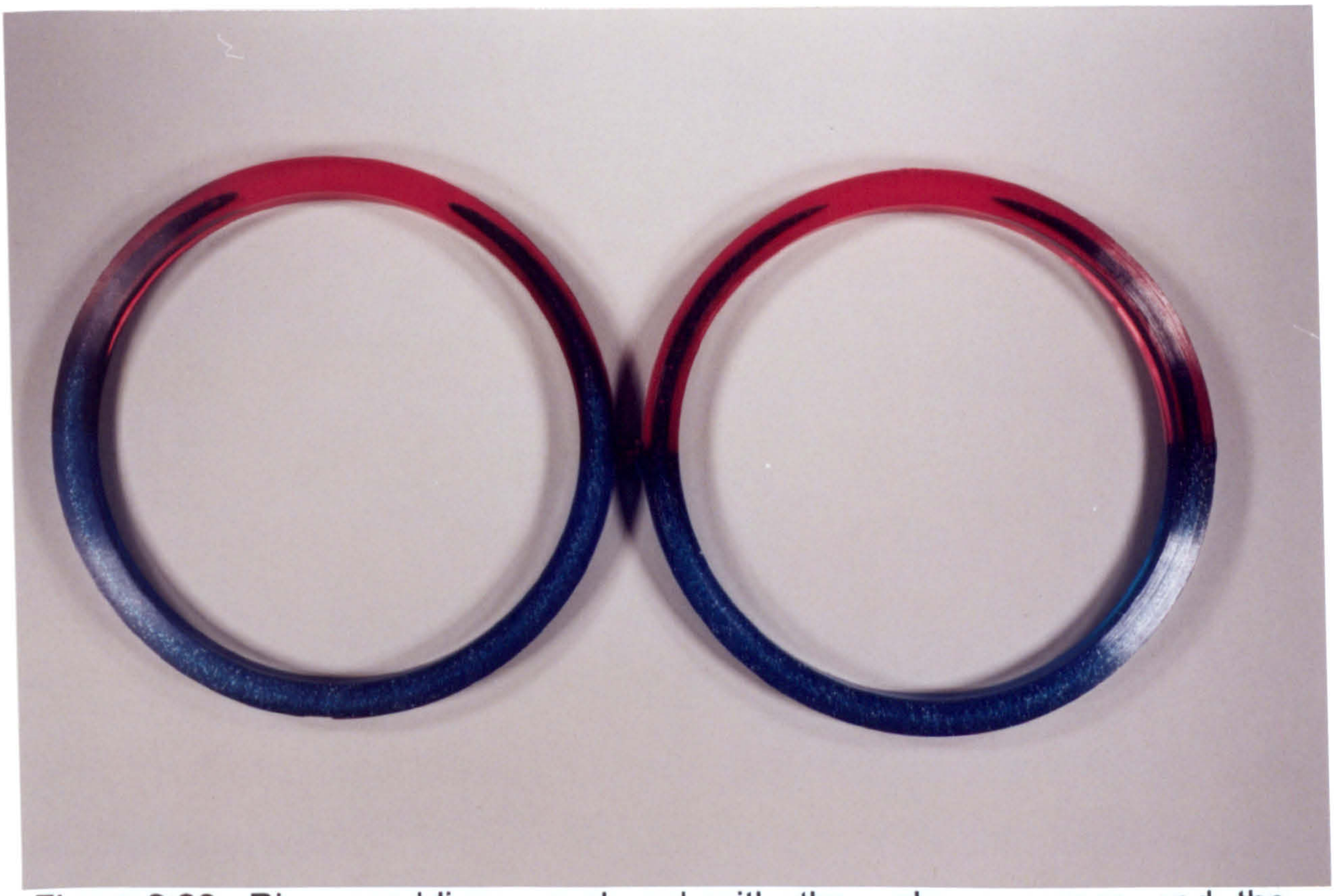

Figure 3.29 Ring mouldings produced with the colour process and the informed application of SCORIM shears.

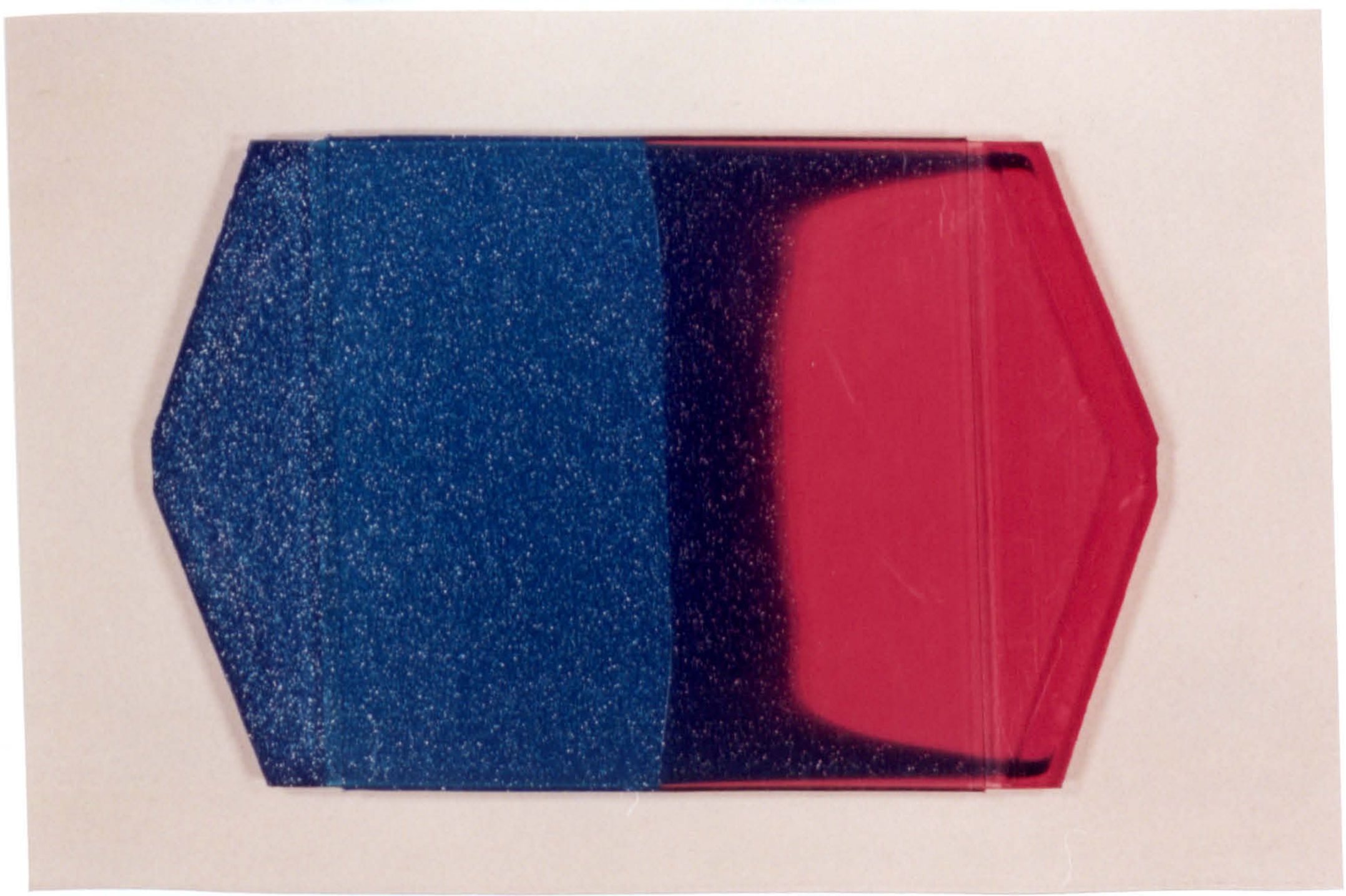

Figure 3.30 A square plaque moulding with two opposing edge fan gates used with the two-colour SCORIM process.

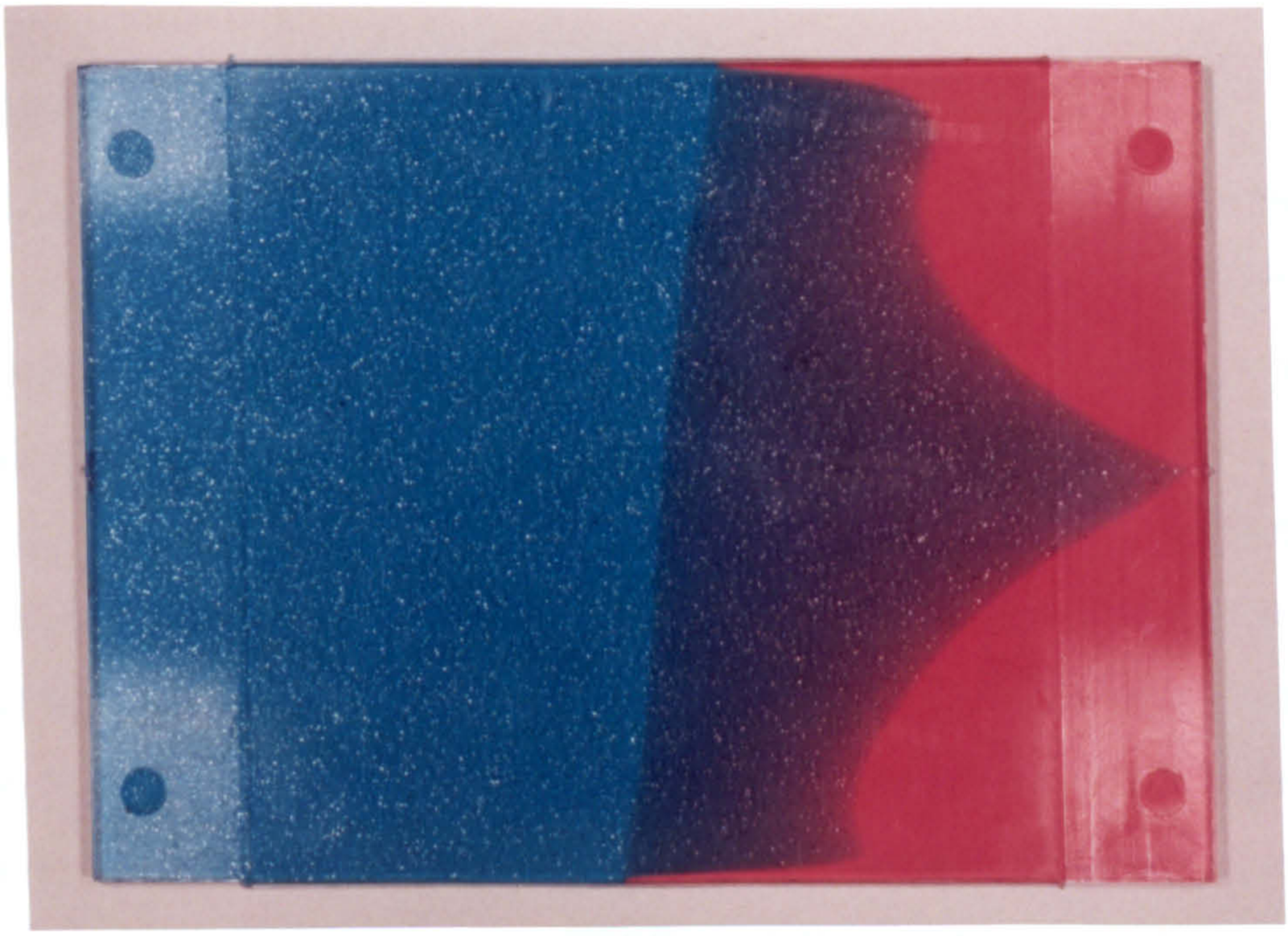

Figure 3.31 Two opposing 1 x 1mm pin gates feeding onto the edge of a rectangular cavity. Mould fill followed by the immediate application of SCORIM shear successfully produced this shear pattern through a small gate.

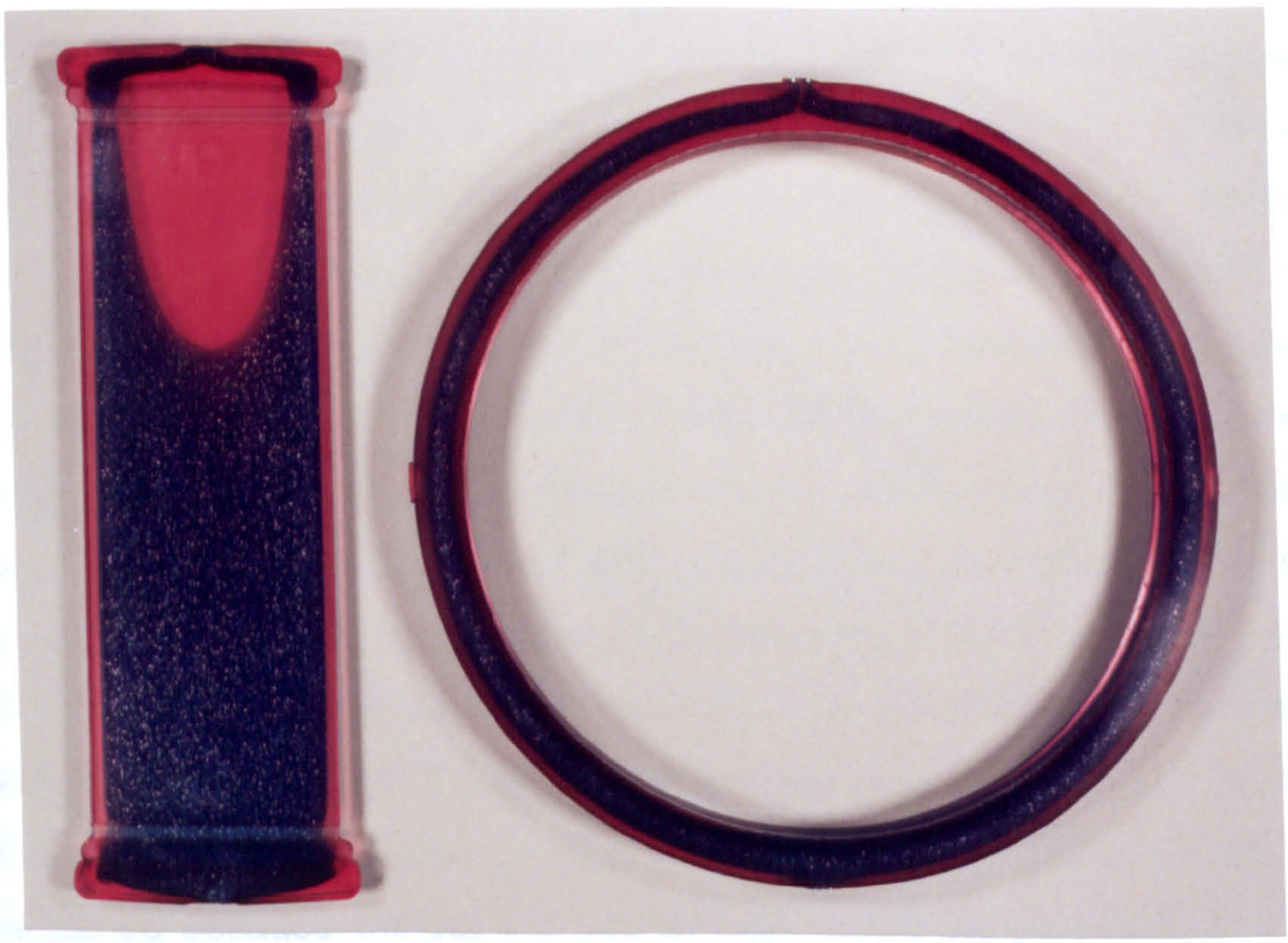

Figure 3.32 Two two-colour mouldings which demonstrate the potential application for SCORIM to be used for the insertion of recyclate (e.g. the blue material) into a virgin skin (e.g. the red material) after initially filling the mould cavity with the skin material.

4. MORPHOLOGICAL CHARACTERISATION RESULTS

SCORIM mouldings were produced using intermittent shears with systematically varied conditions. The unfilled and Al flake filled iPP materials were injected simultaneously to produce two-colour mouldings with initial centralised weld lines. The presence of the Al flake in one of these two materials acted as a suitable marker pigment to delineate between the two materials and identify the positions of the displaced weld interface. This was of particular benefit when viewing microtomed sections using polarised light microscopy. Three principal microscopy techniques were used for the morphological characterisation of samples namely, light microscopy (LM), scanning electron microscopy (SEM) and transmission electron microscopy (TEM). Sample preparation and an introduction to the microscopy techniques are presented in sections 2.5 and 2.6 respectively.

4.1 Polarised Light Microscopy Results

The SCORIM conditions used in tables 4.1 to 4.14 produced the families of mouldings from which the LM micrographs were taken shown in figures 4.1 and 4.2. These illustrate microtomed sections from sequences of mouldings produced using one and two shears respectively. Some scratch marks are evident on the micrographs which are angled to the moulding edge, these were caused by the microtome blade and should be ignored. The sequences are defined by the durations of elapsed cooling time between completion of mould fill and the activation of subsequent shear oscillations. The skin regions are visible with each sample and then further bands relating to each SCORIM oscillation applied to that moulding. The mouldings are symmetrical about their centres, with the size of each band relating to the cooling time allocated before the reverse stroke of the next oscillation. The symmetry was maintained because without the use of high mould temperatures from the induction heating, but a tool temperature of 40°C for heat extraction from the mouldings, there was a relatively minor difference between the cooling rates of the two halves of the tool.

Changes in morphology are evident from the oriented skin region through the highly oriented SCORIM regions, which have contrasting appearance due to the direction of material flow during processing, and finally the unoriented spherulitic core regions. The α-phase and the brighter β-phase spherulites are evident in the core. Where the unoriented phase begins spherulites are prevalent. This is usually coincident with bright β-phase but towards the centre of the core region the α-phase predominates.

Previous work[55, 62, 69, 84] with conventional mouldings has identified three distinct crystalline zones, namely, a highly oriented non-spherulitic skin, a row or shear-nucleated spherulitic intermediate layer and a typically spherulitic core. The thickness of the oriented skin was identified as a function of the polymer melt temperature and varied inversely with temperature. The thickness of the intermediate layer varied with injection pressure, but in a complex manner. With the application of SCORIM this intermediate layer's microstructure can be managerially controlled to impart highly oriented shear regions. The implications of this being that a knowledge of the morphological state of the polymer can assure that mechanical test data is meaningful and that a detailed knowledge of this structure will permit fabrication of injection moulded articles having tailored mechanical properties.

Fujiyama *et al*[61] discuss the molten polymer near the cavity surface experiencing high shear stresses whereby molecular chains are extended. On crystallisation by cooling, molecular chains with a high degree of extension gather first and form fibrous crystals. Then molecular chains with a lower degree of extension pile on the fibrous nuclei by chain folding. Thus a shish kebab structure is formed. At this time, some molecular chains are rejected from forming lamellae, but remain in the space of the main skeleton structure and undergo secondary crystallisation piling epitaxially on the main skeleton structure.

Figures 4.1 and 4.2 illustrate how the initial skin layers form to the same thickness in each of the mouldings, ≈0.15mm. The conventional moulding in figure 4.1 shows that beyond these oriented skin layers there is

the formation of bright β-spherulites representative of unoriented material. These β-phase developed and crystallised during solidification of the stationary melt. With the SCORIM mouldings, the shears manifested themselves under polarised light as layers of polymer brighter than the skin. These shear influenced regions extended some distance into the core of the mouldings whereupon, at a further interface, the presence of β-phase spherulites became prevalent. These parallel interfaces coincided in some areas with additional acutely angled interfaces present in some of the micrographs shown. These are in fact the displaced interfaces of the initial weld line and a clearer example is shown in figure 4.3. These were characteristically angled to the edges of the mouldings where the apparent high β-phase nucleation density to one side of this interface was due to the Al flake present in this material, acting as a heterogeneous nucleant for β-phase.

It was also evident that these β-spherulites were concentrated in layers of the core region close to shear influenced material but did not prevail in the centres of the cores. The lack of β-phase here may be related to the velocity profile of the material as shearing takes place. Tadmor's[12] explanation of this during mould filling is described in section 1.2.1 and the velocity profile is depicted in figure 1.3a. Although flow advancement during SCORIM shear does not exactly map that during mould filling, it may provide an explanation for the selective nucleation of β-phase in the presence of Al flake. In essence, the β-phase is present close to where a maximum shear rate may have induced molecular orientation, only for low heat transfer rates to enable molecular relaxation to occur. This combination of molecular relaxation in the presence of an heterogeneous nucleant, Al flake, may have promoted the formation of β-phase. In contrast, the central core which exhibits little β-phase was subject only to low shear according to the Tadmor[12] model, therefore inducing little molecular orientation. The absence of this orientation and consequent molecular relaxation may have ensured that no β-phase was able to nucleate upon the Al flake in this region. This observation is consistent with Kantz *et al*[55].

Figure 4.1 illustrates how the mouldings were influenced by the action of a single shear with different delay times between mould fill and the shear stroke. Figure 4.2 shows how the sections in figure 4.1 were changed by the action of a second SCORIM shear in the reverse direction to the first. These second shears were initiated after the time quoted had elapsed since the initiation of the first shear. The skin layers formed before the application of the first shear as with figure 4.1, as these stages of the SCORIM sequences were identical. However, figure 4.2 shows the influence of two shear oscillations on the morphology of the mouldings. The second shear layers manifest themselves under polarised light as bright banded regions. The delay incorporated between the first and second shears was the same as that between mould fill and the first shear. The longer this delay the larger the first shear band appeared as more cooling time was allowed to 'freeze in' the oriented structure before the onset of the second shear. The second shear extended some distance into the core of the moulding up to an interface whereupon the shear influenced polymer changed to unoriented polymer detectable by the presence of β-spherulites. The displaced weld interface was also present around these regions characteristically acutely angled to the moulding edge, manifesting itself as a colour change under polarised light. Again, in the spherulitic cores the weld interface was marked by the appearance of β-spherulites nucleated by the Al flake present in the material on one side of this interface. In figures 4.1 and 4.2 the spherulitic core regions exhibited β-phase spherulites predominantly at their edges thinning rapidly towards the core centres.

Figure 4.4 illustrates quite clearly the effect SCORIM has on the displacement of the weld line. This single shear example incorporating a 5 second delay before activation of the shear shows how a flat weld line solidifies in and next to the skin layer whilst the melt is undisturbed. The application of the single shear is evident as a bright band of material, but also the weld line can clearly be seen displaced in the direction of the flowing sheared material. Upon closer inspection, the Al flake is visible within this bright shear band on one side of the displaced weld line. The Al flake can

also be seen to have attained preferred orientation in the flow direction by virtue of SCORIM shearing.

The effect of incorporating ever longer cooling times before the application of shears in figures 4.1 and 4.2, was to increase the amount of oriented material from each shear encapsulated within the moulding. In this way, very few shears are necessary to impart preferred orientation through the majority of the thickness of the moulding. This resulted in the unoriented spherulitic cores being reduced in size as sheared material encroached into it. The extent to which this encroachment occurred was directly related to the amount of cooling time allocated between shears and the number of shears. However, the appearance of the microstructure varied along the length of the cross-section of the moulding depending upon the position of the displaced weld interface at any point.

The use of SCORIM clearly enabled excellent managerial control over the type of microstructure induced into mouldings and the sizes of the banded regions obtained. One limitation when attempting to induce shear influenced microstructure throughout the entire moulding including the core, was the premature 'freeze off' of the thinner cross-sectioned gate. With conventional moulding this effect is designed into a tool to minimise cycle times, however, with SCORIM mouldings a delayed gate 'freeze off' may be desired and may be achieved with the use of a hot sprue.

4.2 SEM Results

SEM was used to reveal the morphology of the shear influenced regions of SCORIM mouldings sectioned parallel and perpendicular to flow. An extensional morphology with orientation parallel to the flow direction appears to be present in figure 4.5, whilst other SCORIM mouldings exhibited similar morphology. The micrograph illustrates clearly the consistent appearance of the SCORIM induced morphology with respect to its length, spacing and uniform direction. By comparison figure 4.6 is a micrograph of the skin at the moulding edge formed when the molten polymer impinged and froze against the tool cavity surface during mould filling. Here shear orientation was

induced by the influence of 'fountain flow' and resulted in a morphology less ordered and less uniform in appearance. Both micrographs were taken at the same magnification and demonstrate clearly the excellent shear orienting properties of the SCORIM technology over and above any orientation obtained during mould filling.

4.3 TEM Results

TEM was able to reveal the morphology of the shear regions of SCORIM mouldings at the highest magnifications of all the microscopic techniques used. At lower magnifications evidence of spherulitic morphology was observed in the core regions. Figure 4.7 shows evidence of chain extensional flow in the flow direction of a region sheared by SCORIM. This manifests itself in this micrograph as rows of ordered structure with preferred orientation in the shear direction. This may be indicative of *shish-kebab morphology*[16] which is known to be present in sheared regions such as these. If so, the crystalline main lamella (shishes) or central backbone are likely to be the clearly visible oriented structure in the shear direction. Also present growing off these chain backbones will be lamella overgrowths (kebabs) oriented perpendicular to the flow direction. The shishes are reportedly[72, 85] about 700Å thick and the kebabs 200Å thick with a scale bar on this micrograph of 2μm. The lamella crystals possess c and a*-axis orientation, where the chain axis is the c-axis and the a*-axis is the shish or kebab axis. Therefore the shishes possess both c and a*-axis orientation parallel to the flow direction. The kebabs which grow on the shishes are expected to have a chain folded structure[16, 61], grown epitaxially onto the shishes. Therefore these kebabs possess c-axis orientation parallel to the flow direction and a*-axis orientation perpendicular to it. Figure 4.7 therefore contains evidence to support the proposal of shish-kebab morphology in shear crystallised isotactic polypropylene[16, 61].

Figure 4.8 shows a sheared region sectioned perpendicular to the flow direction. The morphology appears as terracing presumably containing shish-kebabs sectioned perpendicular to their c-axis orientation. A banded region is

evident which has a different appearance/orientation to the rest of the section, believed to be a shear interface induced into the moulding by SCORIM processing. At such an interface the shish-kebab morphology experienced an alteration in orientation direction, which is an observation consistent with Kalay[72].

Figures 4.9 and 4.10 show the TEM micrographs from the core regions of SCORIM mouldings where shear induced orientation was absent. A spherulitic morphology is observed in figure 4.9 where the individual lamella crystals can be clearly seen radiating from the central nucleus. Figure 4.10 shows the radial lamella of a spherulite at a higher magnification.

Kalay[72, 85] proposed a development of a model by Fujiyama *et al*[61] based on microstructural and x-ray diffraction studies of SCORIM iPP mouldings exhibiting bimodal orientation. A schematic diagram of the model is shown in figure 4.11. The development considered the shishes to have kebabs overgrown onto them at an angle <90°, which is an angular relationship consistent with an 80° epitaxial growth angle proposed by Lotz *et al*[53, 86].

Fujiyama *et al*[61] proposed the model to explain bimodal orientation detected by x-ray diffraction in the skin layers of polypropylene injection mouldings. The model proposes that bimodal orientation was due to further small and nonuniform lamellae (secondary kebabs) with a*-axis parallel to the injection direction initially grown epitaxially on the c-axis kebabs. The formation of these crystal structures occurs as a result of the coiled and entangled molten polymer chains experiencing extensional flow during processing which decreases their entanglement density and causes chain elongation. The high degree of alignment induced crystallises on cooling in fibrillar form (shishes), with those chains not attaining this degree of alignment crystallising epitaxially as chain folded structures (kebabs). Sufficient energy remains within the moulding in the form of heat to enable further reorganisation by slip and rotation of these chain folded blocks, resulting in bimodal orientation. Further, the stretching of tie-molecules

increases their own stiffness and consequently the Young's modulus of the whole moulding.

The spherulitic cores of mouldings can be eliminated in this way by inducing orientation with progressive shearing by the use of SCORIM as solidification takes place. The heat generated by shear does however contribute to the relaxation of oriented molecules aligned in the shear direction. The heat provides energy for recoiling and re-entanglement of molecules previously extended by flow. This would promote the formation of spherulites if an excessive amount of shear heat was generated and therefore the informed application of an optimum level of shearing, designed to impart orientation but enable solidification to encase this without liberating spherulitic growth is required. Live feed moulding needs to be maintained to achieve this however, requiring delayed gate 'freeze-off' to facilitate it.

4.4 Relationship Between Processing Conditions and Morphology

I) Shear orientations with SCORIM produce two closely controlled shear bands adjacent to the solidified outer layers and symmetrical about the mouldings' centreline. Adjacent shear bands have subtly different orientations owing to the direction of shear applied.

II) Shear influenced material induced by SCORIM can be controllably retained within the microstructure by allocating time for solidification of this morphology between reciprocal shear oscillations. In this way, it is proposed that few shear strokes are required to induce shear influenced morphology throughout the thickness of the moulding. This view is supported by the polarised light photomicrograph results.

III) The size of the shear bands solidified from any one SCORIM oscillation, is proportional to the time allocated between reciprocal shears, within an upper limit. The upper limit being the thickness through which any single shear has an influence on the microstructure.

IV) Spherulitic morphology is clearly observed within the core regions using polarised light microscopy. β-phase spherulites predominate at the edges of the core regions with virtually all α-phase spherulites in the central

core region. Evidence of spherulitic morphology between the skin layer and the delayed initial SCORIM shear, suggest it would be possible to produce a laminate microstructure containing alternate layers of shear influenced and spherulitic morphologies, an observation consistent with Kalay *et al*[70].

V) SEM and TEM micrographs reveal a high degree of well ordered molecular alignment achieved by SCORIM. The morphology has the appearance of lamella fibrillar crystals with epitaxially grown chain folded lamellae overgrowths, i.e. *shish-kebab morphology*. Although no γ-phase crystals have been identified by any of the microscopy techniques used, shish-kebab morphology is assumed to be associated with it and α-phase morphology.

Table 4.1 0.5s delay single shear SCORIM sequence

Stage ID	Duration (sec's)	C-time (sec's)	R-time (sec's)	C-Pres (%)	R-Pres (%)	Pistons	Pistons
S00	0.5	0.5	0.5	30	0	NO	None
S01	20.0	20.0	20.0	65	0	N	O

SCORIM Profile: S00, S01

Table 4.2 1.0s delay single shear SCORIM sequence

Stage ID	Duration (sec's)	C-time (sec's)	R-time (sec's)	C-Pres (%)	R-Pres (%)	Pistons	Pistons
S00	1.0	1.0	1.0	30	0	NO	None
S01	20.0	20.0	20.0	65	0	N	O

SCORIM Profile: S00, S01

Table 4.3 2.0s delay single shear SCORIM sequence

Stage ID	Duration (sec's)	C-time (sec's)	R-time (sec's)	C-Pres (%)	R-Pres (%)	Pistons	Pistons
S00	2.0	2.0	2.0	30	0	NO	None
S01	20.0	20.0	20.0	65	0	N	O

SCORIM Profile: S00, S01

Table 4.4 3.0s delay single shear SCORIM sequence

Stage ID	Duration (sec's)	C-time (sec's)	R-time (sec's)	C-Pres (%)	R-Pres (%)	Pistons	Pistons
S00	3.0	3.0	3.0	30	0	NO	None
S01	20.0	20.0	20.0	65	0	N	O

SCORIM Profile: S00, S01

Table 4.5 4.0s delay single shear SCORIM sequence

Stage ID	Duration (sec's)	C-time (sec's)	R-time (sec's)	C-Pres (%)	R-Pres (%)	Pistons	Pistons
S00	4.0	4.0	4.0	30	0	NO	None
S01	20.0	20.0	20.0	65	0	N	O

SCORIM Profile: S00, S01

Table 4.6 5.0s delay single shear SCORIM sequence

Stage ID	Duration (sec's)	C-time (sec's)	R-time (sec's)	C-Pres (%)	R-Pres (%)	Pistons	Pistons
S00	5.0	5.0	5.0	30	0	NO	None
S01	20.0	20.0	20.0	65	0	N	O

SCORIM Profile: S00, S01

Table 4.7 6.0s delay single shear SCORIM sequence

Stage ID	Duration (sec's)	C-time (sec's)	R-time (sec's)	C-Pres (%)	R-Pres (%)	Pistons	Pistons
S00	6.0	6.0	6.0	30	0	NO	None
S01	20.0	20.0	20.0	65	0	N	O

SCORIM Profile: S00, S01

Table 4.8 0.5s delay double shear SCORIM sequence

Stage ID	Duration (sec's)	C-time (sec's)	R-time (sec's)	C-Pres (%)	R-Pres (%)	Pistons	Pistons
S00	0.5	0.5	0.5	30	0	NO	None
S01	0.5	0.5	0.5	65	0	O	N
S02	20.0	20.0	20.0	65	0	N	O

SCORIM Profile: S00, S01, S02

Table 4.9 1.0s delay double shear SCORIM sequence

Stage ID	Duration (sec's)	C-time (sec's)	R-time (sec's)	C-Pres (%)	R-Pres (%)	Pistons	Pistons
S00	1.0	1.0	1.0	30	0	NO	None
S01	1.0	1.0	1.0	65	0	O	N
S02	20.0	20.0	20.0	65	0	N	O

SCORIM Profile: S00, S01, S02

Table 4.10 2.0s delay double shear SCORIM sequence

Stage ID	Duration (sec's)	C-time (sec's)	R-time (sec's)	C-Pres (%)	R-Pres (%)	Pistons	Pistons
S00	2.0	2.0	2.0	30	0	NO	None
S01	2.0	2.0	2.0	65	0	O	N
S02	20.0	20.0	20.0	65	0	N	O

SCORIM Profile: S00, S01, S02

Table 4.11 3.0s delay double shear SCORIM sequence

Stage ID	Duration (sec's)	C-time (sec's)	R-time (sec's)	C-Pres (%)	R-Pres (%)	Pistons	Pistons
S00	3.0	3.0	3.0	30	0	NO	None
S01	3.0	3.0	3.0	65	0	O	N
S02	20.0	20.0	20.0	65	0	N	O

SCORIM Profile: S00, S01, S02

Table 4.12 4.0s delay double shear SCORIM sequence

Stage ID	Duration (sec's)	C-time (sec's)	R-time (sec's)	C-Pres (%)	R-Pres (%)	Pistons	Pistons
S00	4.0	4.0	4.0	30	0	NO	None
S01	4.0	4.0	4.0	65	0	O	N
S02	20.0	20.0	20.0	65	0	N	O

SCORIM Profile: S00, S01, S02

Table 4.13 5.0s delay double shear SCORIM sequence

Stage ID	Duration (sec's)	C-time (sec's)	R-time (sec's)	C-Pres (%)	R-Pres (%)	Pistons	Pistons
S00	5.0	5.0	5.0	30	0	NO	None
S01	5.0	5.0	5.0	65	0	O	N
S02	20.0	20.0	20.0	65	0	N	O

SCORIM Profile: S00, S01, S02

Table 4.14 6.0s delay double shear SCORIM sequence

Stage ID	Duration (sec's)	C-time (sec's)	R-time (sec's)	C-Pres (%)	R-Pres (%)	Pistons	Pistons
S00	6.0	6.0	6.0	30	0	NO	None
S01	6.0	6.0	6.0	65	0	O	N
S02	20.0	20.0	20.0	65	0	N	O

SCORIM Profile: S00, S01, S02

N.B. (C-TIME) = Compression time; (R-TIME) = Relaxation time;
(C-PRES) = Compression pressure; (R-PRES) Relaxation pressure.

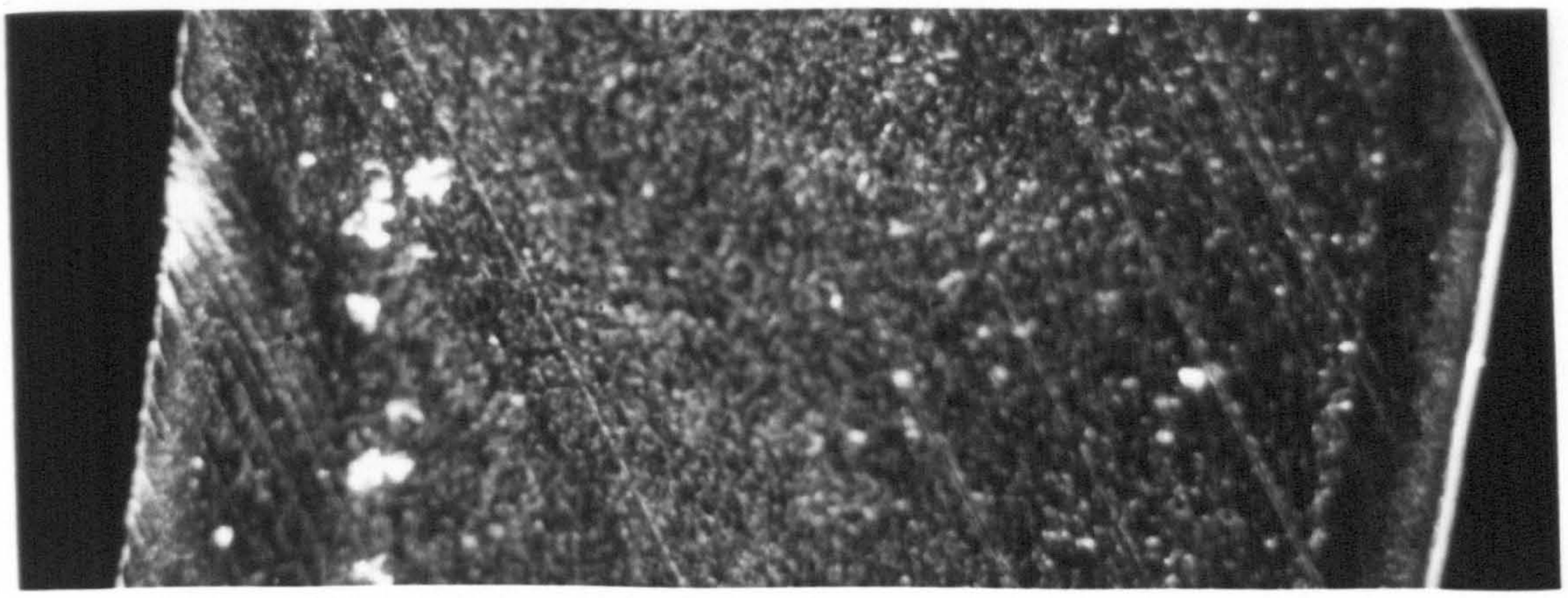

a) Conventional, i.e. no shear

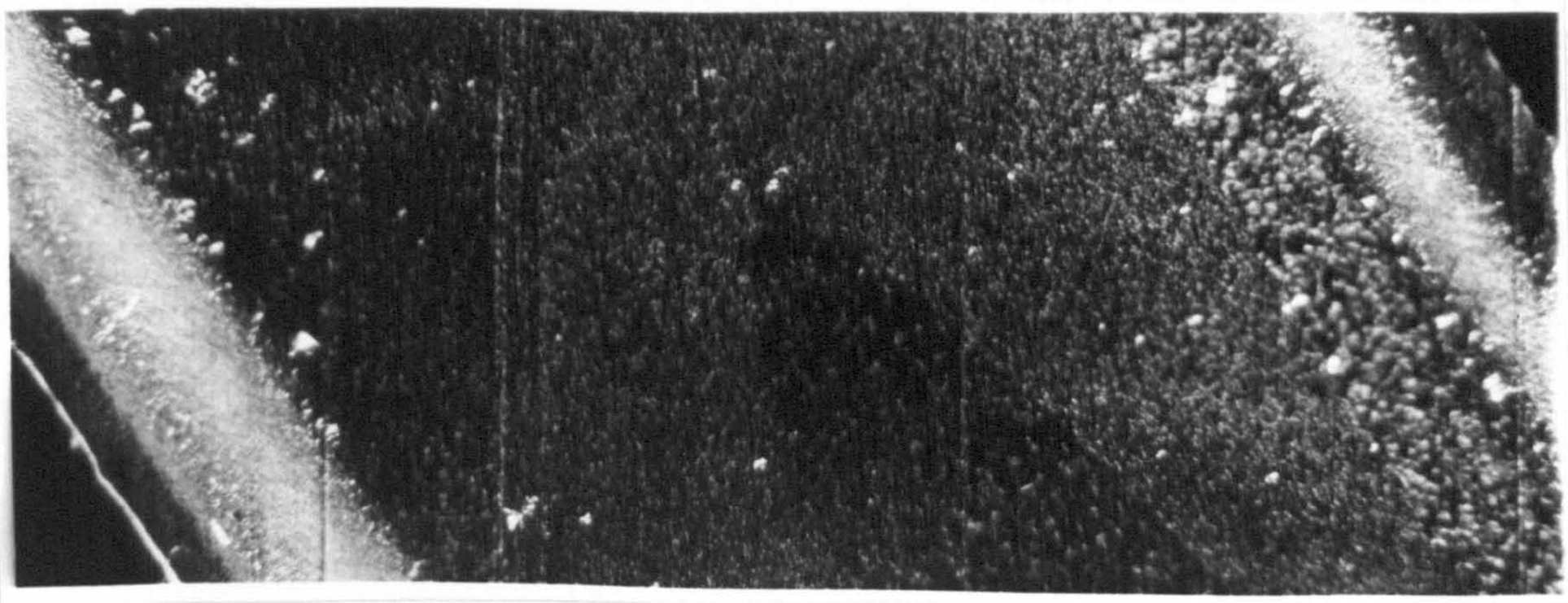

b) 1.0 second delay time

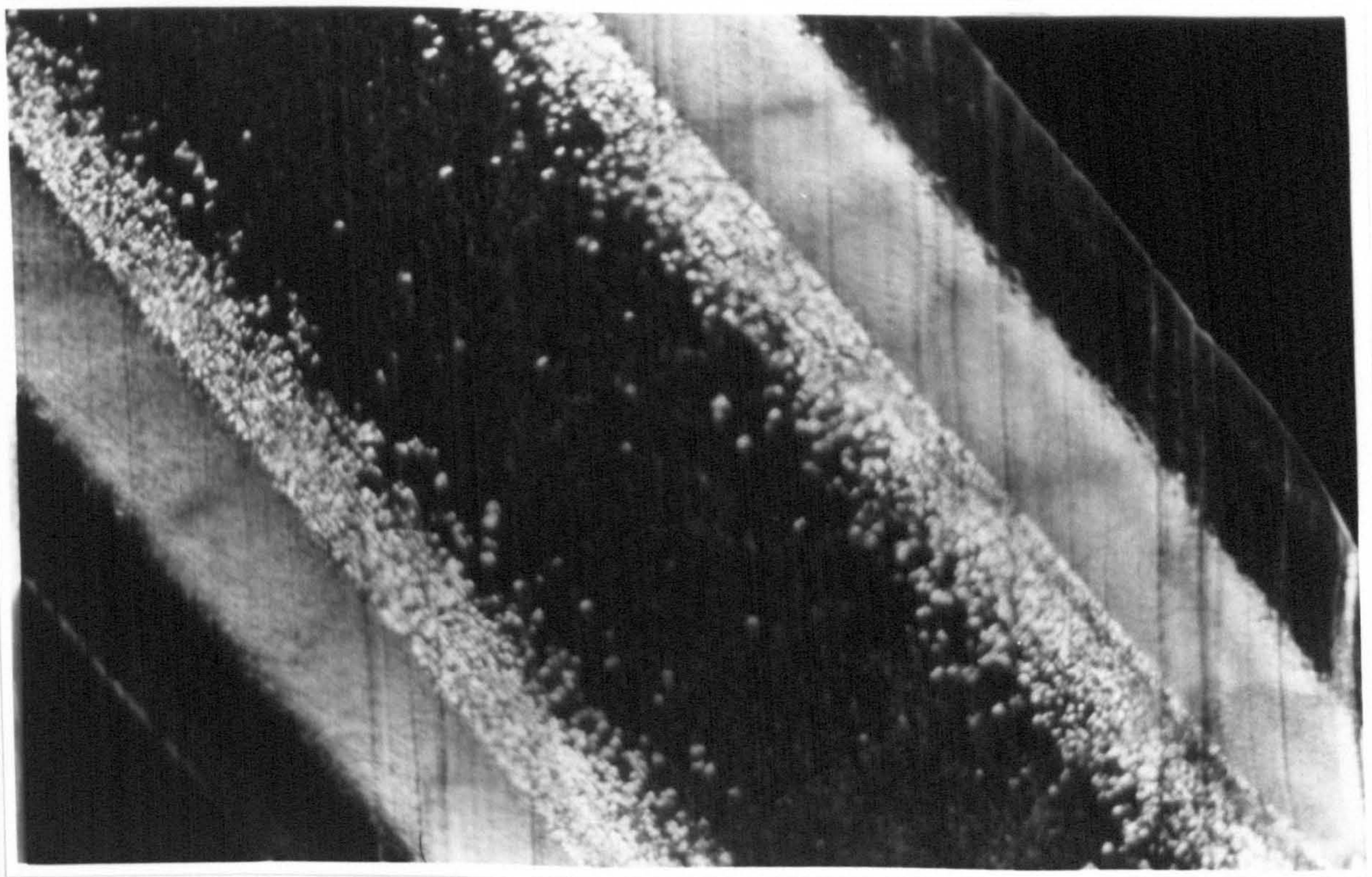

c) 6.0 second delay time

Figure 4.1 Microtomed sections viewed parallel to flow of 2-colour iPP single shear SCORIM mouldings, produced with different delay times. The sections are 4mm wide.

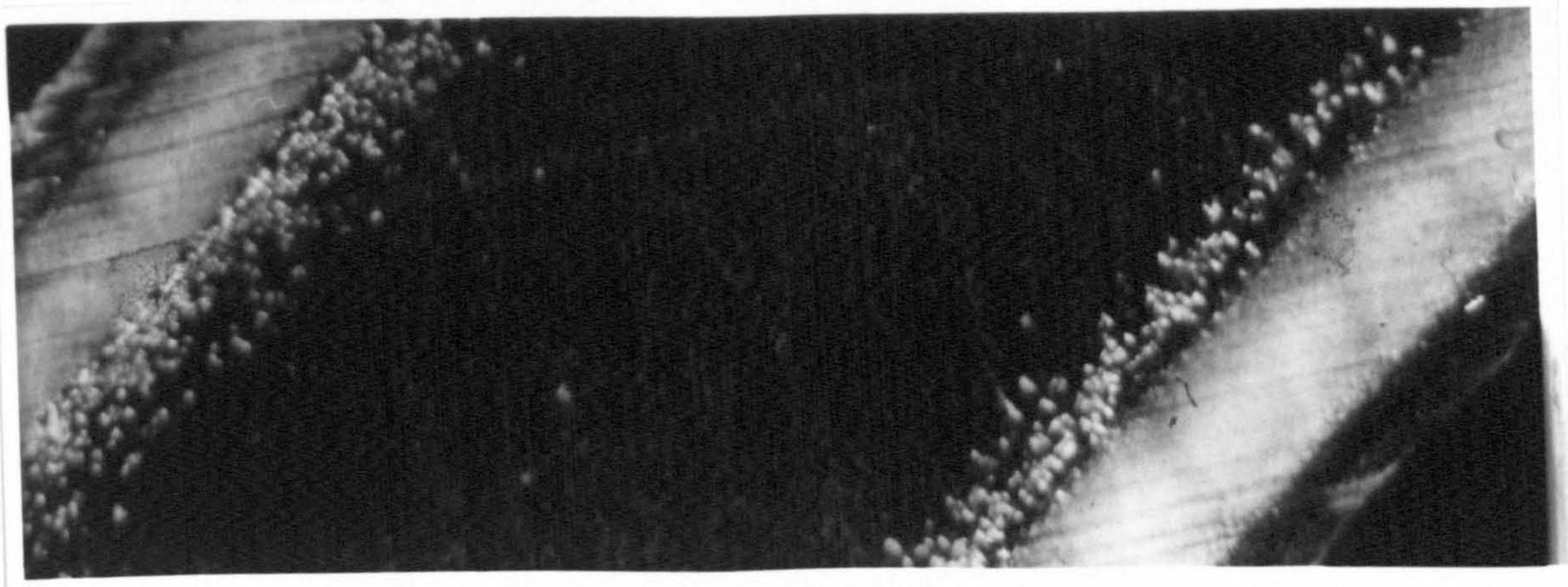

a) 1.0 second delay time

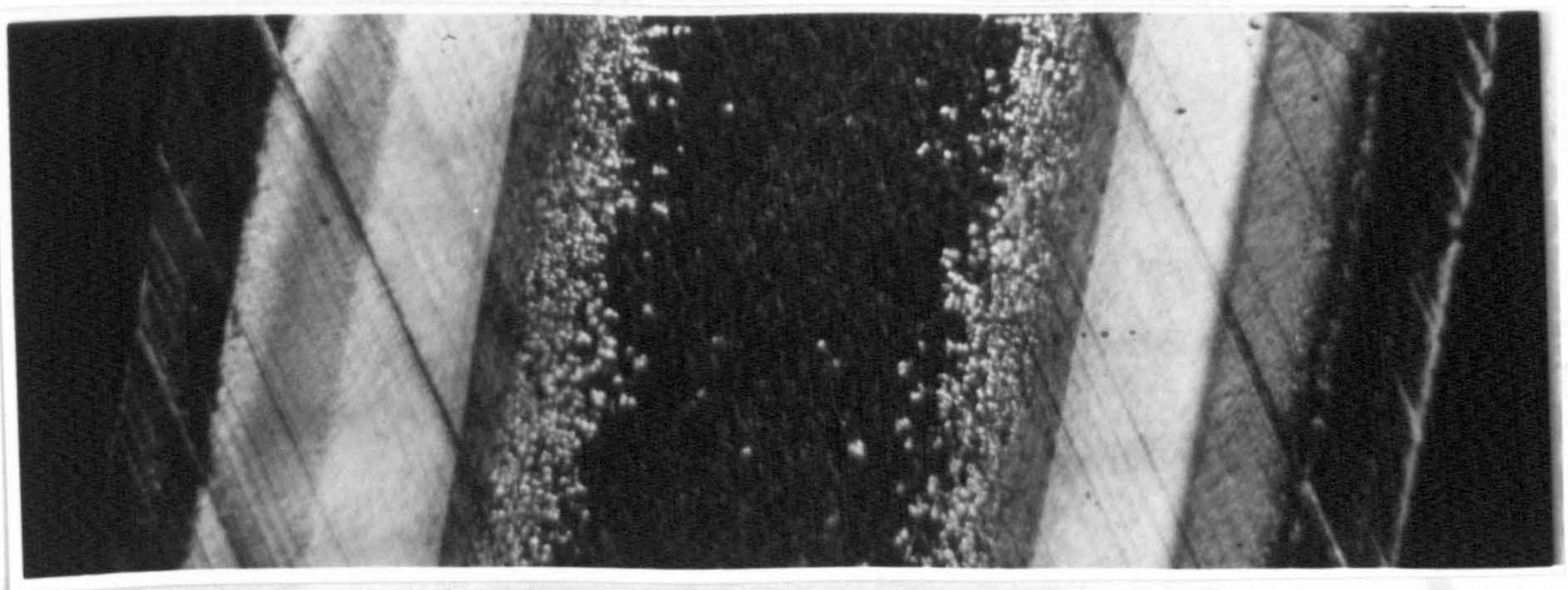

b) 4.0 second delay time

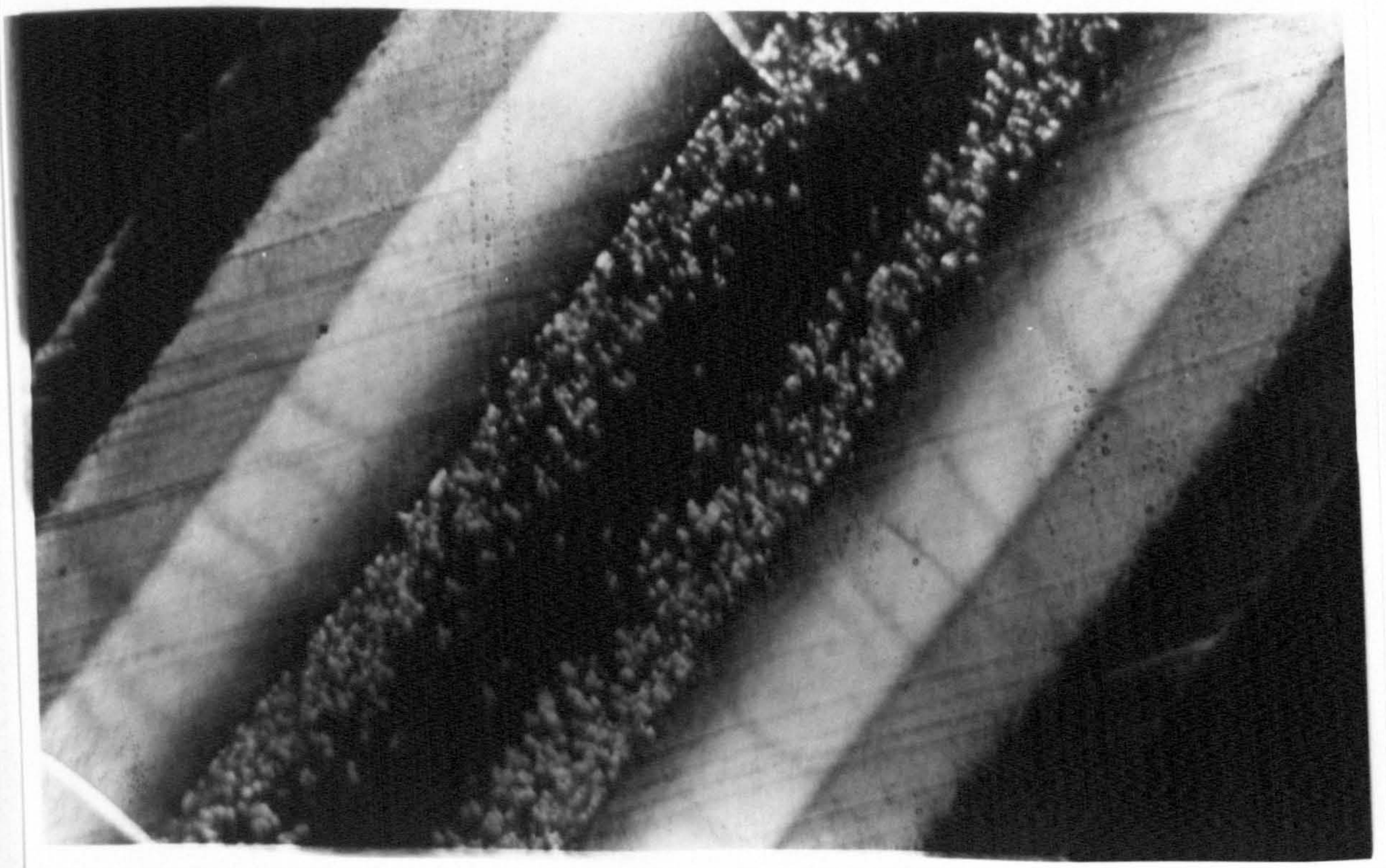

c) 6.0 second delay time

Figure 4.2 Microtomed sections viewed parallel to flow of 2-colour iPP double shear SCORIM mouldings, produced with different delay times. The sections are 4mm wide.

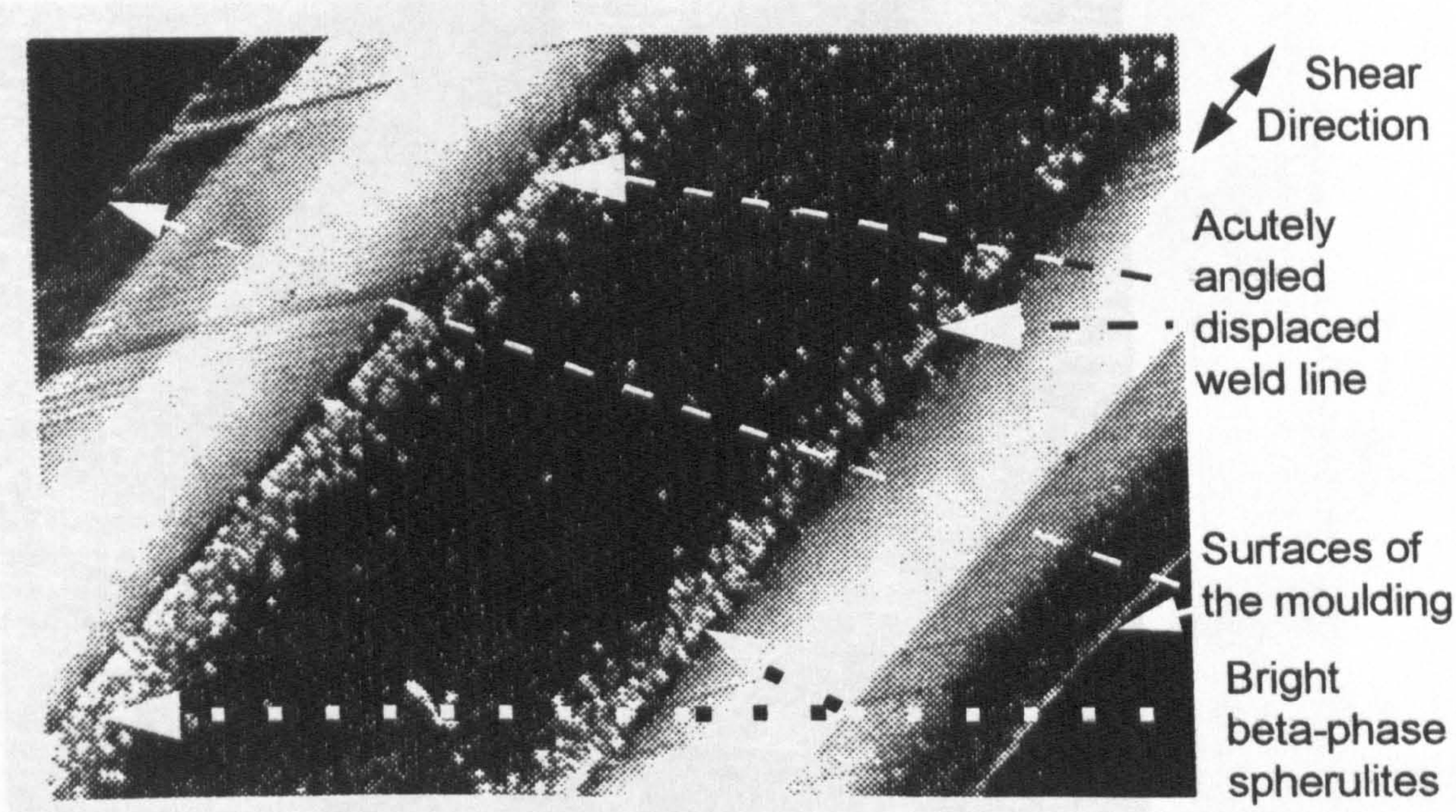

Figure 4.3 Microtomed section of a 2-colour iPP SCORIM moulding produced using a 3.0 second delay time and two shears. The sample is viewed under polarised light and shows the displaced weld line acutely angled to the mouldings surfaces. This interface is marked by the presence of β-spherulites on one side of it.

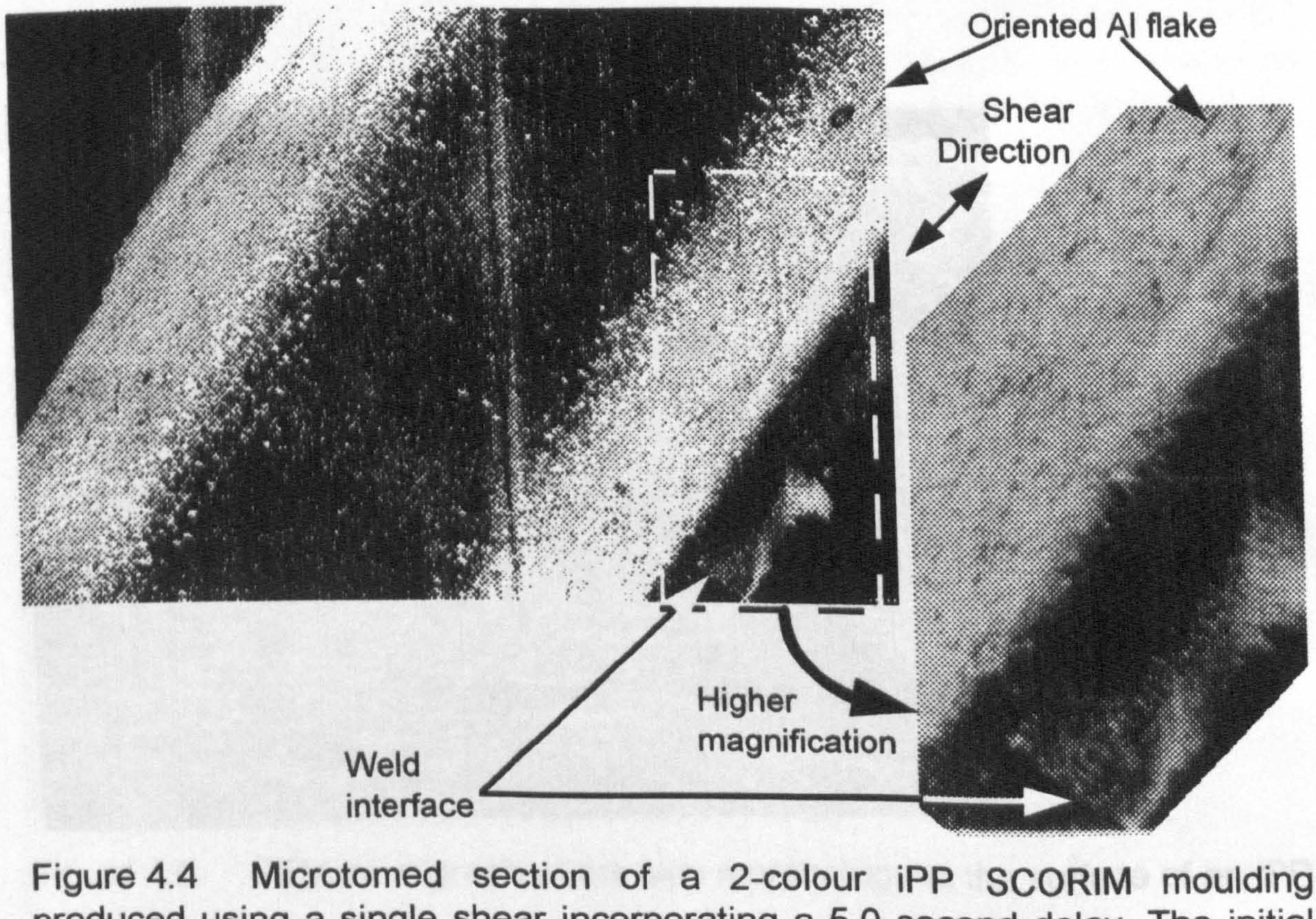

Figure 4.4 Microtomed section of a 2-colour iPP SCORIM moulding produced using a single shear incorporating a 5.0 second delay. The initial weld line can be seen at the edges of the section before SCORIM displaced it. The displaced weld line is acutely angled to the surfaces of the sample, and the Al flake present in the material at one side of this interface can be seen to have oriented preferentially in the flow direction by virtue of shear from SCORIM.

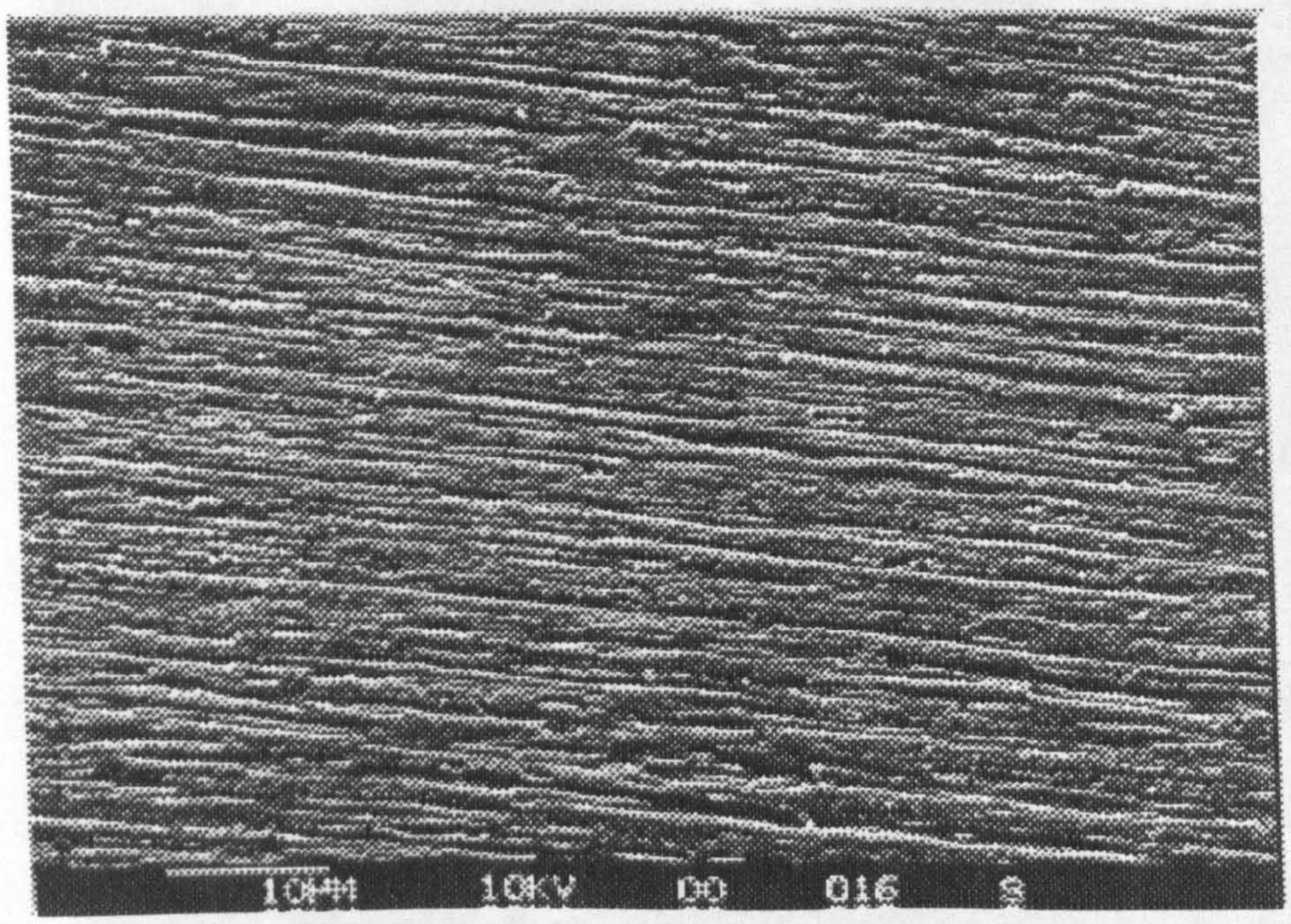

Figure 4.5 SEM micrograph of the lamellar morphology in the shear region of an iPP SCORIM moulding, produced with two intermittent shears containing 6.0 second delays. The scale bar is 10µm.

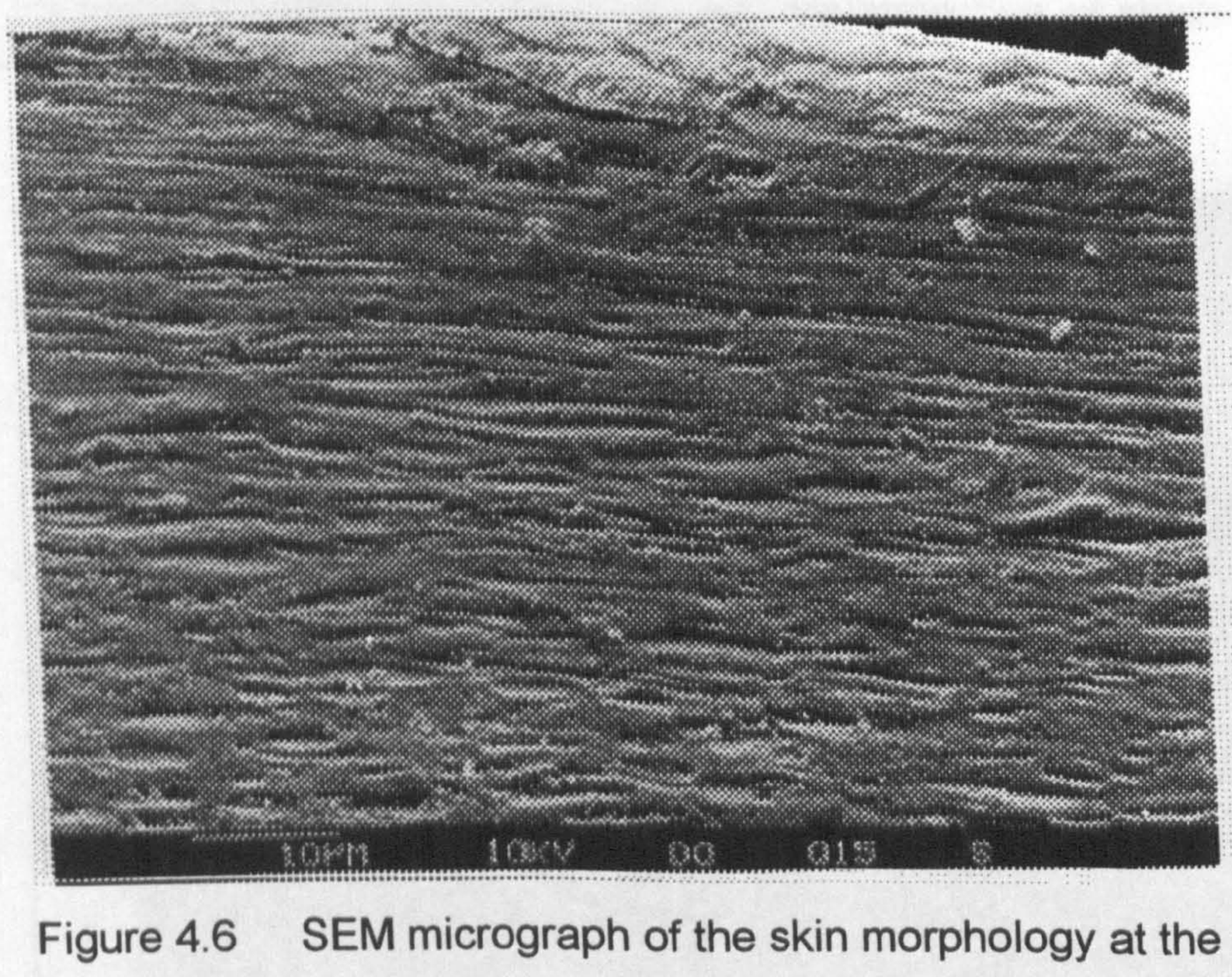

Figure 4.6 SEM micrograph of the skin morphology at the surface of an iPP SCORIM moulding, produced with two intermittent shears containing 6.0 second delays. The region shown was not affected by SCORIM as it had solidified immediately the polymer impinged against the cavity wall. Scale bar is 10µm.

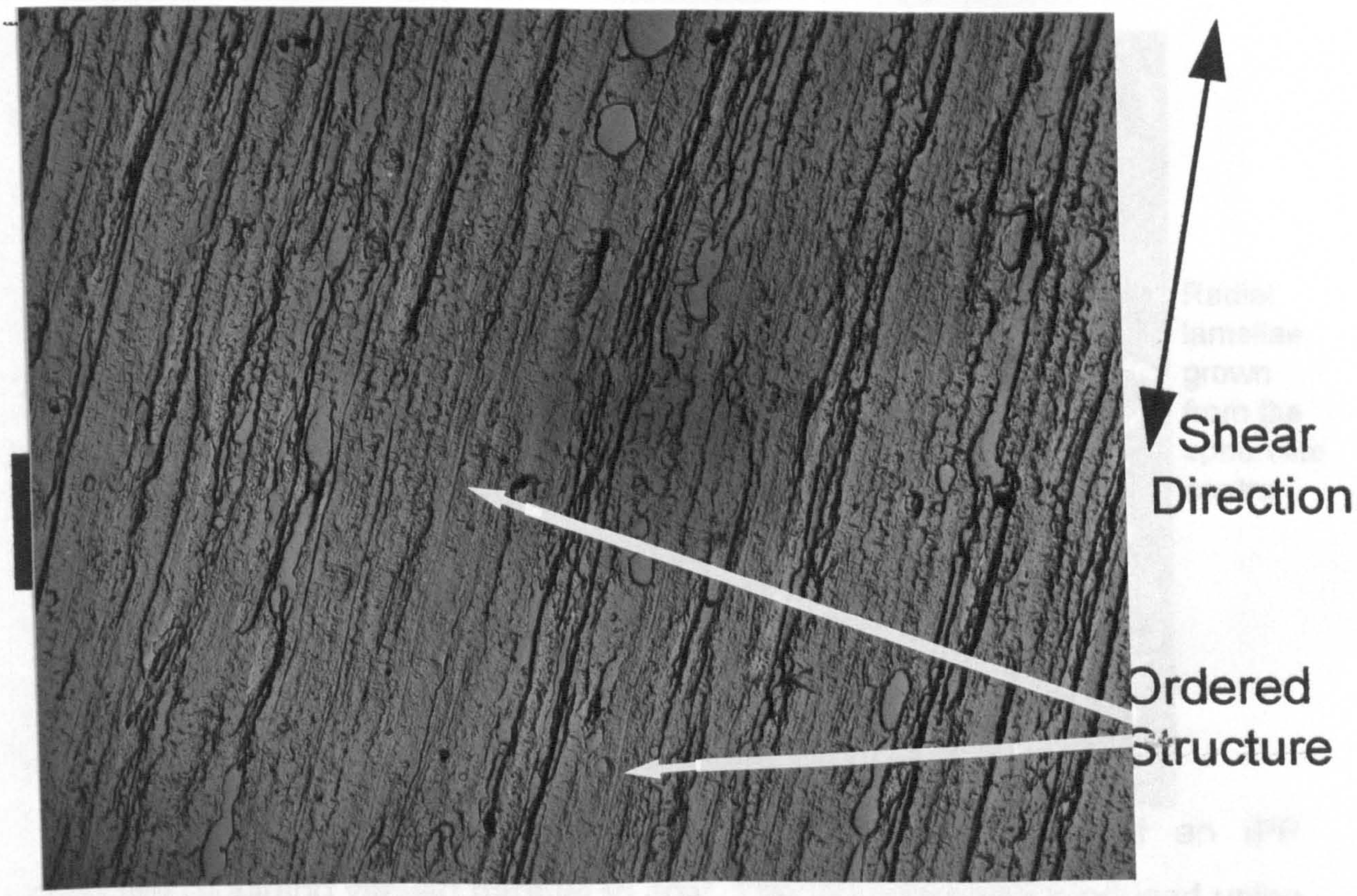

Figure 4.7 TEM micrograph viewed parallel to flow of the shear region of an iPP SCORIM moulding produced with two intermittent shears with 6.0 second delays. The rows of ordered structure present with preferred orientation in the shear direction may be indicative of shish-kebab structure. Scale bar 2μm.

Figure 4.8 TEM micrograph viewed perpendicular to flow of the shear region of an iPP SCORIM moulding. The moulding was produced using 5 shears with no delay inbetween them. The directional change of the flow has been encapsulated within this microstructure as banded regions. Scale bar 2μm.

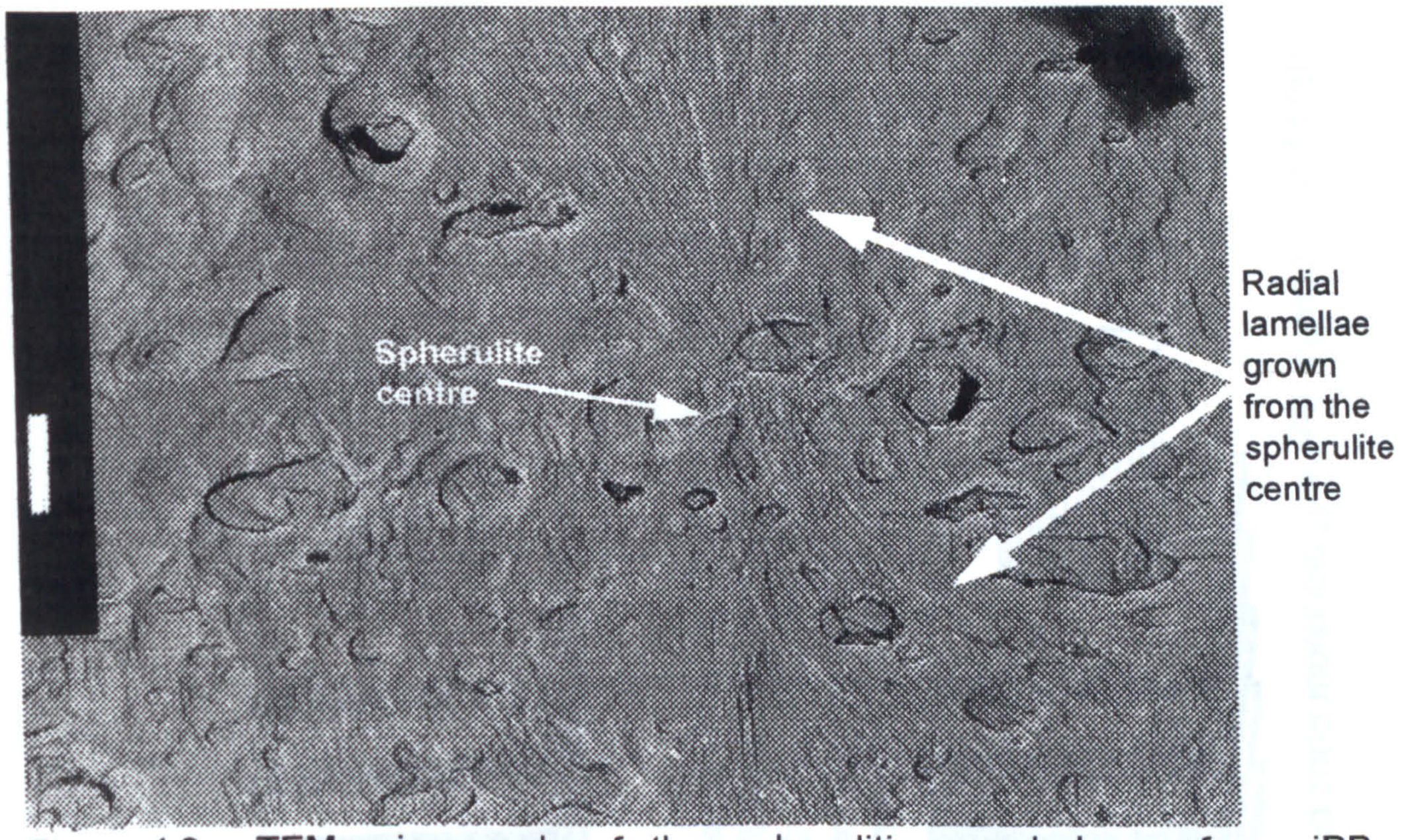

Figure 4.9 TEM micrograph of the spherulitic morphology of an iPP SCORIM moulding viewed parallel to flow. The moulding was produced using 5 shears with no delay inbetween them. Scale bar 1μm.

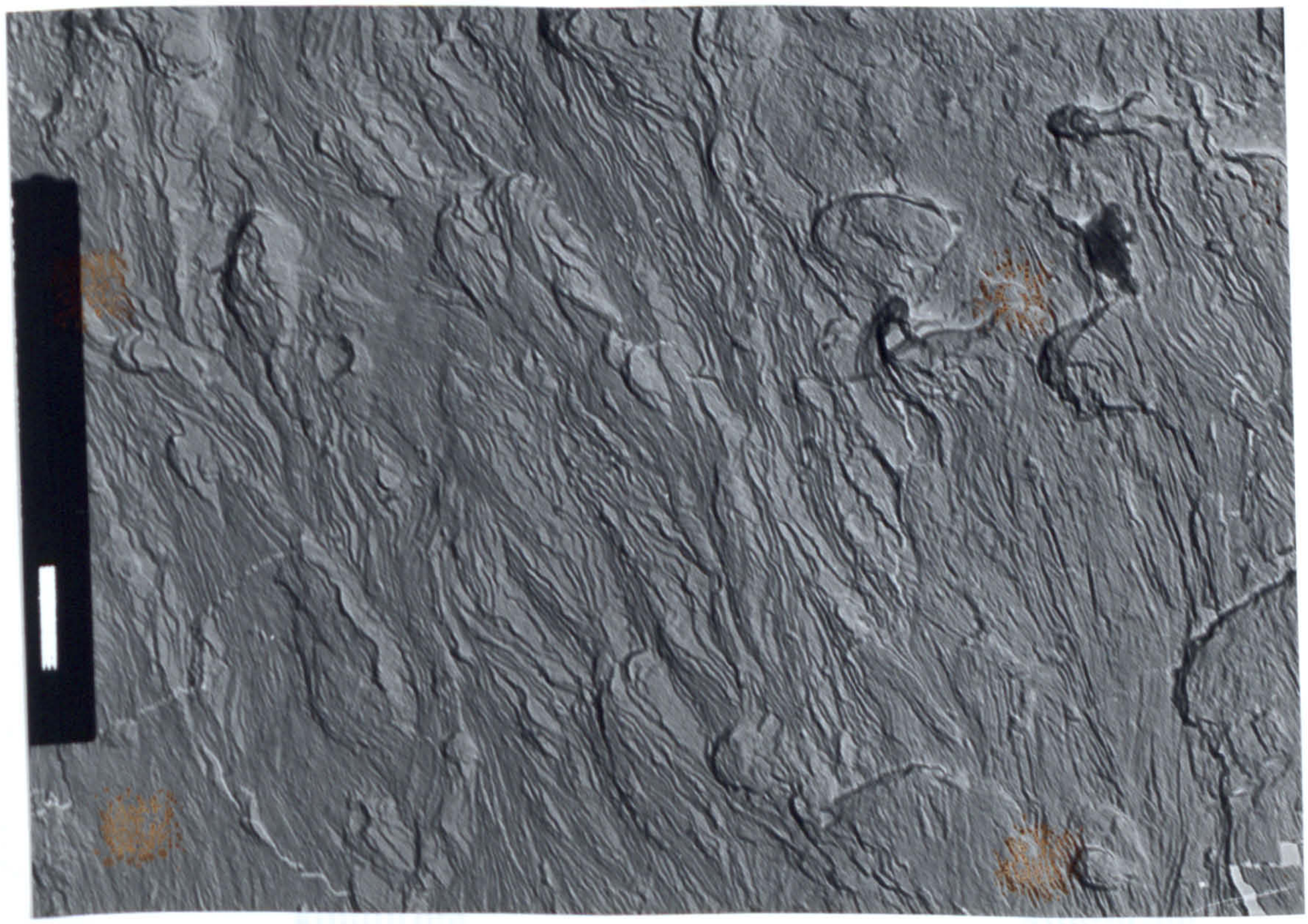

Figure 4.10 TEM micrograph of the lamellar morphology of a spherulite from the core region of an iPP SCORIM moulding. Scale bar 500nm.

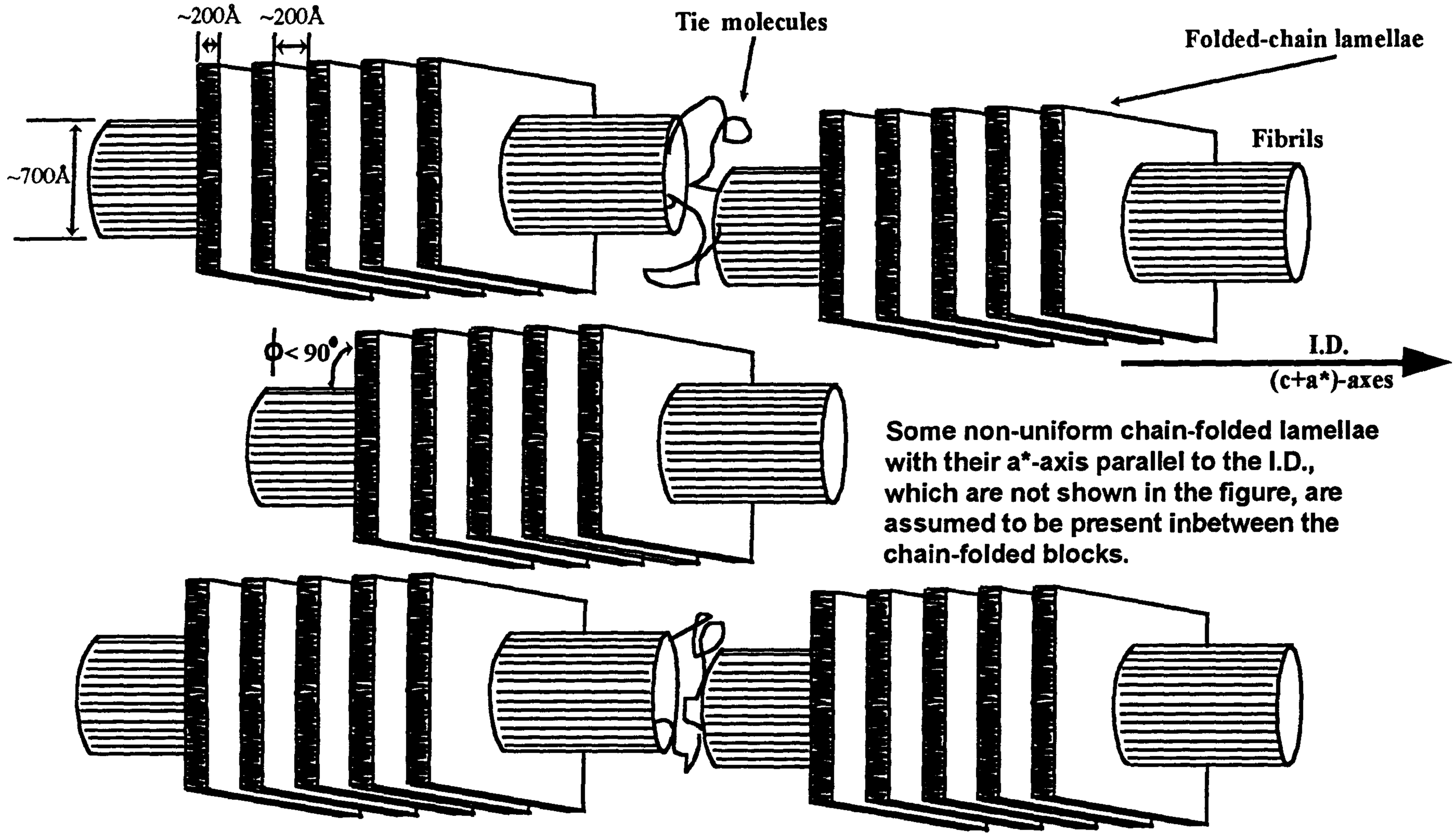

Figure 4.11 Schematic diagram of the model proposed by Kalay[72] for the oriented zone morphology in iPP injection mouldings.

5. CRYSTALLINITY OF α-, β- AND γ-PHASES

5.1 X-Ray Diffraction Profiles

Tables 5.1 to 5.15 summarise measurements of 2θ angles, d-spacings, d* (=λ/d), the relative intensities of the diffraction peaks, crystal phase and their respective Miller indices associated with the reflections recorded from conventional, single and double shear SCORIM PP mouldings produced using time delays between shear strokes. The samples were sectioned from the centreline of the mouldings as illustrated in figure 2.8.

The samples were moulded with unfilled PP and 2% ET2025 Al flake in PP through the twin barrels of the injection moulder. The presence of the Al flake provided a suitable marker material to ensure an initial flat weld interface, before the application of SCORIM. It also provided a visual record of the effects SCORIM was having on the displacement of the internal weld line, ensuring the required processing was successfully occurring. To evaluate the effect of the Al flake on the crystallography of the PP, x-ray diffraction profiles of both materials from a conventional moulding were evaluated, figure 5.1. The percentage crystallinity, α- and γ-phase contents and indices were essentially unaffected by the presence of the Al flake. The only apparent effect of the presence of the Al flake was to introduce a large β-phase which was completely absent in the unfilled material. The β-phase is associated with the spherulitic morphology of the moulding core, and therefore does not influence the morphology of the SCORIM shear regions. The development of a β-phase with the presence of the Al flake is testament to the heterogeneous nucleating properties of this filler material on the PP. This is consistent with the photomicrographs of section 4.

Figures 5.2 and 5.3 show the diffraction profiles obtained for the SCORIM mouldings, with figure 5.4 showing further diffraction profiles with the reflection peaks identified by their respective Miller Indices. For the conventional (i.e. no shear) unfilled section the strongest reflection is that of the $(110)_\alpha$ plane. With the application of SCORIM a strong $(300)_\beta$ peak

developed, synonymous with and proportional to the Al flake present in this sectioned sample. The $(040)_\alpha$ peak also became more intense. The relative intensity of the $(040)_\alpha$ peak became stronger than that of the $(110)_\alpha$ peak with the use of a single shear of 1.0s delay or longer. $(040)_\alpha$ appears to have increased in intensity in proportion to the length of delay time and number of shears applied. Although the $(110)_\alpha$ and $(130)_\alpha$ peaks changed in *relative* intensity and $(060)_\alpha$ and $(220)_\alpha$ peaks retained the same *relative* intensities throughout the families of mouldings presented, their *actual* intensities did increase with increasing delay times and number of shears. This response is a reflection of the increased level of preferred orientation and volume of shear induced crystallisation frozen into the morphology of the moulding with increased delay times and number of shears, as depicted in the photomicrographs of the previous section in figures 4.1 and 4.2. The $(111)_\alpha$ and $(041)_\alpha$ peaks are present in conventional and SCORIM mouldings with various relative intensities dependent upon the height of the most intense peak. Their actual intensities do not however appear to alter much implying their presence is only mildly influenced by the level of shearing induced here.

Tables 5.16 and 5.17 contain the α-phase, β-phase and crystallinity indices, as well as the percentage crystallinities of the one and two shear samples determined from their respective diffraction profiles. The α-phase indices *A* are plotted in figure 5.5 and demonstrate good correlation between *A* and delay times incorporated between shears. The single shear mouldings demonstrate a general rise in *A* with increasing delay times with a reasonable amount of scatter. However, although there is a notable difference between conventional and SCORIM mouldings, the difference between the individual SCORIM mouldings is only small over the processing conditions investigated here. Significantly, the double shear mouldings exhibit excellent correlation between *A* and the delay times incorporated between shears. A rapid increase in *A* from a conventional moulding to one which experienced delayed shears is present. The rate of increase smoothly decelerates with increasing delay time. There are also 10 and 30% increases in *A* over the

range presented here for the one and two shear mouldings respectively, indicating that *A* increases with the:-

- ➢ application of SCORIM relative to conventional moulding.
- ➢ increase in shears from one to two.
- ➢ amount of time incorporated between shears up to at least six seconds.

When these SCORIM mouldings alone are replotted with a logarithmic timescale a near linear relationship emerges between the delay times incorporated between shears and *A*. This is shown in figure 5.6.

Two probable reasons are proposed for this logarithmic relationship when two SCORIM shears are applied to the solidifying melt.

i. The constantly cooling molten polymer increases in viscosity with time.
ii. The width of molten core channel capable of flow under shear decreases with time.

Both these effects result in a proportional increase in the severity of extensional flow taking place through this channel under shear. This results in increased stretching of the coiled and entangled polymer molecules which in turn are proportional to the higher intensities of reflections in the x-ray diffraction profiles. The extent of orientation it is possible to induce in mouldings is dependent upon many factors including,

- ♦ melt temperature,
- ♦ polymer molecular weight and molecular weight distribution,
- ♦ extent of chain branching and side groups,
- ♦ mould temperature (i.e. cooling rate),
- ♦ level of shearing applied (i.e. SCORIM profile),
- ♦ thickness of mould cavity and general flow path geometry.

A limiting factor must exist whereby preferred orientation and *A* reach upper limits. The limiting factor within this work was the prevention of further shearing due to the solidification of the mould gates.

Figures 5.7 and 5.8 graphically illustrate the correlations of crystallinity index *C* and percentage crystallinity with piston delay times for one and two shear mouldings respectively. As the methods of calculation of these two parameters (section 2.7.2) use similar information to those of *A*, it should be expected that all three parameters intensities will closely map each other. This assumption is reflected in the profiles plotted, and consequently it may be considered that the factors influencing the intensities of all three parameters are largely the same. Figures 5.9 and 5.10 illustrate the logarithmic plots of the piston delay times between shears versus *C* and percentage crystallinity respectively, for the two shear mouldings. The approximated linear relationship evident here, with some experimental scatter, supports the findings with *A* that evidence of a linear relationship is present between the logarithmic timescale of the piston delay times and the parameters' intensities.

The intensity of the β-phase index, *B*, is related to the volume of Al flake present in the core of the sample characterised. This information does not therefore offer any clear indication of the way SCORIM influences the value of *B*. The single shear samples exhibit higher values of *B* than the double shear samples simply due to the greater volume of Al flake in the sections measured here.

γ-phase is reported by Turner Jones *et al*[45] to be characterised by five strong x-ray reflections with d-spacings at 6.37, 5.29, 4.415, 4.19 and 4.05Å, four of which lie close to four of the five strong α-phase reflections at 6.26, 5.19, 4.77, 4.19 and 4.04Å. The 4.77Å reflection of α-phase is completely absent in the γ-phase and is replaced by the reflection at 4.42Å[45]. SCORIM mouldings are frequently reported[58, 72, 85, 87] to contain γ-phase at 4.42Å but its presence was only detected in small quantities in these samples. However, figure 5.2 may indicate that samples produced with two SCORIM shears using 4 second delays or longer were beginning to develop γ-phase reflections at 4.42Å. With respect to the other four γ-phase reflections, if present in only small quantities their presence may be masked by the larger quantities of the α-phase reflections.

The γ-phase index was determined for the one and two shear samples. However, γ-phase was present in only very small quantities and was barely distinguishable from the background noise of the diffraction profiles, making accurate quantitative evaluation extremely difficult. Thus suggesting that γ-phase was not able to develop within these samples in any significant quantities, under the relatively low levels of SCORIM shear experienced here. No clear difference was evident between any of these samples.

Figure 5.4 shows two diffraction profiles from the same sample, a PP moulding produced using two SCORIM shears with 6.0 second delays, where the volume of material displaced with the shears was larger than that of the similar moulding of figure 5.3. The sections characterised are schematically represented in figure 2.8. This moulding clearly exhibits the γ-phase reflection at 4.42Å of the $(117)_\gamma$ plane in both the centreline and edge samples. The centreline sample also exhibits a small $(113)_\gamma$ reflection whose presence is inconclusive in the edge sample. Conversely, a $(300)_\beta$ reflection is present in the edge sample and absent in the centreline sample. Further, the $(111)_\alpha$ and $(041)_\alpha$ are a clear doublet in the edge sample but appear merged in the centreline sample. Both samples exhibit $(200)_\alpha$ and $(117)_\gamma$ reflections apparently absent in the samples of figures 5.2 and 5.3. This would imply that a minimum amount of shearing is required in these SCORIM samples before these α- and γ-phases are detectable. Similar findings were reported by Kalay *et al*[87] where only α- and β-phases were detected in conventional mouldings and only α- and γ-phases in SCORIM mouldings.

The different characteristics of the profiles obtained from the centreline and edge samples of the same moulding are synonymous with the 'U'-shaped flow fronts presented in section 3.2. Here, the different amounts of flow in these two regions manifest themselves as subtle differences in reflection intensities.

5.2 Debye Patterns and Molecular Orientation

Debye patterns are consistent with orientation observed in the micrographs of figures 4.1c and 4.2c where 6 second delay times were incorporated. The x-

ray beam was perpendicular to the injection direction for sections cut parallel to the injection direction. Diffraction patterns were taken at 0.25mm increments from the edge through to the centre of the mouldings.

Figures 5.11a & b show the Debye patterns recorded from the longitudinal sections of samples which have undergone one and two shears respectively. Each was produced with delays between mould fill and subsequent shears of 6 seconds. The SCORIM profiles are tabulated in 4.1 to 4.14. Figure 5.12 is a schematic representation of the Debye patterns shown in figures 5.11a & b at 0.75mm, where pronounced orientations were exhibited. The reflections correspond to those identified in tables 5.8 and 5.15, except for those of Miller indices $(300)_\beta$, as this reflection is a shoulder upon the much stronger $(110)_\alpha$ reflection, by which it is masked. Both of these mouldings exhibited preferred orientation in the longitudinal direction characterised, this orientation manifesting itself in reflections of crystal planes with the Miller indices {110}, {040}, {130}, {111}, {041}, {060} and {220}.

Preferred orientation existed at 0.25mm from the edge where orientation was sandwiched between the skin layer and the first SCORIM shear. This orientation was formed during the fountain flow of mould fill, as a consequence of shearing next to the skin layer by the flowing core. Measurements at 0.5mm and some further towards the core, exhibit greatly increased preferred orientation as a consequence of SCORIM. The intensities of these SCORIM induced orientations reflect the effectiveness of the process to facilitate crystallographic change through elongational and extensional flow. Orientation then decayed as the spherulitic core (uninfluenced by SCORIM) was approached, and disappeared completely from 1.5mm to the centre. For this reason only the Debye patterns from the edges to 1.25mm are shown in figure 5.11. The extent of orientation present through the thickness of the mouldings appears to be less in figure 5.11a than 5.11b, reflecting the findings of the corresponding '6 second delay' photomicrographs of figures 4.1c and 4.2c respectively. Both findings illustrate that orientation exists as a consequence of SCORIM, progressing further into the core of the moulding with each successive shear.

It was noted however that the preferred orientation displayed in the Debye patterns was not as pronounced a spot as recorded by Kalay[72, 85] in some SCORIM mouldings. In order to ascertain whether this was due to the level of orientation induced by the SCORIM sequence used during processing, or the influence of any unoriented material adjacent to the SCORIM layers, the same samples were sectioned to exclude all but the most highly oriented SCORIM layers in the 0.5 to 0.75mm regions. This removed the skin and spherulitic core layers, thus eliminating any possible contribution to the Debye patterns by unoriented material. These sections were then re-analysed to produce additional Debye patterns, with an equivalent region from a conventional moulding also characterised for comparison. These Debye patterns are presented in figures 5.13 to 5.15 and represent the conventional, single shear and double shear (incorporating 6 second delays) mouldings respectively.

Figure 5.13 exhibits diffuse rings consistent with no preferred orientation being present in this region of a conventional moulding. The equivalent sections of the SCORIM mouldings in figures 5.14 and 5.15 exhibit preferred orientation by virtue of SCORIM processing alone. It was envisaged that these sections may exhibit very sharp spots on the Debye patterns, indicative of extremely high orientation. However, the spots are relatively broad indicating that the levels of orientation induced are not as high as those observed[72, 85] in iPP mouldings where constant shearing was applied to the solidifying melt without the use of piston restrictors. The levels of orientation recorded in figures 5.14 and 5.15 are no stronger than those of the same regions of figure 5.11, indicating that the degree of preferred orientation exhibited in figure 5.11 was not affected by the adjacent unoriented material.

Figure 5.16 is the Debye pattern from a SCORIM moulding which was produced using 3 shears incorporating 6 second delays encountering some gate 'freeze off' in the process and therefore not representing ideal moulding conditions. The SCORIM profile is shown in table 5.18, with the volume of material sheared with each piston oscillation being greater than those of the

previous samples. The section was again taken from the mouldings' centreline and the x-ray beam passed through the section 1.25mm from the moulding's surface skin. The much more clearly defined spots on the rings of the Debye pattern indicate a much higher level of preferred orientation to be present at this point through this moulding's thickness. It follows that an increased level of orientation must be due to a greater level of shearing within the moulding. This is consistent with the knowledge gained hitherto, that the cavity solidifies in banded layers of thicknesses related to the delay times between SCORIM shears. With a managed and consistent volume of material being sheared with each piston stroke, the material was forced to flow through a constantly thinning core region, inducing a much higher level of preferred orientation with each subsequent shear, due to the greater resistance to flow. This resistance to flow ensured the PP molecular chains disentangled and uncoiled through extensional flow and by the 3rd shear, they were attaining higher degrees of alignment in the flow direction than seen in the other samples. This newly created orientation then solidified before chain relaxation could occur to remove it. The position of this Debye pattern at 1.25mm from the moulding surface is approximately the position of the 3rd shear interface, and hence the higher level of orientation recorded here than when only one or two shears were used as with the previous samples.

Figures 5.17 and 5.18 are Debye patterns taken at 0.5mm from the surface of the same moulding but from the centreline and edge locations respectively, as illustrated in figure 2.8. The moulding was processed using 41 reciprocating shears which were applied consecutively, allowing no delay between flow reversals. The SCORIM profile is given in table 5.19. Figure 5.17 has no preferred orientation at this point which indicates no SCORIM shearing was taking place here. However, figure 5.18 exhibits preferred orientation in the flow direction due to the SCORIM shearing at this edge location. This morphological characterisation is consistent with the visual evidence provided in chapter 3 for the preference of material to flow along the

edges of mouldings during the SCORIM process and less so through the centre.

5.3 Relationship Between Processing Conditions and Crystallinity

The dynamic relationship between SCORIM processing and the different crystallinities which exist within PP mouldings, have revealed detailed information from the characterisations of the families of mouldings presented within this chapter, *viz.*

i) Values of *A*, *C* and percentage crystallinity increased with the application of SCORIM. A linear relationship was discovered to exist between them and the logarithmic piston delay times for two shear mouldings. The limiting factor in this work was gate 'freeze off' preventing further shearing. The values of the above parameters obtained within such a system is a function of temperatures, material rheology and mould geometry.

ii) Evidence from x-ray diffraction and Debye patterns suggest that the edge of a moulding exhibits greater preferred orientation than the centreline. This would be due to more SCORIM shear flow occurring at the edge which is an observation commensurate with visual evidence from other 2-colour mouldings.

iii) The inception of γ-phase with SCORIM moulding was directly related to the level of shearing within the mould. In this research, a greater volume of material sheared with each oscillation was enough for this to occur.

iv) Preferred orientation was recorded further from the surface of mouldings, measured through their thickness, with each successive shear. The delay times incorporated between shears allowed solidification to occur encapsulating the oriented material. Subsequent shears flowed through ever narrowing channels where the preferred orientation induced encroached into the core.

v) The addition of the Al flake to the PP was found to nucleate β-phase spherulitic morphology within the core region of mouldings.

Table 5.1 X-ray data for a conventional moulding

2θ (deg.)	d-spacing (Å)	d* (=λ/d)	Miller Indices (hkl)	Crystal Phase	Relative Intensity (%)
13.91	6.367	0.242	110	α_1	100
15.84	5.594	0.276	300	β_1	32
16.76	5.288	0.292	040	α_2	77
18.38	4.826	0.319	130	α_3	60
21.07	4.216	0.366	111	α_4	55
21.57	4.119	0.374	041	α_4	58
25.27	3.524	0.438	060	α_5	9
28.27	3.156	0.489	220	α_{220}	5

Table 5.2 X-ray data for single shear with 0.5s delay

2θ (deg.)	d-spacing (Å)	d* (=λ/d)	Miller Indices (hkl)	Crystal Phase	Relative Intensity (%)
13.97	6.338	0.243	110	α_1	100
15.95	5.558	0.277	300	β_1	68
16.76	5.288	0.292	040	α_2	93
18.32	4.843	0.318	130	α_3	57
21.11	4.208	0.366	111	α_4	55
21.64	4.107	0.375	041	α_4	54
25.27	3.524	0.438	060	α_5	10
28.21	3.163	0.487	220	α_{220}	5

Table 5.3 X-ray data for single shear with 1.0s delay

2θ (deg.)	d-spacing (Å)	d* (=λ/d)	Miller Indices (hkl)	Crystal Phase	Relative Intensity (%)
13.95	6.348	0.243	110	α_1	99
15.93	5.565	0.277	300	β_1	63
16.74	5.295	0.291	040	α_2	100
18.42	4.815	0.320	130	α_3	60
21.05	4.221	0.365	111	α_4	55
21.68	4.099	0.376	041	α_4	53
25.29	3.521	0.438	060	α_5	10
28.27	3.156	0.489	220	α_{220}	4

Table 5.4 X-ray data for single shear with 2.0s delay

2θ (deg.)	d-spacing (Å)	d* (=λ/d)	Miller Indices (hkl)	Crystal Phase	Relative Intensity (%)
13.99	6.329	0.244	110	α_1	82
15.99	5.543	0.278	300	β_1	48
16.79	5.282	0.292	040	α_2	100
18.44	4.810	0.321	130	α_3	50
21.09	4.212	0.366	111	α_4	41
21.72	4.091	0.377	041	α_4	42
25.40	3.507	0.440	060	α_5	10
28.44	3.138	0.491	220	α_{220}	4

Table 5.5 X-ray data for single shear with 3.0s delay

2θ (deg.)	d-spacing (Å)	d* (=λ/d)	Miller Indices (hkl)	Crystal Phase	Relative Intensity (%)
13.97	6.338	0.243	110	α_1	76
15.99	5.543	0.278	300	β_1	42
16.76	5.288	0.292	040	α_2	100
18.44	4.810	0.321	130	α_3	50
21.11	4.208	0.366	111	α_4	40
21.74	4.088	0.377	041	α_4	42
25.38	3.510	0.439	060	α_5	11
28.52	3.129	0.493	220	α_{220}	5

Table 5.6 X-ray data for single shear with 4.0s delay

2θ (deg.)	d-spacing (Å)	d* (=λ/d)	Miller Indices (hkl)	Crystal Phase	Relative Intensity (%)
13.97	6.338	0.243	110	α_1	79
15.99	5.543	0.278	300	β_1	42
16.79	5.282	0.292	040	α_2	100
18.42	4.815	0.320	130	α_3	46
21.15	4.200	0.367	111	α_4	37
21.39	4.155	0.371	-131	α_4	34
21.68	4.099	0.376	041	α_4	37
25.31	3.519	0.438	060	α_5	10
28.42	3.140	0.491	220	α_{220}	4

Table 5.7 X-ray data for single shear with 5.0s delay

2θ (deg.)	d-spacing (Å)	d* (=λ/d)	Miller Indices (hkl)	Crystal Phase	Relative Intensity (%)
13.99	6.329	0.244	110	α_1	79
16.01	5.536	0.279	300	β_1	48
16.79	5.282	0.292	040	α_2	100
18.47	4.805	0.321	130	α_3	48
21.13	4.204	0.367	111	α_4	38
21.74	4.088	0.377	041	α_4	39
25.40	3.507	0.440	060	α_5	15
28.34	3.150	0.489	220	α_{220}	9

Table 5.8 X-ray data for single shear with 6.0s delay

2θ (deg.)	d-spacing (Å)	d* (=λ/d)	Miller Indices (hkl)	Crystal Phase	Relative Intensity (%)
13.99	6.329	0.244	110	α_1	76
15.97	5.551	0.278	300	β_1	48
16.79	5.282	0.292	040	α_2	100
18.44	4.810	0.321	130	α_3	45
21.07	4.216	0.366	111	α_4	38
21.70	4.095	0.377	041	α_4	37
25.33	3.516	0.439	060	α_5	10
28.42	3.140	0.491	220	α_{220}	3

Table 5.9 X-ray data for double shears with 0.5s delays

2θ (deg.)	d-spacing (Å)	d* (=λ/d)	Miller Indices (hkl)	Crystal Phase	Relative Intensity (%)
13.99	6.329	0.244	110	α_1	91
15.95	5.558	0.277	300	β_1	53
16.79	5.282	0.292	040	α_2	100
18.44	4.810	0.321	130	α_3	55
21.09	4.212	0.366	111	α_4	47
21.76	4.084	0.378	041	α_4	47
25.27	3.524	0.438	060	α_5	10
28.38	3.145	0.490	220	α_{220}	6

Table 5.10 X-ray data for double shear with 1.0s delays

2θ (deg.)	d-spacing (Å)	d* (=λ/d)	Miller Indices (hkl)	Crystal Phase	Relative Intensity (%)
13.99	6.329	0.244	110	α_1	81
15.99	5.543	0.278	300	β_1	35
16.76	5.288	0.292	040	α_2	100
18.47	4.805	0.321	130	α_3	49
21.07	4.216	0.366	111	α_4	35
21.66	4.103	0.376	041	α_4	36
25.35	3.513	0.439	060	α_5	10
28.46	3.136	0.492	220	α_{220}	4

Table 5.11 X-ray data for double shear with 2.0s delays

2θ (deg.)	d-spacing (Å)	d* (=λ/d)	Miller Indices (hkl)	Crystal Phase	Relative Intensity (%)
13.99	6.329	0.244	110	α_1	72
16.03	5.529	0.279	300	β_1	30
16.76	5.288	0.292	040	α_2	100
18.44	4.810	0.321	130	α_3	45
21.09	4.212	0.366	111	α_4	27
21.66	4.103	0.376	041	α_4	28
25.29	3.521	0.438	060	α_5	10
28.42	3.140	0.491	220	α_{220}	4

Table 5.12 X-ray data for double shear with 3.0s delays

2θ (deg.)	d-spacing (Å)	d* (=λ/d)	Miller Indices (hkl)	Crystal Phase	Relative Intensity (%)
13.99	6.329	0.244	110	α_1	67
15.97	5.551	0.278	300	β_1	27
16.79	5.282	0.292	040	α_2	100
18.44	4.810	0.321	130	α_3	41
21.17	4.196	0.367	111	α_4	23
21.68	4.099	0.376	041	α_4	22
25.33	3.516	0.439	060	α_5	10
28.46	3.136	0.492	220	α_{220}	4

Table 5.13 X-ray data for double shear with 4.0s delays

2θ (deg.)	d-spacing (Å)	d* (=λ/d)	Miller Indices (hkl)	Crystal Phase	Relative Intensity (%)
13.97	6.338	0.243	110	α_1	65
15.95	5.558	0.277	300	β_1	29
16.76	5.288	0.292	040	α_2	100
18.42	4.815	0.320	130	α_3	41
21.09	4.212	0.366	111	α_4	20
21.70	4.095	0.377	041	α_4	19
25.27	3.524	0.438	060	α_5	10
28.50	3.131	0.492	220	α_{220}	3

Table 5.14 X-ray data for double shear with 5.0s delays

2θ (deg.)	d-spacing (Å)	d* (=λ/d)	Miller Indices (hkl)	Crystal Phase	Relative Intensity (%)
13.97	6.338	0.243	110	α_1	64
15.97	5.551	0.278	300	β_1	28
16.74	5.295	0.291	040	α_2	100
18.44	4.810	0.321	130	α_3	39
21.05	4.221	0.365	111	α_4	20
21.70	4.095	0.377	041	α_4	18
25.31	3.519	0.438	060	α_5	11
28.50	3.131	0.492	220	α_{220}	4

Table 5.15 X-ray data for double shear with 6.0s delays

2θ (deg.)	d-spacing (Å)	d* (=λ/d)	Miller Indices (hkl)	Crystal Phase	Relative Intensity (%)
13.99	6.329	0.244	110	α_1	62
15.97	5.551	0.278	300	β_1	29
16.76	5.288	0.292	040	α_2	100
18.44	4.810	0.321	130	α_3	37
21.13	4.204	0.367	111	α_4	18
21.68	4.099	0.376	041	α_4	16
25.31	3.519	0.438	060	α_5	10
28.42	3.140	0.491	220	α_{220}	3

Table 5.16 α-phase orientation index *A*, β-phase orientation index *B*, crystallinity index *C* and crystallinities of the conventional and single shear SCORIM mouldings.

Sample ID	*A*	*B*	*C*	Crystallinity (%)
Conventional	0.653	0.021	1.34	38.04
0.5s Delay	0.673	0.193	1.96	42.28
1.0s Delay	0.672	0.167	1.86	40.61
2.0s Delay	0.711	0.133	2.04	42.08
3.0s Delay	0.685	0.111	1.84	42.26
4.0s Delay	0.716	0.122	2.13	45.56
5.0s Delay	0.724	0.133	2.12	45.06
6.0s Delay	0.704	0.145	2.06	42.29

Table 5.17 α-phase orientation index *A*, β-phase orientation index *B*, crystallinity index *C* and crystallinities of the double shear SCORIM mouldings.

Sample ID	*A*	*B*	*C*	Crystallinity (%)
0.5s Delay	0.69	0.129	1.67	41.72
1.0s Delay	0.733	0.082	1.94	43.21
2.0s Delay	0.778	0.075	2.36	44.84
3.0s Delay	0.814	0.07	2.35	46.50
4.0s Delay	0.834	0.083	2.55	47.27
5.0s Delay	0.845	0.084	2.63	47.04
6.0s Delay	0.852	0.09	2.86	47.51

Table 5.18 3 SCORIM shears produced with 6 second delays.

Stage ID	Duration (sec's)	C-time (sec's)	R-time (sec's)	C-Pres (%)	R-Pres (%)	Piston	Piston
S00	6.0	6.0	6.0	30	0	NO	None
S01	12.0	6.0	6.0	65	0	N	O
S02	20.0	20.0	20.0	65	0	O	O

SCORIM Profile: S00, S01, S02

Table 5.19 41 SCORIM shears produced without delays.

Stage ID	Duration (sec's)	C-time (sec's)	R-time (sec's)	C-Pres (%)	R-Pres (%)	Piston	Piston
S00	0.5	0.5	0.5	30	0	NO	None
S01	32.0	0.8	0.8	65	0	N	O
S02	20.0	20.0	20.0	65	0	N	O

SCORIM Profile: S00, S01, S02

N.B. (C-TIME) = Compression time; (R-TIME) = Relaxation time;
(C-PRES) = Compression pressure; (R-PRES) Relaxation pressure.

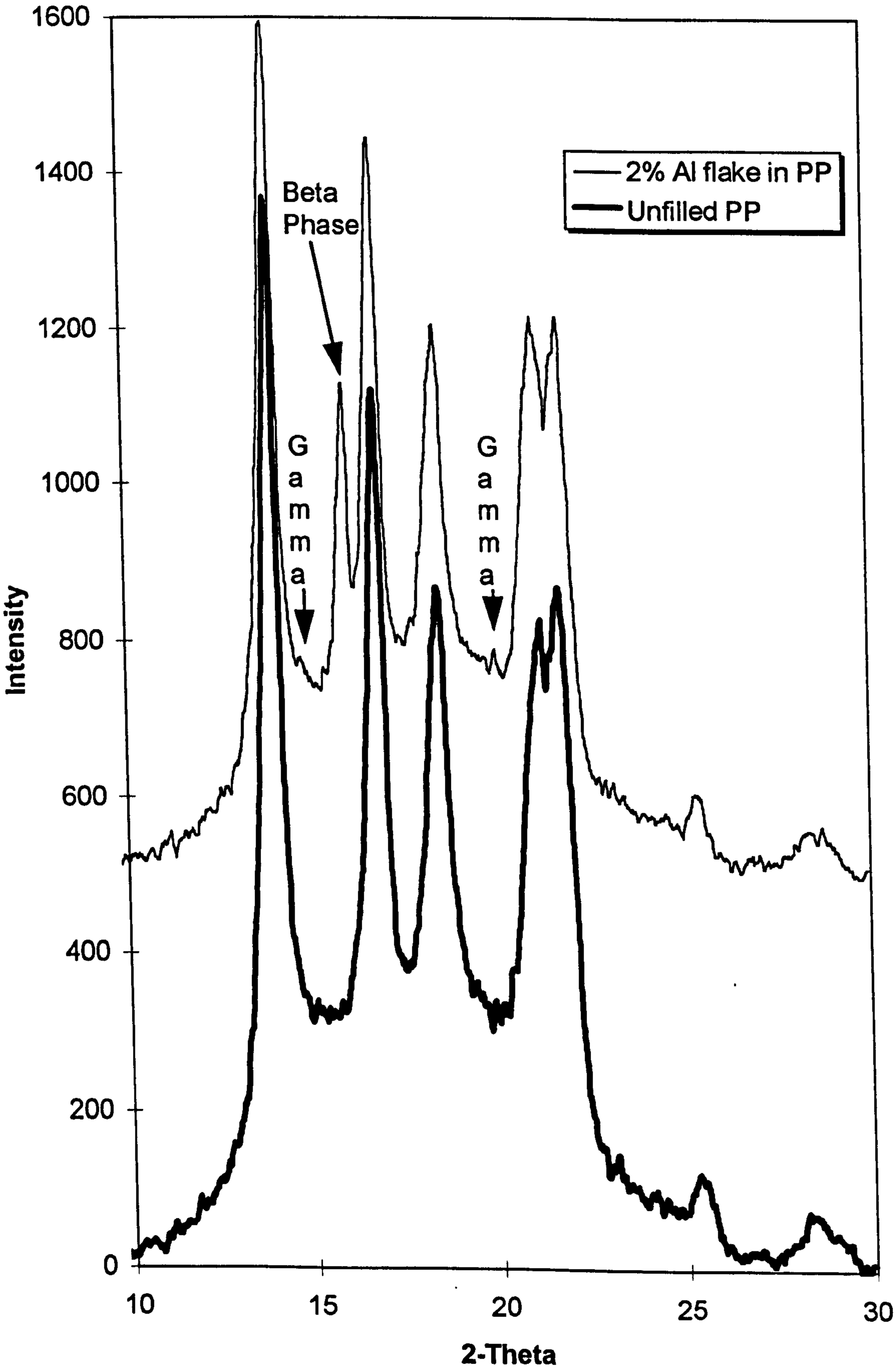

Figure 5.1 X-ray diffraction profiles from a two-colour conventional moulding consisting of 2% Al flake filled PP and unfilled PP.

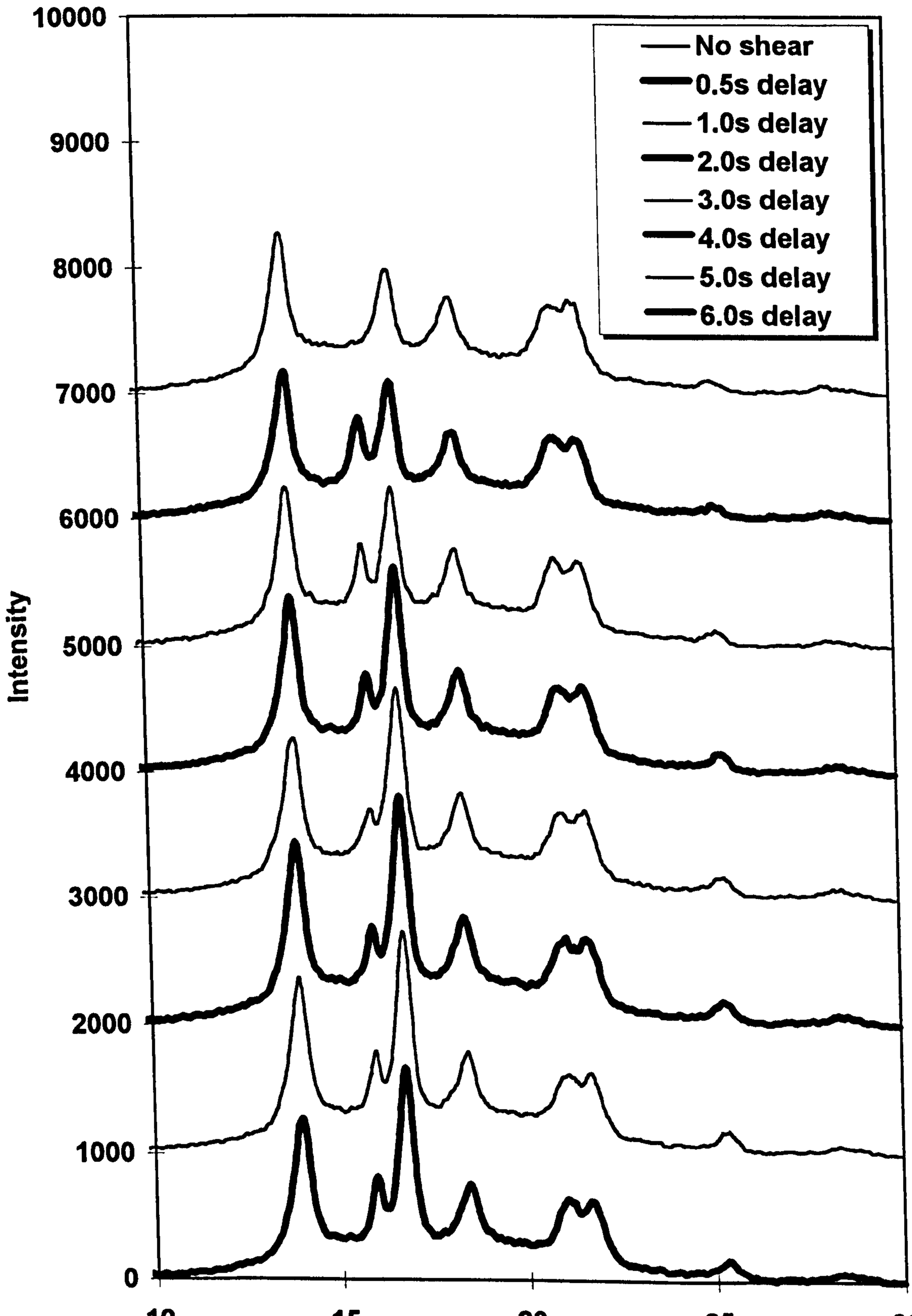

Figure 5.2 Graph of x-ray diffraction profiles of 2-colour iPP mouldings produced using one SCORIM shear with different delays before shearing commenced.

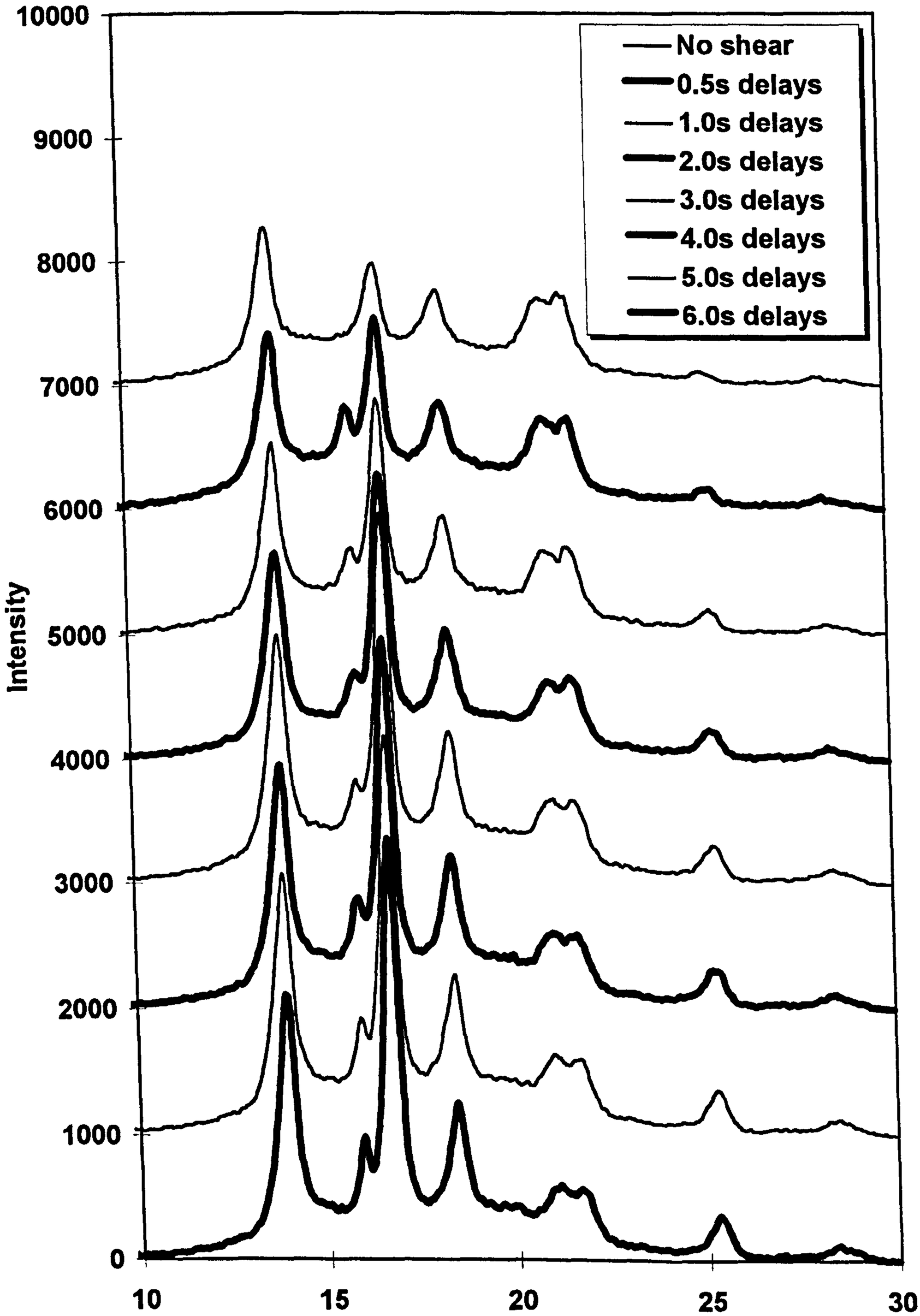

Figure 5.3 Graph of x-ray diffraction profiles of 2-colour iPP mouldings produced using two shears with different delays between shears.

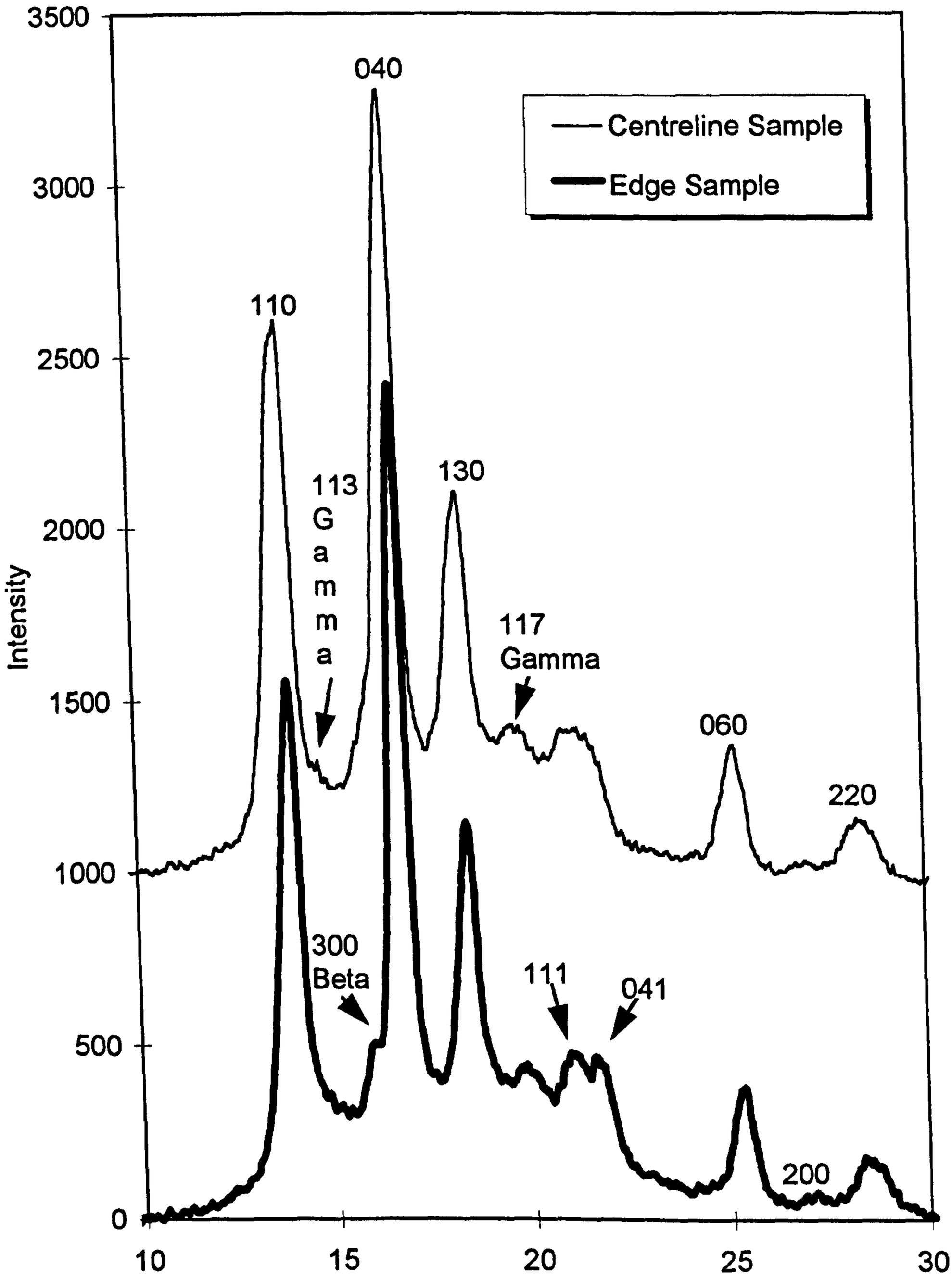

Figure 5.4 Graph of x-ray diffraction profiles of a 2-colour iPP moulding produced using two SCORIM shears with 6.0 second delays. The volume of material sheared with each reciprocation was greater than for the previous samples characterised. Sections for analysis were taken from two locations within the sample. The Miller indices relating to the various reflection peaks are displayed.

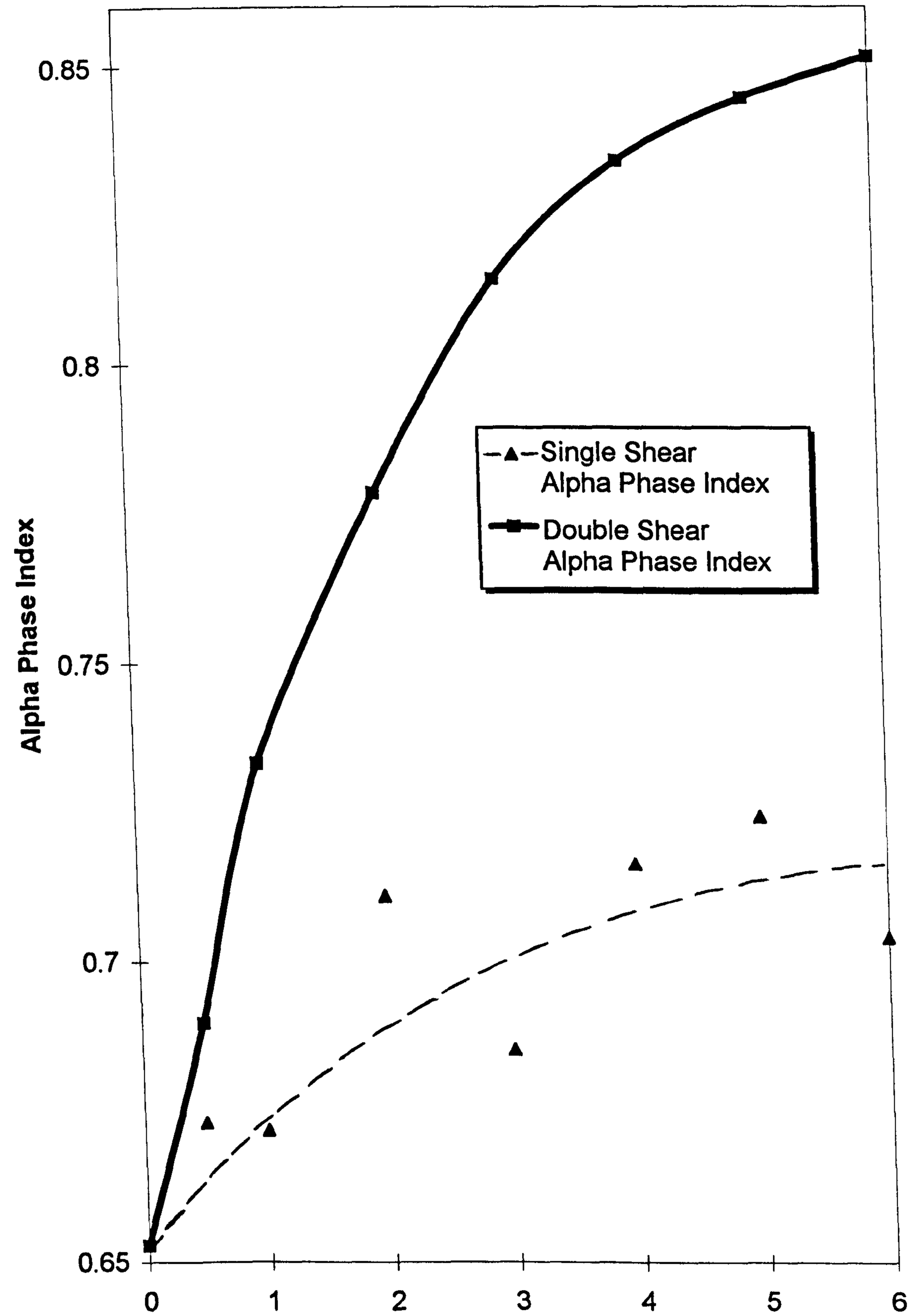

Figure 5.5 α-phase indices *A*, for one and two shear 2-colour iPP SCORIM mouldings produced using different delay times between shears. The value at zero relates to a conventional moulding.

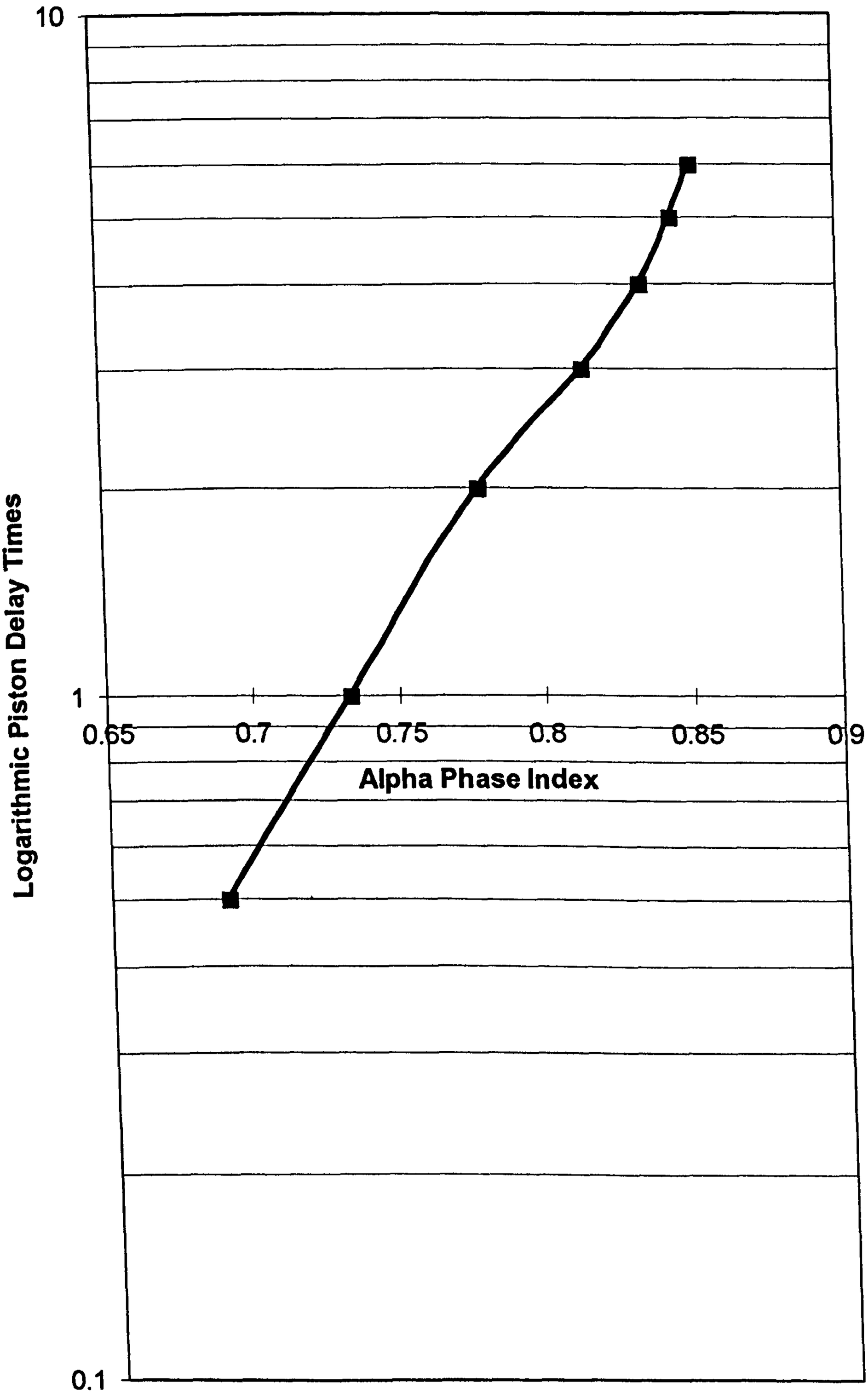

Figure 5.6 Logarithmic piston delay times versus α-phase index *A*, for the 2-colour iPP SCORIM mouldings produced using two shears.

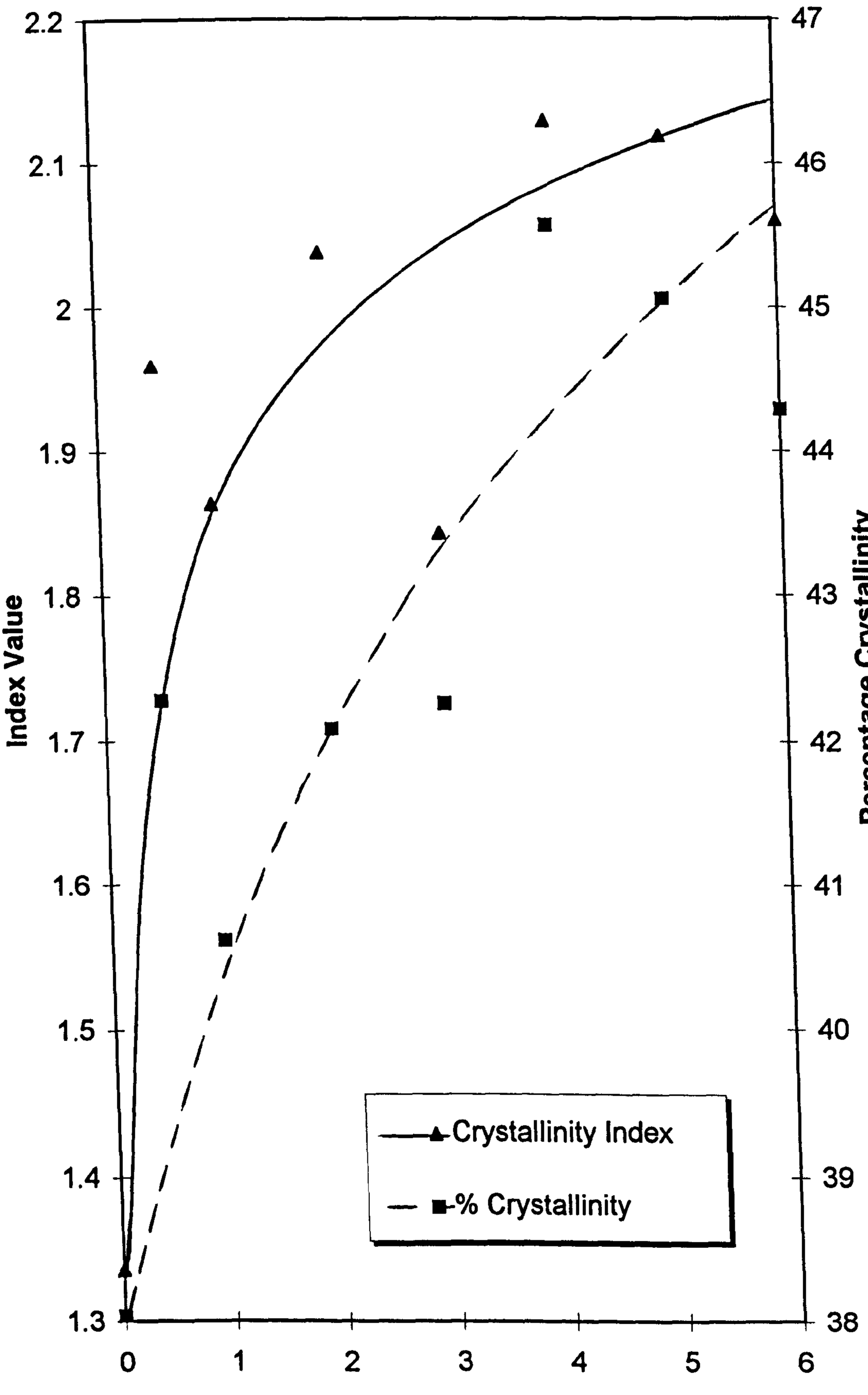

Figure 5.7 One shear 2-colour iPP SCORIM mouldings produced using different delay times between shears. The value at zero relates to a conventional moulding.

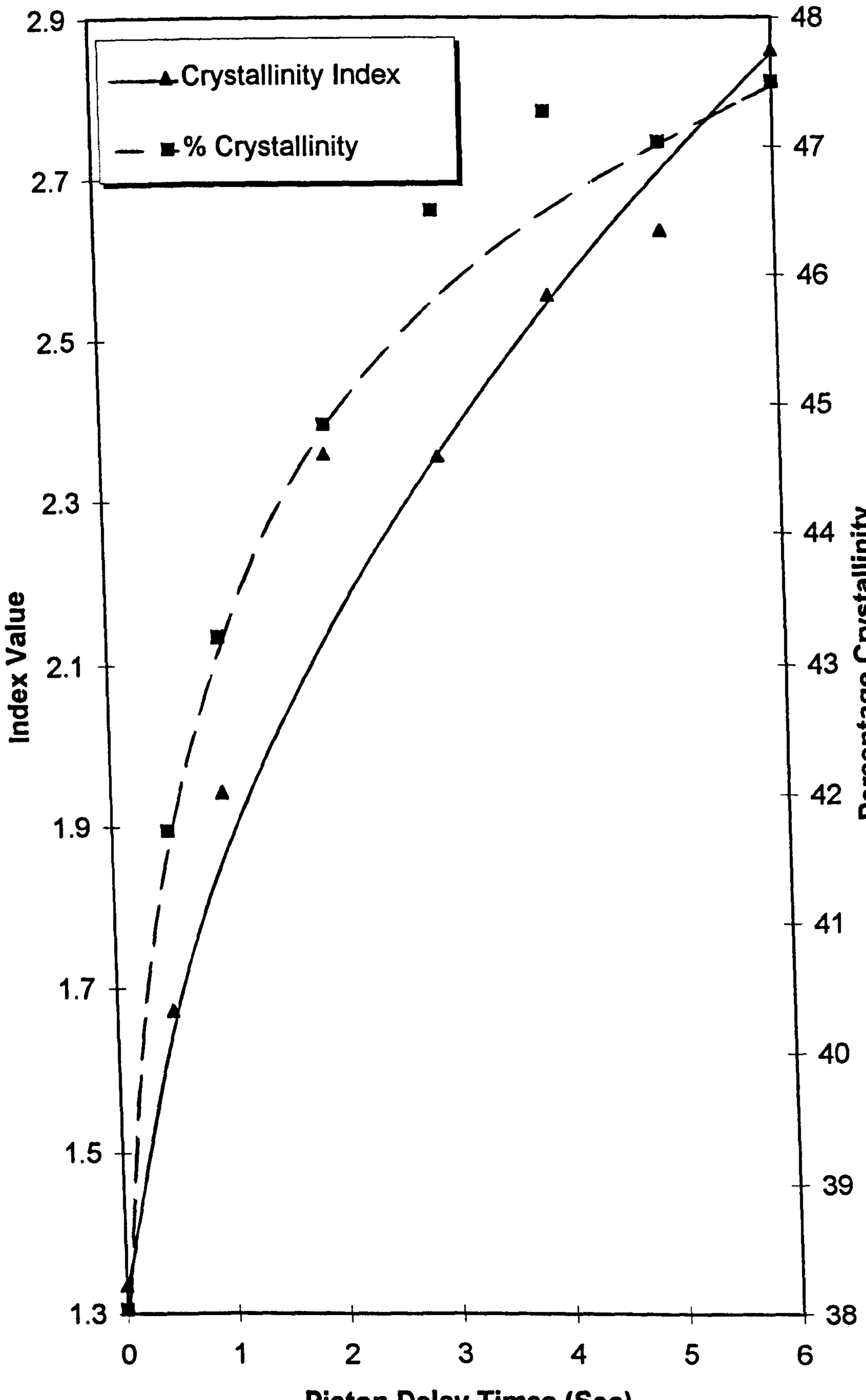

Figure 5.8 Two shear 2-colour iPP SCORIM mouldings produced using different delay times between shears. The value at zero relates to a conventional moulding.

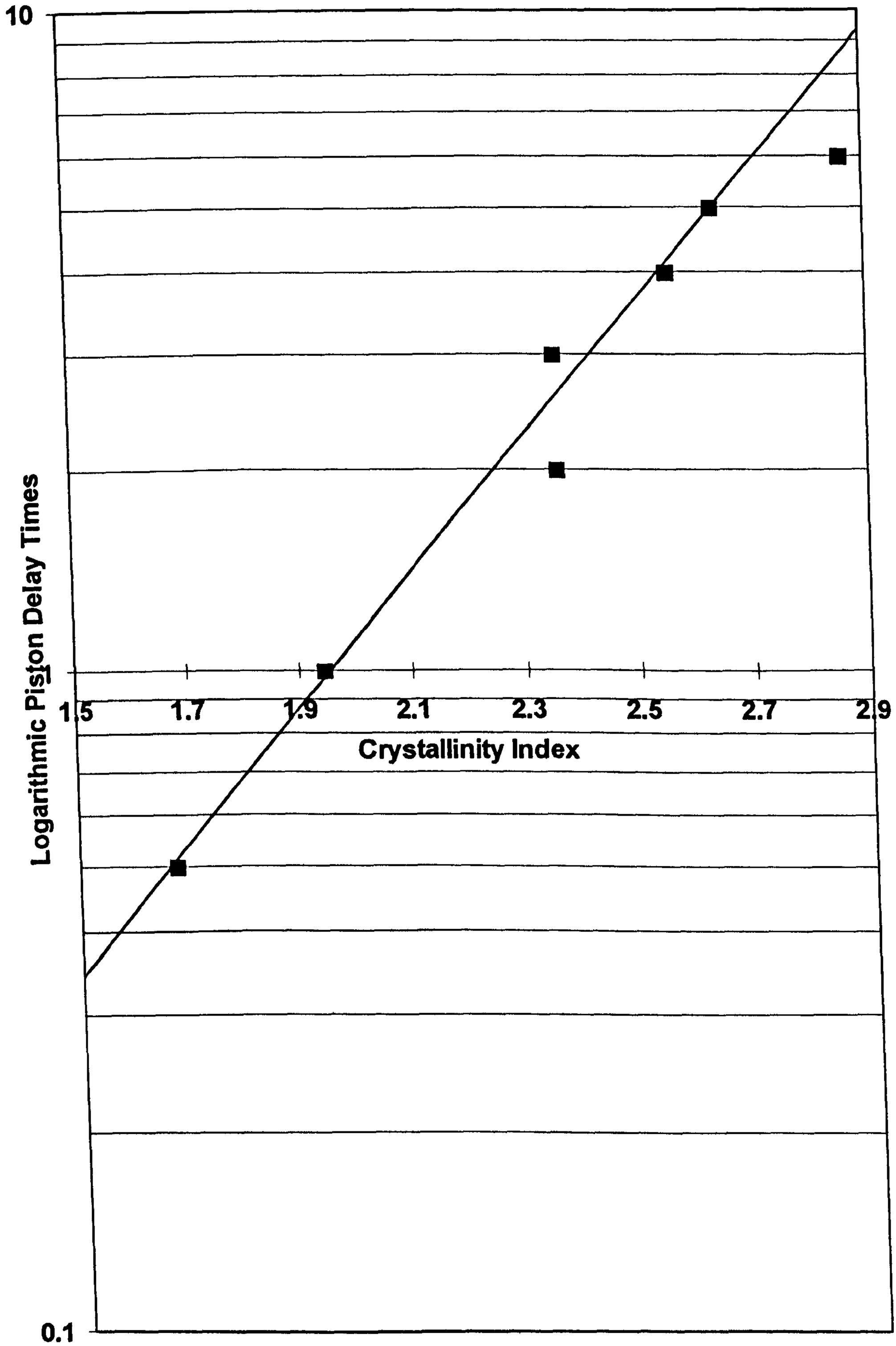

Figure 5.9 Logarithmic piston delay times versus crystallinity index for 2-colour iPP SCORIM mouldings produced using two shears.

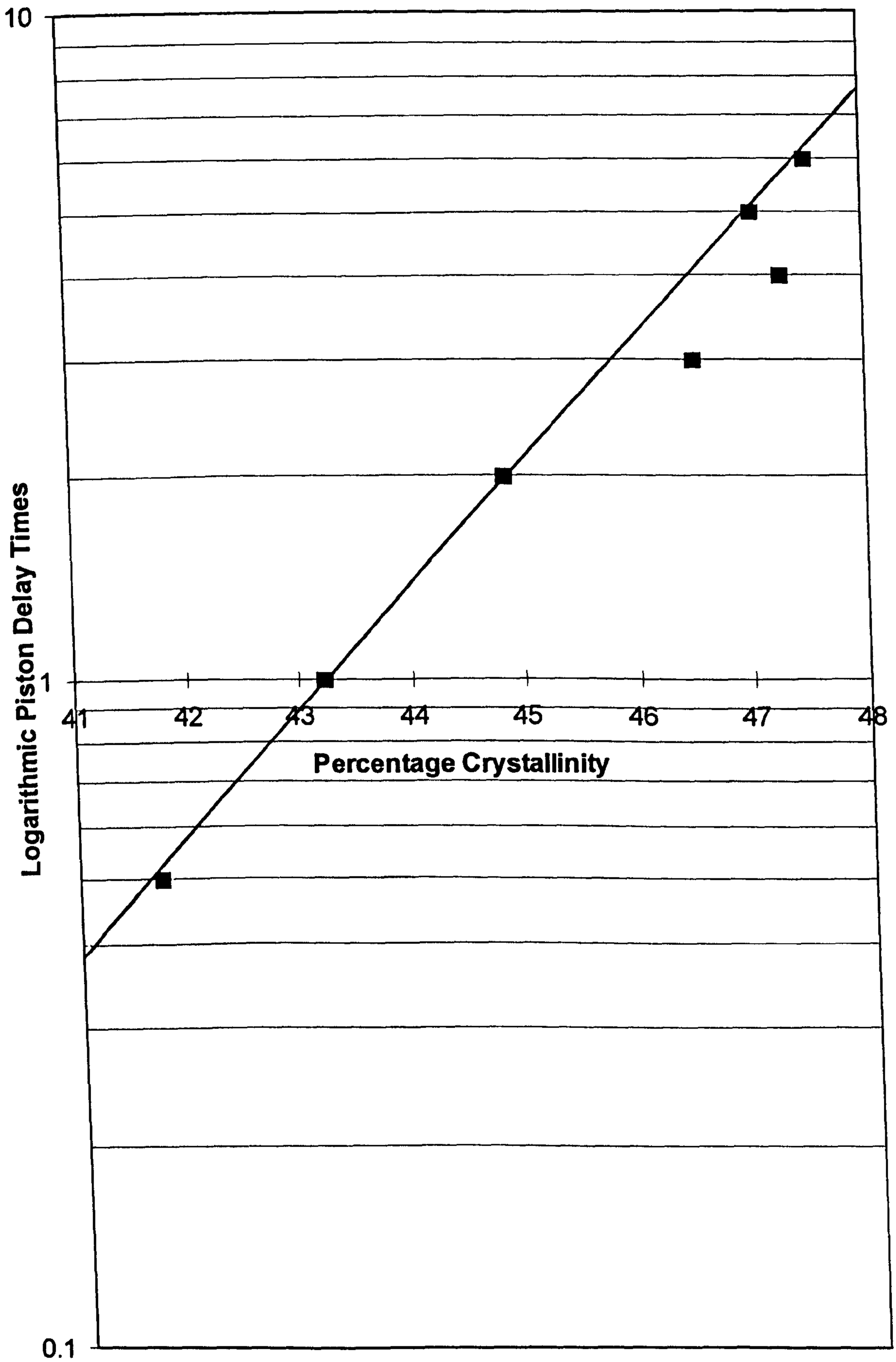

Figure 5.10 Logarithmic piston delay times versus percentage crystallinity for 2-colour iPP SCORIM mouldings produced using two shears.

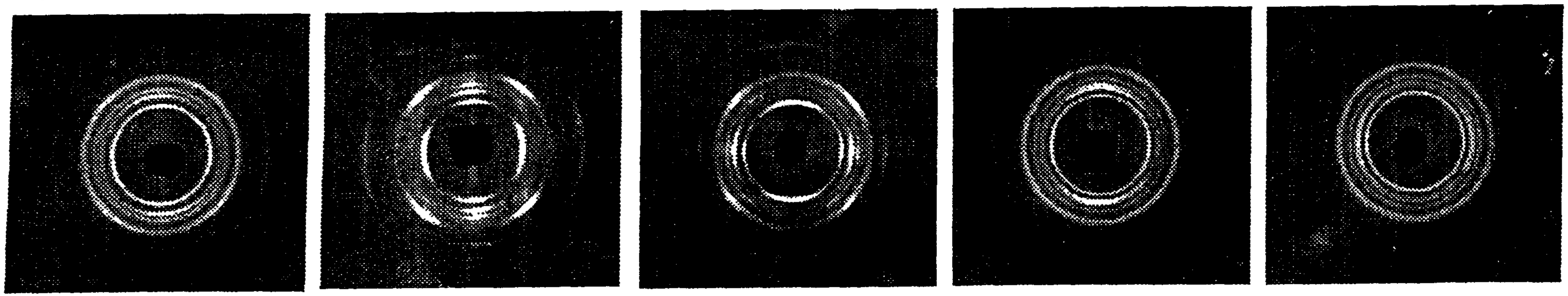

a) 0.25mm 0.5mm 0.75mm 1.0mm 1.25mm

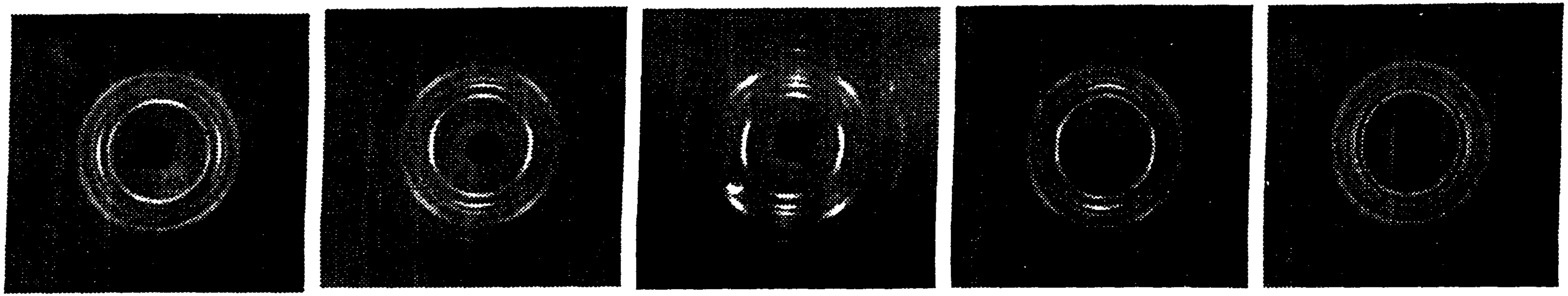

b) 0.25mm 0.5mm 0.75mm 1.0mm 1.25mm

Figure 5.11 Debye patterns from 2-colour iPP SCORIM mouldings sectioned parallel to flow and referenced in millimetres from the edge of the sectioned sample. Mouldings were produced with 6 second delays between shears a) with one shear and b) with two shears.

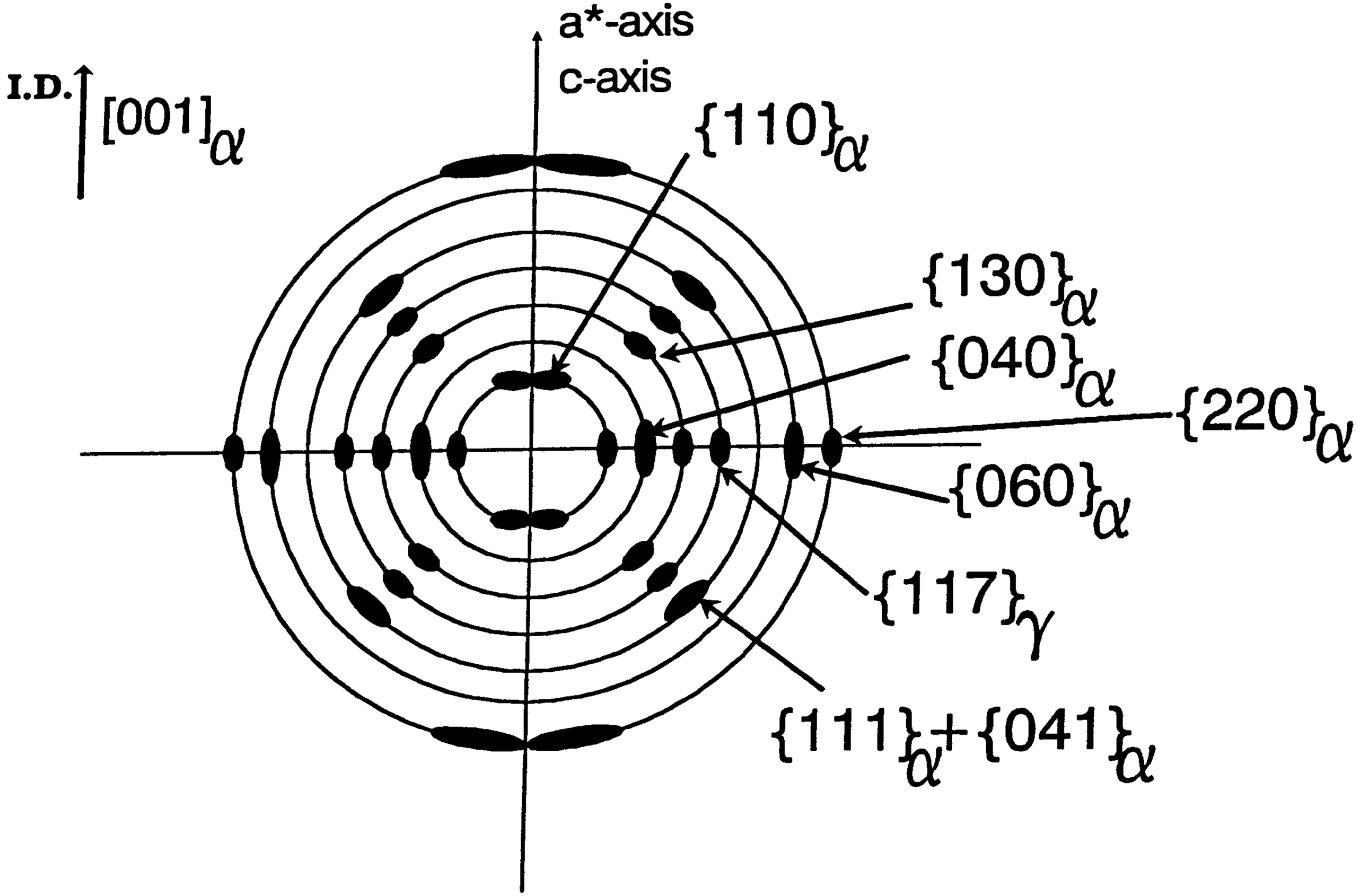

Figure 5.12 Schematic representation of the x-ray diffraction patterns from the longitudinal sections of SCORIM mouldings.

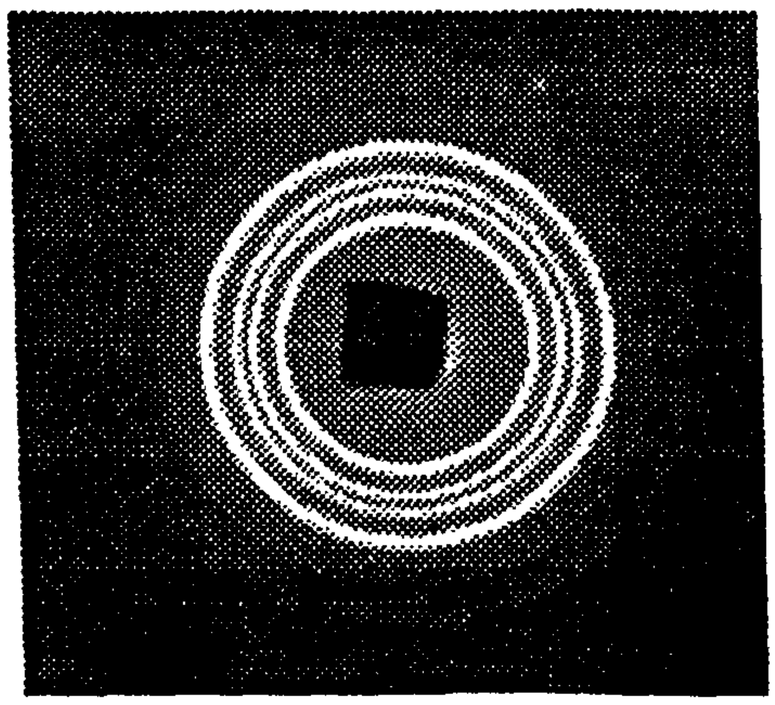

Figure 5.13 Debye pattern from a conventionally moulded iPP section which had skin layers and core region removed, c.f. figures 5.14 and 5.15.

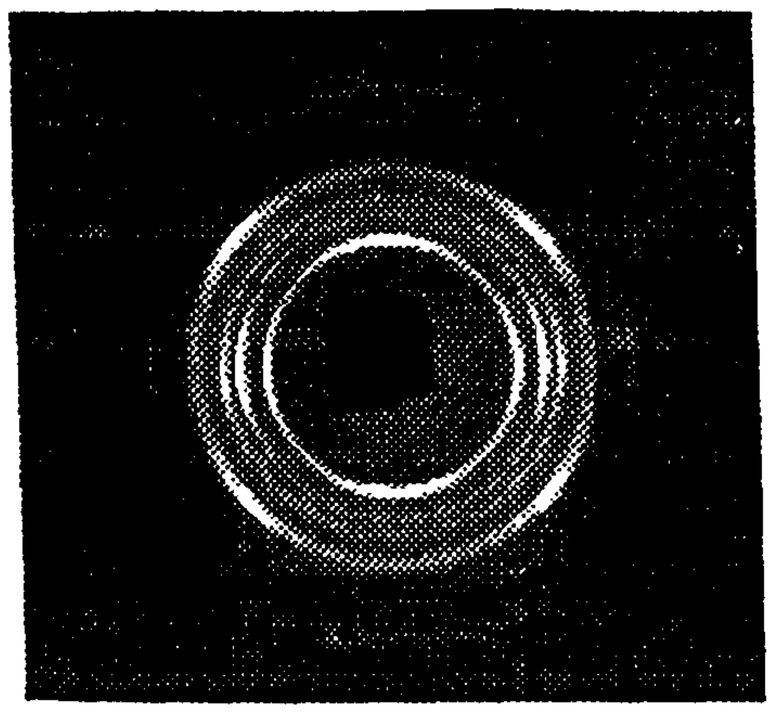

Figure 5.14 Debye patterns from a 2-colour iPP SCORIM moulded section which had skin layers and core region removed to retain only shear influenced zones. Sample produced with one shear with 6 second delay.

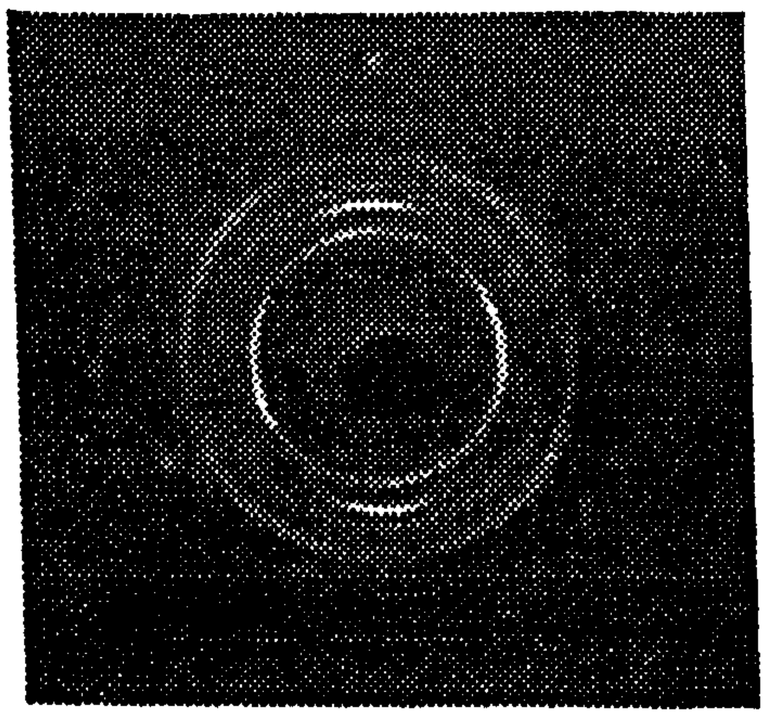

Figure 5.15 Debye patterns from a 2-colour iPP SCORIM moulded section which had skin layers and core region removed to retain only shear influenced zones. Sample produced with two shears with 6 second delay.

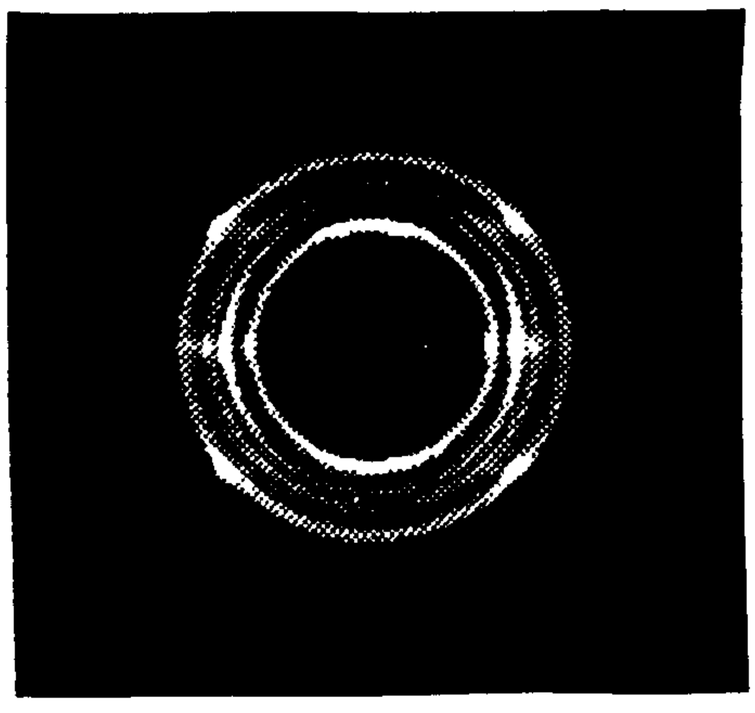

Figure 5.16 Debye pattern of a 2-colour iPP SCORIM moulding produced using 3 shears with 6 second delays. The section was taken parallel to flow along the mouldings' centreline and the x-ray beam focused at 1.25mm from the section edge.

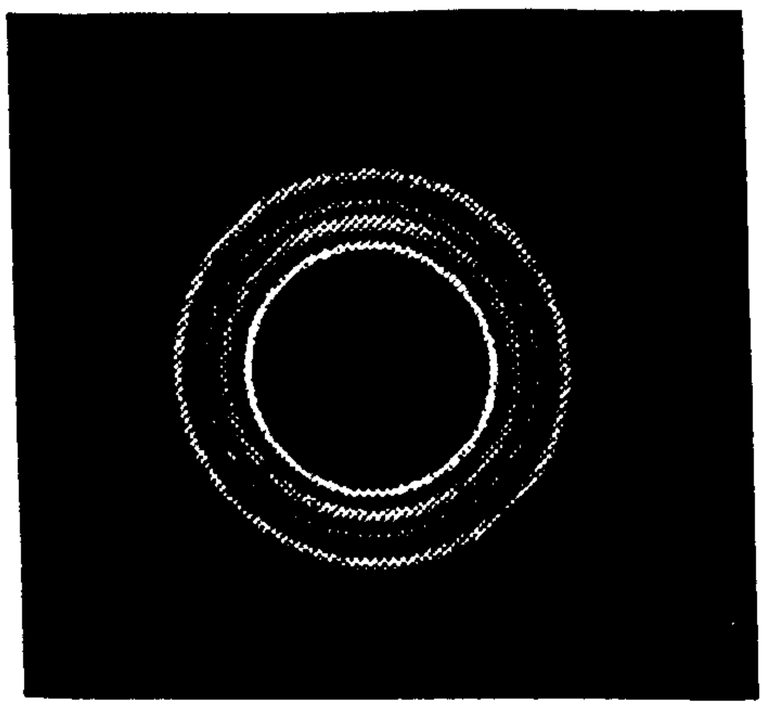

Figure 5.17 Debye pattern of a 2-colour iPP SCORIM moulding produced using 41 shears with no delays. The section was taken parallel to flow along the mouldings' centreline.

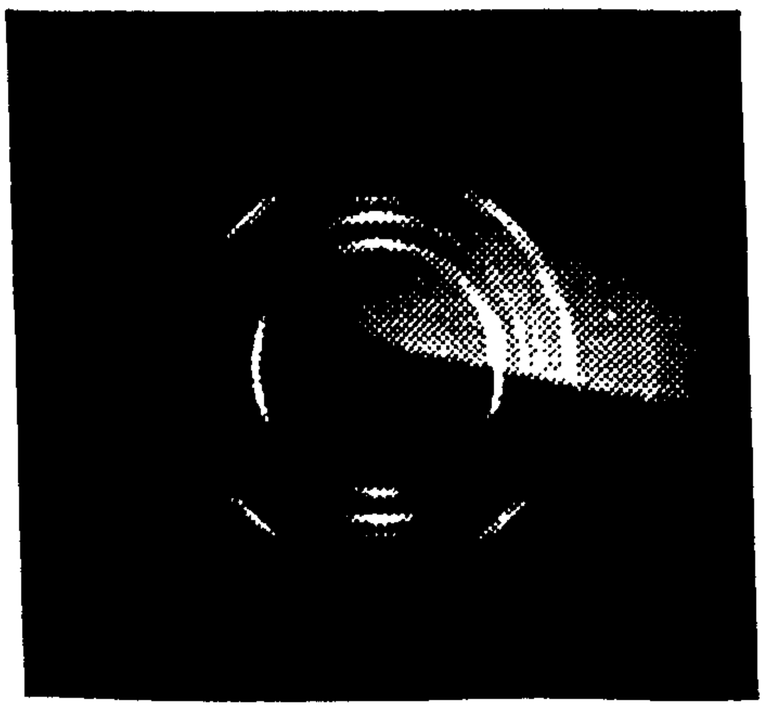

Figure 5.18 Debye pattern of a 2-colour iPP SCORIM moulding produced using 41 shears with no delays. The section was taken parallel to flow close to the mouldings' edge.

6. MECHANICAL PROPERTIES

6.1 Tensile Test Results

Tensile tests were carried out as described in section 2.4 to obtain the modulus and other tensile properties. Six samples were tested in order to obtain representative values with standard deviation (S.D.). Two types of materials were evaluated for comparison, a 2% ET2025 Al flake filled PP and 2% 210-30-E1 Al flake filled PP moulded into dumbbell tensile test bars using conventional moulding, SCORIM, BSM and SBM. The median flake diameters of the ET2025 and 210-30-E1 are approximately 33 and 9μm respectively. These mechanical tests compare the effects on properties of the SBM process with conventionally moulded samples. The use of SCORIM and BSM technologies on their own are also assessed for comparison as are two different types of Al flake. The SCORIM profile used was optimised for removal of the surface weld line and not for mechanical properties which is the subject of other researches[72, 75, 88-90]. The results are presented in table 6.1.

Initial examination of these results reveals that there is minimal difference between the mechanical performances of these two Al flake filled PP materials within experimental error. The most significant difference outside experimental error is between conventional mouldings with no weld line. Here the ET2025 samples have an extremely high value of ultimate tensile strain (ε_u), commensurate with a material of high ductility, but the 210-30-E1 samples have a lower value of ε_u, commensurate with a more brittle material. This is most likely a reflection of their median flake diameters with the smaller 210-30-E1 flake inducing earlier failure in the PP matrix. The only other differences between the two materials outside experimental error are their values of ultimate tensile stress (σ_u) with SCORIM, BSM and SBM. Here, a subtle increase in values is observed for all three processing techniques for the smaller sized 210-30-E1 Al flake. The increases in the mean values of σ_u for SCORIM, BSM and SBM are 4.5, 9.2 and 4.5% respectively. This slight

increase in σ_u compared to the ET2025 Al flake is commensurate with a corresponding decrease in ε_u.

The Young's modulus (E) of all the mouldings characterised are the same within experimental error. This implies that none of the variables considered using these processing parameters had an influence upon E. For σ_u there is no difference between conventional mouldings with or without weld lines, but the application of SBM creates an increase. These values of σ_u were not the optimum obtainable with SCORIM as the SCORIM profile used was intended to optimise weld line removal as shown in figure 3.2. When this SCORIM profile was used alone there was a still greater increase in σ_u, which may suggest that the use of mould heating with SBM is responsible for a reduction in σ_u. This notion is supported by the decrease in σ_u with BSM to a value below both conventional mouldings with ET2025, and a value equal to conventional mouldings with 210-30-E1.

Peak strain (ε_p) was the same within experimental error for conventional mouldings with and without weld lines. The application of SCORIM increased ε_p for 210-30-E1 but for ET2025 there was no increase within experimental error, but an increase in the mean value was observed over conventional mouldings. The use of BSM alone lowered ε_p to values below their respective conventional mouldings values, whilst SBM samples had mean values in-between those of the lower BSM and higher SCORIM values. Again, for ε_p, this appears to suggest BSM is responsible for a slight reduction in property.

ε_u and toughness (*U*) are closely related and therefore reflect one anothers performance. With conventional moulding they are both profoundly influenced by the presence of a weld line, where the absence of a weld line results in an extremely ductile and tough character but the presence of a weld line markedly reduces these parameters. In the case of 210-30-E1, ε_u and *U* increase by 753 and 563% respectively from the presence to the absence of a weld line. This increase was even more distinguished for ET2025 as sample failure did not occur during the test. With the removal of weld lines using SBM, ε_u and *U* increase to values greater than those seen with

conventional weld lines. To emphasise, the SCORIM profiles selected were chosen to optimise visual quality rather than mechanical property with these samples, though the two are by no means mutually exclusive. Therefore these values did not approach those of conventional mouldings with no weld line. When SCORIM was used alone the values obtained were the same as those for SBM within experimental error. With BSM a marked fall in the mean values of ε_u and U occurred to below those of the conventional samples with weld lines. Again this implies that the use of BSM lowers the values obtained for ε_u and U.

These tensile tests were aimed at characterising the effect the different processes had on the mechanical properties of the mouldings as a whole. Flexural tests were also used by Yasuda[5] to assess the mouldings' skin characteristics produced by the different processes, where an increase in flexural strength of SCORIM and SBM over conventional mouldings was reported.

In summary, SBM can be used for the successful removal of surface weld lines whilst maintaining the integrity of the mouldings' mechanical properties. The use of BSM does appear to reduce slightly the mechanical performance of these samples but when used with SBM the improvement in mechanical properties, synonymous with the application of SCORIM, is sufficient to ensure properties comparable or better than those obtained from conventional moulding.

6.2 Vickers Microhardness Test Results

Microhardness testing was carried out to investigate the variation in hardness and texture through the longitudinal and transverse cross-sections of SCORIM mouldings. The results were expressed in graphical form both as indentor diagonal lengths, Y and Z, and Vickers microhardness versus the position of indent as presented in figures 6.1 to 6.4, with corresponding SCORIM profiles presented in tables 4.1, 5.18, 4.7 and 4.14 respectively. Photomicrographs of the surfaces tested are also presented in these figures. The technique proved useful, though other workers[65, 72, 78, 79, 91] found the

technique to be more so with distinctive anisotropy changes with some materials.

Figure 6.1 shows the results for a SCORIM moulding which has undergone a single shear oscillation almost immediately after the mould cavity was filled. Therefore the extensional flow experienced by this sample is restricted to the moulding's edge as photographed in figure 6.1b. The hardness measurements across the section only indicate the skin layer as having a lower hardness value, with the sheared region next to it exhibiting properties similar to the spherulitic core. These properties were largely true of both the longitudinal and transverse sections studied. For all the microhardness samples the indentor diagonal Y was perpendicular to the injection direction and Z was parallel to it. However, no truly discernible anisotropy was detected in this sample.

Figure 6.2 shows the indentor diagonal lengths and Vickers microhardness versus indentor position curves for a longitudinal section. The moulding was produced using 41 shear oscillations which started immediately the mould cavity was full and reciprocated continuously until completion. Thus, the plastic experienced shear extensional flow which was encapsulated adjacent to the moulding's edges by solidification. The moulding's core did not however contain this orientation which had presumably decayed away virtue of the polymers 'memory', causing relaxation through recoiling and re-entanglement of the molecular chains, to yield an unoriented spherulitic morphology. These morphologies manifested themselves in the microhardness plots as relatively soft skin layers adjacent to much harder SCORIM influenced regions. At one edge of the specimen this represented an 88% increase in hardness, at the other edge a 69% increase over the skin layer. The hardest portions of the shear influenced sections do not necessarily appear to be where the main shear bands are present (evident as narrow stripes in the photomicrograph) but in the shear influenced regions between these and the spherulitic core. In the spherulitic core region a hardness intermediate of the two shear influenced regions was present. The core generally appeared to be at its hardest along the centreline of the

moulding. This sample also appeared to demonstrate some degree of anisotropy as most measurements taken perpendicular to flow (i.e. Y values) yielded higher values than those measurements taken parallel to flow (i.e. Z values). This is consistent with the findings of Kalay[72, 58] and also indicates an increase in modulus in the longitudinal direction.

Figure 6.3 shows the indentor diagonal lengths and Vickers microhardness versus indentor position curves for longitudinal and transverse sections with corresponding photomicrograph. The moulding was produced using a single shear from SCORIM 6 seconds after mould fill was complete. This resulted in the development of shear influenced regions, beginning 0.4mm from the surfaces of the moulding and extending a further 0.55mm into the centre. These are visible in the photomicrograph as bright bands parallel to this moulding's surface. The moulding core is again spherulitic. The hardness plots again indicate soft skin layers increasing in hardness rapidly in the first 0.3mm. At 0.4mm a drop in hardness evident in both longitudinal and transverse measurements is consistent with the presence of the shear interface. Beyond this interface towards the core the hardness exhibits a general increase in the shear influenced regions until the spherulitic core is reached which in general has the highest hardness values. The longitudinal plot appears to exhibit a degree of anisotropy, most notably in the shear influenced region at one edge of the moulding which is consistent with Kalay[72, 58] and an anticipated increase in modulus in the longitudinal direction. However, the absence of strong anisotropy at the other edge of this same sample and the apparent presence of some anisotropy in the transverse sample measured, which would not be expected, makes assessment of the levels of anisotropy present difficult to gauge. This in part is due to the inherent difficulties of measuring the indentor diagonal lengths after microhardness indentation because of the visual appearance of the sectioned surface.

Figure 6.4 is the microhardness profile for the longitudinal section of a SCORIM moulding produced using two shears, the first 6 seconds after completion of mould fill and the second reverse shear 12 seconds after the

completion of mould fill. This sample also exhibits a relatively soft skin layer increasing in hardness away from the skin. Changes in hardness values can sometimes be related to interfaces between shear bands. These interfaces appear to have different hardness values than material adjacent to them. The sample generally shows anisotropy where the transverse direction yields higher indentor diagonal lengths than the longitudinal direction. This is consistent with an increase in modulus in the longitudinal direction.

Each of the figures 6.1 to 6.4 exhibit softer skin layers on one side of the moulding than on the other. Although no visual evidence of asymmetry is evident from the mouldings' microstructure in the polarised light photomicrographs, it may be that the different hardness values at the edges of each of the mouldings is a reflection of the differential heat transfer rates from the two halves of the mould tool. This is due to cooling circuit of the moving half being further from the cavity surface than for the fixed half resulting in a lower heat transfer rate. Therefore a higher hardness value may be the result of the slower heat transfer rate from the moving half of the tool, enabling a longer period of time for crystallisation to occur and subsequently the growth of larger crystals. This knowledge could perhaps be utilised for the development of improved scratch resistance of mouldings as it is anticipated that surface hardness is related to this.

6.3 Relationship Between Processing Conditions and Mechanical Properties

i) Ultimate tensile strain and toughness are decreased by the presence of a weld line with conventional moulding.

ii) The use of SBM solely to remove surface weld lines from Al flake filled PP does not reduce the integrity of the mechanical properties of these mouldings. Moreover, subtle increases in mechanical properties were observed with some ultimate properties over a conventional moulding with a weld line. Young's modulus was unaffected by the application of SCORIM and BSM technologies independently or in series. The removal of surface weld lines need not necessitate SCORIM being applied as a means of

optimising mechanical properties, although these two applications of SCORIM within the same moulding cycle are not mutually exclusive.

iii) PP loaded at 2% with one of two Al flakes induced a small increase in ultimate tensile strength, with corresponding reduction in ultimate tensile strain and toughness, for a 33μm flake relative to a 9μm flake.

iv) Microhardness characterisation yielded evidence of anisotropy within some SCORIM mouldings consistent with preferred orientation and increased modulus in the shear direction.

v) Microhardness revealed that the considered use of one or two SCORIM shears, incorporating delay times to allow oriented structure to solidify, is sufficient to induce preferred orientation through a large cross-section of the mouldings thickness. A high frequency of successive multiple shears can induce higher levels of orientation but as shear heating comes into balance with cooling, this only influences a smaller cross-section of the sample.

vi) Microhardness revealed skin layers to be consistently softer than either shear regions or the spherulitic cores. One surface of each moulding was usually harder than the other which is thought to be related to the harder surfaces' slower rate of heat transfer during crystallisation which enabled the growth of larger crystals to occur.

Table 6.1 Mean tensile properties of 2% Al flake filled PP matrixes

	E (GPa)	σ_u (MPa)	ε_p %	ε_u %	U (N/mm)
Al Flake ET2025 (diameter ≈33μm)					
Conventional single feed	1.56 (0.33)	22.76 (0.39)	6.96 (0.24)	Extension exceeded maximum	
Conventional double feed	1.35 (0.18)	23.2 (0.13)	7.07 (0.25)	11.46 (0.55)	9.01 (0.47)
SCORIM	1.51 (0.13)	24.97 (0.08)	7.32 (0.16)	23.55 (8.09)	22.10 (6.7)
BSM	1.39 (0.07)	21.33 (0.89)	4.13 (0.56)	4.76 (0.87)	2.83 (0.98)
SBM	1.47 (0.05)	22.90 (0.30)	5.01 (0.19)	15.93 (4.94)	12.92 (4.33)
Al Flake 210-30-E1 (diameter ≈9μm)					
Conventional single feed	1.68 (0.32)	23.10 (0.12)	6.75 (0.10)	85.36 (15.20)	51.61 (11.69)
Conventional double feed	1.51 (0.14)	23.23 (0.11)	6.83 (0.16)	10.01 (1.25)	7.78 (1.21)
SCORIM	1.65 (0.10)	26.10 (0.09)	7.25 (0.17)	16.81 (3.52)	15.37 (3.31)
BSM	1.27 (0.12)	23.29 (0.48)	5.12 (0.59)	6.8 (2.47)	5.22 (2.55)
SBM	1.68 (0.18)	23.98 (0.16)	5.31 (0.13)	22.41 (7.61)	18.79 (6.56)

Modulus E, ultimate tensile stress σ_u, peak strain ε_p, ultimate tensile strain ε_u and toughness *U*. Standard deviation represented in parenthesis.

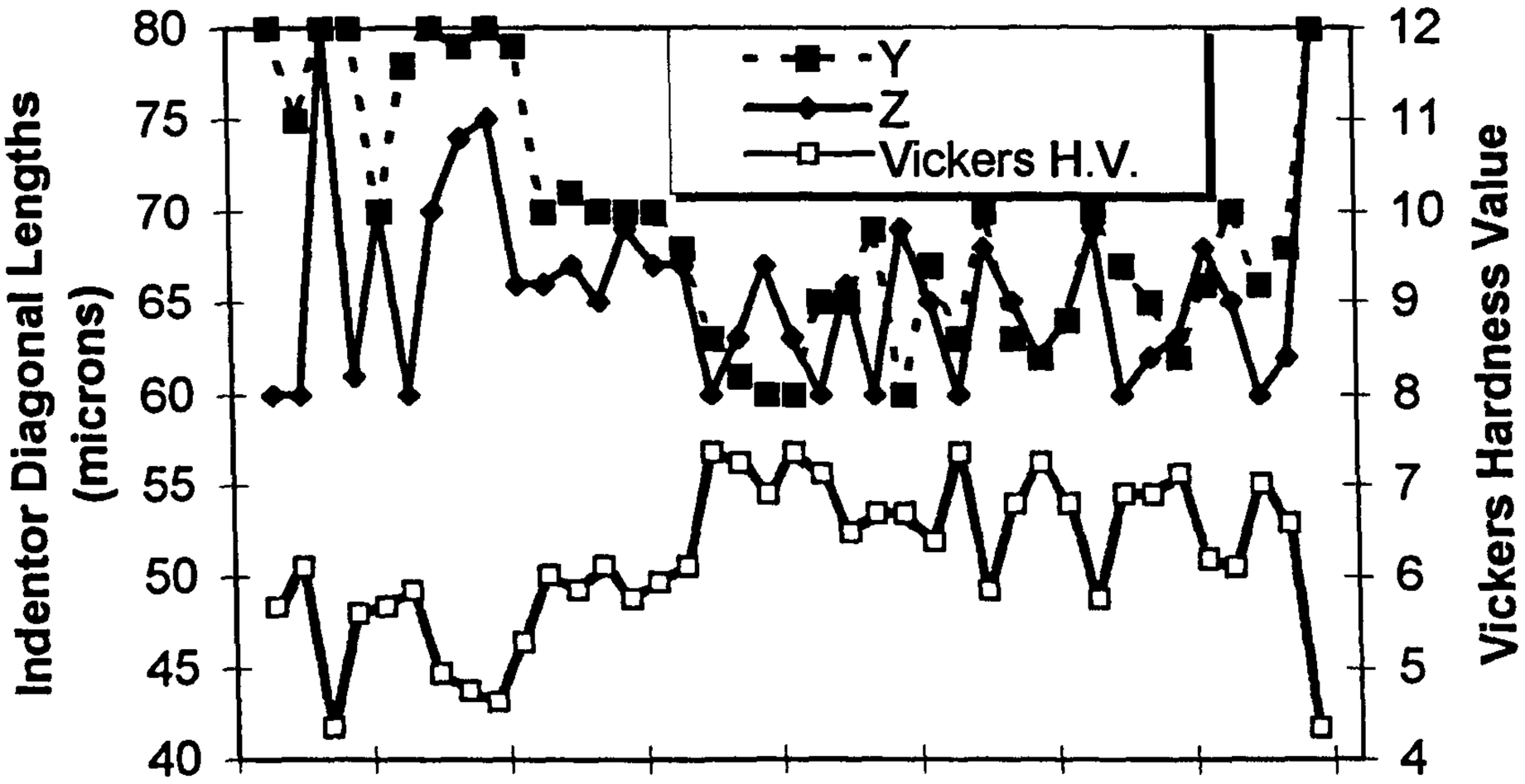

a) Longitudinal section microhardness profile

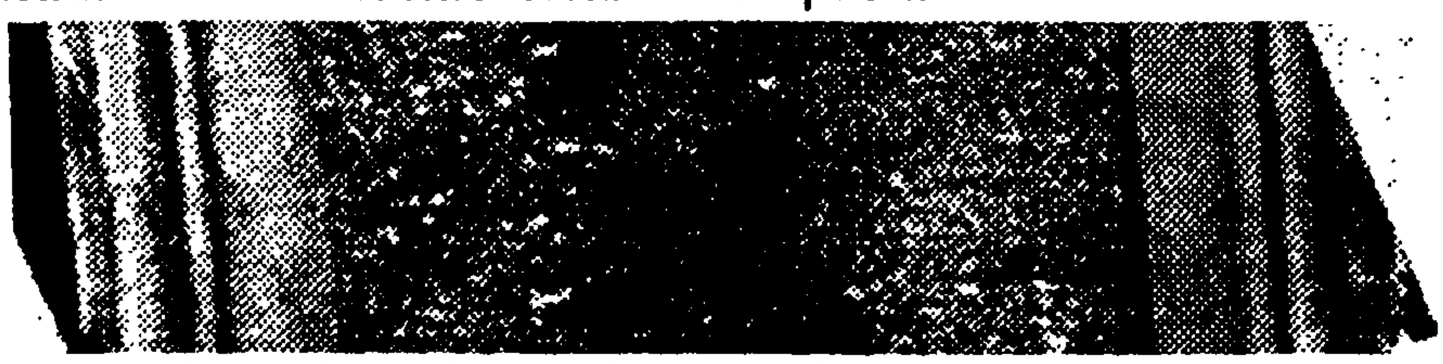

b) Longitudinal section photomicrograph

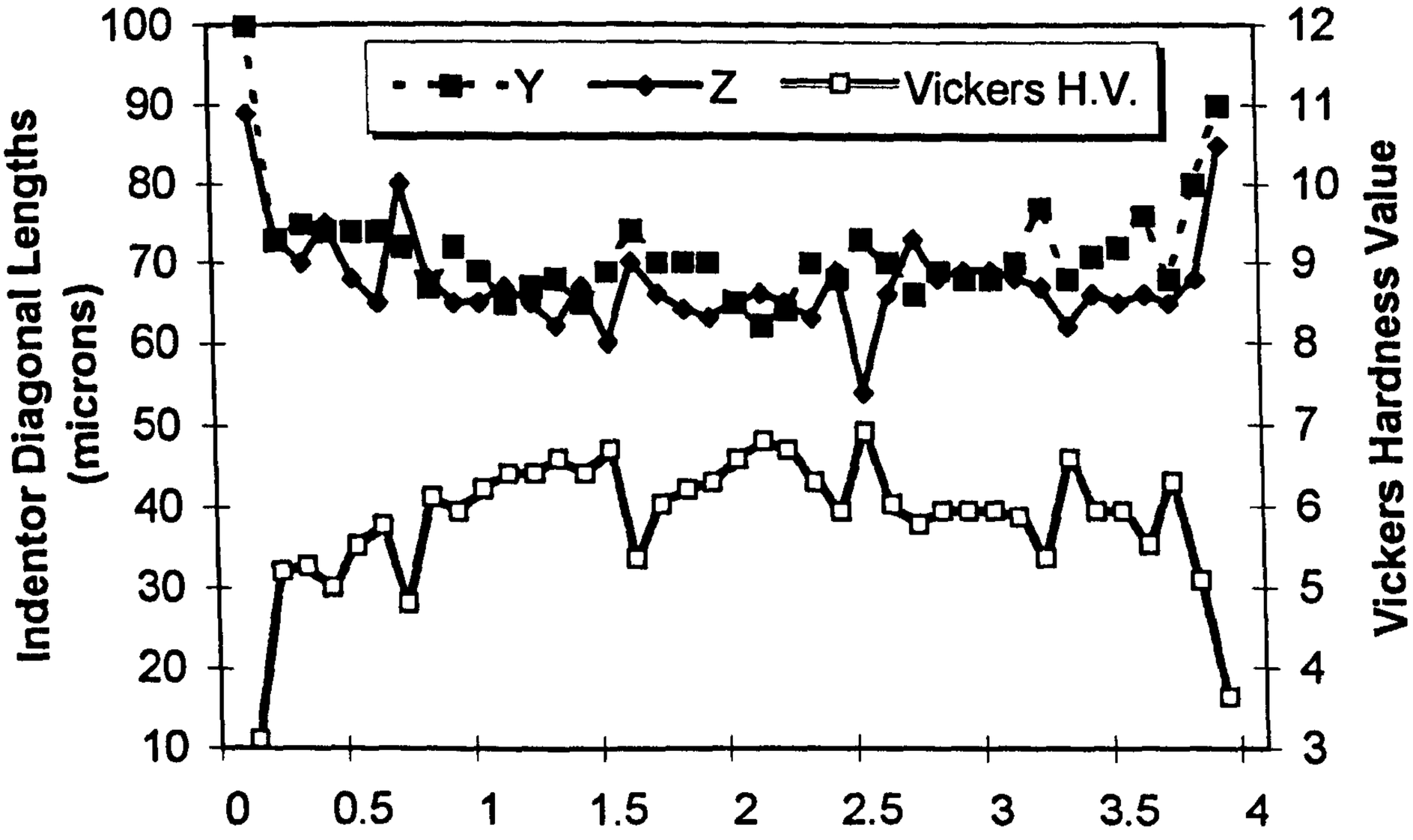

c) Transverse section microhardness profile

Figure 6.1 Microhardness profiles and photomicrograph of a section through a 2-colour iPP SCORIM moulding produced using a single shear with 0.5s delay.

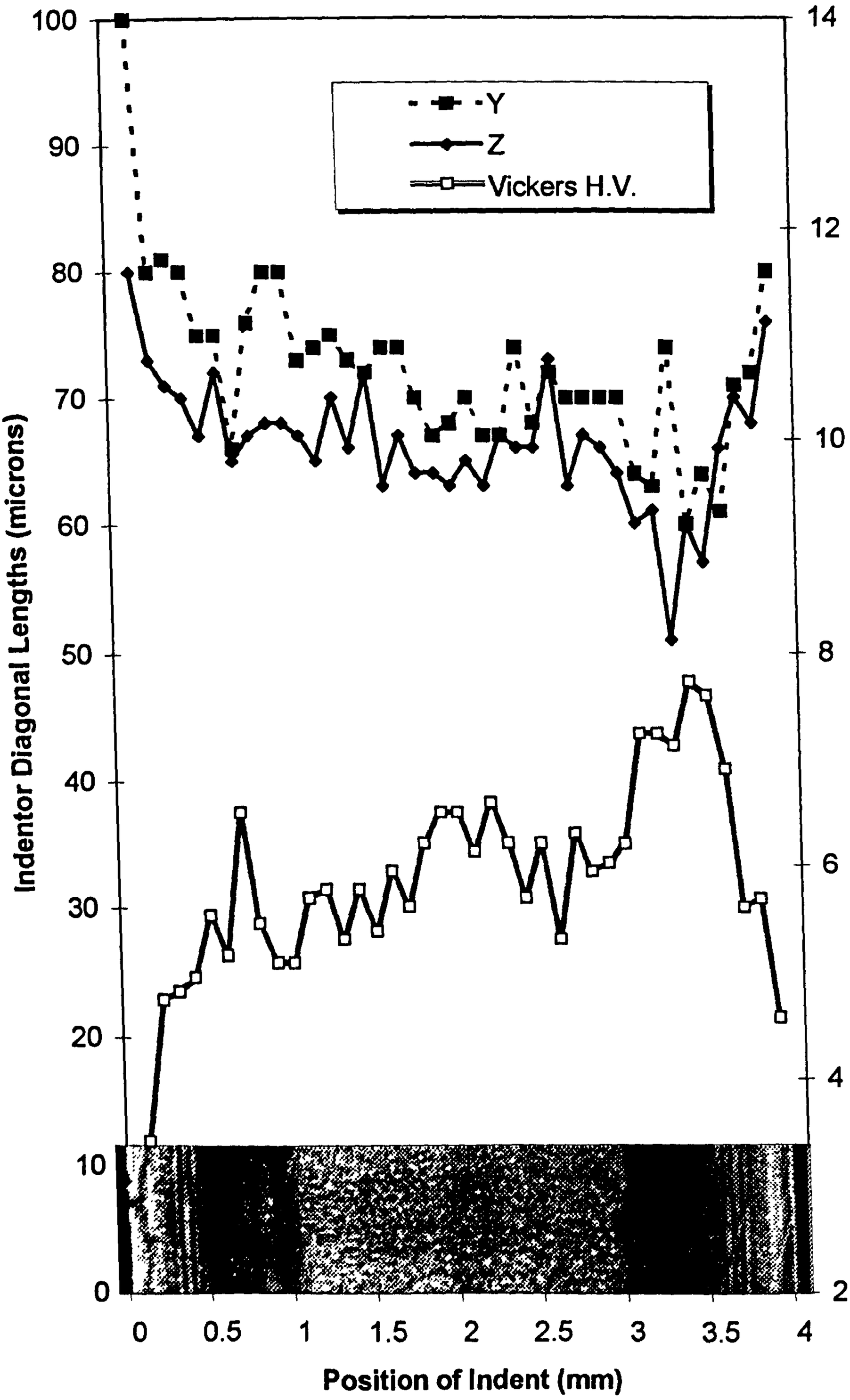

Figure 6.2 Longitudinal section microhardness profile and photomicrograph for a 2-colour iPP SCORIM moulding produced using 41 shear oscillations with 0.8s delays

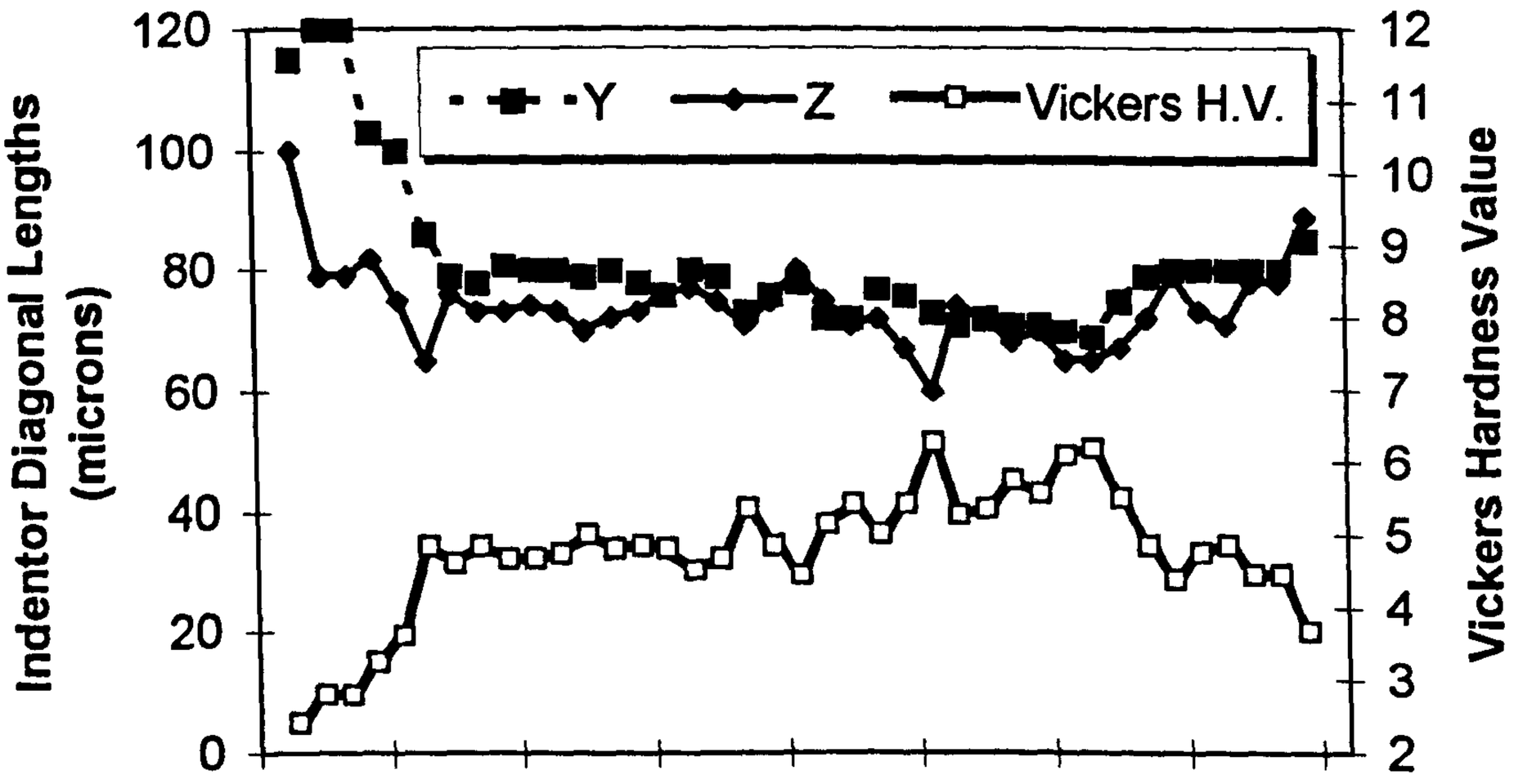

a) Longitudinal section microhardness profile

b) Longitudinal section photomicrograph

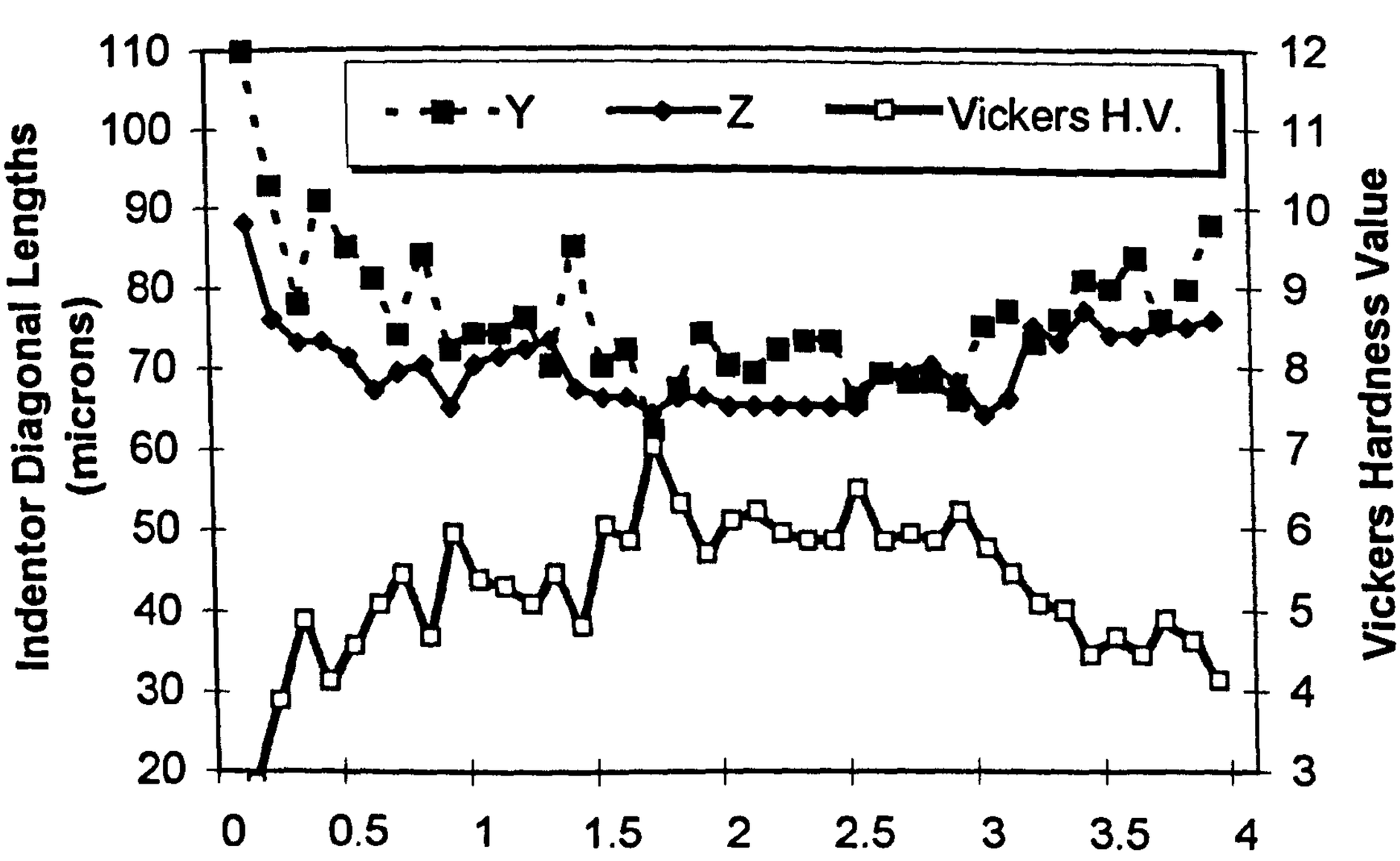

c) Transverse section microhardness profile

Figure 6.3 Microhardness profiles and photomicrograph of a section through a 2-colour iPP SCORIM moulding produced using a single shear with 6s delay.

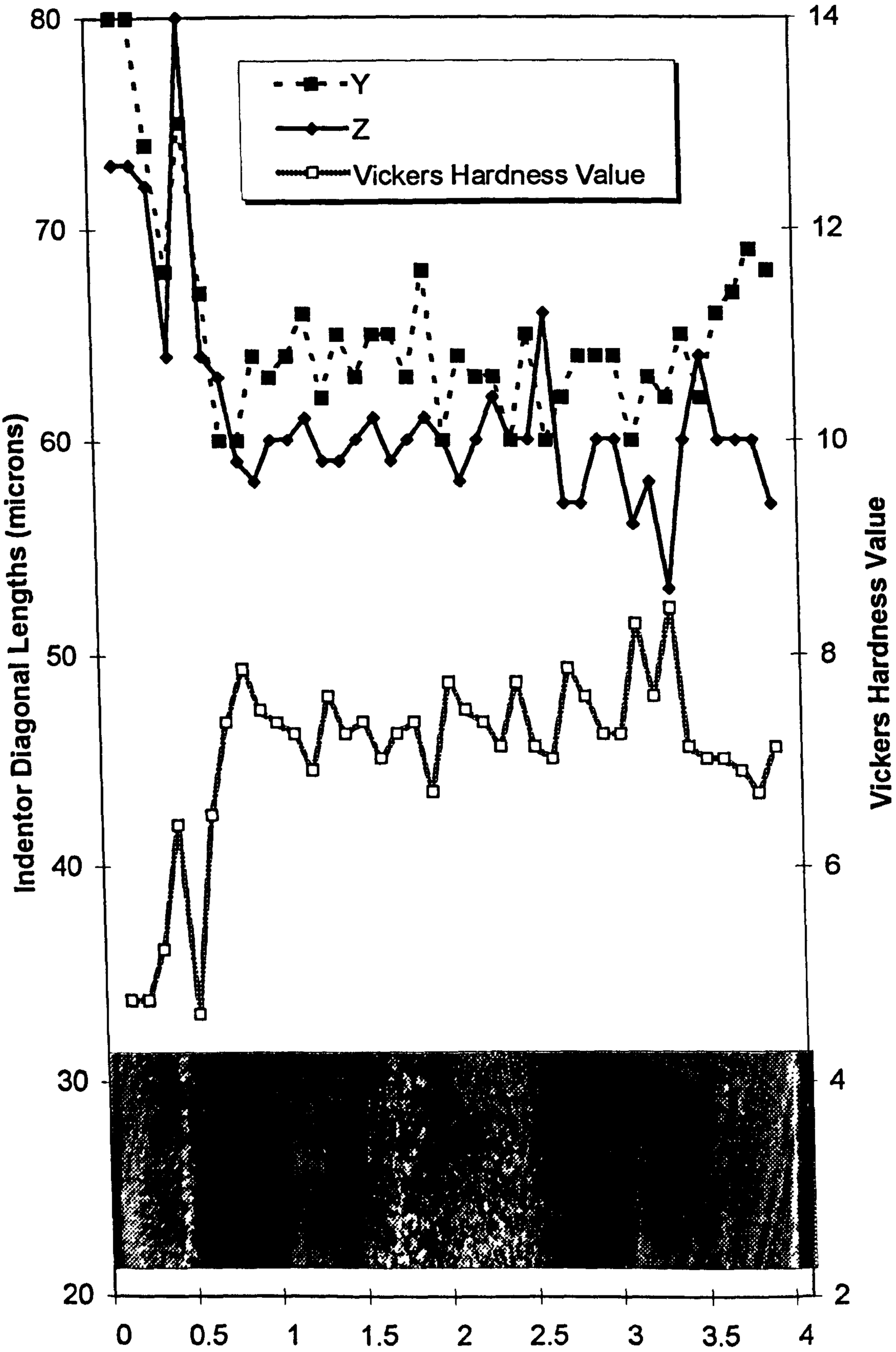

Figure 6.4 Longitudinal section microhardness profile and photomicrograph for a 2-colour iPP SCORIM moulding produced using two shear oscillations with 6s delays.

7. GENERAL DISCUSSION

This thesis covers several areas of research each linked by the use of the SCORIM processing technology, namely the acquisition of processing data relating to this process for the mathematical modelling, the shear flow observations of the two-colour work and related aesthetics, the morphological and induced orientation characterisation of PP mouldings, the removal of weld lines and characterisation of the surface reflectivity from aluminium pigmented PP, and the mechanical property characterisations. This work was carried out to fulfil the original aims of the thesis which are detailed in section 1.1.1 and also to investigate areas of interest not initially envisaged at the start of the work.

The requirement to instrument the injection moulding machine and SCORIM equipment for data acquisition of various selected parameters was fastidiously accomplished prior to the commencement of moulding trials. The requirement for this information by the mathematical modelling group at the University of Wales Swansea, was not however as immediate as anticipated with the data only being used in the latter stages of this work. Therefore the degree of collaboration originally foreseen for the duration of the work did not transpire. This enabled more time for focusing on other aspects of interest, in particular the aesthetic effects achievable with two-colour SCORIM mouldings and the characterisation of the surface reflectivity of the highly reflective aluminium pigmented PP.

The patterns produced with the translucent two-colour mouldings provided a good deal of information as to how SCORIM shear flow propagates through mouldings during their cooling and solidification. This has provided a new level of understanding of the way SCORIM imparts preferred orientation through the width and thickness of the mould cavity. This work also prompted the investigation of using limited numbers of intermittent shears to encapsulate by solidification the displaced material in its displaced position, prior to any reverse shear. Further development of the control of the piston amplitude was also discovered to be desirable to control

the level of shear heat generated and the coloured patterns produced. The way in which the gate dimensions influence the flow and the type of material processed has also been demonstrated to be important. This two-colour study technique will therefore be invaluable to the future development of the mathematical model.

Processing with two-colour iPP using intermittent shears demonstrated for the first time that only one or two shears are required to induce preferred orientation through most of the thickness of the mouldings. Prior to this, the understanding was that the application of continuous reciprocal shears was the way to achieve this effect. However, whilst the application of few intermittent shears bodes well for the preferred alignment of fibre and platelet filled materials, the maximum preferred orientation of polymer molecules may still require more frequent shears as memory induced molecular recoiling will serve to reduce this. This new knowledge will enable a higher degree of control over the tailoring of the materials microstructure to suit its application. The ability to manipulate the microstructure like this highlights the need for a greater degree of control over the pistons' oscillations in terms of their frequency, speed and amplitude.

With injection moulding being the most widely used of all the plastics processing routes, this work is of relevance to a significant niche within the industry. Technical injection moulding, where enhanced mechanical properties are required for engineering applications, would benefit from the knowledge gained herein. It is also envisaged that lower cost commodity thermoplastics could be processed using SCORIM to produce tailored mechanical properties which eliminate the need for higher cost engineering thermoplastics. The additional cost of the SCORIM processing equipment could be offset by reducing cycle times where thinner wall sectioned SCORIM mouldings can achieve the desired properties only previously achievable with thicker sectioned parts.

The need for the SCORIM equipment to be highly reproducible is of the essence if quality parts are to be achieved with each moulding cycle. The full evaluation of the process would however require its statistical assessment

over many hours of continuous processing. This is something which was never intended to be undertaken with this work as it was not considered a priority. However, in light of the importance being placed upon the ability to tailor the microstructure, the reproducibility of SCORIM mouldings is therefore of the essence and this exercise would be justified. The current confidence in the reproducibility of the process is high however, virtue of the many hours processing undertaken using it which have always provided enhanced results.

The GSP characterisation technique has been successfully applied to the quantitative evaluation of Al pigmented mouldings' surface reflectivity properties. This was an evaluation of the aesthetic enhancement achieved by the use of SBM for comparison with conventional, SCORIM and BSM mouldings. The results provided a qualitative assessment of the preferred angle of reflection from the mouldings surface which was related to the angle of orientation of the Al pigment, which in turn was related to the direction and type of processing flow encountered. With this knowledge, it was possible to offer an explanation of the preferred orientation induced by flow, i.e. the 'flip-flop' effect, which is often considered to be unacceptable in terms of quality. The SBM technique was shown to be potentially capable of removing this effect as well as surface weld lines.

SBM was demonstrated to have the potential to produce mouldings with a surface finish comparable to that of a painted component. This can be achieved within one cycle of a fully automated moulding machine. As the cycle time will be increased due to the necessity to heat and cool the surface of the mould tool, the financial benefit would be attained through the omission of costly painting procedures. The use of the SBM technology has so far been demonstrated to be successful with small scale simple shaped mouldings. Initially the technique may only be suited to these components until the process technology becomes established in the manufacturing environment. Progressing the technology to larger area mouldings and more complex shaped geometries will require a knowledge of the induction heating technology coupled with a greater level of experience running the system

continuously than could be attained here. However, it is believed that this is still a feasible goal.

During the course of this work it was also discovered that the Al pigment size was an important factor in determining the ease with which weld lines could be eliminated. The larger the flake was, the easier the weld line could be removed. Other Al pigment parameters such as the concentration, geometry of particles and particle size distribution are also believed to be important.

The compilation of the SCORIM mathematical model has so far developed to a 2-dimensional transient model. It is hoped that this will be further developed into a 3-dimensional transient model and include the effects of gate geometry and hot/cold runner systems.

8. CONCLUSIONS AND FURTHER WORK

8.1 Conclusions

a. Surface weld lines have been successfully removed from injection mouldings with reflective characteristics susceptible to perturbed flow. Through its informed application, the SBM process enabled accurate and reproducible control over the high quality of finish obtained. The potential of SBM for this application was qualitatively demonstrated with several mould geometries.

b. Unique and distinguished aesthetic effects have been produced for the first time with the application of SCORIM within a two-colour moulding arrangement. A wide variety of flow patterns have been observed which are both aesthetically pleasing and highly informative as to the nature of polymer flow during the shearing process. U-shaped shear paths close to the edges of fan gated plaque mouldings were identified consistent with the easiest flow route. These flow fronts are considered to be a consequence of shear heating during mould fill from the cavity edge wall, introducing a temperature gradient which manifests itself during shear in this way. With central edge pin gates shear flow was forced through the centre of the cavity, with further evidence of preferential shear flow along the edges.

c. An opportunity for the application of SCORIM as a tool for inserting recyclate material into the core of mouldings after mould fill has been identified. This is a new processing route for the usage of recyclate in this way and offers an excellent degree of managerial control and reproducibility coupled with a high percentage usage of recyclate with each shot.

d. Large volumes within mouldings produced using SCORIM can be preferentially aligned in the flow direction by the application of only one or two shears. This is fewer than previously thought and is possible by the use of intermittent shearing enabling solidification of aligned material and its encapsulation into the core. Subsequent intermittent shears flow through successively narrower channels consequently orienting the otherwise spherulitic core. A high frequency of successive multiple shears can induce

higher levels of orientation but as shear heating equilibrates with cooling, without delays between shearing to facilitate solidification of oriented material, a smaller cross-section of the final moulding is influenced when processing in this way. This is due to the core material being cooled too slowly to 'freeze in' the orientation and instead enabling molecular relaxation promoted by the molecules memory of their previous orientation. Hence the presence of a spherulitic core.

e. γ-phase was identified with the use of one or two intermittent shears which in turn is consistent with an increase in molecular alignment and improved mechanical properties. The intensity of γ-phase increased with the volume of material sheared.

f. Strong evidence of a linear relationship was identified between the logarithm of the delay times incorporated between two shear mouldings and the values of α-phase index, crystallinity index and percentage crystallinity. The values of each increasing proportionally with the length of delay time used.

g. X-ray diffraction patterns, Debye patterns and two-colour mouldings demonstrate that with the fan gated mouldings more shear occurs along the edges than the centreline resulting in greater preferred orientation in these regions. The maximum level of shear occurs at the melt-solid interface of the displaced material during SCORIM.

h. The addition of aluminium flake to the polypropylene was found to act as a heterogeneous nucleant for β-phase morphology within the spherulitic core. This enabled clear identification of the displaced weld interface under polarised light, of filled and unfilled polypropylene.

i. The use of SBM solely for the removal of surface weld lines did not cause a deterioration in mechanical properties relative to a conventional weld line moulding. Some improvements in mechanical properties were observed. The removal of surface weld lines need not necessitate SCORIM being applied as a means of optimising mechanical properties, although these two applications of SCORIM are not mutually exclusive.

j. Microhardness characterisation revealed anisotropy within SCORIM samples consistent with preferred orientation and increased modulus in the shear direction. The skin layers were characterised as being the softest region through the thickness of the mouldings.

8.2 Further Work

❀ The GSP offers a powerful technique for characterising the surface of polymers. The further evaluation of processing conditions with SBM upon surface weld line removal from mouldings and a quantitative assessment programme of their characteristics as compared with painted components. Likewise, the study of reflective pigments with geometries intended to reflect light diffusely, moulded using SBM and characterised. A more fundamental understanding of the relationship between processing parameters and the 'flip-flop' effect to build upon the knowledge gained herein, and incorporating colour effects in order to evaluate possible new aesthetic finishes to mouldings.

❀ Feasibility studies of two-colour mouldings incorporating delayed SCORIM shears to impart aesthetic effects in 3-dimensional mould cavities with form. The use of pin gates to simulate production requirements and facilitate optimised cycle times with ease of gate removal for a finished article in the as moulded state. This would require heated pin gates to delay gate freeze-off for sufficient time to complete the desired SCORIM sequence. This would enable the examination of shear rheology through such gates in a two-colour moulding and within complex mould geometries. The same arrangement could be used to try to induce and encapsulate oriented microstructure throughout the thickness of the moulding by the use of intermittent shearing to eliminate the effects of relaxation by molecular memory. This essentially represents a development of the work carried out by Gibson *et al*[92].

❀ The study of two-colour mouldings with filler materials consisting of a cocktail of pigments loaded in trace concentrations including dyes, flakes and fibres of various geometries, colours and reflective properties within the

matrix materials. Their GSP characteristics with respect to hue, value and chroma to be determined to ascertain the variation of individual identities of consecutive mouldings. The subtle variations of their relative concentrations should be evaluated with the GSP to determine the statistical probability of two mouldings being produced with the same characteristics. The application of SCORIM to impart clearly visible mixing of the two colours within these mouldings should then be evaluated with the GSP to determine the additional levels of variety achievable. This work has potential applications for security card systems which require fast production cycles for cards with unique characteriseable properties.

❀ The further development of the mathematical modelling completed to date in order to provide a 3-dimensional model of the SCORIM process incorporating gating and hot and cold runner systems. The model should provide a predictive basis for the control of preferred orientation of the resin and any alignable constituents in the moulded plastics as well as the controlled erasure of internal weld lines, thereby leading to the optimum management of microstructure and physical properties including strength, stiffness and aesthetics.

❀ The evaluation of the use of the two-colour SCORIM process with a range of materials possessing rheological properties uncharacteristic of the conventional moulding process. This should include low melting temperature glasses to assess further aesthetic characteristics and shear flow within such a low molecular weight and amorphous material. The processing of foodstuffs is of commercial potential for the ability of SCORIM to impart unique mixing within the tool cavity of colours, flavours and textures from two different but complementary foods, e.g. mint and coffee flavoured chocolate with the same bar.

❀ The investigation of further optimising the use of SCORIM to induce maximum preferred orientation through the mouldings' thickness. This could be achieved by applying a high frequency of shears in mode I to impart maximum preferred orientation but with intermittent pauses incorporated to allow this orientation to solidify. Development would involve acquiring a

knowledge of the optimum frequency, pitch and amplitude of SCORIM in mode I, when shear heating and mould cooling has equilibrated and optimum pause time required to envelop the induced structure.

❀ Development of the SCORIM software to provide control over the volume of material sheared with each piston oscillation, i.e. variable control over SCORIM amplitude as well as the frequency and pitch. The use of damping factors in this way would enable the investigation of different rates of decay of the oscillations in a damped oscillatory system. This additional control would enable a reduction in the volume of material sheared as the mould cavity solidifies eliminating the excessive shear heating which prevents solidification. This control would also benefit investigations with the two-colour work as it would provide for greater flexibility with the management of patterns and also benefit the development of multilayered composite sandwiches within a 2K system.

9. REFERENCES

1. Allan, P. S. and Bevis, M. J., Plast. Rub. Process. Applic., **7** (1987) 3 - 10.
2. Allan, P.S. and Bevis, M. J., British Patent 2170-140-B
3. Allan, P. S. and Bevis, M. J., Composites Manufacturing, **1** (2) (1990) 79 - 84.
4. Allan, P. S. and Bevis, M. J., Materials World, **2** (1) (1994) 7 - 9.
5. Yasuda, K., "Physical Property and Microstructure Control of Filled and Unfilled Amorphous Polymers", Wolfson Centre, Brunel University, 1995.
6. Malguarnera, S. C., Polym. Plast. Techn. Eng., **18** (1) (1982) 1 - 45.
7. Thamm, R. C., Rubber Chem. Technol., **50** (1977) 24 - 34
8. White, J. L. and Dee, H.B., Polym. Eng. Sci., **14** (1974) 212 - 222.
9. Schmitt, L. R., Polym. Eng. Sci., **14** (1974) 797 - 800.
10. Oda, K., White, J. L. and Clarke, E. S., Polym. Eng. Sci., **16** (8) (1976) 585 - 592
11. Wang, K. K., Shen, S-F. F., Hieber, C. A. and Stevenson, J. F., Science and Technology of Polymer Processing (Suh, N. P. and Sung, N. H., Eds.) Mit. Press, Cambridge, Massachusetts, (1979) 293.
12. Tadmor, Z., Appl. Polym. Sci., **18** (1974) 1753 - 1772
13. Folkes, M. J. and Russell, D. A. M., Polymer, **21** (1980) 1252 - 1258.
14. Hegler, R. P., Kunststoffe, **74** (1984) 271 - 277.
15. Hobbs, S. Y., Polym. Eng. Sci., **14** (1974) 621 - 626
16. Young, R J. and Lovell, P. A., "Introduction to Polymers", Second Ed. Chapman and Hall 1991
17. Hagerman, E. M., Plast. Eng., **29** (1973) 67 - 69.
18. Malguarnera, S. C. and Manisali, A., Polym. Eng. Sci., **21** (10) (1981) 586 - 593.
19. Malguarnera, S. C., Manisali, A. I. and Riggs, D. C., Polym. Eng. Sci., **21** (17) (1981) 1149 - 1155
20. Folkes, M. J., Short Fibre Reinforced Thermoplastics, Wiley, Letchwoth, England (1982).

21. Rawson, K. W., "Morphology and Properties of Silica - Polypropylene Composites", M.Sc. Thesis, U.M.I.S.T. 1992
22. Bown, J., Injection Moulding of Plastic Components, McGraw - Hill, London, (1979) 144
23. Rubin, I., Injection Moulding Theory and Practice, Wiley, New York, (1972) 192.
24. Hubbauer, P., Plast. Eng., **29** (1973) 37 - 39.
25. Bright, P.F. and Darlington, M. W., Plast. Rub. Comp. Process. Applic., **1** (1981) 139 - 147.
26. Bright, P. F., Crowson, R. J. and Folkes, M. J., J. Mat. Sci., **13** (1978) 2497 - 2506.
27. Curtis, P. D., Bader, M.G. and Bailey, J. E., J. Mat. Sci., **13** (1978) 377 - 390.
28. Crowson, R. J. and Folkes, M. J., Polym. Eng. Sci., **20** (1980) 934 - 940.
29. Krueger, W. L. and Tadmor, Z., Polym. Eng. Sci., **20** (1980) 426 - 431.
30. Hengesbach, H. A. and Schramm, K., Plastverarbeiter, **12** (1976) 667 - 670.
31. Menges, G., Koenig, D., Luettgens, R., Sarholz, R & Shuermann, E., Plastverarbeiter, **31** (1980) 185 - 193.
32. Holden, A. M., "Multiple Live-Feed Moulding of Fibre Reinforced Thermoplastics", Ph.D. Thesis, Brunel University, 1990.
33. Wada, A. and Kawabata, S., Seikei-Kakou, **3** (2) (1991) 165 - 170.
34. Wada, A. and Yasuda, K., Seikei-Kakou, **4** (9) (1992) 571-6.
35. Pittman, J.F.T., Aguirre, P. & Ding, D., Int. Polym. Processing, "Development of a Computer Simulation of SCORIM: In-mould Shearing with Cooling and Solidification", To be published.
36. Aguirre, P., "Simulation of the SCORIM Process", M.Sc. Thesis, University of Wales Swansea, 1994.
37. Gillespie, J.W. Jr., Vanderschiren, J. A. & Byron Pipes, R., Polym. Composites, **6** (1985) 82 - 86.
38. Vincent, M. & Agassant, J. F., Rheologica Acta, **24** (1985) 603 - 610.
39. Molden, G. F., Materials Science, **4** (1969) 283 - 289.

40. Manz, B., Kunststoffe, **85** (1995) 1346 - 1350.

41. Bürkle, E., Kunststoffe, **87** (1997) 320 - 328.

42. Hartung, M., Hintze-Brüning, H. and Oslowski, H.-J., Kunststoffe, **86** (1996) 350 - 353.

43. Kerr, J. D. and Klein, B., Kunststoffe, **85** (1995) 1130 - 1133.

44. Weigand. M., Kunststoffe, **86** (1996) 362 - 363.

45. Turner-Jones, A., Aizlewood, J. M. and Beckett, D. R., Makromol. Chem., **75** (1964) 134 - 158.

46. Aboulfaraj, M., Ulrich, B., Dahoun, A. and G'Sell, C., Polymer, **34** (1993) 4817 - 4825.

47. Norton, D. R. and Keller, A., Polymer, **26** (1985) 704 - 716.

48. Crissman, J. M., Polym. Sci. Polym. Phys. Ed., **7** (1969) 389 - 404.

49. Keith, H. D., Padden, F. J. Jr., Walter, N. M. and Wyckoff, H. W., Appl. Phys., **30** (1959) 1485 - 1488.

50. Draguan, H., Hubeny, H. and Muschik, H., Polym. Sci. Polym. Phys. Ed., **15** (1977) 1779 - 1789.

51. Varga, J. and Karger-Kocsis, J., Polym. Sci. Polym. Phys. Ed., **34** (1996) 657 - 670.

52. Turner-Jones, A., Polymer, **12** (1971) 487 - 508.

53. Lotz, B., Graff, S. and Wittmann J. C., Polym. Sci. Polym. Phys. Ed., **24** (1986) 2017 - 2032.

54. Padden, F. J. Jr. and Keith, H. D., Appl. Phys., **30** (1959) 1479 - 1484.

55. Kantz, M. R., Newman, JR. and Stigale, F. H., Appl. Polym. Sci., **16** (1972) 1249 - 1260.

56. Piccarolo, S., Scargiali, F., Crippa. G. and Titomaulio, G., Plast. Rub. Comp. Process. Applic., **19** (1993) 205 - 210

57. Murphy, M. W., Thomas, K. and Bevis, M. J., Plast. Rub. Process. Applic., **7** (1987) 241 - 242.

58. Kalay, G., Allan, P. and Bevis, M. J., Plast. Rub. Comp. Process. Applic., **23** (1995) 71 - 85.

59. Murphy, M. W., Thomas, K. and Bevis, M. J., Plast. Rub. Process. Applic., **9** (1988) 3 - 16.

60. Murphy, M. W., Thomas, K. and Bevis, M. J., Plast. Rub. Process. Applic., **9** (1988) 117 - 127.

61. Fujiyama, M., Wakino, T. and Kawasaki, Y., Appl. Polym. Sci., **35** (1988) 29 - 49.

62. Wenig, W. and Herzog, F., Appl. Polym. Sci., **50** (1993) 2163 - 2171.

63. Trotignon, J-P. and Verdu, J., Appl. Polym. Sci., **34** (1987) 1 - 18.

64. Watkinson, K., Thomas, A. and Bevis, M., J. Mat. Sci., **17** (1982) 347 - 358.

65. Bowman, J., Harris, N. and Bevis, M., J. Mat. Sci., **10** (1975) 63 - 76.

66. Bowman, J., J. Mat. Sci., **16** (1981) 1151 - 1166.

67. Wright, D. G. M., Dunk, R., Bouvart, D. and Autran, M., Polymer, **29** (1988) 793 - 796.

68. Fujiyama, M., Int. Polym. Processing, **VII** (1992) 358 - 373.

69. Fujiyama, M., Int. Polym. Processing, **VII** (1992) 84 - 96.

70. Kalay, G., Ogbonna, C., Allan, P. S. and Bevis, M. J., Trans IChemE, **73,** A (1995) 798 - 809.

71. Jerschow, P. and Janeschitz-Kriegl, H., Rheol Acta, **35** (1996) 127 - 133.

72. Kalay, G., "Microstructure and Physical Property Control of Injection Moulded Polypropylene", Ph.D. Thesis, Brunel University, 1994.

73. Gil Medina, E. M., "Alignment and Management of Talc Platelets in Polypropylene Matrix by the Application of Shear Controlled Orientation Injection Moulding (SCORIM) Technology", Ph.D. Thesis, Brunel University, 1996.

74. Liang, H, "The In-situ Formation and Management of Fibres in Moulded Composites of Polyproylene and a Thermotropic Liquid Crystalline Polymer", Ph.D. Thesis, Brunel Univerity, 1995.

75. Wang, L., Allan, P. S. and Bevis, M. J., Plast. Rub. Process. Applic., **25** (1996) 385 - 398.

76. Ogbonna, C. I., Kalay, G., Allan, P. S. and Bevis, M. J., Appl. Polym. Sci., **58** (1995) 2131 - 2135.

77. Pinwill, I. E., Ahmad, F., Allan, P. S. and Bevis, M. J., Powder Metal, **35** (1992) 107 - 112.

78. Lopez, J., Polymer Testing, **12** (1993) 437 - 458.

79. Chua, S. M. and Henderson, P. J., J. Mat. Sci. Letters, **10** (1991) 1379 - 1380.

80. Trotignon, J. P., Lebrun, J. L. and Verdu, J., Plast. Rub. Process. Applic., **2** (1982) 247 - 251.

81. Jeffery Davies, D., Plast. Eng., **53** (1997) 31 - 33.

82. Rösler, G., Kunststoffe, **87** (1997) 304 - 305.

83. Häußling, L., Keil, E. and Reich, W., Kunststoffe, **86** (1996) 354 - 356.

84. Chen, Z., Finet, M. C., Liddell, K., Thompson, D. P. and White, J. R., Appl. Polym. Sci., **46** (1992) 1429 - 1437.

85. Kalay, G. and Bevis, M. J., Polym. Sci. Polym. Phys. Ed., **35** (1997) 265 - 291.

86. Lotz, B. and Wittmann, J. C., Polym. Sci. Polym. Phys. Ed., **24** (1986) 1541 - 1558.

87. Kalay, G., Allan, P. and Bevis, M. J., Polymer, **35** (1994) 2480 - 2482.

88. Kalay, G. and Bevis, M. J., Polym. Sci. Polym. Phys. Ed., **35** (1997) 241 - 263.

89. Kalay, G. and Bevis, M. J., Polym. Sci. Polym. Phys. Ed., **35** (1997) 415 - 429.

90. Wang, L., Allan, P. S. and Bevis, M.J., Plast. Rub. Comp. Process. Applic., **23** (1995) 139 - 150.

91. Bowman, J. and Bevis, M., Colloid & Ploymer Sci., **255** (1977) 954 - 966.

92. Gibson, J. R., Allan, P. S. and Bevis, M. J., Plastics and Rubber International, **16** (5) (1991) 12 - 14.

Appendix

This appendix details a brief outline of the results of the work carried out by Dr J. F. T. Pittman *et al* at the University of Wales Swansea. An introduction to this topic is given in section 1.8, relaying the basic theory behind the one-dimensional transient model employed. The numerical simulation of the SCORIM process was developed alongside the experimental evaluations of this PhD research, which boded for a mutually beneficial collaboration.

The original model described in section 1.8 was compared to the results of two colour SCORIM mouldings produced using one and two shears incorporating delays. This was possible because of clearly defined displaced interfaces, known selective processing conditions via data acquisition and physical property data of the polymer which were known or deduced.

As a consequence of this comparison, it was necessary to adapt and extend the original model incorporating three new factors previously neglected or erroneously considered.

1. The programme had to be extended to simulate the presence of delays between reciprocal piston movements. This required the numerical calculation of the velocity profile at the beginning of each stroke iteratively, incorporating the presence of the frozen skin layer.
2. The type of boundary condition used at the mould wall was changed from a Dirichlet to Fourier type. It was also shown that the thermal resistance within the mould tool could not be neglected. Therefore it was necessary to evaluate the overall heat transfer coefficient between the mould wall and coolant. A decreasing value for this was proposed and justified by consideration of the transient conduction process within the mould tool. The differences between the cooling channels of the two halves of the tool were approximated to a single distance to facilitate the one-dimensional model. This approximation was shown to be suitable.
3. Further, the temperature dependence of density could not be neglected. It was essential to use density values corresponding to the relevant melt temperature, to obtain the correct volumetric flow-rate produced by the SCORIM pistons movements.

The progressive development of this model by the incorporation of these three factors was a contribution made by Mr C. Delahaye to further the progress made by other workers[35, 36] in the Swansea group. These changes yielded results with the model which closer reflected the experimental findings. Any other discrepancies are considered to be mostly related to a lack of reliable physical-property data where the melt viscosity is close to its freezing range.

The model illustrates the ability to realistically simulate the important features of the SCORIM process where complex interactions between flow, heat transfer and phase change are involved. The information deduced with this model relating to the effective overall heat transfer coefficient for mould cooling, is also applicable to conventional moulding.

Future development of this model is hoped to incorporate the insertion of a new subroutine within the programme which facilitates temperature dependence of materials density. Further, an extension to the simulation to include heat conduction through the mould tool would negate the need for estimating the overall heat transfer coefficient.

Bibliography

Delahaye, C., "The SCORIM Injection Moulding Process: Computer Simulations and Experimental Results", Final Year Project, University of Wales Swansea, June 1997.